MISCIBILITY OF POLYMER BLENDS
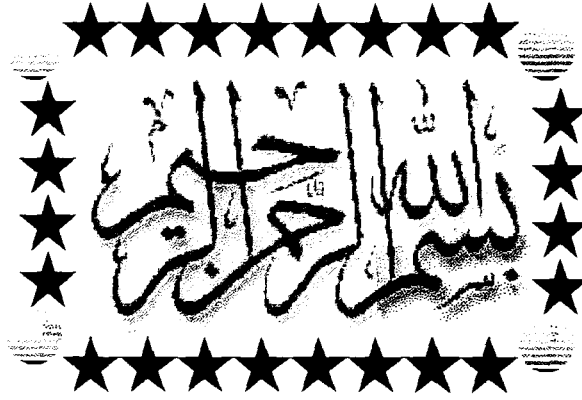
A thesis submitted for the degree of Doctor of Philosophy

by

ALI ASGHAR BHUTTO

Centre for Physical Sciences

Institute of Physical and Environmental Sciences

Brunel University

Uxbridge, Middlesex UB8 3PH

July 1999

بسم الله الرحمن الرحيم

DEDICATION

This work is dedicated to my parents, all the members of my family, my wife, my children and specially my elder brother **Muhammad Anwer Bhutto** and my Uncle **Muhammad Ibrahim Bhutto** for their moral support, struggle, patience and love.

ABSTRACT

In this work an attempt is made to correlate polymer miscibility with diffusion and with molecular interactions. A system with lower critical solubility temperature has been selected, namely polystyrene (PS) and polyvinyl methyl ether (PVME). Most of the published work has been done on polymers in solutions or on solvent cast specimens and therefore on ternary systems. The role of solvent has not yet been fully evaluated and it was of interest to compare the results on solvent cast samples with those prepared by mechanical blending and by diffusion. Molecular interaction is dependent on functional groups present and for this reason experiments have been performed on PVME blends with PS of different levels of sulfonation (SPS). Selective deuteration (d-PS) was used to identify and assign some absorption peaks in the infrared spectra.

DSC measurements have shown that only one T_g is present for all blends prepared by solvent casting. It was necessary to use an extreme quenching rate down to liquid nitrogen in order to preserve the high temperature (above 150°C) phase separated structure, represented by two T_g of homopolymers. The mechanically blended system, on the other hand, did not show a single T_g of the blend, unless annealed for one day at 110°C. This confirms the results obtained by diffusion studies using light microscopy and neutron reflectivity, that the diffusion rates are extremely slow and therefore do not control the phase formation and separation processes. These experiments also indicate that the microstructures of solvent cast samples and samples prepared by mechanical blending are different. The T_g of mechanical blended polymers indicate, that the composition of diffusion swollen PS does not correspond to the phase diagram measured in solutions, confirming thus the above result.

The FTIR studies at different temperatures have shown that changes in spectra of polymer blends, as reported in the literature can be explained by temperature changes in pure homopolymers. This indicates that molecular interactions, which are responsible for miscibility, are not detectable by infrared absorptions and are therefore of unspecified strength and location. The FTIR of SPS/PVME blends show that sulfonate groups on PS affect polymer miscibility through changes in configuration of molecules, rather than through direct interaction with the PVME, as suggested in the literature.

An attempt has been made to study diffusion of SPS and polycarbonate (PC) system by neutron reflectivity. Preliminary results indicate that surface relaxation effects make the data interpretation difficult.

ACKNOWLEDGMENTS

TABLE OF CONTENTS

LIST OF TABLES

LIST OF FIGURES

SYMBOLS

ΔG_m	Gibbs free energy of mixing
ΔS_m	Entropy of mixing
ΔH_m	Enthalpy of mixing
T	Temperature
T_g	Glass transition temperature
$\Delta V_{m.sp}$	Specific volume of mixing
w_1, w_2	Weight fraction of components 1 and 2
k	Boltzmann constant
Q_{12}	Empirical entropic parameter
b_i	Neutron scattering length density of atom i
D_m	Polymer density in bulk
N_A	Avogadro number
M_m	Monomer molar mass
b	Coherent scattering length
c_1 , c_2	Constants
Q	Neutron momentum transfer
q	Wave vector
V	Volume
t	Time
r_{ij}	Fresnel reflection coefficient
R	Reflectivity
R	Gas constant
S	Interfacial area
W	Interfacial width
b/v	Scattering length density
Z_o	Standard deviation of Gaussian function
n_1, n_2	Refractive indices of components 1 and 2
$Nb(z)$	Neutron scattering length density profile
Nb_b, Nb_t	Neutron scattering length density for the bottom and top layer

h	Planck's constant (chapter three)
c	velocity of light (chapter three)

GREEK CHARACTERS

$\Delta\mu_i$	Chemical potential difference of component i.
δ_i	Solubility parameter of component i.
θ	Scattering angle
θ_r	Angle of reflection
θ_i	Angle of incidence
θ_c	Critical angle of incidence
λ	Wavelength of scattering radiation
ν	Wavelength
σ_a	Adsorption cross-section
ρ	Density
$<\sigma^2>$	Root mean square roughness
σ	Gaussian Width
χ_{12}	Interaction parameter

ABBREVIATIONS

UCST	Upper Critical Solution Temperature
LCST	Lower Critical Solution Temperature
PS	Polystyrene
PVME	Poly (vinyl methyl ether)
PMMA	Poly (methylmethacrylate)
PC	Polycarbonate
SPS	Sulfonated Polystyrene
Li	Lithium
Zn	Zinc
dSPS	Deuterated Sulfonated Polystyrene
PVC	Poly (vinyl chloride)
PCL	Polycaprolactone
DSC	Differential Scanning Calorimetry
GPC	Gas Permeation Chromatography
TG	Thermogravimetry
DTA	Differential Thermal Analysis
TMA	Thermomechanical Analysis
DMA	Dynamic Mechanical Analysis
DETA	Dielectric Thermal Analysis
EGD	Evolved Gas Detection
EGA	Evolved Gas Analysis
EDA	Electron – donor – acceptor
FTIR	Fourier Transform Infrared
NMR	Nuclear Magnetic Resonance
NR	Neutron Reflectivity
INS	Inelastic Neutron Scattering
CRISP	Critical Reflection Investigation of Surface Phenomena
SCPE	Solution Chlorinated Polyethylene

CHAPTER ONE

INTRODUCTION

1.1   OBJECTIVES

Commercial polymers are mixtures of several compounds including stabilisers, antioxidants, UV stabilisers, processing aids, lubricants, extenders and fillers. Mixing with other polymers has also been commercially successful and some of the best polymer systems or copolymers or polymer blends. The blending of the polymers is therefore of industrial importance and has been extensively studied. The most successful polymer systems were, however, developed empirically and there is great shortage of fundamental knowledge of the basic principles of miscibility.

This work attempts to evaluate the thermodynamic parameters, microstructure, molecular interaction and diffusion in polymer blends. The polymer systems investigated were PS and SPS blended with PVME and also with polycarbonate. The techniques used were FTIR spectroscopy, light microscopy, DSC and neutron reflectivity. The interpretation of the FTIR spectra was aided by utilisation of deuterated compounds. The main object of this work was to correlate miscibility with, diffusion and molecular interaction.

1.2   BACKGROUND

A polymer blend is a mixture of at least two polymers or copolymers [1,2] that exhibits homogeneity on a microscopic scale [3,4]. Blending polymers is an engineering technique used to develop new polymeric materials which have specific properties different from those of the pure homopolymers. Polymer blends can be characterised by the degree of miscibility, and classified into three types as shown below:

Polymer 1

Miscible
- Single phase
- Single T_g

Partially miscible
- Phases separate as ratio progresses toward 50/50
- The two T g are between the Tg's of constituent polymers

Immiscible
- Two phases
- Two T_g's are similar in constituent polymers

(a)   (b)   (c)
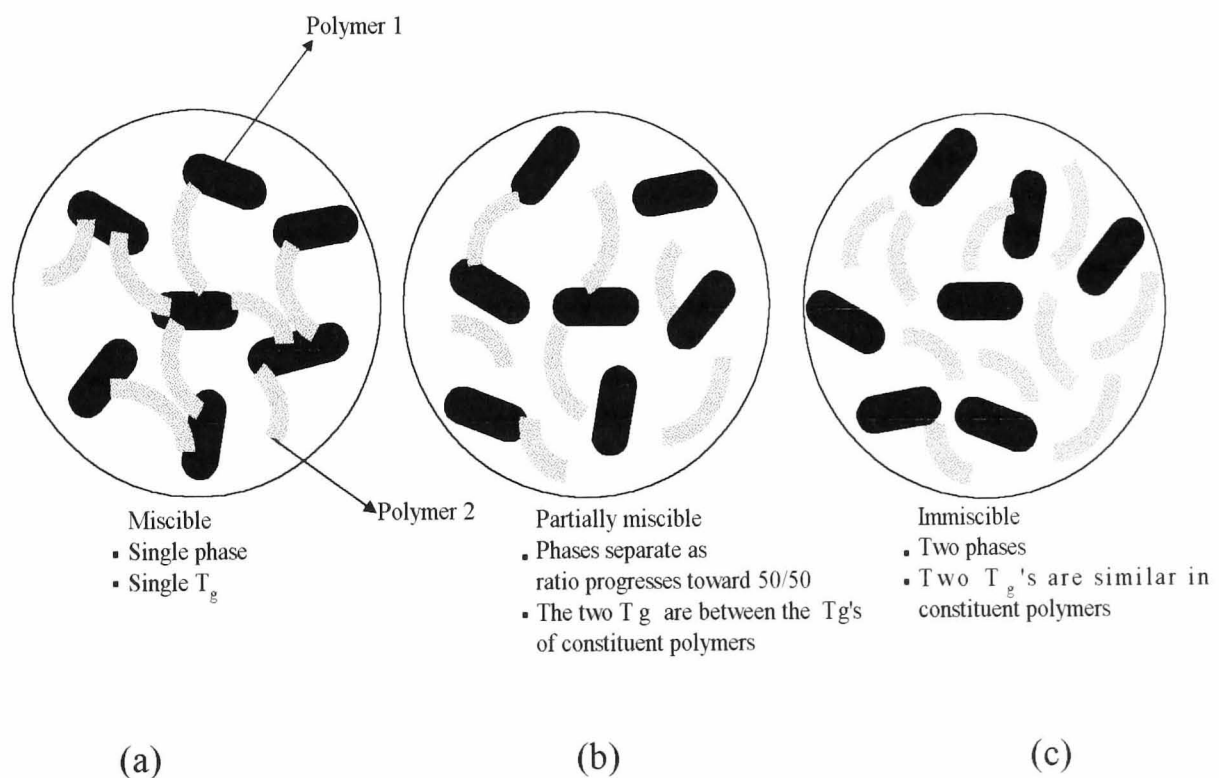
Figure 1.1   Morphologies of a polymer blend [3] (a) miscible (b) partially miscible (c) immiscible.

Miscibility is defined as a state of two polymers where the level of molecular mixing is adequate to yield macroscopic properties expected of a single-phase material [5]. It happens when the two polymers have the total interaction energy

between their monomers (after blending) lower than the combination of interaction energy of each polymer before blending. These interactions are the combination of attractive and repulsive forces of the functional groups between and within the molecules. Unlike the small molecular systems, the entropies of large molecules are small and contribute less to the miscibility of high molecular weight systems.

Partially miscible polymers exhibit at least two miscible phases where each phase may comprise a high concentration of one component with a smaller dissolved portion of the other. The largest group of commercial alloys and blends falls into this category [3].

Immiscibility is a state of the system where two phases are present in macroscopic and/or microscopic properties. This occurs when the blend of two polymers has on unfavourable interaction energy (repulsion or no attraction between different polymer molecules). A block, graft copolymer or polymeric plasticizer can cause an immiscible blend to have a smaller domain size and increase the interfacial area [3] by attracting one part of the molecule into one phase and attracting the other into the second. It also produces a covalent bond at the interfaces and joining the two phases together, the result will be better properties, especially the mechanical properties.

The same polymer blend can exhibit miscibility, partial miscibility or immiscibility, depending on the conditions and methods of blend preparation such as temperature, pressure or shear rate. An *upper critical solution temperature* (UCST) occurs when the immiscible blends become miscible at high temperature, and *lower critical solution temperature* (LCST) occurs when the miscible blends

become phase separated at high temperature. Properties of polymer blends can be divided into three categories as shown below in the figure 1.2. [4]
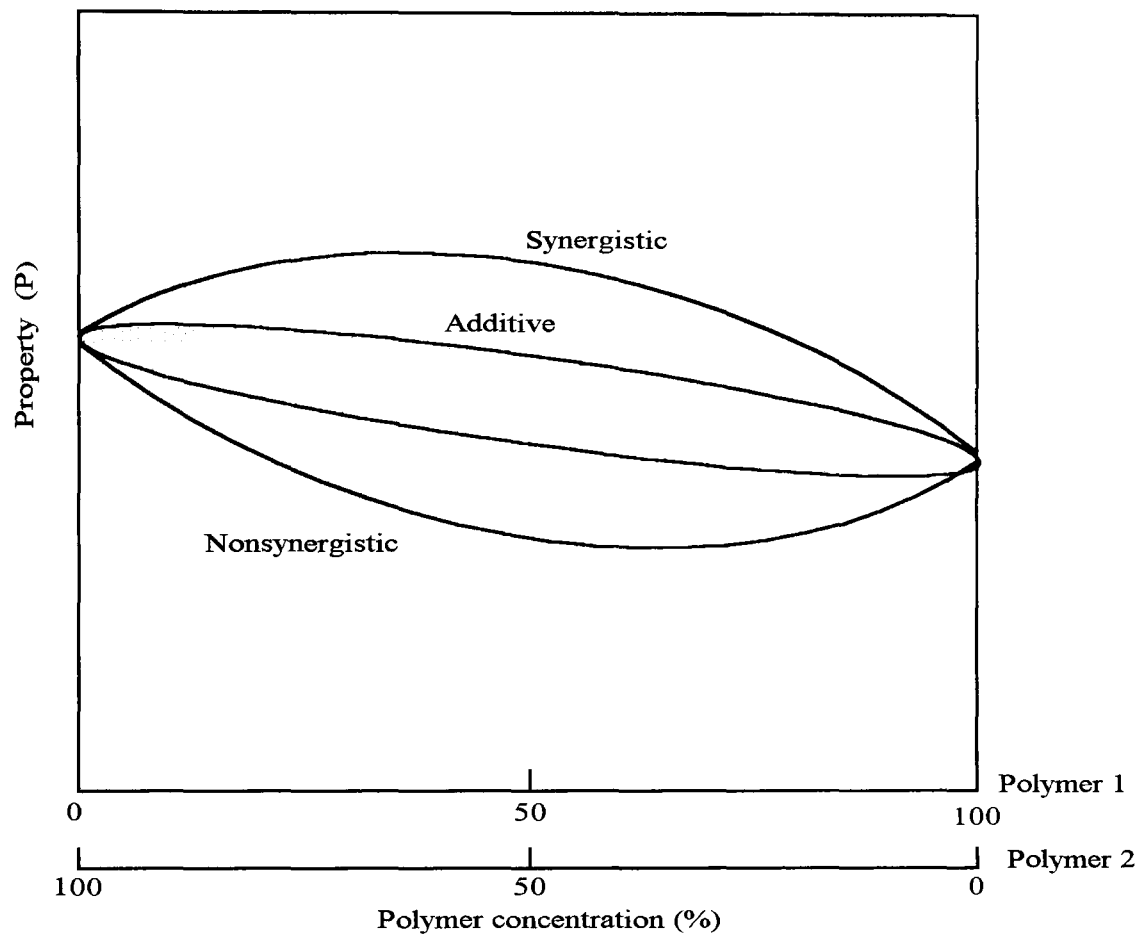
Figure 1.2   Possible functions of mechanical properties vs. two – component compositions.

The polymer blends behave synergistically when the properties of the polymer blends are better than those of both pure polymers. The additive blends are the polymer blends that have their properties fall between both pure components. Most polymer blends fall into this category. Immiscible polymer blends usually

behave nonsynergistically and the properties are less favourable than those of both pure components.

Making polymer blends is relatively inexpensive compared to creating a new homopolymer [3]. The blend's properties can be improved (synergistic) or be a weighted average between those of the two pure polymers (additive)[1]. This method allows the producers to vary the quality and price of their products to suit the applications. For example, amorphous polymers usually have low chemical resistance but high dimensional stability and high impact properties. Crystalline polymers usually have high chemical resistance, but have a low impact and low dimensional stability. The appropriate blends between the two may show an improvement over the properties of then individual polymers [3].

The subject of this thesis is to investigate the miscibility of two different blends through polymer – polymer diffusion. The first case studied is a model system, the blend of polystyrene (PS)/poly(vinyl methyl ether) (PVME). The standard characterisation of this blend was carried out using *differential scanning calorimetry (DSC)*, *light microscopy* and complemented by *FTIR spectroscopy* studies as a function of temperature. The second system investigated was that of sulfonated polystyrene/polycarbonate blends where interfacial diffusion was studied using the neutron reflectivity technique. Diffusion in the bulk was difficult to observe in the PS/PVME blend.

These two case studies are linked by a detailed *FTIR* study into the changes in polystyrene, occurring on a molecular level, as a function of sulfonation and deuteration.

1.3   ORGANIZATION OF THE THESIS

In this thesis I will present the results of the research on the mechanism of polymer miscibility by different experimental methods. Because the different aspects of this work are easily divided into sub-projects, I have chosen to depart somewhat from the strict conventional thesis format and I am presenting each sub-project as a separate chapter.

In chapter two, an outline of the theory of polymer blends miscibility which is relevant to this project is given. In the third chapter, some information about the experimental techniques employed in the course of the Ph.D. project is provided. The work performed on *PS/PVME* and *Na-SPS/PVME* blends is reported in chapter four, where results obtained by three different techniques are discussed. Chapter five presents the results of FTIR study of hydrogenous atactic polystyrene and its selectively deuterated variants, and a corresponding series of atactic sodium sulfonated polystyrene. This research is a continuation of previous work [6] using inelastic incoherent neutron scattering. Here infrared spectroscopy was used instead. Chapter six contains an independent study of ionomer blends using neutron reflectivity. The blends under investigation are *Li-dSPS/PC* and *Zn-dSPS/PC*. Finally, seventh chapter contains the conclusions of the research described in the preceding three chapters, and gives recommendation for future work.

References

1. Utracki, L. A., *Polymer Alloys and Blends* **1989**.

2. Sperling, L. H., *Introduction to Physical Polymer Science* **1986**.

3. Kienzle, S. Y., *Engineering Material Handbook, Vol. 2-Engineering Plastics* **1988**, 487-492.

4. Jacqueline, I. K., *Concise Encyclopaedia of Polymer Science and Engineering* **1990**.

5. Olabisi, O.; Robeson, L. M.; Shaw, M. T., *Polymer – Polymer Miscibility*, Academic Press: New York, **1979**.

6. Gabrys, B. J.; Huang, D; Nardi, F; Peiffer, D. G.; and Tomkinson, J., *Macromolecules* **1993**, 26, 8, 2007.

CHAPTER TWO

POLYMER MISCIBILITY: THEORY AND BACKGROUND

2.1 MISCIBILITY OF POLYMER BLENDS

2.1.1 Introduction

During the last few decades, efforts have been made to modify the traditional concept of mixing in order to explain the thermodynamic behaviour of polymeric systems. The thermodynamics of mixing can be applied to polymers in order to explain the changes in the properties of mixtures and the mixing behaviour at various conditions of temperature, pressure and concentration. Thermodynamics usually predict the final characteristics i.e. equilibrium states of the blends when the environment changes, the polymer blend has to find a new thermodynamic equilibrium. These changes may be caused by many things such as the methods of preparing blends, changes in working condition, etc.

Polymer blends behave differently from mixtures of normal small organic molecules because the former has huge molecules with various kinds of monomers that have special characteristics. For this reason, the behaviour of polymer blends is difficult to predict and the blends are difficult to process. If only we understood completely the reasons for their behaviour, then perhaps we could create economically new materials from mixtures of selected polymers in selected process conditions.

Only a few pairs of polymers show mutual compatibility at a thermodynamic level, for example a model system of polystyrene (PS) and poly(vinyl methyl ether) (PVME). Results obtained for this blend show the compatibility of PS and PVME over a wide range of compositions[1] and temperatures. This compatibility is also dependent upon the nature of the solvent [2] used for mixing. The compatible films show reversible phase separation at high temperatures [3], and the cloud point temperature is associated with the _lower critical solution temperature_ (LCST)[4].

In order to study the phase behaviour of polymer-polymer mixtures, the PS and PVME system is frequently chosen as both polymers are amorphous and their blend has an accessible phase diagram. PS is available in monodispersed form but not PVME.

In this chapter, some attempts to predict and explain the special characteristics of polymer blends will be briefly discussed, starting with the miscibility study or how to detect the miscibility and phase behaviour of the polymer blends. The Flory – Huggins theory of mixing and related equations will also be described: these are the basic concepts related to mixtures of small molecules. This will provide an introduction to mixing and will illustrate the difference between the thermodynamic properties of such mixtures and those formed by polymers.

2.1.2 Thermodynamics of blend miscibility

The basic thermodynamic equation for describing miscibility of a polymer blend which relates the Gibbs' free energy of mixing, $\triangle G_m$, to the enthalpy and entropy of mixing, $\triangle H_m$ and $\triangle S_m$, respectively, is given by

$$\Delta G_m = \Delta H_m - T\, \Delta S_m,$$ 2.1

where T is the absolute temperature.

The conditions for a single phase structure to exist are that the Gibb's free energy of mixing is less than or equal to zero, and the second derivative of the Gibb's free energy of mixing with respect to the composition is always positive:

$$\Delta G_m \leq 0,$$ 2.2

and

$$\frac{\partial^2 \Delta G_m}{\partial \phi^2} > 0.$$ 2.3

The number of ways small molecules can arrange themselves with each other is very large and as a result the entropy of mixing is also large. Therefore in low molecular weight systems the term $T\Delta S_m$ in equation 2.1 is large enough to make ΔG_m negative. Polymers however have very long chains and it can assume a large number of conformation. This means that for polymers the entropy of mixing contributes very little to ΔG_m. Despite this, many polymer pairs are miscible due to some *specific interactions* (such as hydrogen bonding) between the polymers which make ΔH_m negative. As a result ΔG_m is negative and mixing occurs. Since

ΔH_m is temperature - dependent, the stability of the system will vary with temperature.

If the molecular weight of a component in a polymer is increased, the entropy of mixing ΔS_m decreases, thus $T\Delta S_m$ is smaller and ΔG_m is less negative (therefore the components are less miscible). This means that for high molecular weight polymer the temperature at which the system phase separates is lower.

Figure 2.1[5,6,7] shows a typical dependence of ΔG_m on composition ϕ for a system which is miscible at the temperature of observation, T_0, and which shows LCST behaviour. The corresponding miscibility varies with temperature and composition.

It is seen that, for any composition between ϕ_1 and ϕ_2 (here ϕ_1 and ϕ_2 are the volume fraction of the components), the system can reduce ΔG_m by separating into two phases with composition ϕ_1 and ϕ_2. The solid line in diagram (b) is called the *binodal* and is defined by the points of common tangent of ΔG_m. At these compositions the chemical potentials (the term *chemical potential* is used to describe a partial molar Gibb's free energy), μ_1 and μ_2 are equal and two phases can coexist.:

$\mu_1 = \mu_2.$ 2.4

The dashed line in figure 2.1 (b) is the *spinodal*, defined by the points of inflexion where the following condition holds

$$\frac{\partial^2 (\Delta G_m)}{\partial \phi_2^2} = 0 \qquad\qquad 2.5$$

These points are denoted ϕ_1' and ϕ_2' in diagram 2.1(a). For compositions between ϕ_1' and ϕ_2' are determined by the condition

$$\frac{\partial^2 (\Delta G_m)}{\partial \phi_2^2} > 0 \qquad\qquad 2.6$$

and the system is unstable to all small concentration fluctuations. The phase separation process is called *spinodal decomposition*. Between ϕ_1 and ϕ_1' and ϕ_2 and ϕ_2',

$$\frac{\partial^2 (\Delta G_m)}{\partial \phi_2^2} < 0 \qquad\qquad 2.7$$

so that small fluctuations are damped out and phase separation can proceed only by a nucleation and growth process.
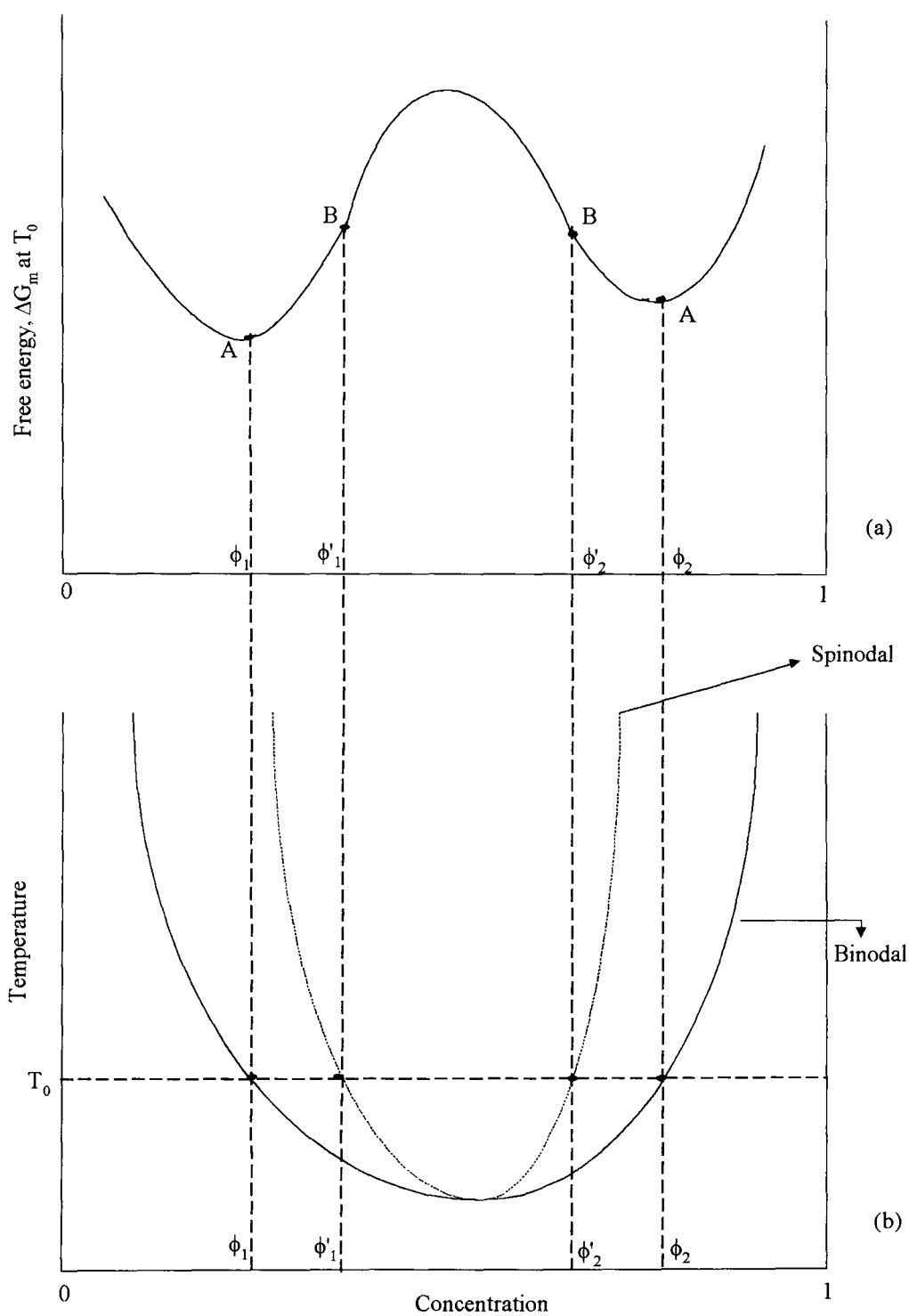
Figure 2.1   (a). Plot of the free energy of mixing as a function of polymer concentration.

(b). Corresponding phase diagram of a polymer blend exhibiting LCST behaviour [5]. (see description in text)

2.1.3   Specific Interactions Occurring in Polymer Blends

Specific interactions between chemical groups of two blend components can play important roles in polymer mixtures. Specific attractive interactions lead to exothermic mixing which favours miscibility, and there is a range of such interactions of varying strength, which has been identified in polymer blends. Olabisi [8] classifies seven types of interactions: (1) random dipole -induced dipole, (2) dipole - induced dipole, (3) dipole - dipole, (4) ion - dipole, (5) hydrogen bonding, (6) acid - base, and (7) charge transfer. These interactions are described below. *Specific interactions* is a genetic term used in chemistry and biochemistry, and such interactions are generally defined for small molecules. It should be noted that the extension of this concept to polymers is not always straightforward: it is more difficult to identify interactions in polymers, the spectroscopy is more complex, and molecular conformations are less certain. This situation is further complicated because researchers use different names and definitions to describe similar interactions.

(1). Random Dipole - Induced Dipole Interactions

The dipole moment is a measure of the degree to which the centre of the negative charge distribution (electron) of a molecule differs from the centre of the positive charge distribution. The magnitude and the direction of charge asymmetry is the dipole moment, a vector quantity. A single ground-state oscillation of charge in any molecule can create a temporary, fluctuating, random dipole moment in a molecule. Exposing a molecule to an electric field will also produce a dipole moment, an induced dipole. The size of the induced dipole moment depends on

the polarizability of the molecule as well as the field strength. A temporary, random dipole moment propagates a fluctuating electric field, which induces dipole moments in neighbouring molecules; then, in turn, the induced dipole radiates electric field back to the original molecule. The net result of these interactions is an attractive force between the two molecules [9]. This force is called the dispersion or the London force after London who first described it[8]. The strength of this force is proportional to $1/r^6$, where r is the intermolecular distance. The interaction energy, U, is expressed as:

$$U = -\frac{3I_1I_2\alpha_1\alpha_2}{2(I_1+I_2)r^6}$$
                                            2.8

where I_1 and I_2 are the ionisation potentials of the molecules and α_1 and α_2 are the polarizabilities. The dispersion force is relatively weak; for example, the dispersion force between two water molecules 0.3nm apart would be of the order of $3.4kJ\ mol^{-1}$ [9].

One blend in which the dispersion forces are thought to play a role in polymer - polymer miscibility is poly(4-methyl styrene) / poly(2,6-dimethyl-1,4-phenylene oxide) where there is a strong dispersion interaction between the phenyl and phenylene rings [10].

(2). Dipole - Induced Dipole Interactions

The interaction between a permanent dipole and the dipole it induces in a neighbouring symmetric molecule is called the induction force. The expression for the energy of this interaction is given by

$$U = \frac{-(a_1\mu_2^2 + a_2\mu_1^2)}{r^6}$$

2.9

where μ is the dipole moment [8,9].

McClellan includes the dipole moments of some common polymers in his book of experimental dipole moments [11].

(3). Dipole - Dipole Interactions

Dipole - dipole interactions are generally stronger than either of the two interactions above. The interaction between two permanent dipole moments is very sensitive to the orientations of the dipoles. Head -to- head and tail -to- tail configurations are repulsive, head-to-tail arrangements are attractive. If all arrangements were equally probable, the net force would be zero, but because favourable orientations are preferred, particularly at lower temperatures, the net result of dipole pairs is an attractive interaction. The potential for randomly oriented permanent dipole pairs falls off with an r^6 dependence and an inverse temperature, T^{-1}, dependence:

$$U = \frac{-(2\mu_1^2\mu_2^2)}{3kTr^6}$$

2.10

where k is Boltzmann's constant.

In the case of the optimum alignment of the dipoles, the distance dependence decreases to $1/r^3$. For well aligned water dipoles at T=300K, the dipole potential

is 15 kJ mol^{-1} [see also hydrogen bonding (5)]. An example of a dipole - dipole interaction in a polymer blend is provided by the mixture of polycaprolactone (PCL) and poly(vinylidene chloride-co-acrylonitrile) (Saran). There is thought to be an interaction between the carbon-chloride dipole of the Saran and the carbonyl dipole of the PCL. Hydrogen bonding is hindered in this blend because there is no α hydrogen atom in the Saran [12].

(4). Ion - Dipole Interactions

Ion - dipole interactions are stronger and farther reaching than the dipole only interactions discussed above. The potential energy of a water molecule interacting with a monovalent ion is 59kJ mol^{-1}, which is four times the strength of the maximum dipole - dipole interaction. The expression for the potential energy is:

$$U = \frac{-q_1 \mu_2}{r^2}$$
2.11

where q_1 is the charge on the ion.

The effective value of the ionic charge can be reduced at longer range by the presence of counter ions.

An example of ion - dipole interactions between blended polymers is in a mixture of poly(alkyl oxide) (ethylene or propylene) and an ionomer, poly(styrene-co-methacrylic acid) neutralized with an alkali metal. The dipole is provided by the oxygen on the poly(alkyl oxide) and the ion is the cation, lithium, sodium or potassium, from the ionomer [13,14].

(5). Hydrogen Bonding Interactions

Hydrogen bonds are one of the most important interactions in polymer blends and are frequently cited as the reason for blend miscibility. Hydrogen is ubiquitous in polymers and electronegative atoms such as nitrogen, oxygen, fluorine and chlorine are also common. Hydrogen bonding is a type of dipole - dipole interaction, but it is particularly strong because of the small radius of the hydrogen atom; the participating atoms can get close to each other, The term $1/r^6$ is thus large. A hydrogen bond involves two electronegative atoms or groups (X, Y) and a hydrogen atom (H) covalently bonded to one of the electronegative moieties:

$$^{\delta-}X - {}^{\delta+}H \ldots {}^{\delta-}Y \qquad\qquad 2.12$$

Orientation is again important here; the most effective orientation is to have the hydrogen bond at 180^0 to the covalent bond. Typical bond strengths are of the order of 12 to 25 kJ mol^{-1} [15,16].

There are many examples of hydrogen bonding in the polymer blends to be found in the literature. In many cases the presence of hydrogen bonding has been conclusively shown by Fourier transform infrared spectroscopy (FTIR)[17]. The most common hydrogen bonding acceptor groups found in polymers is the carbonyl group; popular donor groups are N-H and CC-H groups, particularly when there is an electronegative moiety such as chlorine attached to the carbon atom.

(6). Acid – Base Interactions

According to the Lewis definition [18], an *acid* is a substance, which can accept electrons and a *base* is one which can donate electrons. Thus an acid – base reaction involves the acid accepting electrons from the basic donor:

$$X + Y \rightarrow X^- + Y^+$$
                                        2.13

The interaction results from the ionic attraction between the two charged species[19]. An expression for the potential energy of such an interaction is given by:

$$U = \frac{\beta^2}{I_d - A_a + C}$$
                                        2.14

where I_d is the ionic potential of the electron donor, A_a is the electron affinity of the electron acceptor, β is the electron exchange energy and C is a constant[15]. When the acid is also an acid by the Bronsted/Lowry definition [20], i.e. a proton donor, the acid – base reaction may also be called a proton transfer reaction:

$$X - H + Y \rightarrow X^- + H - Y^+$$
                                        2.15

A proton transfer interaction is distinct from, and stronger than, a hydrogen-bonding interaction, the proton is not actually transferred in hydrogen bonding.

However some researchers do consider hydrogen bonding to be a subset of acid
– base interactions [21].

Reports of acid-base interactions in polymer blends are not as common as those
of hydrogen bonding. Eisenberg [19,22-25] has studied a number of blend systems
where he reckoned that proton transfer takes place. Percec, Pugh and Rodriguex-
Parada [26,27] describe electron-donor-acceptor (EDA) interactions in copolymer
blends, which contained carbazolyl electron donor groups and 3,5-dinitrobenzoyl
acceptor groups. Weiss et al [28] used acid-base interactions to enhance the
miscibility of modified polystyrene and oligomeric poly(alkylene oxide) blends.

(7). Charge Transfer Interactions

Charge transfer interactions involve the formation of a two molecule complex
through electronic delocalization. An electron moves from an orbital centred on
one molecule to an orbital centred mostly on the second molecule:

$$X + Y \rightarrow X^- Y^+$$

2.16

One area of chemistry where charge transfer interactions are often found is
organo-metallic chemistry, in the interactions between metals and organic
ligands: electrons move from ligand centred orbitals to metal centred ones or vice
versa, forming co-ordination complexes. This type of specific interaction is also
found in polymer blends, particularly in blends containing ionomers.

Peiffer et al[29] studied a blend of zinc neutralized sulphonated EPDM with
poly(styrene-co- vinyl pyridine), while Belfiore[30] used NMR to investigate a

similar interaction in a blend of poly(vinyl pyridine) and poly(ethylene-co-methacrylic acid) partially neutralized with zinc. A blend of copper neutralized carboxyl terminated polybutadiene with poly(styrene-co-vinyl pyridine) was found by Weiss et al[31] to have enhanced miscibility due to the presence of a charge transfer interaction.

2.2   PHASE BEHAVIOUR OF POLYMER BLENDS

2.2.1   The Phase Diagram

There are basically two types of phase diagrams describing a mixture of two components: as temperature increases, one that demixes *lower critical solution temperature behaviour* (LCST) and the other that mixes *upper critical solution temperature behaviour* (UCST). Any given mixture can show either of these behaviours, none or both. This is important for industry, to know the limits of application.

In figure 2.2 are some examples of types of phase diagram for two components blends: (a) fully miscible at all compositions and temperatures, (b) completely immiscible, (c) a single phase at high temperature and phase separated at low, (d) a single phase at low temperature and phase separated at high [the converse of (c)], and (e) a single phase at intermediate temperatures but in two phases at the extremes of temperatures, (c) and (d). The diagrams in figure 2.2 represent the idealised symmetric cases; these are rarely (if ever) found experimentally. It is usual that the phase boundaries are skewed by differing molecular weights, polydispersity, interaction ratios and other factors.
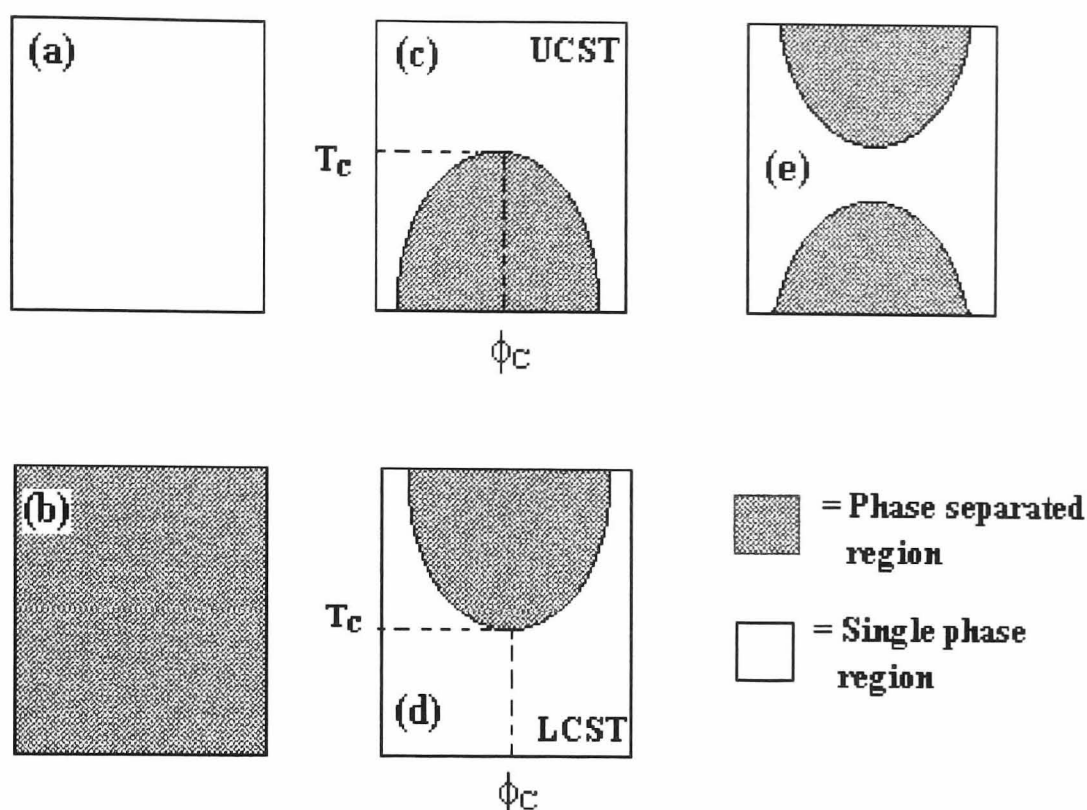
Figure 2.2   Forms of phase diagrams [8] (a) fully miscible (b) completely immiscible,
(c) a single phase at high and phase separated at low temperature, (d) a
single phase at low and phase separated at high temperature, (e) a single
phase at intermediate temperatures

Beside the limiting cases of (a) and (b), the most common phase diagrams for
polymer blends are the types (c) and (d). Type (c) exhibits an _Upper Critical
Solution Temperature_, UCST, phase diagram. The upper critical solution
temperature, T_c, is the highest temperature at which phase separation begins, and
the corresponding composition for this is called the critical composition ϕ_c (see
figure 2.2). This kind of phase behaviour is found in blends with endothermic
heats of mixing, in blends of similar polymers, or in blends where the component
polymers have low molecular weights.

The phase diagram for (d) is called the *Lower Critical Solution Temperature*, LCST. It is rarely observed for lower molecular weight solutions but is very often the behaviour observed for polymer blends. An LCST phase diagram is indicative of a blend which mixes exothermically. In cases where specific interactions are the principal cause of blend miscibility, the phase diagram is of the LCST type.

Imagine a blend where there are no specific attractive interactions, composed for instance of two polymers of very similar structure. ΔH_{mix} will be positive and thus the only contribution to miscibility will come from the entropic term. The more negative this term is, the more miscible the system will be, and this can be achieved by increasing temperature. This is also the case of low molecular weight components, and it represents the UCST. Instead, if there are important attractive interactions as for instance in PS/PVME (solution of polystyrene / poly (vinyl methyl ether), ΔH_{mix} will be negative and hence the mixture will be miscible. Increasing the temperature may have a strong effect on these interactions: the internal energy (vibrational, rotational) of the molecules will increase so much that it will be able to break the attractive forces between polymer molecules. This is the case of LCST.

There are two kinds of phase boundary: the *binodal* and the *spinodal* phase boundaries as described in figure 2.1. And there are three kinds of phase regions: a single phase region below the binodal boundary, a metastable region between the binodal and the spinodal boundary and a phase separated region above the spinodal, as shown in figure 2.3
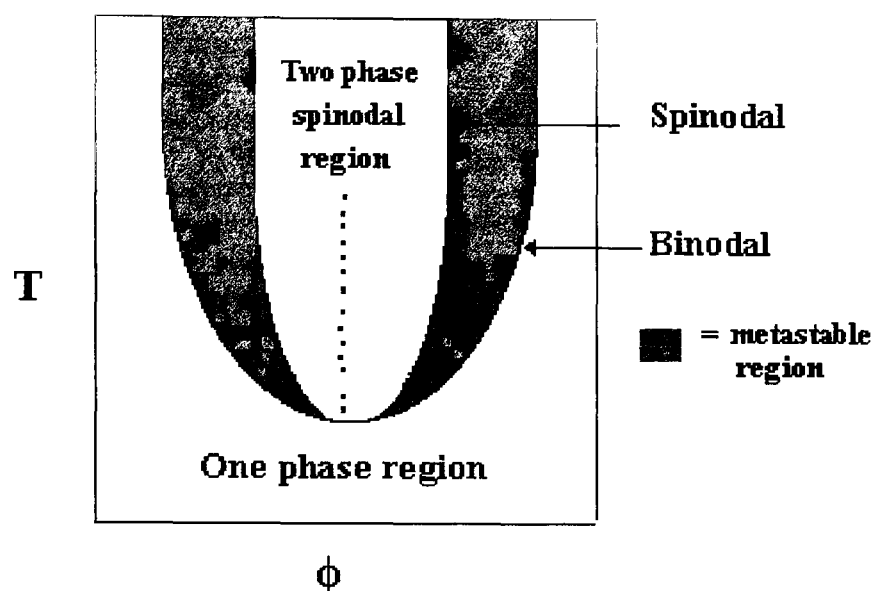
Figure 2.3 Temperature as a function of blend composition ϕ : an LCST phase diagram showing the spinodal and binodal phase boundaries and the metastable, one phase and two phase regions.

The binodal boundary can be defined as a locus of co-existing phase compositions. Consider a blend of A and B at compositions ϕ_0 and temperature T_0 (figure 2.4). This blend phase-separates into two phases, 1 and 2, moreover the compositions of the two phases lie on the binodal boundary and are joined by the constant temperature tie line. These two phases coexist in equilibrium, hence the chemical potentials, μ, of the two phases are the same:

$$\Delta(\mu_A)_1 = \Delta(\mu_A)_2 \quad \text{and} \quad \Delta(\mu_B)_1 = \Delta(\mu_B)_2 .$$ 2.17

On the plot of ΔG_{mix} as a function of blend composition for a given fixed temperature, the binodal compositions ϕ_1 and ϕ_2 have a common tangent to the ΔG_{mix} curve (figure 2.1).

Figure 2.1 can also be used to explain the spinodal phase boundary, which is the locus of points in the composition and temperature plane when $\frac{\partial^2 \Delta G_{mix}}{\partial \phi^2}$ is negative. On the ΔG_{mix} versus ϕ plot in figure 2.1 (a), the points, which lie on the spinodal boundary, are inflection points on the curve.
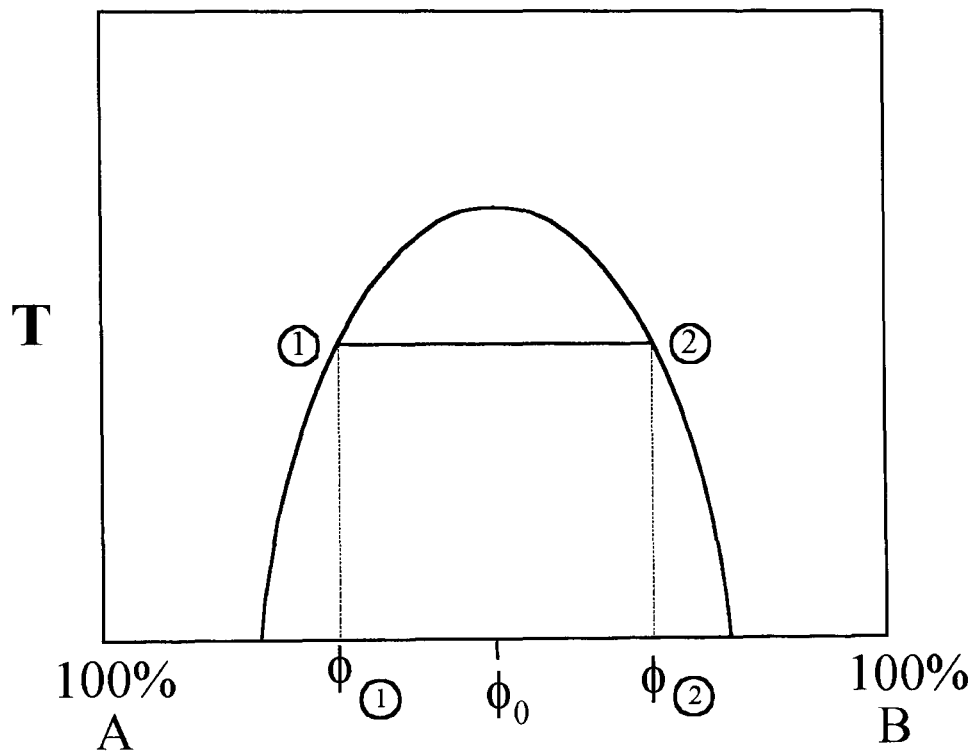
Figure 2.4   The binodal curve on a temperature versus composition; phase 1 and 2 coexist in equilibrium.

2.2.2   Phase Separation Mechanism

A principal distinction between the spinodal and the binodal boundaries is the method of phase separation. In the metastable region between the binodal and spinodal boundaries, phase separation takes place by a nucleation and growth mechanism, while inside the spinodal phase boundary, the mechanism is one of

spinodal decomposition. The morphology of the phase-separated blend is dependent, to some extent, on the mechanism of separation; the phases in a nucleating blend tend to discrete "blobs" from the start, while the phases in a blend undergoing spinodal decomposition have a much higher degree of interconnectivity, although in the later stages, the structure does coarsen. In the early stages of spinodal decomposition, orientation of the phases is random and the spacing of the pattern is constant. One the other hand, the spacing between the domains which phase-separate by nucleation and growth mechanism is quite irregular.

Nucleation and Growth: In a metastable region, most small concentration fluctuations are quickly damped out. In order to form a nucleation site, the surface energy barrier must first be overcome, small nuclei below a critical size are unstable. However, once a stable nucleus has been formed, the growth of the site is thermodynamically favoured and phase-separation proceeds without hindrance. The nucleating phase grows by accretion of material from the homogenous, two-component, parent mixture; the composition of the nucleating phase is determined by the thermodynamics of the system and is independent of the kinetics of phase separation. The rate of growth of the nucleating phase is controlled by the diffusion rate of the nucleating component through the parent.

Spinodal Decomposition: In the spinodal region, the system is unstable to small concentration fluctuations and so the phase separation proceeds continuously and spontaneously. The initially homogenous mixture separates into two phases by "uphill" diffusion against the concentration gradient, to produce two distinct phases, each richer in one component. In the early stages, the size scale of the phase separation is constant while the concentrations of the two phases change.

In the intermediate stages both the phase size and the phase concentrations vary with time. And finally in the late stage, the phase composition remains constant while the phase size are enlarged by coalescence of smaller phases.

Spinodal decomposition is one of the few solid state transformations for which there is a well developed quantitative kinetic theory. The theory was originally proposed for small molecules, particularly metals, by Chan (who is credited with the first use of the term spinodal decomposition) [32] and Hilliard [33]. The Cahn-Hilliard theory is able to explain the "uphill" diffusion which takes place in spinodal decomposition by the inclusion of higher order terms in the diffusion equation which take into account the thermodynamic contributions to the energy gradient terms [34]. The theory was later modified by deGenns [35], Pincus [36], and Binder [37] for specific application to spinodal decomposition in macromolecules.

Experimental studies of phase separation in polymers includes work on the polystyrene – poly(vinyl methyl ether) blend system [34,38] and more recent work on the kinetics of spinodal decomposition in hydrogenous and deuterated 1,4 polybutadiene blends by Bates and Wiltzius [39]; a general chapter on polymer phase separation has been provided by Hashimoto [40].

2.3   DIFFUSION IN POLYMERS

2.3.1   What is Diffusion?

Diffusion is the relative motion between molecules, caused by a number of different forces like chemical potential, pressure or a concentration gradient [41.42]. A single flexible polymer molecule in solution or the melt experiences several

types of motion, each on a different molecular level. There are vibrational and rotational modes of single atoms and the articulated motion of short chain segments within the polymer molecule.

On a large scale one can distinguish between "rotational motion", in which the centre of mass of the molecule is fixed but the principal axes of gyration are allowed to move, and "translational motion" in which motion of the centre of mass is considered. Here we will be mainly concerned with this latter type of motion, although all of the above are intimately related to one another [43,44].

In polymer systems molecules are not isolated and the diffusion of each molecule is hindered by the presence of the surrounding chains. This allows one to distinguish between two basic types of diffusion: The diffusion of a chain within a matrix of chemically identical molecules, the only difference being their molecular weights, is known as "self – diffusion" or "intradiffusion". If the molecules forming the matrix and the test chain have different chemical structure, the diffusion process is termed "interdiffusion".

Interfacial mixing begins when two polymer surfaces are brought into contact with each other [45] and the extent and rate of interdiffusion depend on the interaction between the two polymers [46]. General theories regarding polymer interdiffusion and the techniques used to study polymer – polymer interfacial mixing and the measurement of diffusion coefficients are described in two recent reviews[47,48]. The present work falls within the area of the interfacial composition profile and the diffusion of the interface during interfacial mixing of a polymer pair with a large mismatch in their respective molecular mobilities and for which intermolecular interactions occur.

Diffusion of low molecular weight species is usually Fickian with a constant diffusion coefficient [49]. For polymer solutions or melt where both components are relatively mobile, interdiffusion is Fickian but with a concentration-dependent diffusion coefficient. As a result, the interface moves linearly with respect to the square root of time in the direction of the species with the higher mobility [50-52]. However, certain general patterns of diffusion behaviour are recognised.

2.3.2 Diffusion Coefficient

One of the most important aspects of diffusion is the rate at which the process takes place, which can be determined by measuring the diffusion coefficient for the system. There are two approaches for the definition of the diffusion coefficient:

The first one consists of following the centre of mass motion of a single macromolecule in the melt. The diffusion coefficient D is defined as [53]

$$D = \lim_{t \to \infty} \frac{r^2(t)}{6t} \qquad\qquad 2.18$$

where $r(t)$ is the position of the centre of mass at a time t.

Another approach consists of setting up a fluctuation in the melt and observing its relaxation with time. The type of fluctuations that we will be concerned with are fluctuations in concentration. For such a situation, the diffusion coefficient is defined by Fick's law as the proportionality parameter between J, the rate of transfer of the diffusing substance through unit area of a section, and the concentration gradient measured normal to the section:

$$J = -D \frac{\partial C}{\partial z} \qquad\qquad\qquad 2.19$$

where C is the concentration of the diffusing substance and z is the space-coordinate measured normal to the section.

Diffusion frequently takes place effectively in one direction only. For example, let us suppose that there is a gradient of concentration only along the z-axis. For such a case and considering the mass-balance of an element of volume, the fundamental differential equation takes the form

$$\frac{\partial C}{\partial t} = D \left(\frac{\partial^2 C}{\partial z^2} \right) \qquad\qquad\qquad 2.20$$

provided D is a constant.

In many polymer systems, however, D varies markedly with concentration. Also, in some cases the medium is not homogenous and D varies from point to point. In these situations equation 2.20 becomes

$$\frac{\partial C}{\partial t} = \frac{\partial}{\partial z} \left(D \frac{\partial C}{\partial z} \right) \qquad\qquad\qquad 2.21$$

This second approach to the definition of the diffusion coefficient is very widely used experimentally. Diffusion coefficients are very often obtained by analysing concentration-distance curves. This case will be illustrated with an example. Let us calculate the solution to the diffusion equation for the simple case of two effectively infinite media brought together at $t = 0$ and allowed to mix. The diffusion coefficient and its concentration dependence can be deduced from the

concentration profile obtained at some subsequent times. For the case of a constant diffusion coefficient D and assuming that there is no overall change of volume on mixing, the solution to the diffusion equation is given by

$$C = \tfrac{1}{2} C_0 \, erfc \frac{z}{2\sqrt{Dt}}$$ 2.22

where $erfc$ is the error function complement and C_0 is the concentration at $t = 0$. For this case the numerical value of the diffusion coefficient can be calculated by comparing the theoretical solution (equation 2.22) with an experimentally determined concentration profile at a given time. An example of such a profile is shown in figure 2.5
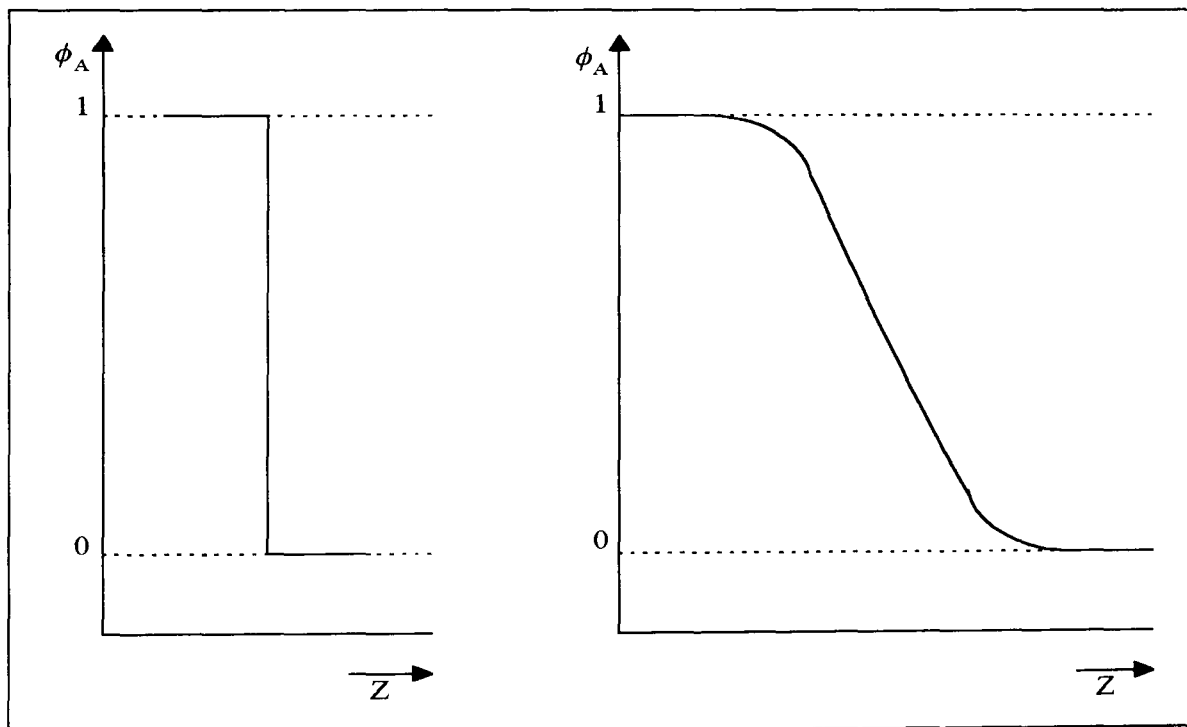
Figure 2.5   Time evolution of a Fickian concentration profile between two blocks of pure polymers A and B brought into contact at $t = 0$ and allowed to mix. The z-axis has been expanded in the second figure.

The case of a concentration – dependent diffusion coefficient is a bit more complicated but the solution for this case are also well advanced [54].

In the treatment described above, the diffusion process has been characterised in terms of a single diffusion coefficient D. How can this be possible if there are two species present in the system? One would think that there should be a diffusion coefficient for each component in the mixture. The single diffusion coefficient arises from the idea that in diffusion the motion of the different molecules are essentially linked. It is therefore not meaningful to talk of a separate diffusion coefficient for each species, but only of one coefficient for the particular two – component system under consideration. Since there are only two species in the system, once the concentration profile for one of the components is known, the profile for the second species can be deduced automatically.

2.4   THERMODYNAMIC THEORIES OF BINARY MIXTURES

Thermodynamic theories as applied to mixtures of small molecules had been well established by the turn of the century. These theories were later modified in order to make them applicable to polymer solutions and mixtures.

2.4.1   Flory-Huggins "lattice" theory of polymer solutions

Flory [55,56] and Huggins [57,58], working independently, successfully used a rigid "lattice" model to derive the expression for the ideal entropy of mixing ΔS_m for chemically similar, low molecular weight components. They used this model to obtain the following expression for the entropy of mixing of polymer solutions:

$$\Delta S_m = -k[n_1 \ln \phi_1 + n_2 \ln \phi_2] \qquad\qquad 2.23$$

where k is the Boltzmann constant.

Here $\phi_1 = \dfrac{n_1}{n_1 + rn_2}$; $\phi_2 = \dfrac{rn_2}{n_1 + rn_2}$,

n_1 is the number of molecules of solvent, n_2 is the number of molecules of polymer, ϕ_1 and ϕ_2 are the volume fractions of the solvent and polymer, respectively, and r is the degree of polymerisation.

Equation 2.23 assumes that the system is completely random. This is a good approximation for weakly interacting molecules because strong interactions induce short range order and therefore lower the entropy of the mixture.

For polymer solutions ΔS_m is small compared to that involving small molecules because there are fewer ways in which the same number of lattice sites can be occupied by polymer segments. The forces between a polymer and a simple molecule are similar to those between pairs of simple molecules. The heat of interaction between a polymer molecule and its surroundings should vary linearly with the composition. Flory therefore wrote an expression for the heat of mixing of a polymer solution, similar to that used by Scatchard [59], for simple molecules:

$$\Delta H_m = kT\chi_{12}n_1\phi_2 \qquad\qquad 2.24$$

χ_{12} is the Flory-Huggins interaction parameter; it is independent of the concentration and molecular weight of the components. The free energy of mixing ΔG_m is obtained by a combination of equations 2.23 and 2.24.

$$\Delta G_m = kT\left(n_1 \ln\phi_1 + n_2 \ln\phi_2 + n_1\phi_2\chi_{12}\right) \qquad\qquad 2.25$$

Extension of Flory-Huggins theory to polymer-polymer mixtures

The Flory-Huggins equation for the free energy of mixing of a polymer-solvent system was later extended to polymer-polymer systems. By analogy with equation 2.23 the entropy change of mixing two polymers is given by:

$$\Delta S_m = -k\left[n_1 \ln \phi_1 + n_2 \ln \phi_2\right]$$

  2.26

As the molecular weights of the two polymers tend to infinity, n_1 and n_2 tend to zero and ΔS_m tends to zero. For high molecular weight polymers the following holds [57]

$$\Delta S_m \cong 0$$

  2.27

Substituting equation 2.27 into equation 2.1.

$$\Delta G_m \cong \Delta H_m$$

  2.28

By analogy in a equation (2.24), the enthalpy of mixing of two polymers is

$$\Delta H_m = kT\chi_{12}n_1 r_1 \phi_2$$

  2.29

The free energy of mixing, ΔG_m, of high molecular weight polymers is therefore determined by the enthalpy of mixing, ΔH_m, since ΔS_m is negligible. A negative ΔH_m (which implies an exothermic heat of mixing) is therefore necessary for two high molecular weight polymers to mix spontaneously.

The Flory-Huggins theory was only able to predict miscibility for low molecular weight mixtures (oligomers) which generally show upper critical solution temperature (UCST). This is because these systems mix endothermally (ΔH_m is positive) and ΔS_m is large and positive. An increase in temperature therefore makes ΔG_m more negative and miscibility is improved. Phase-separation occurs on reduction of temperature when the term $T\Delta S_m$ is offset by the positive value of ΔH_m, equation (2.1).

Although the "lattice" theory has some merits it also has several disadvantages. It assumes that the interaction parameter is only temperature dependent and fails to account for concentration, pressure and molecular weight dependence. A modified interaction parameter χ suggested by Tompa [60] have been extensively used to describe binary mixtures.

$$\chi = \chi_1 + \chi_2 \phi_2 + \chi_3 \phi_2^2 + \ldots\ldots\ldots\ldots \qquad 2.30$$

where χ_1, χ_2, χ_3 are the interaction parameters and ϕ_2 is volume fraction.

A similar empirical function, g, has also been introduced by Koningsveld and Kleintjens [61] to replace the interaction parameter χ_{12}:

$$g = g_{k,1} + g_{k,2} / T + g_{k,3} T + g_{k,4} \ln T \qquad 2.31$$

The parameters $g_{k,i}$ depend on measurable physical quantities such as the heat of mixing and molecular weight. This g function is related to χ_{12} as follows:

$$\chi_{12} = g(1 - \phi_2)\frac{\partial g}{\partial \phi_2}$$ 2.32

It has been used by Koningsveld et al [66] when only the second and third terms of equation (2.31) are used to describe the phase boundaries of mixtures. However, no satisfactory molecular interpretations of g exist [62,63,64].

The Flory-Huggins theory neither predicts lower critical solution temperature (LCST) nor does it explain all the observed LCST behaviour which is a common feature in high molecular weight polymer mixtures. It does not predict miscible high molecular weight polymer pairs, of which there are now known to be many. A compilation of these miscible polymer blends has been made by Paul and Newman [65] and by Olabisi et al [8].

2.4.2 Flory's Equation -of -State

In deriving this equation, Flory combined some features from the corresponding states theory and the cell models of Prigogine [66], while he attempted to correct some of their shortcomings. He therefore treated the intermolecular energy in a more empirical way, following the ideas originally suggested by Hildebrand and Scott [67]. Based on the ideas developed by Tonks [68], Eyring et al [69], Hirschfelder et al [70] and Rice [71] for pure liquids, Flory then obtained the free energy directly from the partition function.

The equation of state parameters, P*, V*, T*, which may be evaluated from the pure component data (density, thermal expansion coefficient and thermal pressure coefficient) were used to characterise each pure component while the properties

of the mixture were calculated by using an interaction term χ_{12} (Flory et al[71,72]).

The main difference with the lattice theory is that it considers a volume change in the mixing process. It can predict LCST behaviour. However, it still requires an empirical entropy correction parameter, Q_{12}, to fit detailed behaviour; it has been successfully used to predict the effect of the various contributions to the phase boundaries of hypothetical mixtures [4]. It has also been successfully used to simulate the phase boundaries of miscible, high molecular weight polymer blends[73,74,75].

2.5   ONWARDS

The next chapter gives a theory of thermal analysis, spectroscopy and reflectivity techniques, which were used in this research project. And it relates how the techniques have been used to observe and to quantify the homopolymer and blend behaviour, which has been presented in this thesis.

References

1. Bank, M.; Leffingwell, J.; Thies, C. *Macromolecules* **1971**, 4, 44.

2. Bank, M.; Leffingwell, J.; Thies, C. *Macromolecules* **1971**, 4, 1.

3. Bank, M.; Leffingwell, J.; Thies, C. *J. Polym. Sci.* (A-2) **1972**, 10 1097.

4. McMaster, L. P. *Macromolecules* **1973**, 6, 760.

5. Utracki, L. A. *Polymer Alloys and Blends*, Oxford University Press: New York, **1989**.

6. Guo, W.; and Higgins, J. S. *Polymer* **1990**, 31, 699.

7. Voight-Martin, I. G.; Leister, K. H. *J. Polym. Sci., Part B: Polym. Phys. Ed.* **1986**, 24, 723.

8. Olabisi, O.; Robeson, L. M.; Shaw, M. T. *Polymer-Polymer Miscibility*, Academic Press: New York, **1979**.

9. Richards, E. G. *An Introduction to Physical Properties of Large Molecules in Solution*, Cambridge University Press: Cambridge, **1980**.

10. Wellinghoff, S. T.; Keonig, J. L.; Baer, E. *J. Polym. Sci., Polym. Phys. Ed.* **1977**, 15, 1913.

11. McClellan, A. L. *Tables of Experimental Dipole Moments*, Freeman, San Francisco, **1963**.

12. Garton, A.; Aubin, M.; Prud'homme, R. E. *J. Polym. Sci., Polym. Phys. Ed.* **1983**, 21, 45.

13. Hara, M.; Eisenberg, A. *Macromolecules* **1987**, 20, 2160.

14. Hara, M.; Eisenberg, A. *Macromolecules* **1984**, 17, 1335.

15. Tsuchida, E.; Abe, K. *Interactions Between Macromolecules in Solution and Intermacromolecular Complexes*, Advances in Polymer Science, 45, Springer-Verlag, Berlin, **1982**.

16. Pimental, G. C.; McClellan, A. L. *The Hydrogen Bond,* Freeman, San Francisco, **1960**.

17. Garton, A. in *Current Topics in Polymer Science, Vol. I'*, Ottenbrite, R. N.; Utracki, L andInoue, S. Eds., 203, Hanser, Munich, **1987**.

18. Breck, W. G.; Brown, R. J. C.; McCowan, J. D. *Chemistry for Science and Engineering*, McGraw-Hill Ryerson, Toronto, **1981**.

19. Natansohn, A.; Eisenberg, A. *Macromolecules* **1987**, 20, 323.

20. Moore, W. J. *Physical Chemistry*, Longman, London, **1972**.

21. Fowkes, F. M.; Tischler, D. O.; Wolfe, J. A.; Lannigan, L. A.; Ademu-John, C. M.; Halliwell, M. J. *J. Polym. Sci., Polym. Chem. Ed.* **1984**, 22, 547.

22. Murali, R.; Eisenberg, A. in *Structure and Properties of Ionomers NATO ASI Series*, Pineri, M.; and Eisenberg, A. Eds., p307. D. Reidel Publishing Company: Dordrecht, **1987**.

23. Smith, P.; Eisenberg, A. *J. Polym. Sci., Polym. Lett. Ed.* **1983**, 21, 223.

24. Rutkowska, M.; Eisenberg, A. *Macromolecules* **1984**, 17, 821.

25. Natasohn, A.; Rutkowska, M.; Eisenberg, A. *Polymer* **1987**, 28, 885.

26. Pugh, C.; Percec, V. *Macromolecules* **1986**, 19,65.

27. Rodriguez-Parada, J. M.; Percec, V. *Macromolecules* **1986**, 19, 55.

28. Weiss, R. A.; Beretta, C.; Sasongko, S.; Garton, A. *J. Appl. Polym. Sci.***1990**,

29. Peiffer, D. G.; Agarwal, P. K.; Lundberg, R. D. *J. Polym. Sci., Polym. Lett. Ed.* **1986**, 24,581.

30. Belfiore, L. A. *Polymer Preprints* **1988**, 29, 17.

31. Sen, A.; Weiss, R. A.; Garton, A in *Multiphase Polymers, Blends and Ionomers: ACS Symposium Series*, Utracki, R. A.; Eds. p353, American Chemical Society, Washington, **1989**.

32. Cahn, J. W., Transactions of the Metallurgical Society of AIME **1968**, 242, 166.

33. Hillard, J. E. *Phase Transformation*, Chap:12, American Society for metal, Chapman & Hall Ltd, **1970**.

34. Nishi, T.; Wang, T. T.; Kwei, T. K. *Macromolecules* **1975**, 8, 227.

35. DeGennes., P. G. *Macromolecules* **1976**, 9, 587.

36. Pincus, P. *J. Chem. Phys.* **1981**, 75, 1996.

37. Binder, K. *J. Chem. Phys.* **1983**, 79, 6387.

38. Voight-Martin, I. G.; Leister, K. H.; Rosenau, R.; Koningsveld, R. *J. Polym. Sci., Part B: Polym. Phys. Ed.* **1986**, 24, 723.

39. Bates, F. S.; Wiltzuis, P. *J. Chem. Phys.* **1989**, 91, 3258.

40. Hashimoto, T. *in Current Topics in Polymer Science, Vol. II*, Ottenbrite, R. N.; Utracki, L.; Inoue, S.; Eds. P119, Hanser, New York, **1987**.

41. Fujita, H.; Kishimoto, A.; Matsumoto, K. *Trans. Faraday Soc.* **1960**, 56, 424-437.

42. Frisch, H. L. *J. Polym. Sci., Part: B Polym. Phys.* **1965**, 3, 13.

43. Doi, M.;Edwards, S. F. *The Theory of Polymer Dynamics* , Clarendon Press: Oxford, **1982**.

44. Ferry, J. D. *Viscoelastic Properties of Blends*, 3rd ed.,Wiley, New York, **1980**

45. Voyutskii, S. S. *J. Adhes* **1971**, 3, 69.

46. de Gennes, P. G., *C. R. Acad. Sci. Paris, Ser. II*, **1981**, 292, 1505.

47. Kausch, H. H.; Tirrell, M., *Annu. Rev. Mater. Sci.* **1989**, 19, 341.

48. Jabbari, E.; Peppas, N. A. *J. M. S.-Rev. Macromol. Chem. Phys.* **1994**, C34 (2), 205.

49. Crank, J., *The Mathematics of Diffusion*; Claredon: Oxford, **1956**.

50. Brochard, B.; deGennes, P. G. *Europhys. Letter* **1986**, 1(5), 211.

51. Kramer, E. J.; Green, P. F.; Palmstrom, C. J. *Polymer* **1984**, 25, 473.

52. Fernandez, M. L.; Higgins, J. S.; Penfold, J.; Shackleton, C. *J. Chem. Sco., Faraday Trans.* **1991**, 87 (13), 2055.

53. Chandrasekar, S. *Rev. Mod. Phys.* **1943**, 15, 1.

54. Crank, J.; Park, G. S. *The Mathematics of Diffusion* 2nd ed. Oxford Univ. Press: **1975**.

55. Flory, P. J. *J. Chem. Phys.* **1941**, 9, 660.

56. Flory, P. J. *J. Chem. Phys.* **1942**, 10, 51.

57. Huggins, M. L. *J. Chem. Phys.* **1941**, 9, 665.

58. Huggins, M. L. *Ann. N.Y. Acad. Sci.* **1942**, 43, 01.

59. Scatchard, G. *Chem. Rev.* **1931**, 8, 321.

60. Tompa, H. *Polymer Solutions*, Butterworthw Scientific Publications: London, **1956**, 118, 170.

61. Konningsveld, R.; Kleintjens, L. A. *Macromolecules* **1971**, 4, 637.

62. Konningsveld, R.; Kleintjens, L. A. *British Polymer Journal* **1974**, 9, 212.

63. Konningsveld, R.; Kleintjens, L.A.; Onclin, M. H. *J. Macrom. sci. Phys.* **1980**, B18(3), 363.

64. Konningsveld, R.; Kleintjens, L.A.; Schaffelers, H. M. *Pure Appl. Chem.* **1977**, 39, 01.

65. Paul, D. R.; Newman, S., Eds. *Polymer Blends*; Academic Press: New York, **1978**; Vols. I and II.

66. Prigogine, I.; Bellmans, A.; Near-Collin, C. *J. Chem. Phys.* **1957**, 26, 751.

67. Hildebrand, J. H.; Scott, R. L., *The solubility of Non-electrolytes*, Dove Publications: New York, **1964**.

68. Tonks, L. *Phys. Rev.* **1936**, 50, 955.

69. Eyring, H.; Hirschfelder, J. *J. Phys. Chem.* **1937**, 41, 249.

70. Rice, O. K. *J. Chem. Phys.* **1944**, 12, 01.

71.   Flory, P. J.; Orwoll, R. A.; Verij, A. *J. Chem. Soc.* **1964**, 86, 3507.

72.   Flory, P. J. *J. Am. Chem. Soc.* **1965**, 87:89, 1833.

73.   Olabisi, O. *Macromolecules* **1975**, 18, 316.

74.   Rostami, S.; Walsh, D. J. *Macromolecules* **1985**, 18, 1228.

75.   Chai, Z.; Walsh, D. J. *Eur. Polymer. J.* **1983**,19, 519.

CHAPTER THREE

EXPERIMENTAL TECHNIQUES

3.1 INTRODUCTION

This chapter contains a brief description of the techniques used in this work. Three techniques, namely Differential Scanning Calorimetry (DSC), Light Microscopy and Fourier Transform Infrared (FTIR) spectroscopy have been used to investigate the miscibility and phase behaviour of the polystyrene (PS) and sulfonated polystyrene (SPS) with poly(vinyl methyl ether) (PVME) blends. The neutron reflectivity was used to investigate the interfacial mixing of two ionomer blends, Li-dSPS/PC and Zn-dSPS/PC. In addition, the vibrational spectra of a series of atactic polystyrenes with selectively deuterated variants, and a corresponding series of atactic sodium sulfonated polystyrenes were analysed by using FTIR spectroscopy. Details of the samples used in this thesis are presented in each related chapter.

3.2 THERMAL ANALYSIS

The term *thermal analysis* refers to the group of methods in which some physical properties of the sample and /or of its reaction products are measured as a function of temperature [1,2]. Thermal analysis comprises thermogravimetry (TG), which gives gain or loss of weight (mass change); differential scanning calorimetry (DSC) and differential thermal analysis (DTA), which give changes in specific-heat capacity (rate of enthalpy change); thermomechanical analysis

(TMA) and thermodilatometry, which give penetration or expansion (dimension change); dynamic mechanical analysis (DMA) and dielectric thermal analysis (DETA), which give loss moduli; evolved gas detection (EGD) and evolved gas analysis (EGA)[2,3,4]. From this group, DSC has been used to characterise a series of PS/PVME blends. .

3.2.1 Differential Scanning Calorimetry (DSC)

Differential scanning calorimetry [5,6] is the dominant technique for the thermal analytical investigation of polymeric materials. It measures the difference in energy inputs into the sample and a reference material as they are subjected to a controlled temperature program. Practically all physical and chemical processes involve changes in enthalpy or specific heat, and the applicability of DSC to condensed-phase systems is almost universal. Its measurement process is quantitative and the change of enthalpy is usually a linear function of the reaction co-ordinate.

DSC followed the older technique, DTA, or differential thermal analysis. In DTA, the signal recorded is the difference in temperature between a sample and a reference material heated at the same rate. In DSC, a servo system is used to measure the quantity of heat, which must be added to the sample cell to maintain it at the same temperature as the reference cell. An important advantage of DSC over DTA is that it allows the enthalpy of transitions to be obtained directly by integration of the scanning curves. The signal obtained in DSC is proportional to the difference in the heat capacity, C_p, of the sample and the reference cell. DSC requires a very small amount of specimen, 10-20 mg, and has sophisticated controlled rates of heating and cooling.

The differential scanning calorimeter used in this study at Imperial College is the Pyris model – 1; there is a separate heater and thermometer for the sample and reference cells [7]. The power to the individual heaters is varied so as to keep the temperatures measured by the two thermometers equal. The instrument records the differential power between the sample and the reference cell as a function of time.

When a T_g is measured by DSC, the transition is marked by a change in the heat capacity of the material; in the signal versus temperature scan, this appears as a sudden endothermic shift in the baseline as shown in figure 3.1. The introduction of rotational freedom as the polymer undergoes the change from a glassy to a rubbery material results in an increase in heat capacity. There may be an endothermic overshoot associated with the glass transition event on heating [figure 3.1(b)]; this is common to many amorphous thermoplastics [8]. Annealing of the polymer allows the formation of a lower enthalpy glass which, when heated, tends to superheat. The endothermic peak represents the "catch up" period of the glass as it returns from a superheated state to equilibrium.

3.2.2 Glass Transition Temperature Determinations

Polymers go through various stages as they are heated from a very low temperature. All polymers can be cooled to form a brittle solid; for example rubber can be broken like glass when cooled in liquid nitrogen. As the temperature is raised, the polymer changes from a glassy state to a rubbery one. This change is not sharp but occurs over a small range of temperatures. The temperature of this transition is called the _glass transition temperature T_g_. All polymers exhibit this phenomenon which takes place in their amorphous region. The glass transition temperature is very important because at or in the vicinity of

this temperature various physical properties of a blend or homopolymer are altered. The second common way of determining miscibility limits is to observe the T_g of the systems. For a truly homogeneous system all molecules are in the same environment and only a single, well defined T_g which is a monotonic function of composition is observed. In the heterogeneous system two T_gs at temperatures identical to those of the pure components will be observed, providing the component polymers themselves have T_gs differing by about 20°C. The partially miscible system shows a single broad T_g in one phase region of the phase diagram; this splits into two T_gs on crossing a phase diagram into the two phase regions. As the blend becomes more segregated, the glass transition temperatures appear increasingly like those of the pure components.

There are two ways of obtaining T_g from the DSC curve. The first method is to find the onset of T_g. This method uses the intercept to represent T_g: the intercept is between the base line and the tangential line from the slope of the step line of T_g. The second method is the so-called mid-point T_g. This method uses the half way point between both intercepts between the tangential line and upper and lower base line to represent T_g. In this research both methods were used to determine the T_g. These two methods are sketched in figure 3.1)

There has been a number of equations proposed to model or predict the glass transition temperature for a one-phase blend of given composition. For amorphous miscible blend systems, the T_g - composition dependence can be well described by the Fox equation or by several other theoretical and empirical equations [9,10,11,12]. Two such equations are presented below:

(i)   The Gordon – Taylor equation[10]:

$$T_g = \frac{w_1 T_{g_1} + K w_2 T_{g_2}}{w_1 + K w_2}$$ 3.1

(ii)   The Fox equation[11]:

$$\frac{1}{T_g} = \frac{w_1}{T_{g_1}} + \frac{w_2}{T_{g_2}}$$ 3.2

where T_g is the glass transition temperature of the blend, T_{g1} and T_{g2} are the glass transition temperatures of the constituent polymers (1) and (2), with respective weight fractions of w_1 and w_2, and K is the ratio of the heat capacity change in PS to the change in PVME.

Each of these equations has its merit, the suitability of a particular equation depends on the blend, the information available and the desired accuracy. For example M. Bank et al [13] have compared the validity of these two equations for PS/PVME blends and found experimental agreement with the Gordon – Taylor equation.

The DSC instrument used for our measurements is a PYRIS model – 1, located in the analytical laboratory of the Chemical Engineering Department of Imperial College London. Samples of 10-15 mg weight were scanned at 20°C min^{-1} to avoid an over– heating effect. The blends were examined for phase separation upon heating. Lower critical solution temperature (LCST) behaviour was observed by use of a DSC technique as described previously by Weiss [14] and Zheng, et al[15,16] on other systems.
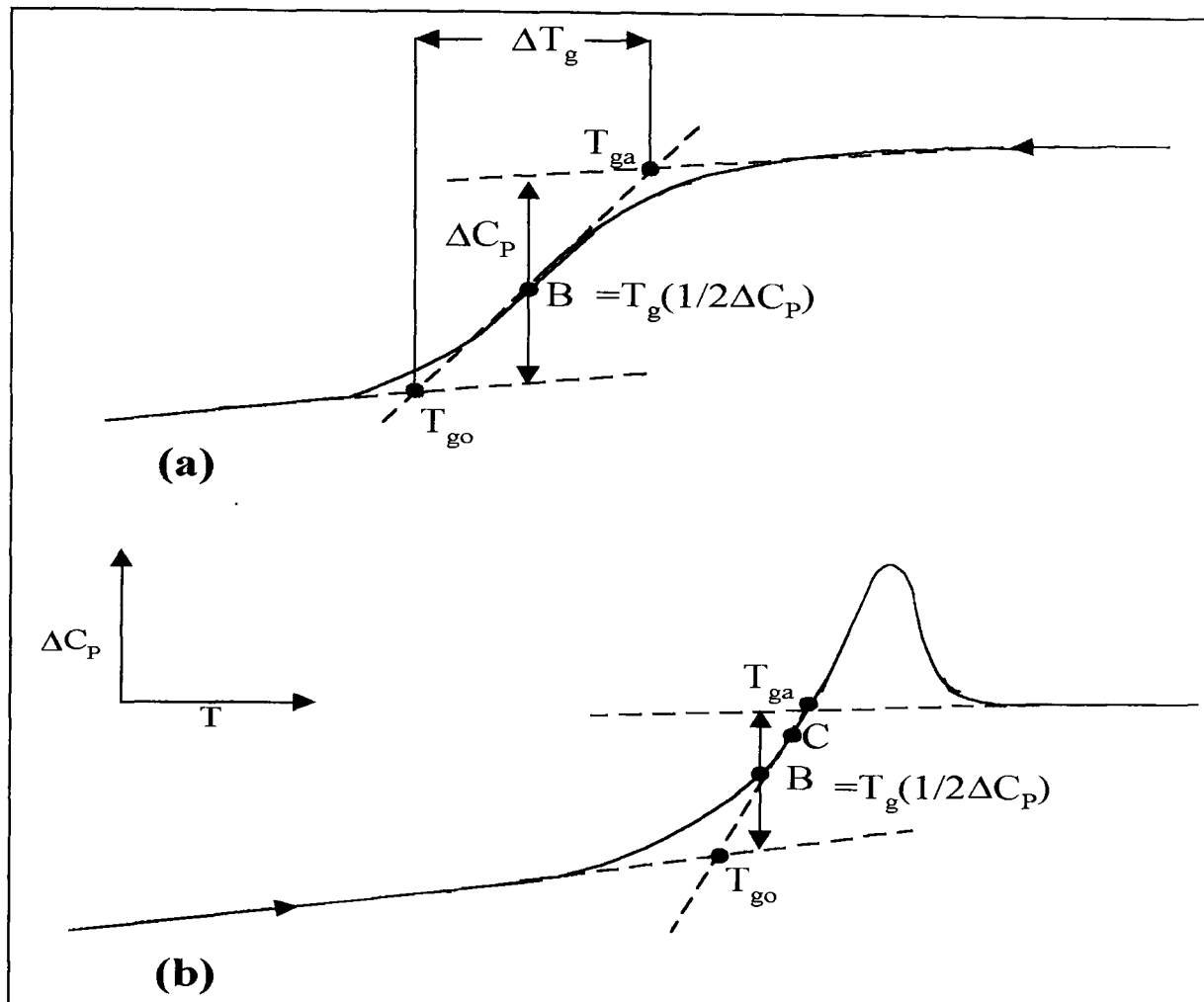
Figure 3.1   The glass transition region (a) for cooling and (b) subsequent reheating, showing some commonly used definitions of T_g : T_{go} is the extrapolated *onset* and T_{ga} the extrapolated end, the width ΔT_g is defined by $\Delta T_g = T_{ga} - T_{go}$, B is the *midpoint* where half the specific heat increment has occurred, C is the point of inflection[17].

3.3   INFRARED SPECTROSCOPY

3.3.1   Introduction

The term *spectroscopy* refers to the study of the interaction of light with matter[18-25]. When a beam of light is focused on a sample, it can be reflected or if the sample is transparent to the frequency or frequencies of the incident light, simply transmitted with no change in energy. The light is only absorbed if its energy and hence frequency correspond to the energy difference between two quantum levels in the sample. This is described by the Bohr frequency condition:

$$\Delta E = E_2 - E_1 = h\upsilon \qquad\qquad 3.3$$

where h is Planck's constant and υ is the frequency of the light in cycles per second (Hertz, Hz).

The *infrared spectroscopy* is the technique of spectroscopic measurement in the infrared region of the electromagnetic spectrum. It involves the vibrational energy levels of molecules but often provides only part of the complete vibrational spectrum. It is probably one of the most widely used analytical techniques in the field of identification and analysis of organic compounds. It is an extremely versatile technique, enabling the evaluation of samples in liquid, solid or gaseous state relatively simply. Its main application in the area of fingerprinting or obtaining functional group information enables unknown materials to be correlated with known standard spectra. The technique can also be used to determine the concentration of individual components in a mixture of known compounds. However, the FTIR spectroscopy provides interesting

information on the interactions at the molecular level of the components.

3.3.2   Infrared Spectrum

The infrared spectrum (IR) is said to be one of the most characteristic properties of a compound. It refers broadly to the part of the electromagnetic spectrum contained between the visible and microwaves regions, as shown in figure 3.2. When infrared light is passed through a sample of an organic compound, some of the frequencies are absorbed while other frequencies are transmitted through the sample without being absorbed. If percent absorbance or percent transmittance against frequency is plotted, the result is an infrared spectrum.

All molecules are made up of atoms linked by chemical bonds. Their motion can be regarded as being composed of two components, the stretching and bending vibrations. The frequencies of these vibrations are not only dependent on the nature of the particular bonds themselves, such as the C - H or C - O bonds, but are also affected by the entire molecule and its environment. Similarly, the vibrations of bonds, which accompany electric vibrations, will increase their amplitude if an electromagnetic wave (infrared beam) strikes them. Therefore, only the infrared beam with a frequency exactly corresponding to that required to raise the energy level of a bond will be absorbed, the amplitude of the particular vibration is increased suddenly by a certain amount and not gradually. When the frequency of the infrared beam is changed continuously and the sample is irradiated by it then certain regions of this infrared beam will be absorbed by the molecules: it is consumed to stretch or bend the respective bonds. The transmitted beam corresponding to the region of absorption will naturally be weakened, and thus a recording of the intensity of the transmitted infrared beam versus wave number or wavelength will give a curve showing

absorption bands. This is the _infrared spectrum_.
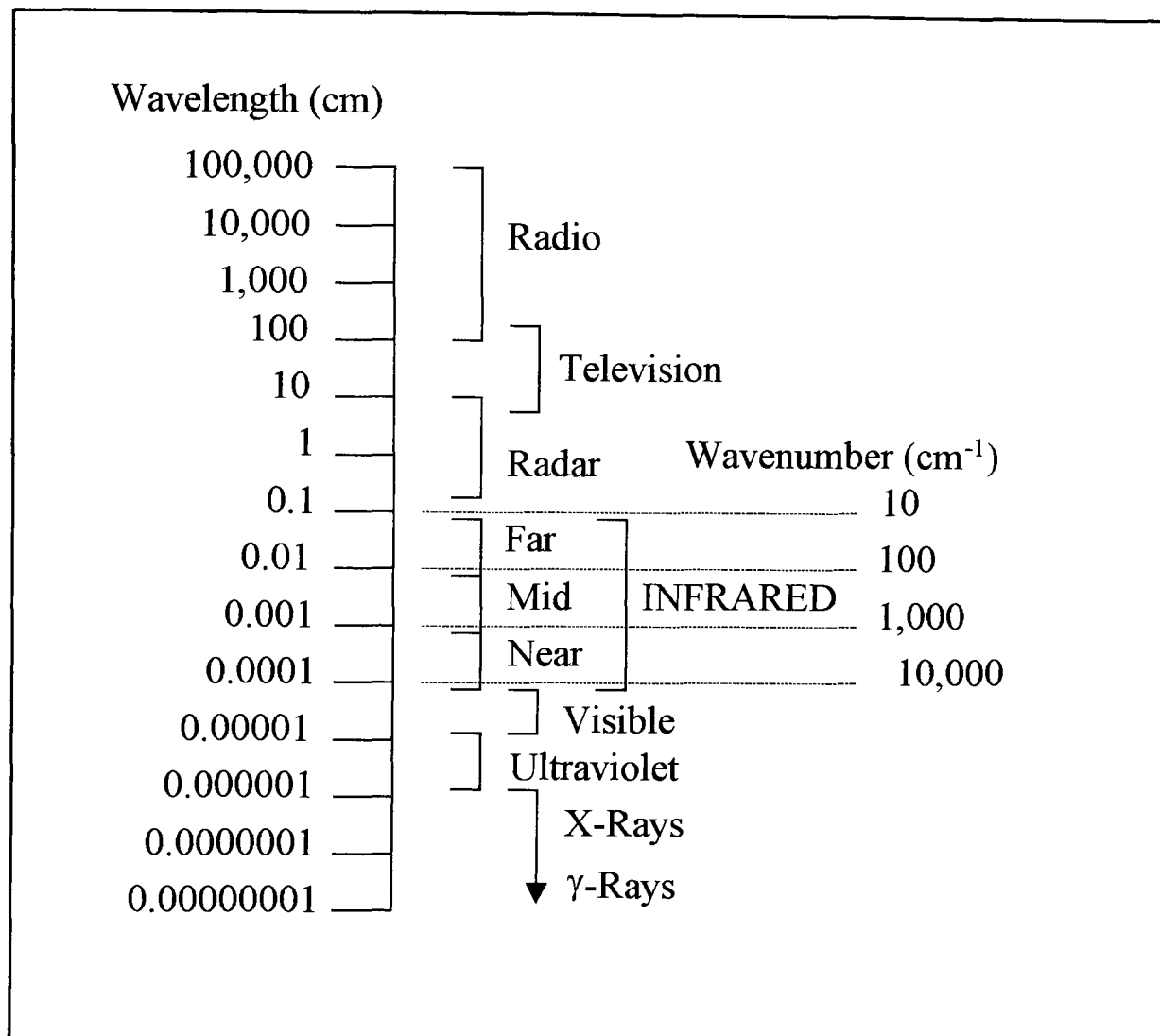
Figure 3.2   Frequency ranges for different types of spectroscopy.

3.3.3   Infrared Region

The study of infrared energy and its interaction with matter comprises a very broad field. Since much of the electromagnetic spectrum falls in the infrared region, the breadth of wavelength included in this region requires a variety of experimental techniques for its application and measurement. One micrometer (μm) is equal to 10^{-4} cm (10^{-6} m) or equal to 10,000 angstroms ($\overset{\circ}{A}$). For all

wavelengths, a frequency unit (v, the wave cycles per second) may also be used to characterise the radiation. Since the velocity of light, ($c=3 \times 10^{10}$ cm/sec) is the same for all wavelengths, the frequency varies inversely with wavelength ($v= c/\lambda$). Since both are dependent upon energy (E) according to the fundamental Planck equation, $E = hv$, $= hc/\lambda$, where h is Planck's constant (h = 6.62391×10^{-27} erg-sec). The wavenumber and frequency are related to the wavelength as shown in figure 3.3. The usual unit of the wavenumber is the reciprocal centimetre (cm^{-1}). In term of this unit, the wavenumber is the reciprocal of the wavelength (λ), when λ is expressed in centimetre.

The infrared radiation usually falls in the wavelength range of 0.1 to 0.00025 cm, or as it is more commonly expressed 10 to 4000 cm^{-1} (wavenumbers), from just outside the visible region and extending up to the microwave region as shown in figure 3.2. On the basis of experimental techniques and applications, the overall infrared region may be subdivided as shown in table 3.1. Two types of spectrophotometers are available, those linear in wavelength and those linear in wavenumbers, but the wavenumber unit is more widely used today.

Table 3.1   Common subdivisions of the Infrared region.

Infrared Region	λ (cm)	v (cm^{-1})
Near	7.8×10^{-5} to 2.5×10^{-4}	12,800 to 4000
Middle	2.5×10^{-4} to 5×10^{-3}	4000 to 200
Far	5×10^{-3} to 1×10^{-1}	200 to 10
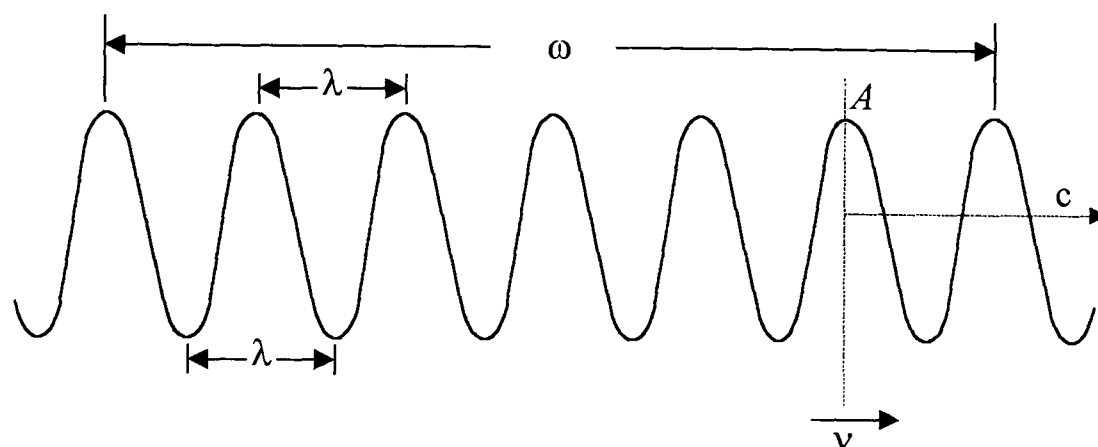
Figure 3.3   The relationship of wavenumber and frequency to wavelength where: λ = wavelength; v = number of waves passing point A per second; ω = number of waves per centimetre (wavenumber); c = velocity of light; $\lambda = c/v$; $\omega = v/c = 1/\lambda$.

3.3.4   Principles of Infrared Spectroscopy of Polymers

The fundamental principles of infrared absorption are considered for small molecules in terms of the *degree of freedom* of the molecule in question. However, all the motions that excite by whacking can be broken down into the sum (or difference) of just a few types of motion, called the *normal modes* of vibration. The number of normal modes available to a molecule depends upon the number of atoms it contains and hence its *degrees of freedom*. The motion of any atom in a molecule, be it the result of an internal vibration or rotations and transitions, can be resolved into components parallel to the x, y and z axis of a cartesian system. Subsequently, the atom is described as having three degrees of freedom: a system of N nuclei has 3N degrees of freedom. However, for a non-linear molecule six of these degrees of freedom correspond to translations and

rotations of the molecule as a whole and therefore have zero vibrational frequency, so there are 3N-6 vibrational degrees of freedom or normal modes of vibration. For strictly linear molecules, such as carbon dioxide, the rotation about the molecular axis does not change the position of the atoms and only two degrees of freedom are required to describe any motion. Consequently, linear molecules have 3N-5 normal vibrations. Theoretically, for an infinite polymer chain only the three transitions (stretching, bending, scissoring) and one rotation have zero frequency and there are 3N-4 degree of vibrational freedom. Each normal mode consists of vibrations, although not necessarily significant displacements, of all the atoms in the system. It is therefore surprising, given the number of atoms per molecule, that the absorption spectra of polymers are relatively simple [26]. The reason for this being so is that many of the normal vibrations have almost exactly the same frequency and therefore appear in the same absorption band. Also, due to the selection rules for polymers being more strict than those for small molecules, only a few of the many normal vibrations are active. For example, consider an idealized case of polystyrene where all of the repeat units have the same geometrical configuration [27] as shown blow.
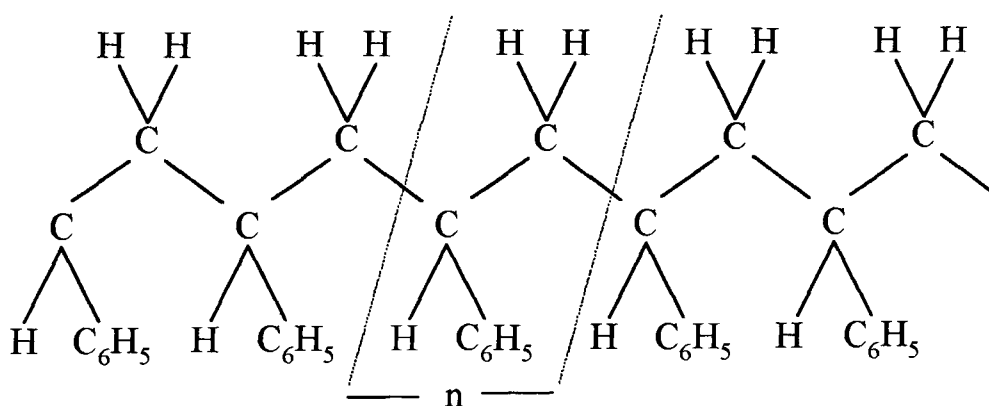
The repeat unit may be considered as consisting of 16 atoms, therefore it has 3N-4= 44 normal vibrations. As the molecule has no symmetry, all of the

vibrations are infrared and Raman active with both aromatic and aliphatic constituents. Applying this to the polymer chain, each repeat unit still has the same normal vibrations but due to the proximity of neighbouring atoms, these are affected by mutual interaction.

If the coupling between two adjacent repeat units is low, then each normal vibration is doubly degenerate. Similarly if we have N coupled repeat units in the chain, each frequency will be split N-fold. The amount of splitting will be related to the degree of interaction and is usually small for characteristic group vibrations but large for skeletal vibrations. For the characteristic vibrations of the benzene ring in PS, the splitting is too small to be observed when compared with the CH_2 group vibrations in normal hydrocarbon chain which can show considerable splitting. It must be noted, however, that the splitting of individual bands can be observed for a polymer of a narrow molecular weight distribution and in the crystalline state. For common crystalline polymers, the splitting of an absorption band is different for chains of varying length and therefore the observed spectrum is an average of the individual bands showing little fine structure.

Intermolecular interaction due to weak forces such as O-H coupling can affect the infrared absorption and can induce band shifts. In the amorphous regions, the interaction between adjacent chain segments is random and a broadening of the absorption band is observed. In crystalline regions, the interchain coupling is regular and well defined. This interaction may well cause absorption bands to split, the number of bands in the infrared spectrum can be as high as the number of chains passing through the unit cell. Polyethylene exhibits splitting into two of the CH_2 bending and rocking doublets.

The application of infrared spectroscopy in the characterization of polymer blends is extensive in the literature. In particular, two authors Coleman and Painter have published several papers and two books, "Theory of vibrational spectra and its Application to polymeric Materials"[28] and "Specific interactions and the Miscibility of Polymer Blends"[29], but only those papers of direct relevance to the polymers used in this work have been cited. An introduction to various modern spectroscopic methods for polymeric systems was published by Klopffer[30], with the applicability of each of these methods being clearly presented. The fundamental aspects as well as principles of experimentation using FTIR instruments were discussed.

3.3.5 Instrumentation

In this research work two instruments have been used to acquire infrared spectra: One of them is a Nicolet 710 spectrometer located in analytical laboratory of the Materials Engineering Department. It is a room temperature DTGS detector with a resolution of 4 cm^{-1}, within the waveband range 4500 - 400 wave number (cm^{-1}).

The Second instrument used in this work is a Nicolet 60SXB spectrometer with a Mercury - Cadmium liquid nitrogen cooled detector. For the 60SXB spectrometer, a high temperature cell is connected, that cell allows for spectroscopic studies to be made on a solid sample (28mm diameter) at temperatures between ambient and 500°C. The inner cell body is constructed from stainless steel and the middle portion of the outer body from anodised aluminium. The sample temperature was monitored by means of chromel /alumel thermocouple which passes through a vacuum tight seal into the sample cavity. Heating was controlled by a variable transformer 0.3v AC. With this cell

the spectra of PS, PVME and various composition of PS/PVME blends were obtained at high temperature to follow the dynamics of thermally induced phase separation.

3.4 NEUTRON REFLECTIVITY

3.4.1 Introduction

Neutron reflectivity is a technique of choice for probing the interface between two polymers. This technique provides the composition variation normal to the surface of the polymer film, with an accuracy on a sub-nanometer length scale [31-35].

There are several important features that make neutron reflectivity a powerful technique for investigating interfacial phenomena, despite the number of other surface characterisation techniques that are available. The wavelength of thermal neutrons is much shorter than that of light, making neutron reflection suitable for investigating layer thicknesses on the molecular scale. The neutron refractive index, n, of any material is directly related to composition and density as given by equation 3.4:

$$n = 1 - \frac{\lambda^2 \rho_z}{2\pi} \qquad \qquad 3.4$$

where λ is the neutron beam wavelength, and ρ_z is the scattering length density given by

$$\rho_z = \frac{\sum b_i D_m N_A}{M_m}$$
                                                                                3.5

where $\sum b_i$ is the sum of the monomer atomic coherent scattering lengths, D_m is the bulk polymer density, N_A is the Avogadro constant and M_m is the monomer molar mass.

In contrast to X-rays, neutron scattering lengths vary randomly from element to element and, most importantly, different isotopes can have different values. In particular the difference in the scattering lengths between hydrogen (H) and deuterium (D) isotopes is large. Hence isotopic substitution can be used to manipulate the refractive index profile, and the use of H/D isotopic substitution is especially important in application of the technique to problems in surface chemistry. Deuteration is therefore an important labelling technique to highlight whole molecules or specific section of the polymer and produce a large contrast variation with the normal hydrogenous molecules around it.

In addition, neutron reflectivity measurements do not require high vacuum containment, which allows samples to be measured under normal atmospheric conditions, as is the case of light and X-ray techniques.

3.4.2   Theoretical Background of Reflectivity Measurements

Reflectivity is defined as the ratio of reflected intensity from a flat sample surface to the incident radiation intensity. In a typical specular reflectivity measurement, the reflectivity is measured as a function of the angle of the incident radiation at a given wavelength or as a function of the wavelength of

the radiation at a given incident angle. The reflection of thermal neutrons can be explained in terms of classical laws of optics [36]. As illustrated in figure 3.4, neutrons can be reflected or refracted after impingement on a surface. The logical construction is "if the surface is flat then the angle of reflection, θ_r is equal to the angle of incidence, θ_i". This is the "specular" reflection.
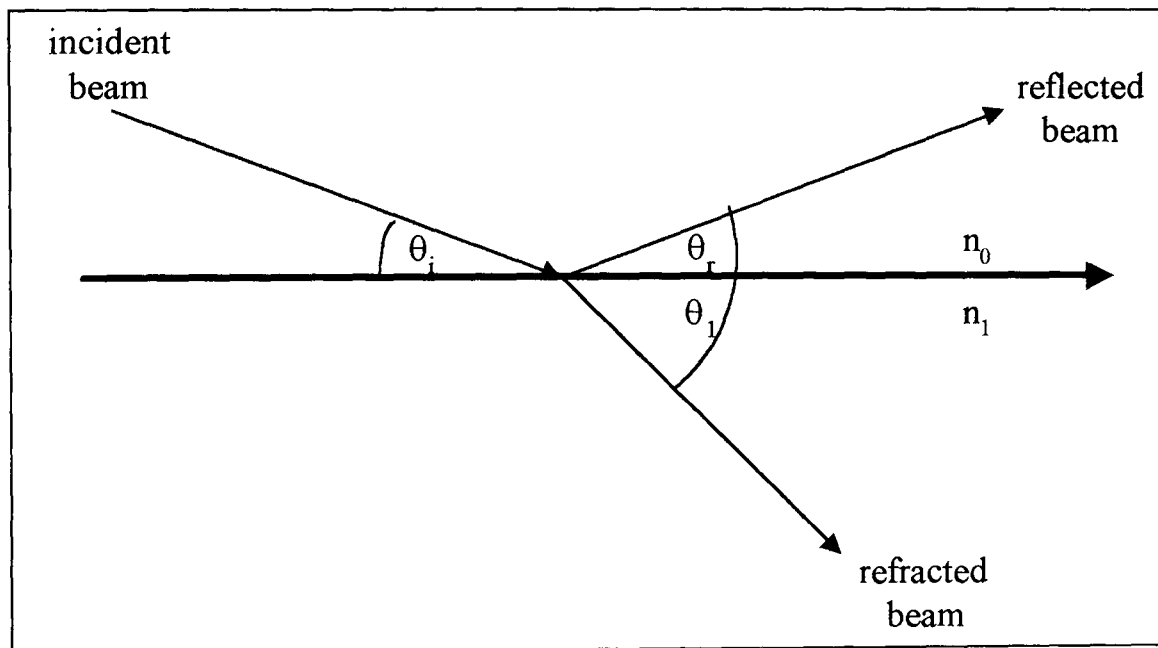
Figure 3.4   Schematic diagram of an incident neutron beam on a flat interface between two media, showing the reflected and refracted beams.

The neutron refractive index of a material is given by equation 3.6 below. For most materials (with an exception of those containing the elements lithium Li, boron B and cadmium Cd) the absorption cross section is effectively zero, i.e. $\sigma_a \approx 0$, and the imaginary part of equation 3.6 disappears to yield equation 3.7. Thus

$$n = 1 - \frac{\lambda^2 Nb}{2\pi} + i\frac{\lambda N\sigma_a}{4\pi}$$ 3.6

but when $\sigma_a \approx 0$ equation 3.6 becomes

$$n = 1 - \frac{\lambda^2 Nb}{2\pi}$$ 3.7

In the above equations N is the atomic number density per cm^3, b is the coherent scattering length, the product $Nb = \rho_z$ is the scattering length density, σ_a is the absorption cross-section and λ is the neutron wavelength. Substitution for Nb yields.

$$n = 1 - \frac{\lambda^2 \rho_z}{2\pi}$$ 3.4

The neutron scattering length b is a nuclear property describing the interaction between the neutron and the atomic nucleus [37]. The value of b varies randomly across the periodic table and also between isotopes of the same element [38]. Here neutrons present a big advantage over other radiation such as light or X-rays, with isotopic substitution providing enhanced contrast between two otherwise equivalent species.

Figure 3.4 shows a neutron beam incident on an interface between two infinitely thick media with refractive indices n_0 and n_1, where the interface is also infinitely sharp. The beam can be either reflected at an angle, θ_r, equal to that of the incident beam, or refracted at an angle θ_1 according to Snell's law: [39]

$$n_0 \cos\theta_i = n_1 \cos\theta_1$$ 3.8

For any pair of refractive indices, an incidence angle will exist below which

total reflection occurs. This is the critical angle θ_c. Clearly, for total reflection $\theta_1 = 0$ and hence one obtains

$$\cos\theta_c = \frac{n_1}{n_0} \qquad\qquad 3.9$$

If the incident beam is travelling through air or vacuum then $n_0 \approx 1$ and equation 3.4 gives

$$\cos\theta_c = 1 - \frac{\lambda^2 \rho_z}{2\pi} \qquad\qquad 3.10$$

The neutron refractive index of most condensed media is of the order 10^{-6}. Hence the critical angle is very small, so that reflection can be deduced to occur at glancing angles. Equation 3.10 can be simplified by expanding the cosine term to yield:

$$\theta_c \approx \lambda\left(\frac{\rho_z}{\pi}\right)^{1/2} \qquad\qquad 3.11$$

Usually in a neutron reflectivity experiment we are interested in not merely a single surface but a series of layers as shown later in this section. Above the critical angle, the beam will be partially reflected and partially refracted at each interface. For a single layer, or the unusual case where all the layers are of same thickness, the thickness of the layer can be determined from Bragg's law ($\lambda = 2d\sin\theta$). However, in practice such layers with infinitely sharp interfaces do not occur and Bragg's law can only be used to make an initial estimate of the

dominating thickness from the distance between through of the reflectivity profile. Instead Fresnel's law is used to build up an equation describing the interactions between the waves reflected from each surface. The relevant detailed mathematics is complex and described in various forms in the literature[31,34]. Here only some important conclusions are stated that are particularly relevant to the diffusion at interfaces. (I presume)

3.4.3 Reflectivity from an Interface of Two Bulk Media.

Figure 3.4 shows an example of a wave passing from one medium to another. The specular reflection at the sharp interface of two bulk media is described by Fresnel's law. For $\theta < \theta_c$, where θ_c is the critical reflection angle, a total reflection occurs and the reflectivity R is unity. For $\theta > \theta_c$, the reflectivity is

$$R = r_{01}^2 = \left| \frac{n_0 \sin\theta_i - n_1 \sin\theta_1}{n_0 \sin\theta_i + n_1 \sin\theta_1} \right|^2$$

3.12

where n_0, n_1 are refractive indices of the two media, θ_i is the glancing angle of incidence, θ_1 is the angle of refraction, and r_{01}^2 is the Fresnel coefficient.

3.4.4 Reflectivity From a Layer of Thin Film

Figure 3.5 shows a wave of radiation passing through a thin film with a thickness d. The expression for the reflectivity from the film, with sharp boundaries resting on a substrate, can be obtained exactly as

$$R = \left| \frac{r_{01} + r_{12} \exp(i2dq_1)}{1 + r_{01} \exp(i2dq_1)} \right|^2$$

3.13

where r_{ij} is the Fresnel coefficient at the i j interface such that

$$r_{ij} = \frac{n_i \sin \theta_i - n_j \sin \theta_j}{n_i \sin \theta_i + n_j \sin \theta_j}$$

3.14

and q_1 are the z-components of the radiation wavevector in the film given by $q_1 = (2\pi / \lambda) n_1 \sin \theta_1$. The subscripts 0, 1, 2 refer to the air, film, and the substrate, respectively.

The reflectivity spectrum given by equation 3.13 exhibits a series of fringes, commonly referred to as Kiessig Fringes. Successive minima of the Kiessig Fringes result when the argument of the exponential function in equation 3.13, $2dq_1$, is an even multiple of π. Consequently, the thickness of the film can be determined directly from the equation

$$d = \frac{\pi}{\Delta q_1} \propto \frac{\pi}{\Delta q_0}$$

3.15

where Δq_0 is the period of z-component of the wavevector between two successive minima in the reflectivity spectrum.

Equation 3.15 indicates the determination of the thickness is essentially independent of the refractive index of the medium. This results from the fact that the wavevector for X-rays or neutrons in a medium, q_1, is almost the same as that in the air, q_0, and the relative difference is of the order of 10^{-6}. It is

important to note that the thickness can be determined without the assumption of any models and is one unique parameter that can be obtained from reflectivity measurements directly.
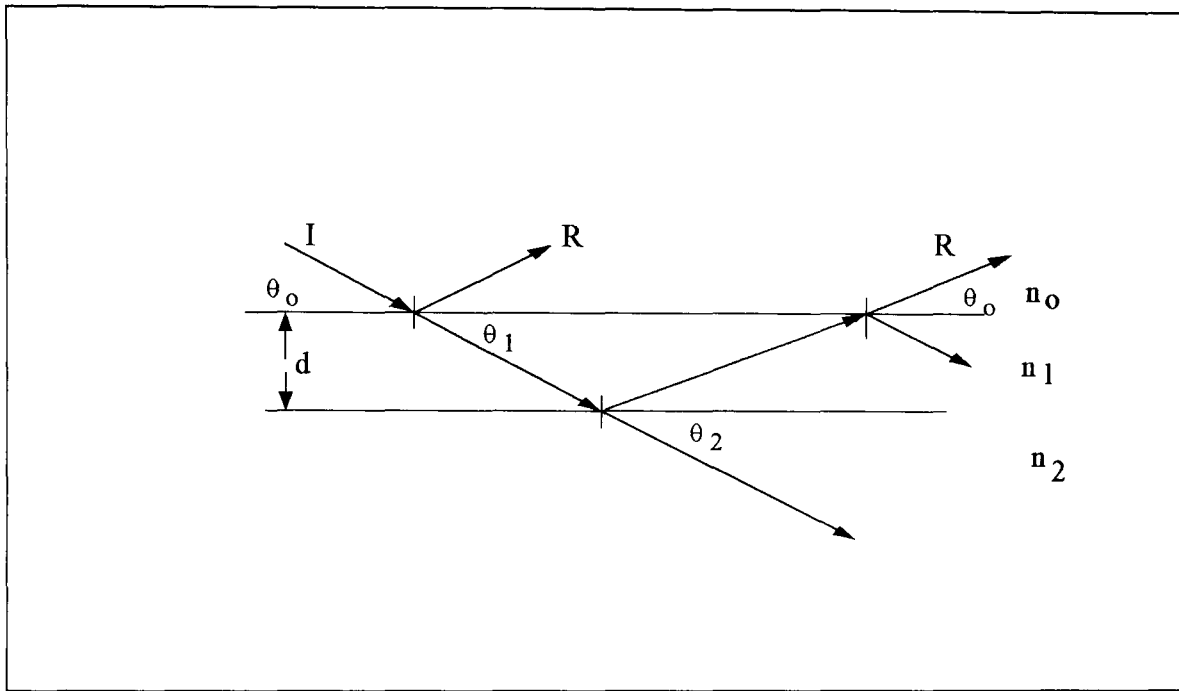
Figure 3.5. The wave passing through a thin film of refractive index n_1 between two media of refractive indices n_0 and n_2.

3.4.5   Reflectivity From a Multilayer of Thin Films

To consider the reflectivity from a medium with many discrete layers, a general solution can be adopted. Although many alternative forms exist, a convenient method is that of Abeles [40] which defines a characteristic matrix per layer in terms of Fresnel coefficients and a phase factor. The characteristic matrix M_i for the ith layer is written as:

$$M_i = \begin{bmatrix} \cos(d_i q_i) & -(i/k_i)\sin(d_i q_i) \\ -ik_i \sin(d_i q_i) & \cos(d_i q_i) \end{bmatrix}$$ 3.16

where $k_i = n_i \sin\theta_i, d_i$ is the thickness of the *ith* layer, and q_i is the z-component of the radiation wavevector in the *ith* layer. The overall matrix for calculating reflectivity is then obtained from the product of these matrices:

$$M = [M_1][M_2][M_3]....[M_n] \qquad\qquad 3.17$$

The result is a 2 × 2 matrix.:

$$M = \begin{bmatrix} M_{11} & M_{12} \\ M_{21} & M_{22} \end{bmatrix} \qquad\qquad 3.18$$

and the reflectivity is given by

$$R = \left| \frac{(M_{11}+M_{12}k_s)k_a-(M_{21}+M_{22})k_s}{(M_{11}+M_{12}k_s)k_a+(M_{21}+M_{22})k_s} \right|^2 \qquad\qquad 3.19$$

where the subscript, a, refers to the outer (air) medium and s, to the final (substrate) medium.

3.4.6 Reflectivity from Rough and/or Diffuse Interfaces

Equations given above are applicable only to ideal interfaces, e.g., infinitely sharp interfaces; some considerations must be given to interfacial imperfections. If the interfaces are rough or not sharp, but diffuse, their effects on the average refractive index profile normal to the interface n (z) are identical, and it is impossible to distinguish between the two cases. In either case, the reflectivity is modulated by an exponential decay.

For a bulk interface of a Gaussian distributed roughness or diffuseness profile, Nevot and Croce [41] showed that the reflectivity takes the form of

$$R = R_F exp(-q_0 q_1 <\sigma>^2)$$
3.20

where R, R_F are the reflectivities with and without roughness or diffusion. R_F is given by equation 3.12, and $<\sigma>$ is the root mean square roughness or diffuseness. Cowley and Ryan [42] extended this treatment to the case of thin films by applying a similar Gaussion factor to the Fresnel coefficient in equation 3.15, such that

$$r_{ij} = \frac{n_i Sin\theta_i - n_j Sin\theta_j}{n_i Sin\theta_i + n_j Sin\theta_j} \exp\left(-\frac{q_i q_j <\sigma>^2}{2}\right)$$
3.21

This approach has been further extended to the general multilayer case using Abeles method by Penfold [43] and provides a good approximation for the treatment of interfacial roughness and diffuseness. It is clear from equation 3.20 and equation 3.21 that the interfacial roughness or diffuseness diminishes the magnitude of the reflectivity, especially at high values of q.

3.4.7 Instrumentation

The essence of a neutron reflection experiment is to measure the specular reflection from a sample as a function of the wavevector transfer, Q perpendicular to the reflecting surface. Q is shown in figure 3.6, and its modulus is given by the equation

$$Q = \frac{4\pi}{\lambda} \sin \theta$$

3.22
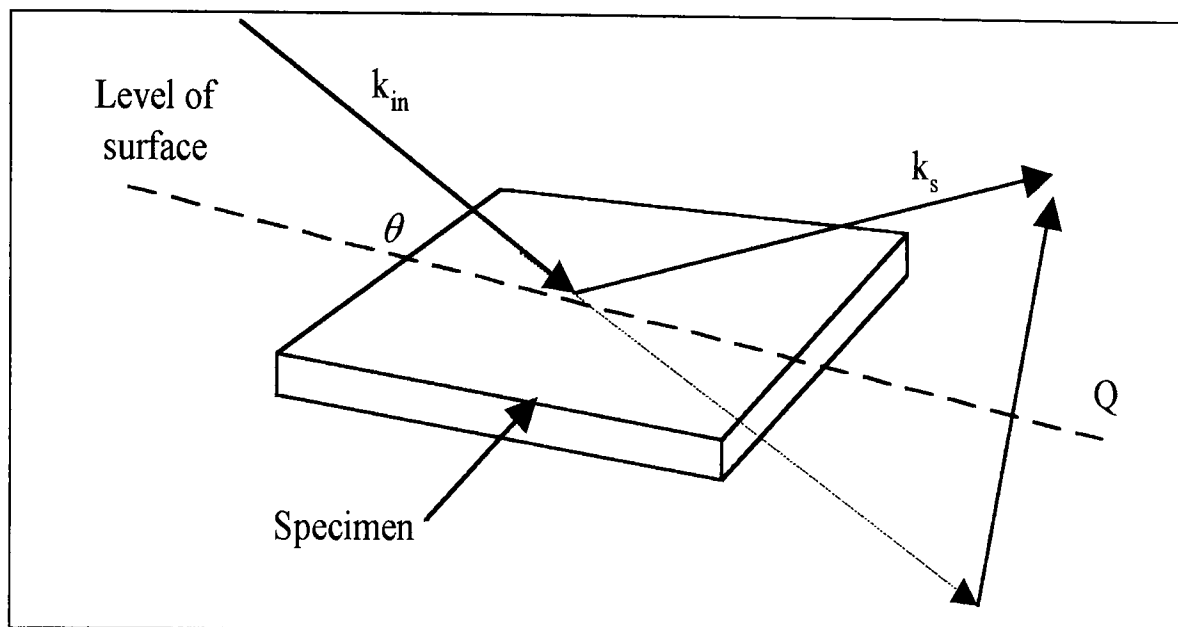
Figure 3.6   Schematic of a reflection experiment showing the incident and specularly

reflected beam and wave vector transfer, Q. [44]

As mentioned in section 3.3.1, the reflectivity is directly related to the density and composition profile normal to the surface or interface. The reflectivity profile can be measured by either keeping the wavelength of the neutrons constant and varying the incident angle or by varying the wavelength of the neutron at constant angle. CRISP like other pulsed neutron source reflectometers has a fixed wavelength range, therefore at each incident angle on the sample a limited Q range is obtained. The Q range can easily be extended by running two or more incident angles and combining the data [45]. In the present study, three angles were used. Analysis of the data was facilitated by keeping the area of illumination and the instrument collimation constant for all the angles. This was achieved by altering the collimation slit width. The overlap between the Q ranges was large, in order to avoid changing to a different angle so affecting the

reflectivity profile.

The neutron reflection experiments performed as part of this thesis were carried out at the ISIS pulsed neutron source, Rutherford Appleton Laboratory, on the CRISP reflectometer [46]. This is typical of a pulsed source time-of-flight (TOF) spectrometer, which utilise a white neutron beam with a wide range of wavelengths. Hence the data can be collected over a large Q range without moving the specimen or detector, hence removing the problems of illuminated area and vibrations. Figure 3.7 illustrates schematically the general layout of the instrument.
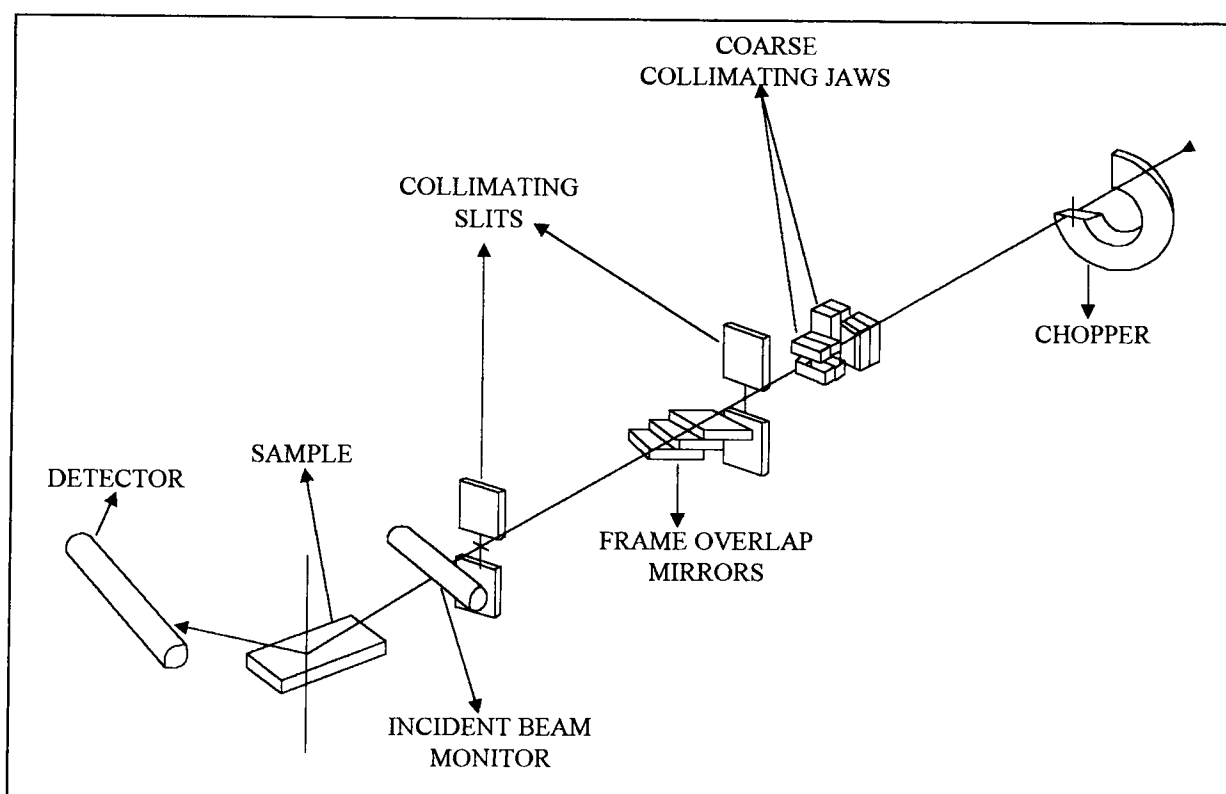
Figure 3.7   Schematic layout of the time-of-flight neutron reflectrometer CRISP at the ISIS Facility, Rutherford Appleton Laboratory [35].

The moderated neutrons pass through a double set of choppers, firstly, a disc chopper to select the wavelength range and then a prompt pulse suppressing nimonic chopper. The beam is coarsely collimated by neutron absorbing jaws before entering the experimental measurement area. Fine collimation is achieved by two slits before the sample, which define the illuminated area and resolution at the sample position. The beam profile and intensity is monitored just before reaching the sample by a scintillator detector. Generally, a one-dimensional detector is used to measure specular reflection, although a two dimensional detector is available to collect not only the specular, but also the off-specular profiles. In this study, we measured the reflection from the film at the specular angle by a single well-collimated detector. Samples prepared for neutron reflectivity (NR) need to be flat enough to minimise the off-specular scattering of the sample, which is deleterious to the specular reflectivity. Typically, for the investigations of polymer – polymer interfaces such flat samples are prepared by spin coating thin polymer films from solution onto optically flat substrates such as silicon or quartz. In our case we have used silicon substrates as described in more detail in chapter six.

Once the raw data has been collected, it must be reduced to the reflectivity profile as a function of Q. For the cell data this also involves correcting for the fact that the neutron beam must travel through the quartz windows in the perspex box and the silicon block before reaching the surfaces and interfaces of interest. The data for different Q ranges are then combined and the data normalised such that below the critical angle, R=1 (where R is reflectivity). There are in principle, four ways of analysing the reflectivity profiles arising from polymer interfaces:

(1) Model fitting

(2) Approximation techniques

(3) Direct inversion of the reflectivity data into scattering density profiles

(4) Model free fitting

These methods are discussed in detail in the general references [31,32,33]. In this study a model-fitting procedure has been used to analyse the reflectivity data. The detail procedure of the data analysis is given in chapter six.

3.5   LIGHT MICROSCOPY

3.5.1   Optical Light Microscopy

The term *microscopy* is the study of the fine structure and morphology of objects with the use of a microscope. There is a wide range of microscopy instruments available, which can resolve details ranging from the millimeter to the nanometer size scale (Table 3.2). The size and distribution of spherulites can be observed by optical techniques, but more detailed studies require electron microscopy. Single lameller crystals can be seen with phase contrast optical microscopy but need TEM for detailed image and measurements.

Polarized light microscopy is an optical technique that enhances contrast in crystalline materials. Phase contrast optical techniques enhance contrast between polymers that are transparent but which have different optical properties, such as refractive index and thickness. Combinations of these microscopy techniques provide images of the morphology of polymer materials.

Table 3.2   Characterisation techniques: size ranges

Transmission electron microscopy (TEM)	0.2 nm – 0.2 mm
Scanning electron microscopy (SEM)	4 nm – 4 mm
Optical microscopy (OM)	200 nm – 200 μm

3.5.2   Instrumentation

The microscopic study of the PS/PVME blends prepared by solvent cast and mechanical blending samples were performed in the Material Engineering Department. A Leitz – Laborlux polarising microscope was used in conjunction with a Linkam heating stage. The stage was equipped with a temperature control system, which enabled samples to be heated and cooled at an adjustable rate. The development of the phases was followed by photography at appropriate intervals with a Nikon camera attached to the microscope. The magnification of each run was calibrated by photographing a stage micrometer (calibrate scale).

3.6   Onwards

Results of experiments on polymer blends using the techniques described above are presented in chapters four to six.

References

1.   James, W. D.; Kenneth, H. T., *Thermal methods*, Johm Wily & Sons, New York, **1987**.

2.   Richardson, J. M. *Polymer Testing* **1984**, 4, 101.

3.   Rabek, J. E., *Experimental Methods in Polymer Chemistry*, Johm Wily & Sons, New York, **1980**.

4.   Wendlandt, W. W., *Thermal Analysis*, 3rd edition, (chemical analysis vol:19), Johm Wily & Sons, New York, **1986**.

5.   Richardson, J. M. in., *Comprehensive Polymer Science*, vol.1, Pergamon press: Oxford, **1989**, 868.

6.   Wendlandt, W. W.; Gallagher, P. K in, *Thermal Characterization of Polymeric Materials*, Academic Press: New York, **1981**.

7.   Mraw, S. C., *Rev. of Scientific Instruments*, **1982**, 53, 228.

8.   Wunderlich, B in, *Thermal Analysis in Polymer Characterisation*, (Turi E, ed.), 2, Heyden and Philadelphia, **1981**.

9.   Couchman, P. R., (a). *Macromolecules* **1978**, 11, 1156, (b). *Macromolecules* **1980**, 13, 1272.

10.   Gordon, M.; Taylor, J. S., *J. Appl. Chem.* **1952**,2, 493.

11.   Fox, T. G. Bull, *Amm. Phys. Sco.* **1956**, 2, 123.

12.   Utracki, L. A, *Polymer Alloys and Blends*, Oxford University Press: New York, **1989**.

13.   Bank, M.; Leffingwell, J.; and Thies, C. *Macromolecules* **1971**, 4, 43.

14.   Weiss, R. A.; Lu, X. *Polymer* **1994**,9, 35.

15.   Zheng, S.; Huang, J.; and Yang, X. *European Polymer Journal* **1996**, Vol.32, No. 6.

16.   Zheng, S.; Huang, J.; and Guo, Q., *J. Polym. Sci., Polym. Phys. Ed.* **1997**, 35, 1383.

17.   Richardson, M. J.; Riesen, R.; Schuijff, A., _Calorimetry and Thermal Analysis of Polymers, chapter. 6_, Hanser Publishers, New York, **1994**.

18.   Jan, F. R., _Experimental Methods in Polymer Chemistry_, John Wiley & Sons, New York, **1980**.

19.   Brown, D. W.; Floyd, A. J.; and Sainsbury, M., _Organic Spectroscopy_, John Wiley & Sons, New York, **1988**.

20.   Coleman, M. M.; Painter. P. C. _Applied Spectroscopy_ **1984**, 20, 255.

21.   Bower, D. I.; and Maddams, W. F., _The vibrational Spectroscopy of Polymers_, Cambridge University Press: London, **1992**.

22.   Norman, B. C.; Lawrence, H. D.; and Stephen, E. W., _Introduction to Infrared and Raman Spectroscopy_, 3rd Ed., New York, **1990**.

23.   Dudley, H. W.; and Ian Fleming, _Spectroscopic methods in organic Chemistry_, Fifth Ed., McGraw-Hill, London, **1995**.

24.   Pavia., D. L., _Introduction to Spectroscopy_, 2nd Ed., Harcourt Barace College Publishers, New York, **1996**.

25.   Painter, C. P.; Coleman, M. M., _Fundamentals of Polymer Science_, Technomic Publishing Company, Inc, New York, **1997**.

26.   Liang, C. Y.; Krimm, S.; and Sutherland, G. B., _J. Chem. Phys._ **1956**, 25, 543.

27.   Zbinden, R., _IR Spectroscopy of high polymer_, Academaic Press: New York, **1964**.

28.   Coleman, M. M.; Koenig, J. L.; Painter, P. C., _Theory of vibrational spectra and its Application to Polymeric Materials_, Wiley: New York, **1982**.

29.   Coleman, M. M.; Painter, P. C.; Koenig, J. L., _Specific Interactions and the Miscibility of Polymer Blends_, Technomic Publishing Company Inc., Lancaster, New York, **1991**.

30.   Klopffer, W., _Introduction to Polymer Spectroscopy_, Springer Verlag, **1984**.

31. Russell, T. P., _Materials Science Reports_ **1990**, 5, 171.

32. Penfold, J.; Thomas, R. K., _J. Phys. Condes. Matter_ **1990**, 2, 1369.

33. Thomas, R. K., _Scattering methods in polymer science_, Ed. Richards, R. W., Ellis Horwood, **1995**.

34. Higgins, J. S.; Benoit, H. C., _Polymers and neutron scattering_, Oxford University Press: **1994**.

35. Higgins, J. S.; Bucknall, D. G., _Neutron Reflection Studies of Polymer-Polymer Interfaces_, Technical Report of Central Laboratory of the Research councils **1997**.

36. Lekner, J., _Theory of Reflection_, Martinus Nijhoff, Dordrecht **1987**.

37. Koester, L., in Bonse, U.; Rauch, H.; Eds.; _Neutron Interferometry_, Oxford Science Publications: Oxford **1979**.

38. Sear, V. F., _Neutron News_ **1992**, 3, 26.

39. Born, M.; Wolf, E., _Principles of Optics_, 6th edition, Pergamon Press: Oxford, **1980**.

40. Heavens, O. S, _In Optical Properties of Thin Films_, Butterworth, London, **1995**.

41. Nevot, L.; Croce. P. _Phys. Appl._ **1980**, 15, 761.

42. Cowley, R. A.; Ryan, T. W., _J. Phys., Ed. D_, **1987**, 20, 61.

43. Penfold, J., _J. de Physique, C7 Supplement No. 10_, **1989**, 50, 99.

44. Richards, R. W.; Penfold. J, _Rev. TRIP_ **1994**, vol. 2, No. 1, 5

45. Bucknall, D. G.; Penfold, J.; Webster, J. R. P., _ICANS XIII Proceeding, PSI Pro 95-02_, **1995**, 1, 123.

46. Boland, B.; Whapman, S., Eds.; _ISIS User Guide: Experimental Facilities_, December **1992**.

CHAPTER FOUR

STUDY OF PS/PVME AND SPS/PVME BLENDS

This chapter reports an investigation of the nature of the interaction responsible for the miscibility of polystyrene (PS) and sodium sulfonated polystyrene (Na-SPS) with poly(vinyl methyl ether) (PVME) blend. The semiquantitative evaluation of the strength of interaction between the components of the blend was performed with DSC (Gordon-Taylor equation). The DSC measurements were also made in order to find the phase boundary of this LCST blend system as functions of temperature and composition. Quantitative information on the molecular interaction has been obtained from FTIR by evaluating the peak position and intensity.

4.1   INTRODUCTION

There has been a considerable interest in the study of polymer blends because of their importance in practical applications. Particularly, much attention has been paid to miscibility and phase behaviour in polymer blends [1-3]. In general, the miscibility of a polymer pair is dictated by the change in the Gibbs free energy of mixing, ΔG_{mix}. Since the change in entropy of mixing, ΔS_{mix}, is usually small for polymers, miscibility of a polymer pair will be improved if the change in enthalpy of mixing, ΔH_{mix}, is negative. For this reason a number of studies have been focused on polymer mixtures with specific interactions, such as hydrogen bonding [4-7] or charge-transfer complex formation[8].

The typical and well-known polymer mixture exhibiting a lower critical solution temperature (LCST) is polystyrene (PS) and poly(vinyl methyl ether) (PVME) blend. Earlier studies [9-12] have demonstrated that these two amorphous polymers are miscible at low temperature over the entire range of compositions. It was suggested that the miscibility at low temperature of this particular polymer pair originates from the specific interaction between the lone-pair electrons of PVME and the phenyl ring of PS. These attractive interactions have been observed through the changes in i.r. absorption peaks of both PS and PVME upon mixing and with increasing temperature[13-15]. In this chapter, this hypothesis is being investigated through several experimental techniques.

The recent quasielastic neutron scattering experiments [16], however, do not support these conclusions. In order to clarify this issue a series of measurements on this blend was carried out using FTIR spectroscopy and the results obtained are supported by DSC measurements.

The PS/PVME system also offers the opportunity to generate heterogeneous blends by demixing the polymers at high temperature, followed by quenching at ambient temperature [17]. In this chapter, an investigation of miscibility and phase behaviour of this type of blend is reported. As for determination of the phase boundary of polymer blends by DSC techniques, several articles have been published [18-20]. However to our knowledge the phase boundary of PS/PVME blends has not been measured using DSC technique. In this work the miscibility and phase behaviour of this blend has been studied by differential scanning calorimetry (DSC), light microscopy and fourier transform infrared (FTIR) spectroscopy measurements. In addition, an attempt has been made to study miscibility through diffusion between these two polymers using light microscopy.

However the diffusion between PS and PVME was not observed in the time available.

Furthermore, specific interactions between the two components of these blends (ranging from 10% to 90% PS by weight) were examined experimentally by FTIR spectroscopy, and the composition dependence of the glass transition temperatures T_gs of these blends was determined by DSC. The compositional variation of the glass transition temperature was analysed in terms of the Fox, and Gordon-Taylor equations. The results obtained were compared to those previously reported [9,17] by DSC and dilatometric measurements [18] and show a good correlation with results presented here.

4.2   EXPERIMENTAL

4.2.1   Polymers

Polystyrene (PS) remains one of the world's highest produced thermoplastics. This is because it combines its low cost with many desirable properties: it is clear, transparent, easily coloured and easily fabricated, and has a reasonable chemical resistance. Its glass transition temperature (T_g) is about 100°C, hence it is "glassy" at room temperature. It also has reasonably good mechanical and thermal properties, but its two major defects in mechanical properties are its brittleness and its relatively low heat deflection temperature of about 80°C, which means that polystyrene articles cannot be sterilized. The chemical structure of polystyrene is as follows:

$$\left[-CH_2-CH-\right]_n$$
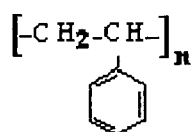
A number of attempts have been made to modify PS for improved impact strength with use of rubber additives to produce blends of greatly improved toughness. A wide range of elastomers have been investigated as possible impact modifiers for PS. One of them is Poly(vinyl methyl ether) PVME $[CH_2CHOCH_3]_n$, an elastomer which was first made available in Germany just before 1940, it is a water soluble (cold water), viscous liquid or tacky solid at room temperature. It has a low T_g of (-28°C) and its main applications are in the adhesive and rubber industries. These blends have been extensively investigated, as explained in 4.1.

4.2.2 Materials

PS and SPS with different level of sulfonation (1.18, 2.7 and 5.2 mol. %) were obtained as powder from Exxon Chemicals of USA with $\overline{M_w}$ = 300,000 g.mol^{-1} and $\overline{M_w}$ / $\overline{M_n}$ = 1.06. Poly(vinyl methyl ether) PVME, was purchased from Scientific Polymer Products, Inc. (Ontario, New York), as a 50% (w%/w%) solids solution in toluene. Its molecular weight $\overline{Mw}$ = 95,000, quoted by the company as determined by gel permeation chromatography (GPC). Both polymers were used without further purification.

4.2.3 Preparation of blends for DSC measurements.

Polymers containing PS, PVME and PS/PVME mixtures of 1% concentration ratio at different compositions were prepared by solvent casting from a common solvent *toluene* .SPS blends were prepared by dissolving in solution of 90:10 *toluene/methanol* at room temperature. Reported PS/PVME concentration ratio are on a (wt. %/wt. %) basis. During preparation it is extremely important to avoid moisture since PVME is hygroscopic. All solutions prepared by solvent casting were stirred with a magnetic stirrer and subsequently cast onto a glass surface only for compositions up to 70% PS. For 50 and 30% PS blends, a Teflon-coated surface was used to facilitate the release of films. Finally, to avoid handling of the 20%, 10% PS and pure PVME films that are soft and sticky, the solution was poured into small aluminium pans. In order to remove the residual solvent, all films were put in a vacuum oven at a temperature above the (single) glass transition temperatures of the blends. The temperature was slowly increased up to 60°C, and the final temperature was maintained for 3 days. Finally the dried films were left at room temperature in the oven until used. The mechanical blending was performed by hand mixing the polymers placed on a glass slide, on a hot –stage with a thermocouple.

4.3   MEASUREMENTS

4.3.1   Differential scanning calorimetry

The calorimetric measurements were performed on a *Pyris model-1* differential scanning calorimeter in a dry nitrogen atmosphere in the analytical laboratory of the Chemical Engineering Department, Imperial College of Science, Technology and Medicine, London. The instrument was calibrated with indium and lead standards for low and high temperature regions, respectively. All the samples used in the DSC cell were about 10 mg in weight. They were first heated from -70°C to 150°C and held for 5 min, followed by quenching to -70°C. A heating rate of 20°C min^{-1} was used in all cases to avoid a super-heating effect. The glass transition temperature (T_g) was taken by both methods as described in chapter three, the *mid-point* of the heat capacity change and *onset* of the transition (the change of the specific heat) in the heat flow curves, respectively.

Phase separation processes were investigated by annealing the homogenous blend samples at the upper temperature for 10 min. The samples were then quenched to -70°C and scanned up to the next higher temperature at the heating rate of 20°C min^{-1}. The upper temperature was changed in 10 degrees intervals. This procedure was repeated until the occurrence of phase separation was observed. The annealing temperature corresponding to the appearance of two T_gs corresponding to the T_gs of the pure polymers was taken to be the phase separation boundary.

4.3.2   Fourier transform infra-red spectroscopy

Infrared spectra were obtained using a *Nicolet - 710* and *60SXB* FTIR spectrophotometer of the Materials Engineering Department, Brunel University.

The number of scans per sample was two hundred and the resolution of the measurements was 4 cm^{-1}. The recorded wavenumber range was 400 - 4500 cm^{-1}. The measurements were carried out either on thin films onto potassium bromide (KBr) discs or using a solid thin solvent-cast film. Blends of various compositions were prepared by dissolving appropriate amounts of the components in a common solvent toluene at room temperature to yield 1% (w/w) solutions.

Thin films for FTIR studies were obtained by casting the polymer solutions of pure PS and composition up to 30% PS on to a teflon - coated surface (Petri dish) at room temperature, and subsequently kept in a vacuum oven at 60°C for one week. For pure PVME (due to it being soft and sticky) potassium bromide discs at room temperature were used. These films were sufficiently thin to exhibit absorbance in the range where Beer's law is obeyed. The solvent was then rapidly evaporated by placing the sample in a vacuum oven at 40°C for 3 days. All the spectra were recorded at room temperature. Films were subsequently annealed up to 160°C (both homopolymers and the PS/PVME (50:50) blend) at 25 degree intervals.

4.3.3 Light microscopy

A polarised – light microscope (_Leitz Laborlux_) was used to examine the morphology of the (solvent – cast and mechanical blending) samples and also for the study of the diffusion layers at Materials Engineering Department, Brunel University. The film samples for optical examination were prepared using a procedure similar to that described in section 4.2.3, except that glass slides and cover slips were used to sandwich the films. The films for light microscopy were sufficiently thinner than the required resolution.

For diffusion studies using the light microscopy, samples were prepared by the following procedure: A thin PS film was produced by compression-moulding the stabilised powder in a heated barrel; after moulding, a small amount of PVME was placed on the upper surface of the PS thin film in preparation for annealing. A vacuum oven was used for this purpose, and the temperature set below and above the glass transition temperature of PS. Annealing was performed on a number of samples for a range of annealing times.

After annealing, the boundary of PS/PVME was assessed by examination of thin sections. These sections were cut at room temperature perpendicular to the PS/PVME boundary, using a microtome with a glass knife, and examined under the light microscope, equipped with an eyepiece graticule calibrated in hundredths of a millimetre.

4.4 RESULTS AND DISCUSSION

4.4.1 DSC Results

Mixing of the two polymers PS and PVME by solvent casting in toluene resulted in optically clear samples. This observation indicates that PS/PVME blends present a single homogenous amorphous phase at room temperature, i.e., phase separation did not occur, at least on a scale with dimension of phase domains exceeding the wavelength of visible light.

The determination of the glass transition temperature is a commonly used tool to evaluate the miscibility of a polymer blend. A miscible polymer blend shows a single T_g different from, and in general intermediate between, those of the two pure components [3]; on the contrary, an immiscible blend exhibits two different T_gs corresponding to those of the single constituents, as discussed in Chapter Three.

All the blends were first characterised by DSC. Figure 4.1 shows DSC thermograms of pure PS, PVME and PS/PVME blends of several compositions prepared by solvent casting. Pure PS shows a T_g at 106°C, and pure PVME shows a T_g around -28°C. A single T_g was observed at intermediate temperature between those of the pure polymers and varied with blend composition. The presence of a single T_g and optical clarity were used as an indication of miscibility. These results also suggest that the PS/PVME blends have a single amorphous phase, i.e. the two polymers are miscible in the amorphous state over the whole composition range. The results correspond to those obtained previously [9,17]. These results show that PS and PVME are miscible throughout the whole range of compositions. In order to establish the phase diagram, i.e. the

temperature dependent miscibility, further work was required, as described later in this section.
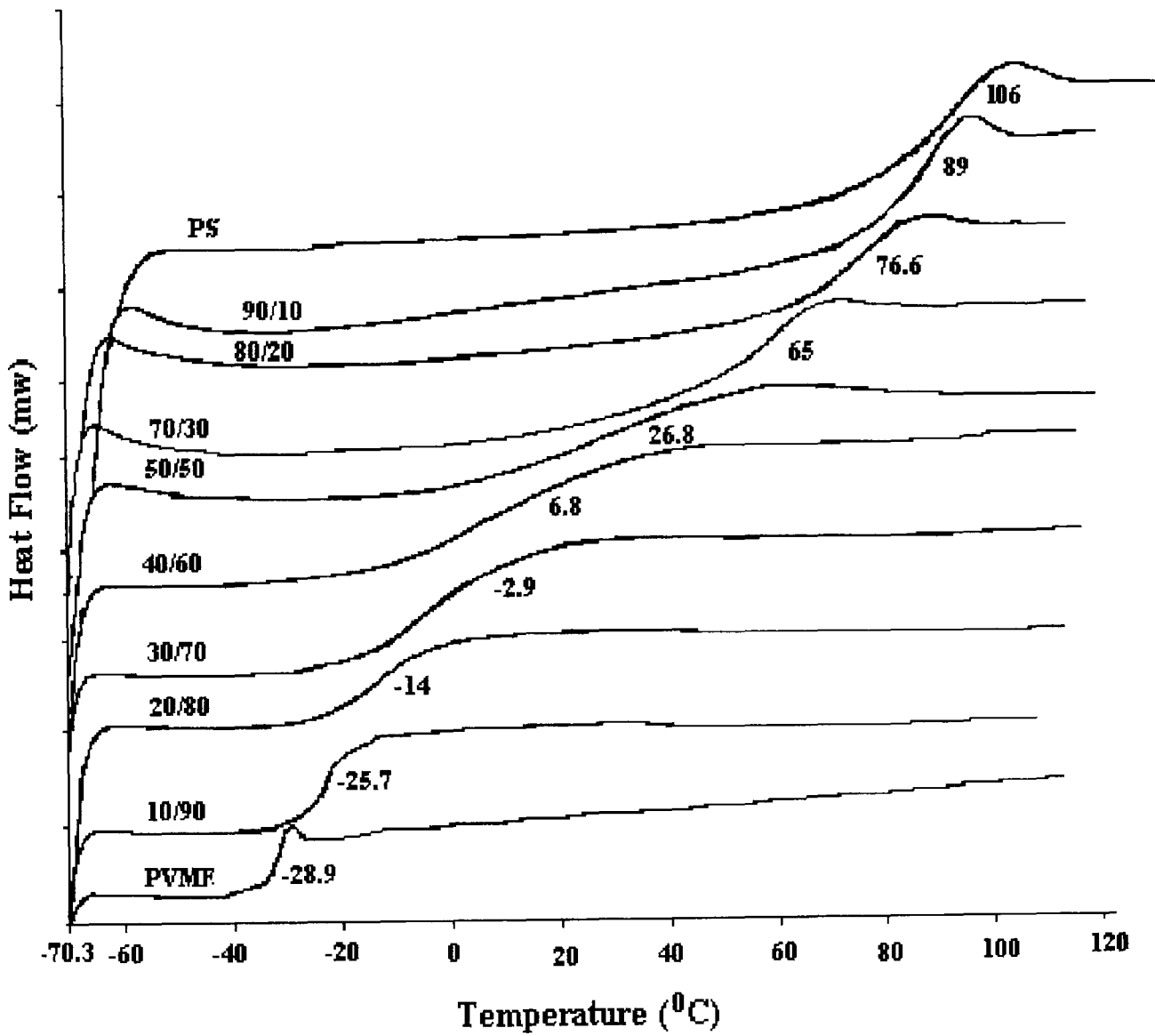

Figure 4.1   Representative DSC thermograms of miscible PS/PVME Blend system for mixtures containing various wt. % PS prepared from toluene.

Representative thermograms in figure 4.1 show that the transition is broad, diffuse and does not have a thermal peak under experimental conditions used in this study except for homopolymers. Both homopolymers exhibited the endothermic peaks normally observed during the first and second runs respectively, when cooled at similar rates. However, in at least two cases [80/20 and 90/10 PS-PVME] annealing at temperatures just below the transition point yielded a small endothermic peak, similar to the effect of annealing a homopolymer, which is common to many amorphous thermoplastics [22]. The broad glass transition region as measured by DSC is similar to the appearance of the well known broad glass transition for other miscible polymer blends [23-24].

Sodium sulfonated polystyrene (Na-SPS) and PVME were also found to be miscible over all the composition range. Na-SPS/PVME blends exhibit a single T_g, which varies with blend composition. The changes in T_g of PS and SPS with different level of sulfonation are shown in figure 4.2. The T_g of SPS increases with sulfonation level [25]: for the pure PS, T_g is 106C°, which for the 1.18, 2.7 and 5.2 mol. % Na-SPS, the T_g increases to 108, 111 and 115C°, respectively. Figure 4.2 shows an approximately linear increase with increasing sulfonation level of SPS (within experimental error). For a 50/50 composition SPS/PVME blend, a single, broad and composition-dependent T_g, was observed similar to those of PS/PVME blends. The T_g of the blends increases linearly with increasing sulfonation level of SPS (see figure 4.3). This indicates that the sulfonation as well as PVME composition affect the T_g of the blend.
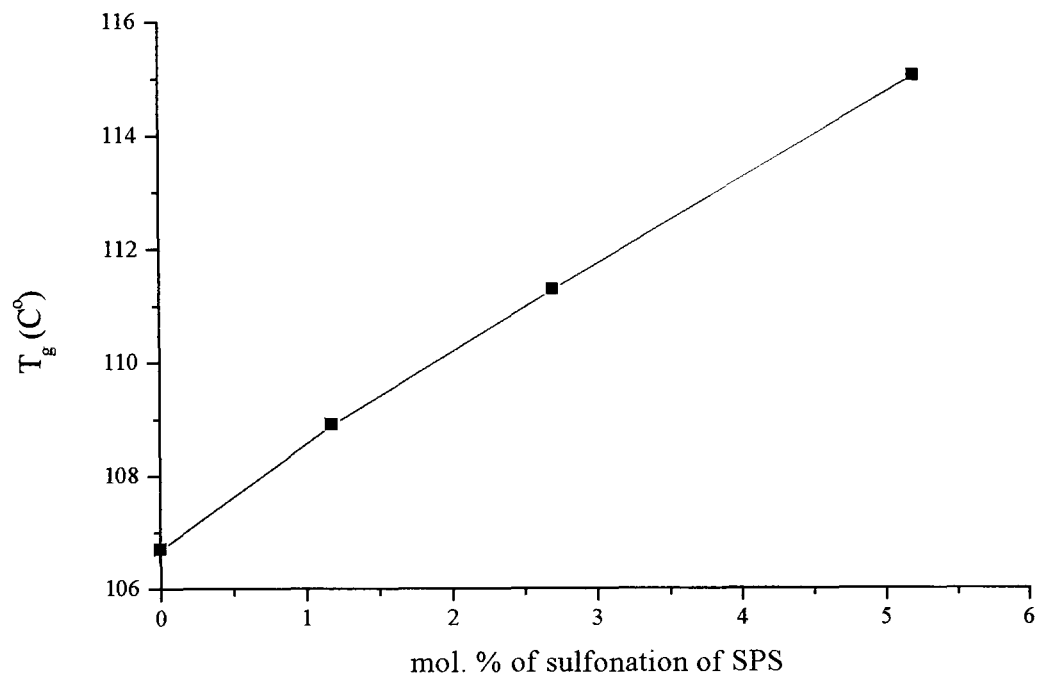
Figure 4.2   Effects of sulfonation level of SPS on the T_g.
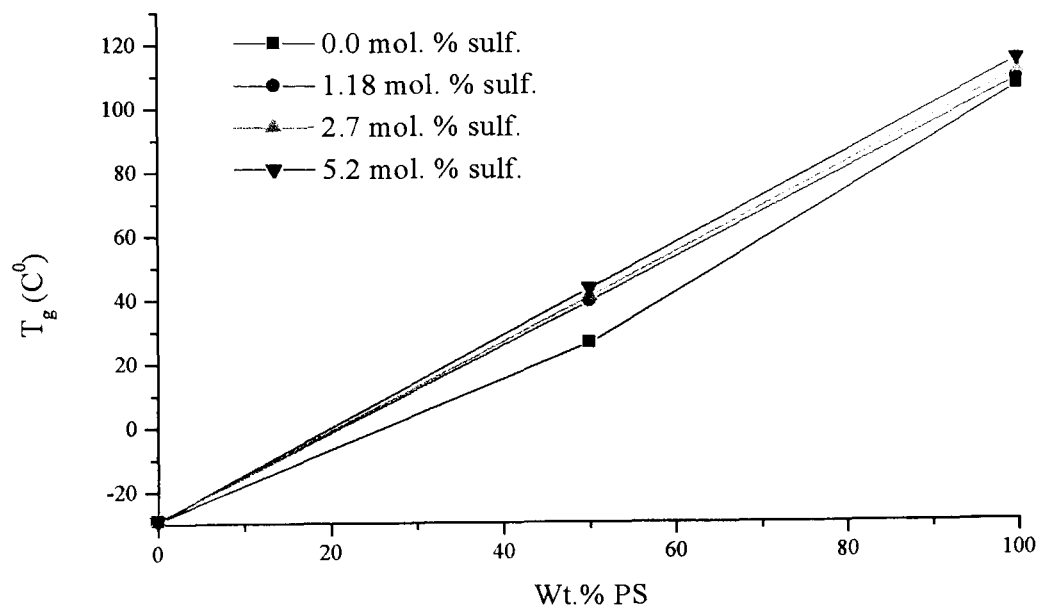
Figure 4.3   Effects of sulfonation level of SPS and PVME content on the T_g of the blends.

Table 4.1   Effect of composition on the glass transition temperature (T_g) of
PS/PVME blends cast from toluene

W% PS	Glass Transition Temperature (°C)		
	Half-height methods	Onset methods	Data of M. Bank et al
100	106.72	102.87	102
90	89.21	81.56	80
80	76.63	65.68	66
70	64.53	52.51	42
60	38.68	13.9	9
50	26.27	0.48	-14
40	6.81	-13.19	-20
30	-2.94	-16.61	-24
20	-14.13	-24.57	-24.5
10	-25.72	-29.92	-27
0	-28.95	-31.38	-28

Figure 4.4 shows T_g values as a function of PS weight % calculated from the DSC curves using the onset and mid-point methods as discussed in Chapter three. T_g values defined by both methods gave similar curves when plotted against composition, assuming that the polymers are compatible (single, composition dependent T_g). The precise method used for defining T_g is not very

important but it must always be self-consistent. T_g values are reported in Table 4.1 as a function of composition. As PS content decreases, the glass transition temperature decreases from 106°C (T_g for PS) to -28°C (T_g for PVME), in accordance with the values reported in literature [9,17].

Several theoretical and empirical equations have been proposed, in order to correlate or predict the dependence of T_g on the composition of the polymer blend as mentioned in section 3.2.2. Herein we have applied the Gordon-Taylor and the Fox equations.

The Gordon – Taylor equation [26] is

$$T_g = \frac{w_1 T_{g_1} + K w_2 T_{g_2}}{w_1 + K w_2}$$

and the Fox equation [27] is

$$\frac{1}{T_g} = \frac{w_1}{T_{g_1}} + \frac{w_2}{T_{g_2}}$$

where T_g is the glass transition temperature of the blend, T_{g_1} and T_{g_2} are the glass transition temperatures of the components 1 and 2, respectively; w is the weight fraction, and $K = \Delta C_{P2} / \Delta C_{P1}$ (i.e. ratio of heat capacity change in PS to the change in PVME).

The plot of the glass transition temperatures T_gs for the miscible blends versus PS weight fraction is presented in figure 4.4. The T_gs, predicted by Fox equation (curve C) are compared with the experimental data calculated by mid-point

method (curve A) showing the best overall fit. However, curve B comprising T_gs calculated by the onset method, displays a slight sigmoidal positive deviation from the Fox equation, especially at lower PS contents. It is seen that T_g of each blend varies progressively between T_gs of the homopolymers obeying the Fox equation calculated from the end points. This deviation can be explained as follows: for the PS/PVME blends with specific intermolecular interactions, a negative volume of mixing or densification might result in a higher T_g due to a reduction in free volume, i.e. a positive deviation of T_g from the Fox equation[28].
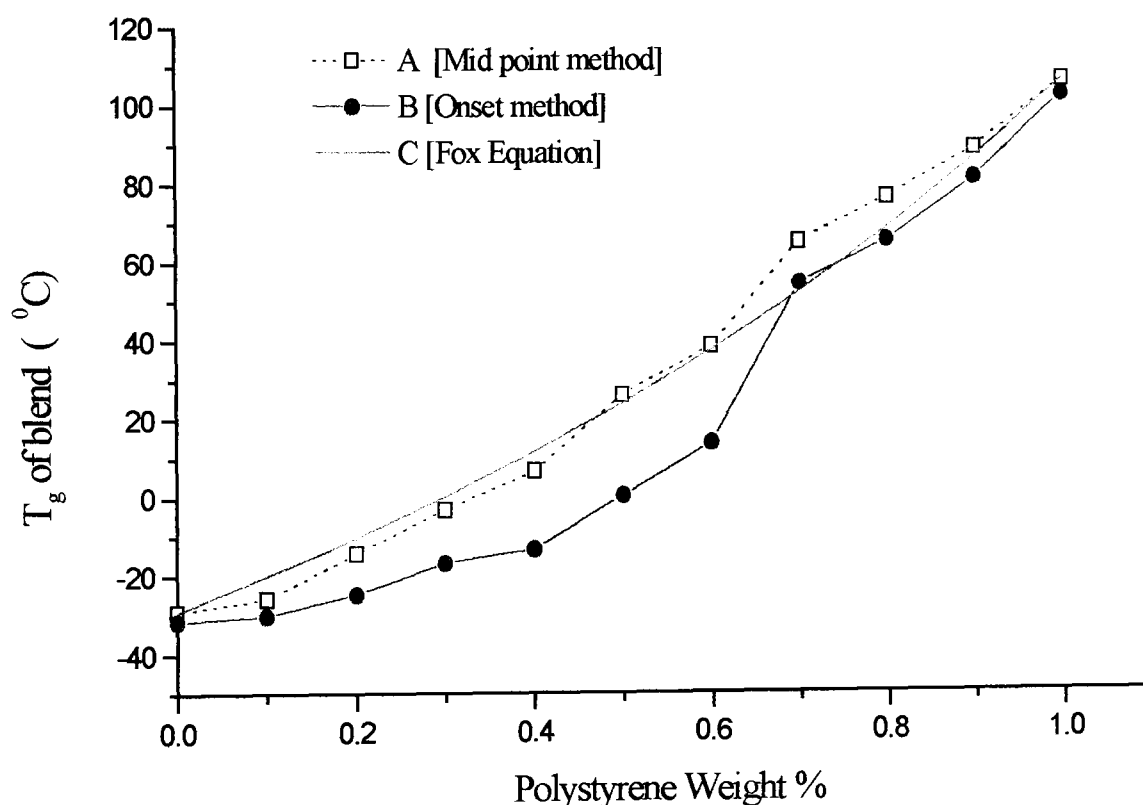

Figure 4.4   Glass transition temperature of PS-PVME blends as a function of PS concentration: A, experimental curve by mid-point methods; B, Experimental curve by Onset methods and C, Fox equation.

The results obtained from the onset method for the PS/PVME system agree with that reported earlier by M. Bank et al[9] who stated that the Gordon - Taylor equation describes well the T_g - composition relationship. They tested this equation by varying the values of the constant K between 0.5 and 0.25. However, a reasonable fit of the experimental data to this expression occurs only at high PS contents but large deviations still occur at lower PS concentrations. To better describe this relationship, the Gordon - Taylor equation was used again. The fitted K values of 0.5 and 0.25 were used respectively as shown in figure 4.5.

However in our results by varying the constant K, the Gordon- Taylor equation can be adjusted to give the best fit at low PS contents, but still large deviations occur at higher PS concentrations. The experimental curve shows a slope at < 60 % PS content, indicating that the composition dependence of the transition is not uniform. This result is in agreement with that previously reported [9]. It is well known that T_g depends on chain mobility, especially on segmental mobility, and the increase in T_g is usually attributed to a decrease in the mobility of the polymer chain.

The difference between the theoretical and experimental curves may stem from the assumption of simple additivity of specific volume. Thus it is suggested that the specific volume change due to mixing ($\Delta V_{m.sp}$) is not zero but either positive or negative for the PS/PVME blend system [29]. The partial molar volumes depend on interactions between molecules as well as on glassy or rubbery environments, and the experimental temperature T is chosen so that $T_{gB} > T > T_g$ (mixture) as demonstrated in figure 4.6. If the mixing of two polymers occurs on a molecular scale, then the chains of polymer B in the mixture will be in a rubbery environment. The partial molar specific volume of polymer B in the mixture is

expected to be closer to V_{1B}, the extrapolated specific volume from the liquid state to T, than to V_{gB}, the specific volume in the glass state at T. On the other hand, if microscopic domains of sufficient size exist, the partial molar specific volume of polymer B in the mixture will be essentially identical with V_{gB}. The partial molar specific volume of polymer A is V_{1A} in either case. Similar reasoning can be applied to the partial molar specific volume of polymer A in the mixture if T_g > T.
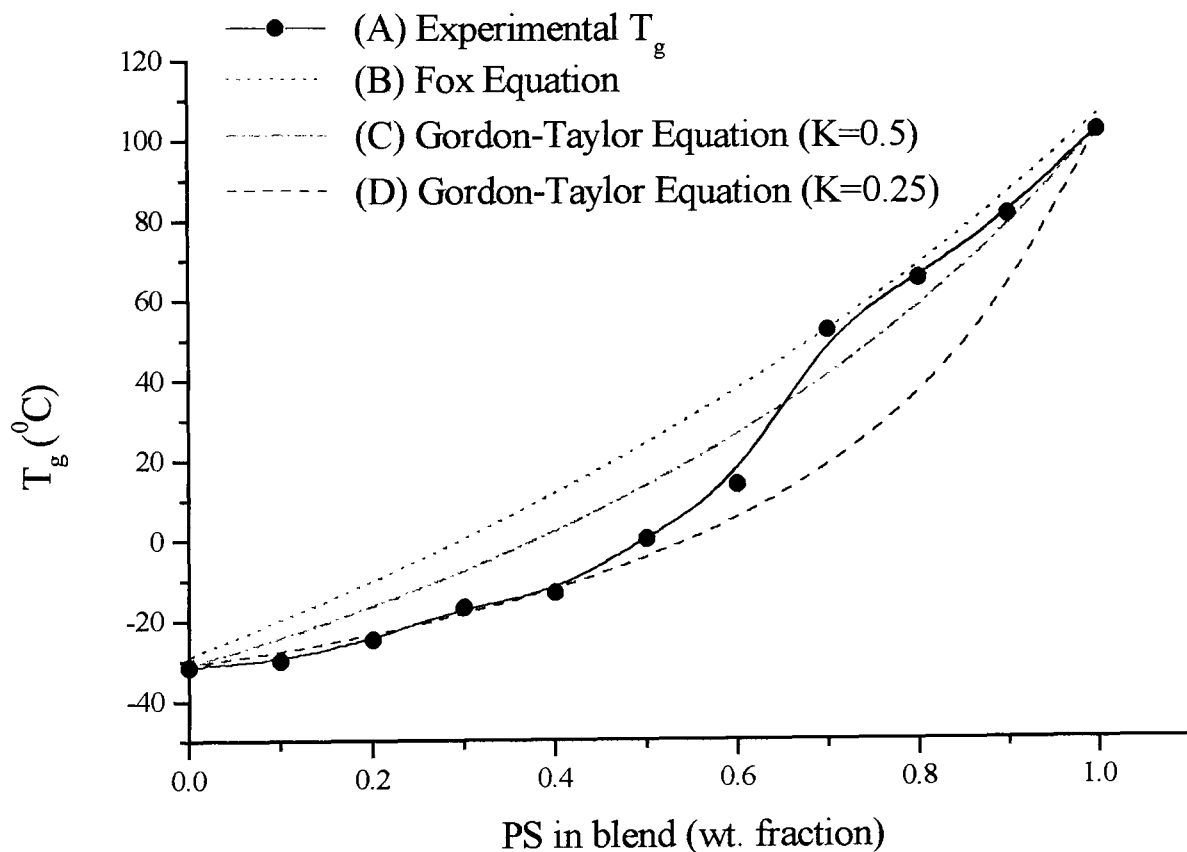

Figure 4.5 Glass transition temperature of PS-PVME blends as a function of PS concentration: A, experimental curve by onset methods; B, Fox equation; C, Gordon-Taylor equation, K = 0.5; D, Gordon-Taylor equation, K = 0.25.
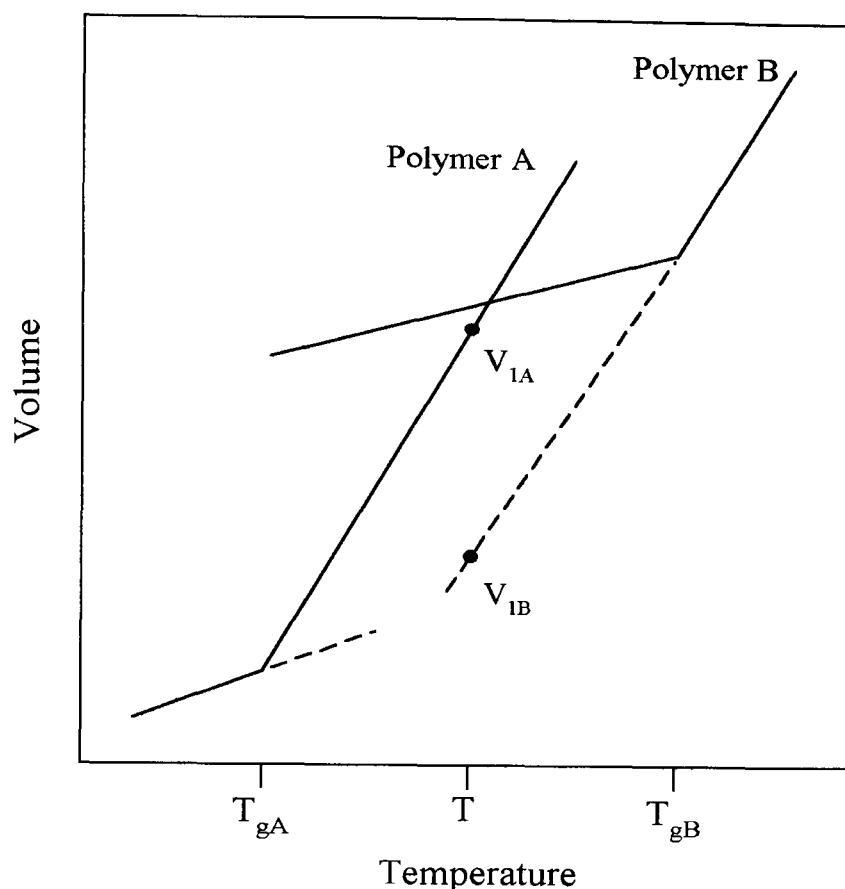
Figure 4.6   Schematic representation of volume-temperature curves of two polymers having glass transition temperatures widely separated from each other.

Schneider and Brekner[30] have shown that the composition dependence of the glass transition in the miscible PS/PVME blend exhibits deviations from the additivity rules (these rules were derived assuming the continuity of the thermodynamic excess functions of mixing). It was noted that at the T_g of the blend, the pure components are in a mixed phase, one (PVME) in the liquid, and the other (PS) in the glassy state. They concluded that only the acceptance of an additional adjusting parameter, which accounts for possible differences in interactions between the components in the mixed phase would enable a full interpretation of experimental T_g data. This adjusting parameter was quite different for the blends of PVME with oligomeric and high molecular weight PS, respectively, due to the mobility of the chain ends in oligomeric PS. In their

explanation the chain-end mobility creates supplementary free volume in the blend, thus causing a substantial depression of the T_g.

Prud'homme et al. have suggested[31,32] that the K value can be taken as a semiquantitative measure of the strength of interaction between the components of the blend. For instance, in blends of poly(vinyl chloride) (PVC) with chlorinated (CPVC), K increases from 0.26 to 1.0. The predicted T_gs from the Gordon-Taylor equation for the PS/PVME blends fitted the experimental data quite well and yielded a K value of 0.25. The agreement of the Gordon-Taylor equation with experimental data indicates that any specific interaction that may occur between PS and PVME is relatively weak.

Determination of phase diagram

It is well proved that miscible polymer blends have a single glass transition temperature and immiscible polymer blends have two glass transition temperatures, one for each phase. In this study PS/PVME homogenous blends were demixed at high temperature and then quenched at ambient temperature. Samples prepared in this way exhibited heterogeneous blend behaviour, and showed two glass transition temperatures, indicative of phase-separation[9,17].

Typically, a quench of the polymer blend is achieved by a rapid change of temperature which forces the blend into the unstable or metastable regions of the phase diagram. In the metastable region of the phase diagram, between the binodal and spinodal lines, phase separation takes place by nucleation and growth[33]. Phase separation in the unstable region occurs via spinodal decomposition bounded by the spinodal line [33,34]. The initially miscible blend develops domains that are preferentially enriched in one of the components and

these become less connected during the phase separation. For a wide range of blend compositions both phases should be connected and the interface should be diffuse in the early stages of spinodal decomposition. In the present study, the blends are believed to be phase-separated mainly by spinodal decomposition, since phase separation was carried out above the cloud points (lower critical temperature) commonly believed to occur above the spinodal decomposition temperature [35].
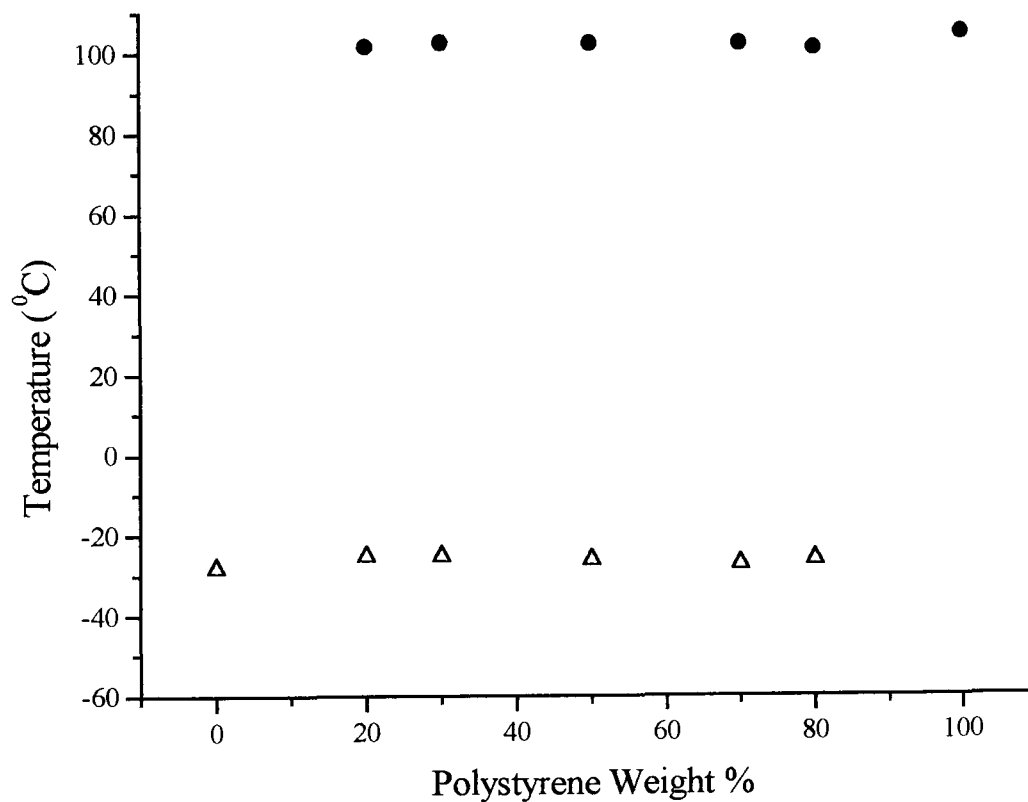

Figure 4.7   Glass transition temperatures of PS/PVME blends heated for 10 min at 150 – 170°C and quenched in liquid nitrogen after the first scan. (●) PS - rich phase or pure PS, (Δ) PVME - rich phase or pure PVME.

All PS/PVME blends quenched in liquid nitrogen after the first heating at temperature 150°C possessed a two-phase structure as shown by the appearance of two glass transition temperatures in the second DSC scan, (shown in figure 4.7).

Figure 4.8 contains representative DSC thermograms that illustrate this point. Before being heated to the critical point, the blends have a diffuse transition, which is composition-dependent and falls between the glass transition temperatures of the homopolymer components. After quenching in liquid nitrogen samples subsequently heated to the critical temperature, two glass transitions T_gs are detectable. T_g values fall at temperatures characteristic of the T_g of PS and PVME. This was observed for all the samples studied.

Bank et al [9] reported that the phase behaviour of these blends depended on the solvent. Two-phase behaviour was reported for blends cast from trichloroethylene or chloroform, whereas films cast from toluene or xylene exhibited single-phase behaviour. Further studies indicated that initially single-phase films cast from the appropriate solvent exhibited phase separation when heated above 125°C. Moreover, the two-phase films cast from the trichloroethylene or chloroform solvents remained in a phase separated state after thermal treatment consisting of extensive annealing and slow cooling. The above result have been confirmed by McMaster[36] and hence toluene has been used exclusively in this work.
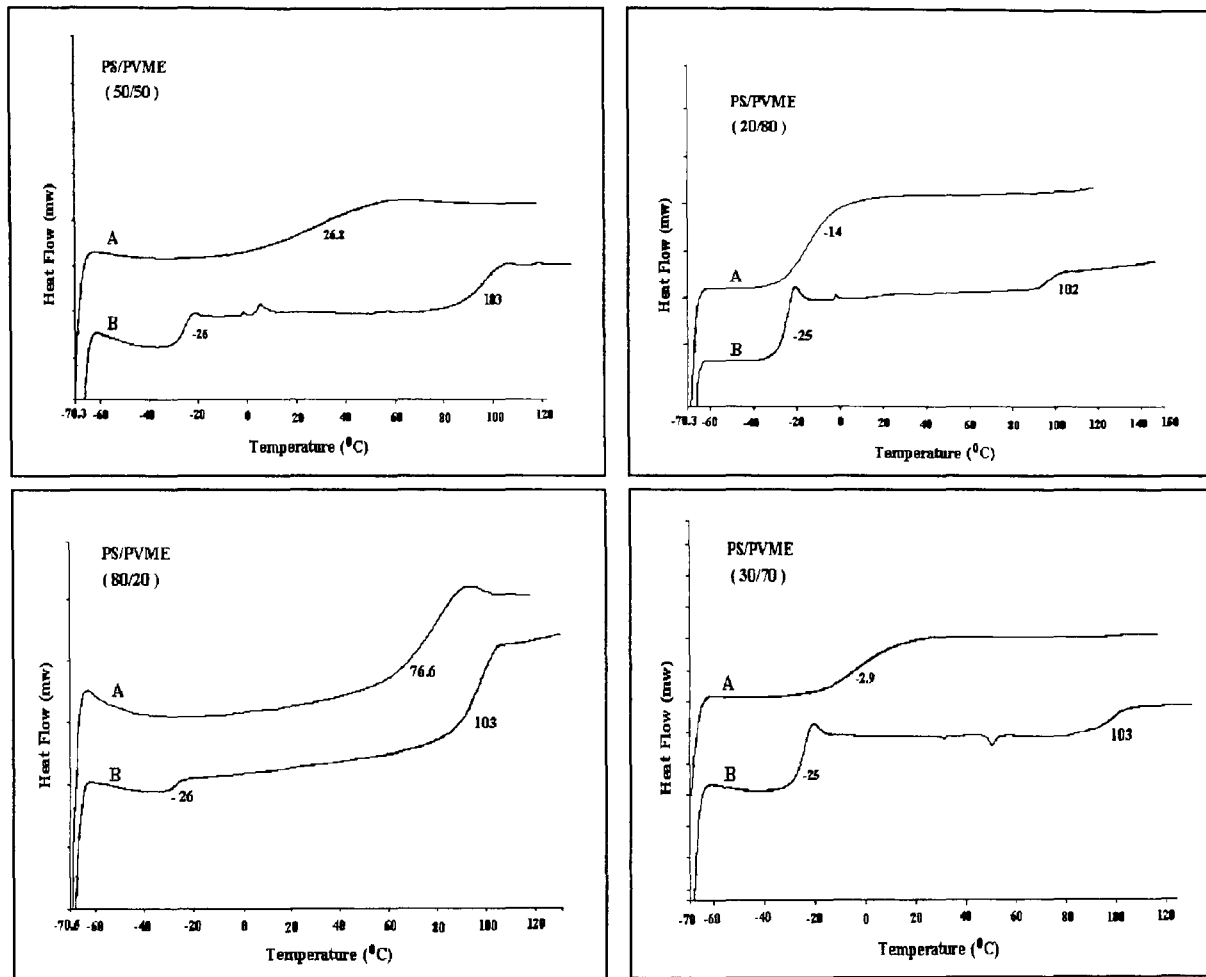
Figure 4.8   DSC thermograms for PS-PVME mixture: (A) before phase separation; (B) after phase separation.

In this study the phase separation boundaries were determined by DSC. The homogeneous blend samples were annealed at temperatures just below LCST for 10 min and then quenched to -70°C; after quenching the specimen was scanned in DSC to temperatures above LCST. The annealing temperature was then increased by 10°C steps up to LCST. The annealing temperature corresponding to the appearance of two glass transition temperatures (which were close to T_g's of both homopolymers) was taken as the phase separation boundary, as shown in figure 4.9. The phase diagram of this blend system has the LCST at critical composition of between 20 and 30 wt % PS content. This is not an accurate method of LCST determination, and is used here only for correlation of our results with those already available in the literature[37]. The weight fraction of PS

at the LCST depends on the molecular weight of each component in the blend

[37]. The system with the molecular weight of PS larger than that of PVME, LCST is located at the PVME –rich content (PS poor content), as in the present case.
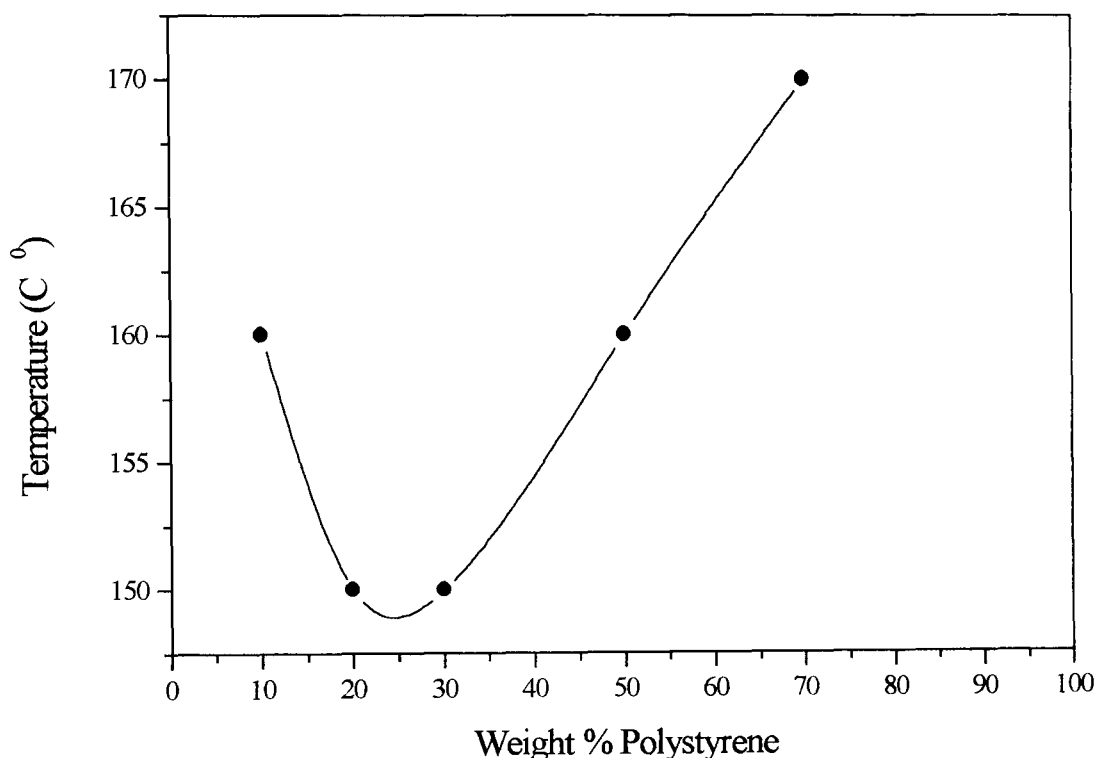
Figure 4.9   Phase separation boundary diagram of PS/PVME blends determined by DSC.

The phase boundary has been established by heating the sample in the DSC instrument to various temperatures (10°C intervals) and cooling rapidly. It has been found that even the cooling rate of 10°C/min or even 250°C/min was not sufficient to observe phase separation and single T_g has always been observed. In order to observe the phase boundary a rapid cooling to liquid nitrogen had to be used. The phase boundary temperature for a given composition has been

established as a transition, below which a single T_g has been observed and above which two T_gs (corresponding to the homopolymers) have been shown.

The DSC results show for the first time by this method, that a phase diagram can be constructed. This diagram corresponds to diagrams measured by different techniques [38,39]. In addition it is shown that the rate of separation is very fast and the phases can only be preserved using the fastest possible cooling rate (e.g. N_2). The DSC measurements of T_g for mechanically blended samples show two T_gs, corresponding to pure homopolymers. After annealing for 24 hours at 110°C a T_g at 67°C can be observed. This means that a slow diffusion process is forming one phase. The composition of this phase can be evaluated from a known dependence of T_g on composition (Figures 4.1, 4.4, 4.9 and Table 4.1) and is about 70% PS and 30% PVME. This shows that for mechanical blending a different phase diagram is observed than for solvent cast samples, confirming the conclusions obtained by light microscopy.

4.4.2 FTIR Spectroscopy Results

In order to elucidate the role played by intermolecular interactions in the miscibility of these blends, i.r. absorption of the individual polymer components, PS, SPS and PVME was measured and compared to that in the mixtures. The spectra of pure PS, pure PVME and their blends at mass ratios 90/10, 70/30, 50/50, and 30/70 (PS/PVME) at room temperature are shown in figures 4.10 to 4.15, respectively, in order to give an overview of the changes that occur with composition. All the infrared spectra show a similar pattern. In the infrared spectrum of PS, a number of bands showed small changes in position or shape when PS is blended with PVME. The assignment of these bands is tabulated in Table 4.2, which serves to identify the conformational changes as discussed below.
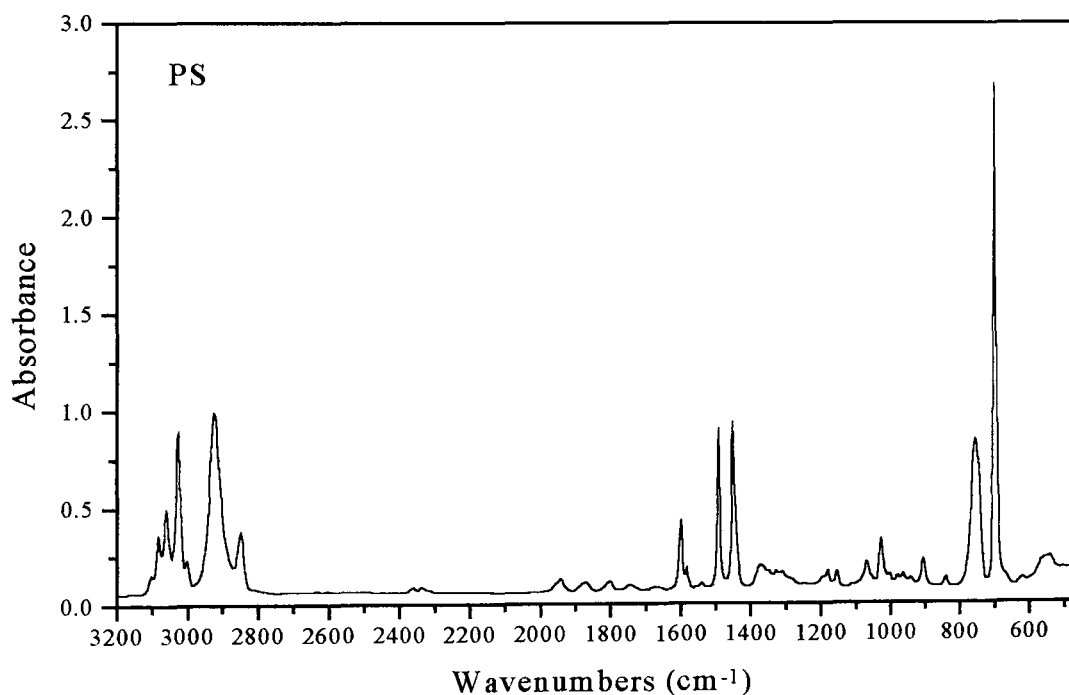

Figure 4.10 Infrared spectra of pure PS casted from toluene solution and measured at room temperature.

Table 4.2. IR Absorption Assignment for PS/PVME blends at room temperature.

| Assignments	Wavenumbers (cm^{-1})		
	PS	PVME	Blend
C - H aromatic stretching vibration	3002 - 3103	-	3001 - 3102
C - H asymmetrical stretching vibration of CH	2924	2931	2926
C - H symmetrical stretching vibration of CH$_2$	2850	2886	2850, 2883
C - H asymmetrical stretching vibration of CH$_3$	-	2969	2969
C - H stretching vibration of CH$_3$	-	2820	2820
C - C stretching frequency of ring in plane	1601	-	1601
C - H stretching vibration of ring in plane	1583	-	1583
C – H bending vibration of CH$_2$	1493	-	1493
C - H bending vibration of CH$_2$	1452	-	1452
C - H deformation of CH$_3$	-	1462	-
C - O stretching vibration	-	1132	1131
C - C stretching vibration	-	1107	1107
CH$_3$ rocking mode	-	1085	1085
C - H bending vibration of ring in plane	1069	-	-
C - H bending vibration of ring in plane	1028	-	1028
C - H out - of - plane bending vibration of ring	840	-	840
C - H out - of - plane bending vibration of ring	756	788	758
C - H out - of - plane bending vibration of ring	698	-	700
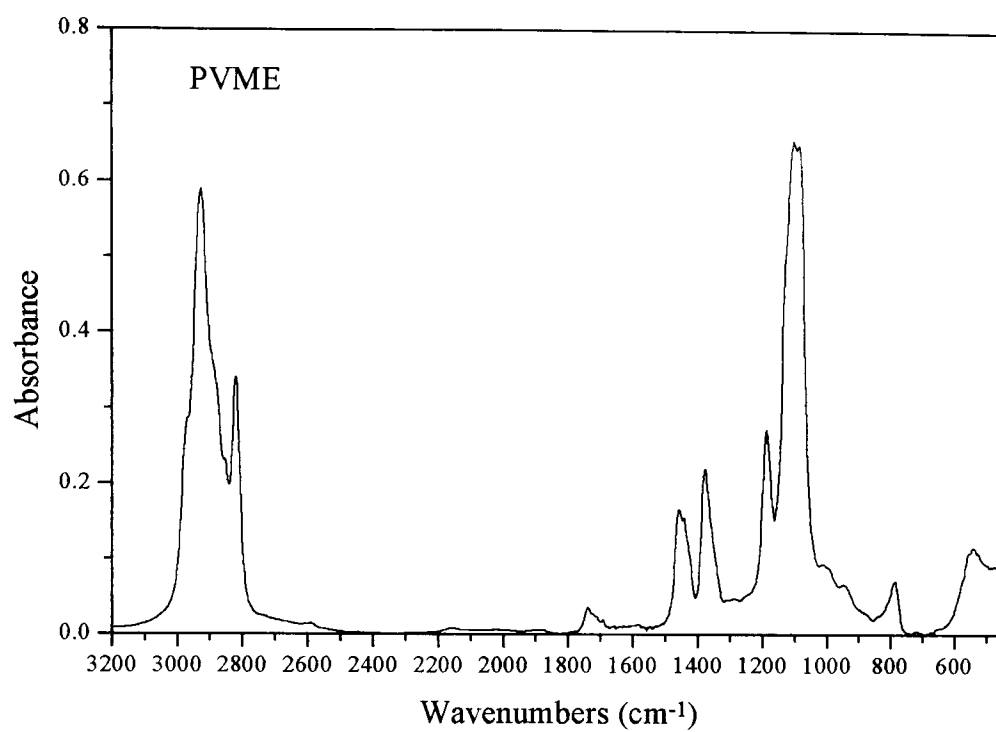
Figure 4.11   Infrared spectrum of Pure PVME prepared from toluene solution and measured at room temperature.
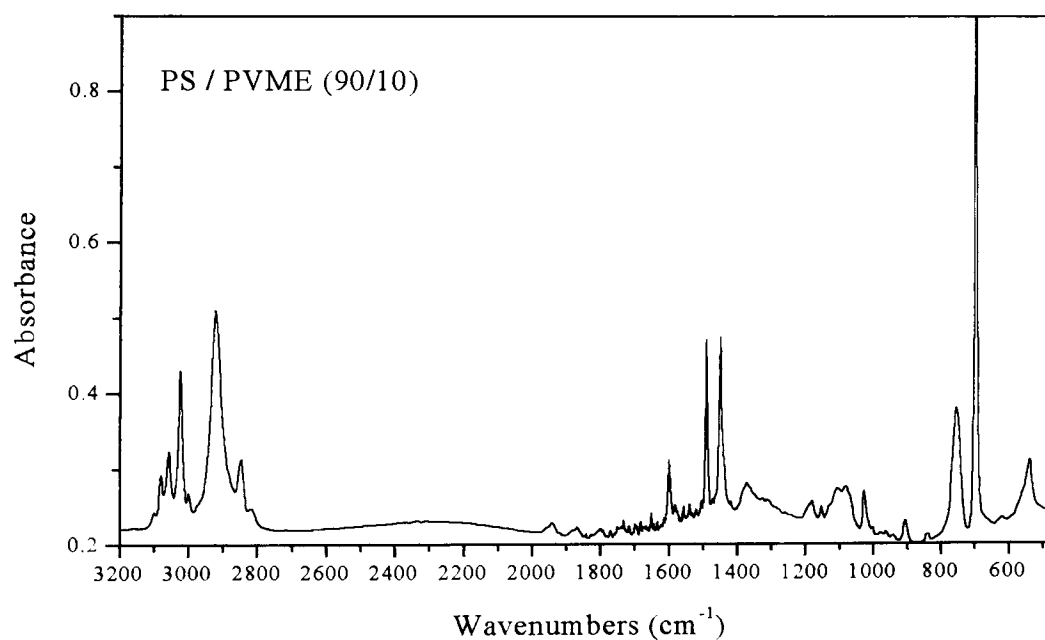
Figure 4.12   Infrared spectrum of compatible 90:10 (w/w) PS/PVME blends in toluene.
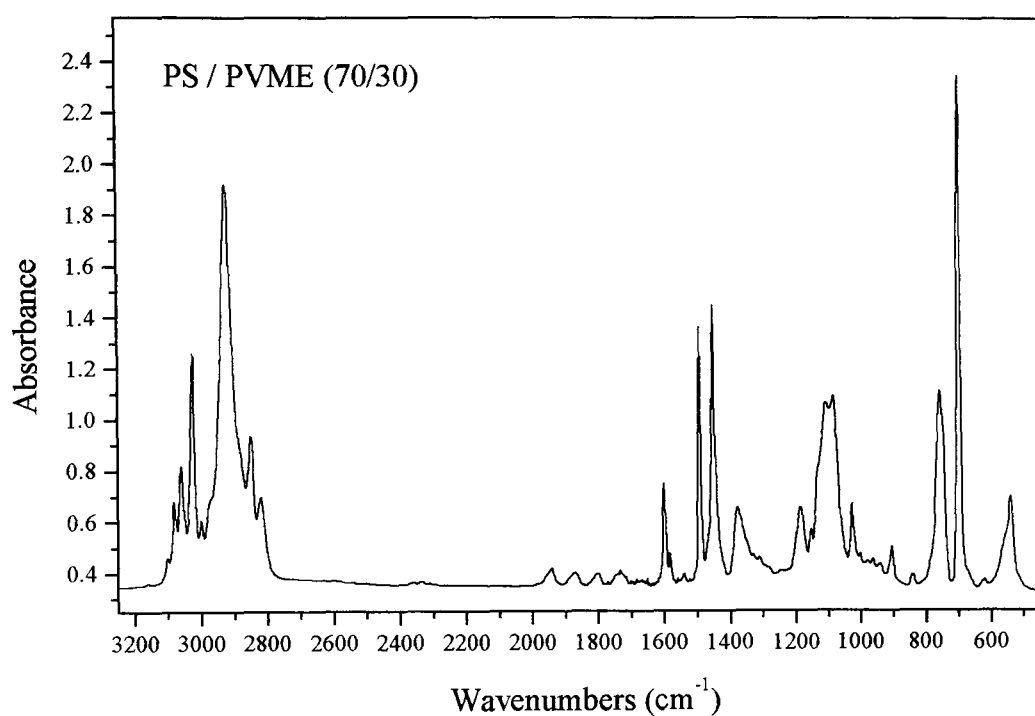
Figure 4.13 Infrared spectrum of compatible 70:30 (w/w) PS/PVME blends in toluene.
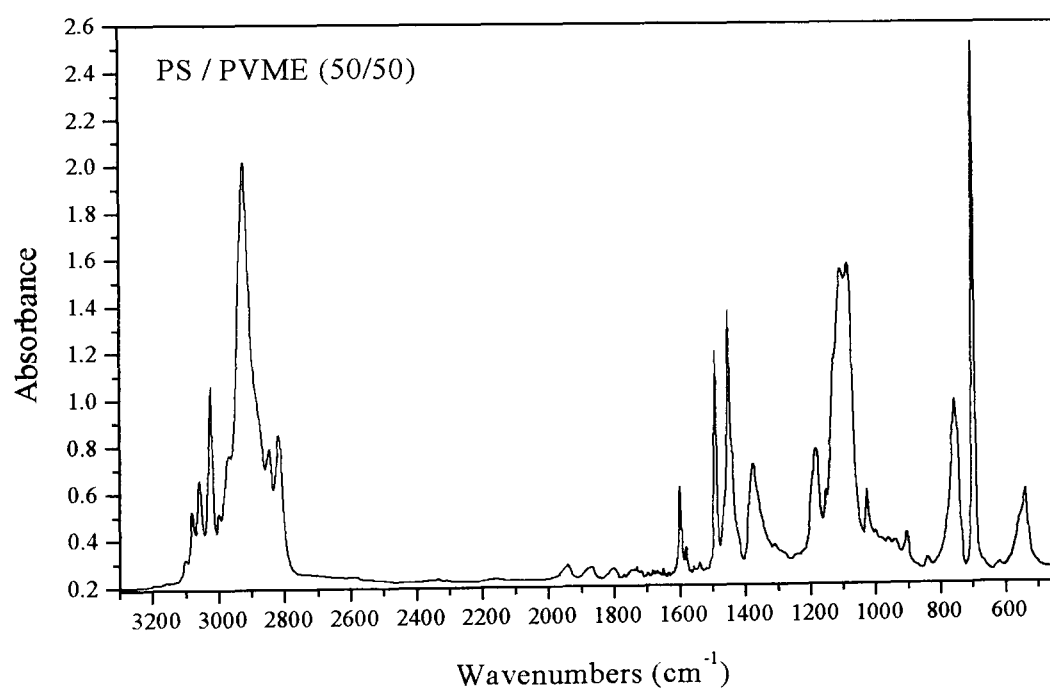
Figure 4.14 Infrared spectrum of compatible 50:50 (w/w) PS/PVME blends in toluene.
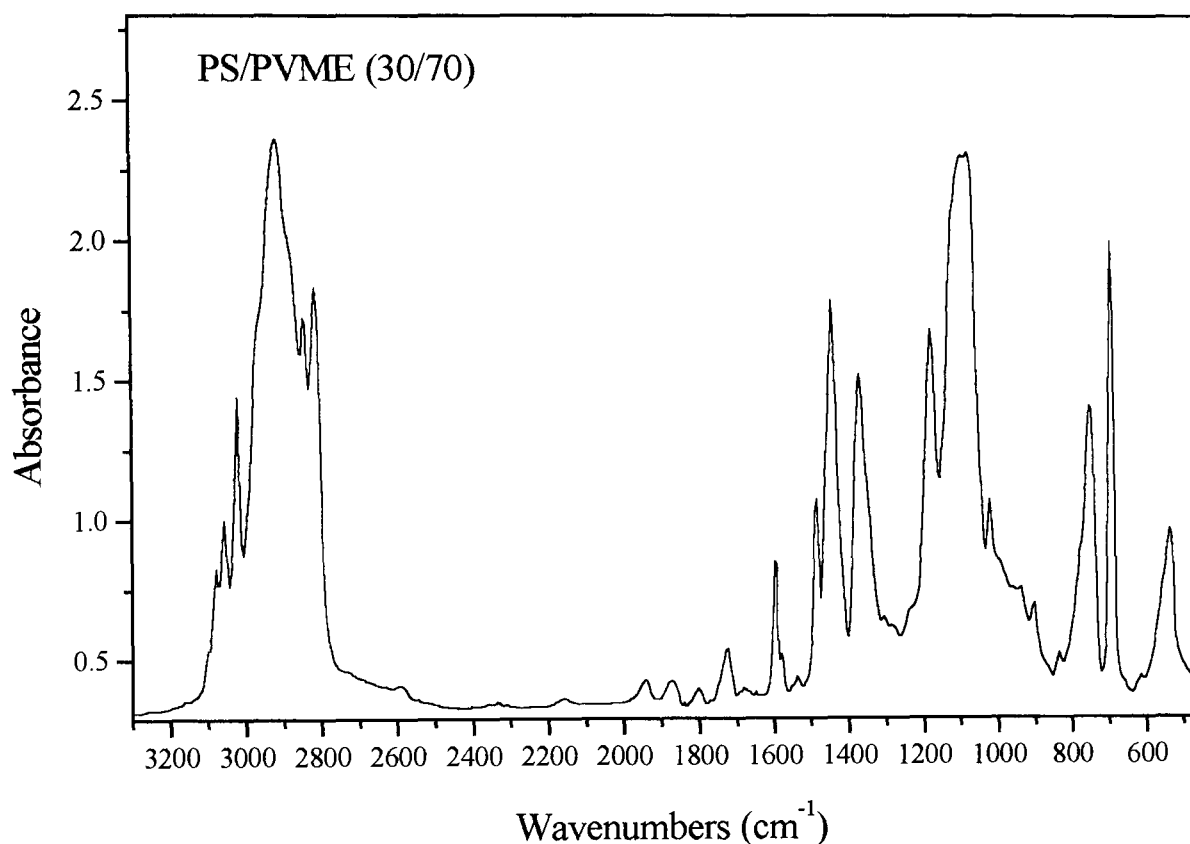
Figure 4.15 Infrared spectrum of compatible 30:70 (w/w) PS/PVME blends prepared from toluene solution and measured at room temperature.

The assignment of the C-H stretching bands of molecules with a $(CH_2)_{n-2}$ chain has been the object of several experimental and theoretical studies[40-45]. The generally accepted assignment of the asymmetric and symmetric methylene stretching modes corresponds to the bands observed in the infrared spectra at around 2925 and 2850 cm^{-1}, respectively. The symmetric stretching of the methyl group occurs at 2870 cm^{-1}, and a band assigned to the asymmetric CH_3 stretching is measured at about 2960 cm^{-1}. The aromatic stretching vibration is also expected around 3000 to 3100 cm^{-1}.

Figure 4.16 Infrared spectra of pure PS at high-frequency in the 3200 to 2700 cm^{-1}

regions measured at room temperature.

Figure 4.16 and 4.17 show the FTIR spectra of PS and PVME, respectively in the high-frequency region from 2700 to 3200 cm^{-1}. The high-frequency spectra of PS consist of seven absorption bands. The bands with peak locations at 3002, 3026, 3060, 3082 and 3103 cm^{-1} are due to the C-H stretching of benzene ring CH groups on the PS side chain. The bands with peak positions of 2924 and 2850 cm^{-1} are due to the C-H stretching vibration of the CH and CH$_2$ groups on the main PS chain, respectively. The high-frequency spectrum of PVME consists of four absorption bands. The bands with peak positions at 2886, 2931, and 2969

104

cm^{-1} are due to the C-H stretching vibration of the CH$_2$, CH and CH$_3$ groups on the main chain, respectively. The band at 2820 cm^{-1} is the C-H stretching of the CH$_3$ group of the methoxy side chain, as shown in figure 4.17. In this region, three peaks were found most sensitive to the changes in the composition of PS/PVME blends. These are the band at 2820 in PVME, and in PS the bands appearing at 2850 and 2924 cm^{-1} (figures 4.18 – 4.21).
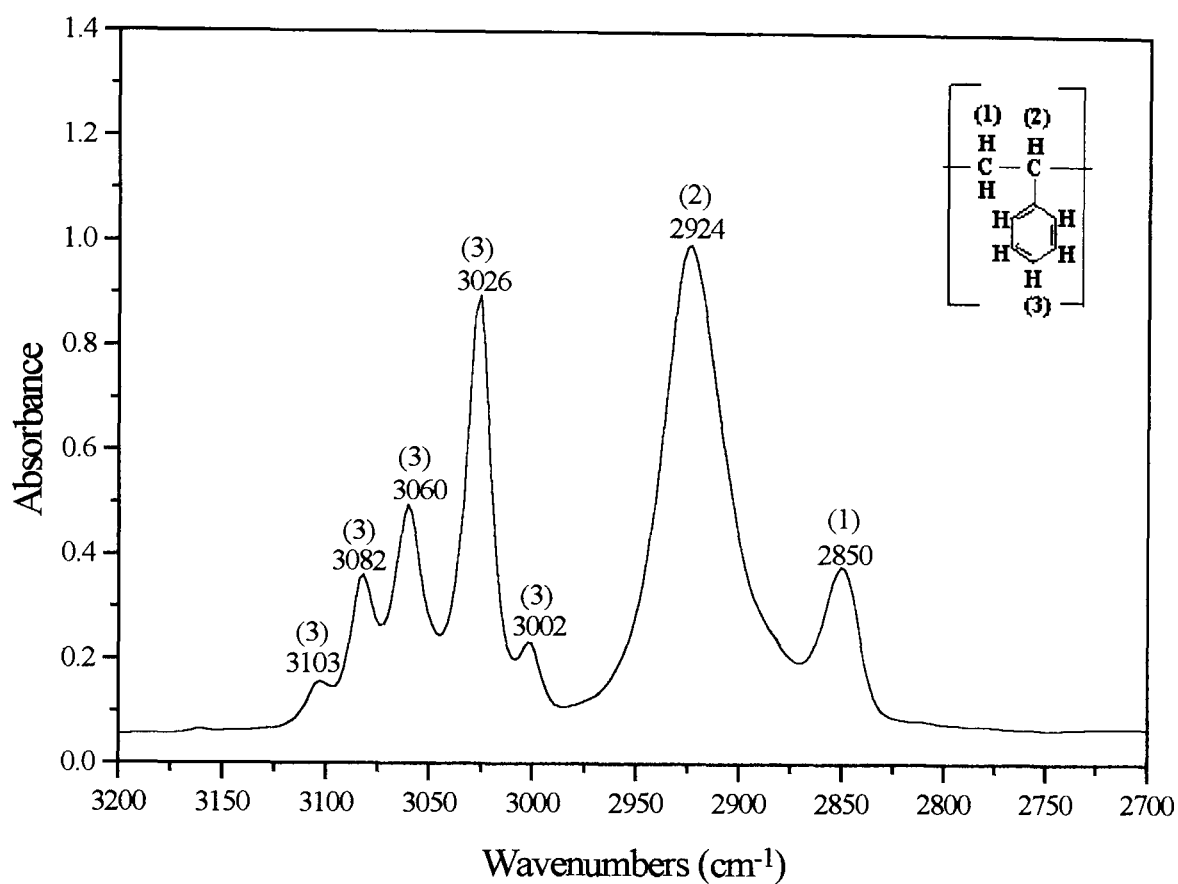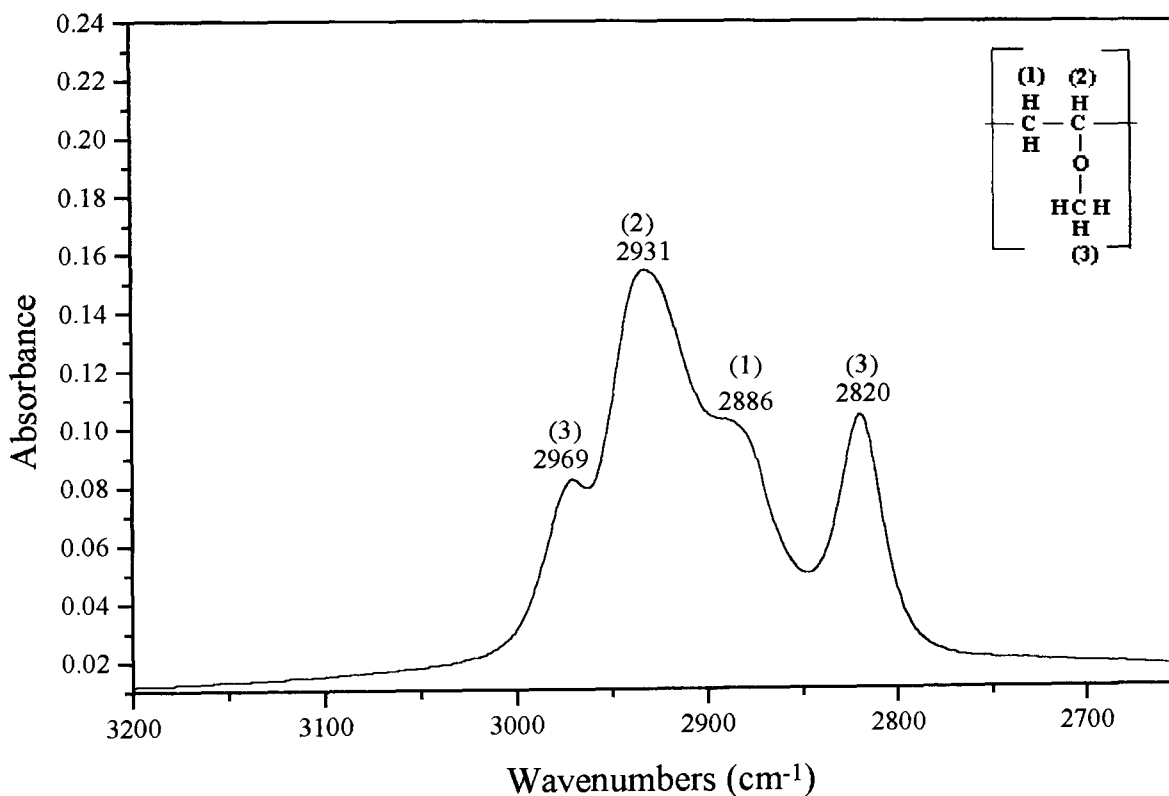

Figure 4.17 Infrared spectrum of PVME at high-frequency in the 3200 to 2650 cm^{-1} region measured at room temperature.
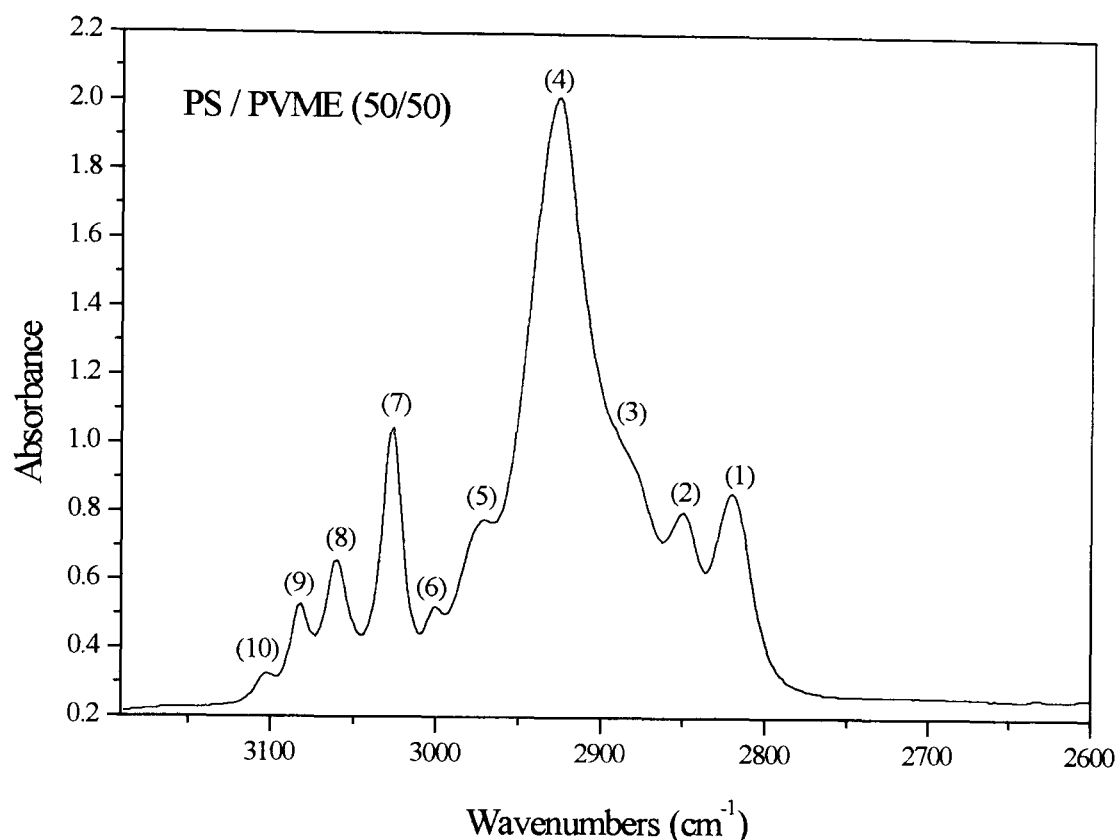
Figure 4.18 Infrared spectrum of 50:50 (w/w) PS/PVME blends at room temperature in high frequency from 3200 to 2600 cm^{-1} regions. Peak frequencies (1) - (10) are 2820, 2850,2886,2926,2971, 3001, 3026, 3060, 3082, and 3103 cm^{-1}, respectively.

Figure 4.18 shows the FTIR spectrum of the 50/50 (w/w) PS/PVME system. The seven absorption bands of PS and the four bands of PVME in the high-frequency region combine to give ten bands with the PS and PVME bands at 2926 cm^{-1} superimposed. However, it was observed that the band which is assigned to C - H stretching of the CH group on the main PS chain at 2924 cm^{-1} in pure PS shifts slightly to higher frequency when PS blends with PVME. This difference in peak position can be expected from simple addition of two closely spaced broad peaks of different absorbance and cannot be interpreted as a result of some

interactions. As shown in figure 4.22 (the spectrum of a (50:50) PS/PVME and SPS/PVME blends at room temperature) this band is found at 2926 cm^{-1} in both sulfonated and unsulfonated blends. Previous studies [14,46] have shown that similar small changes in position of the CH out-of-plane bending vibration of PS in the lower frequency region of the spectrum (700 cm^{-1} region) occur with blending. However, no significant change in position or shape of the absorption bands was observed in the above work in the higher frequency region of the spectrum as a function of temperature and compatibility, as we demonstrated here.
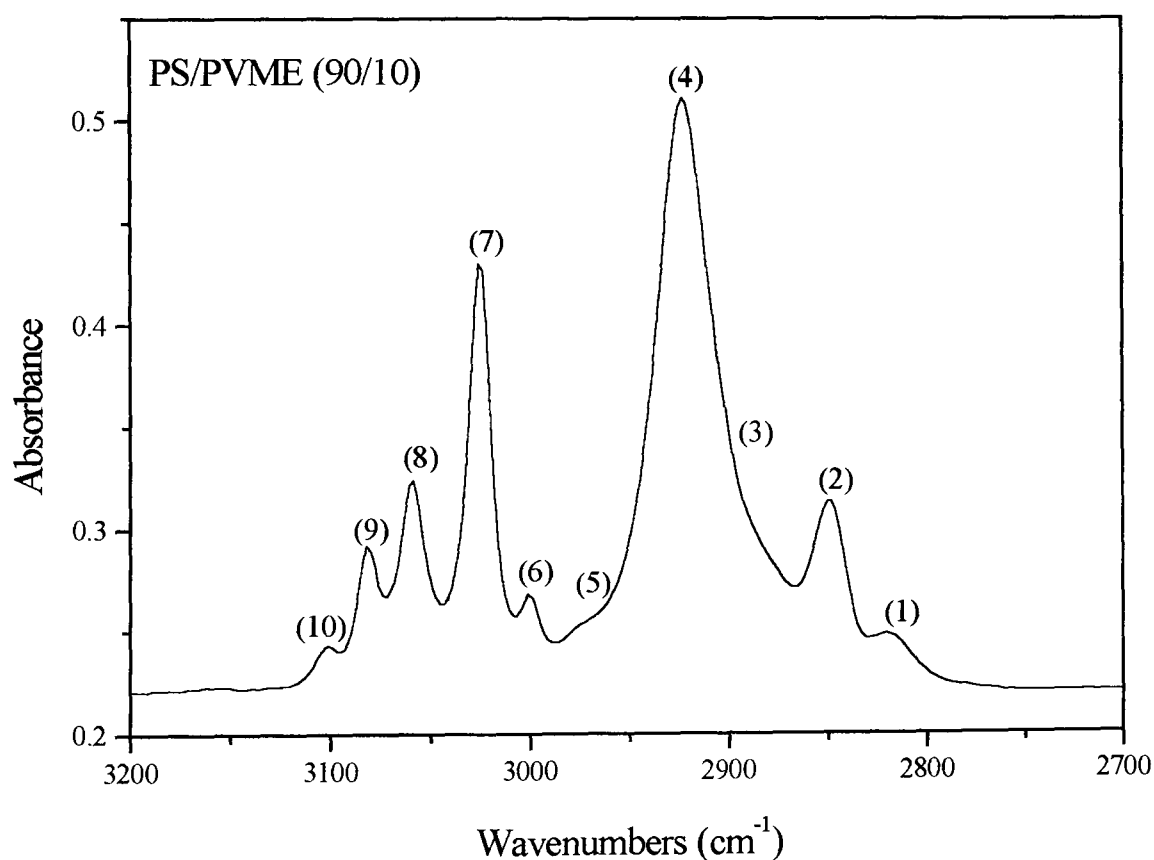
Figure 4.19 Infrared spectrum of 90:10 (w/w) PS/PVME blends in the high frequency region.
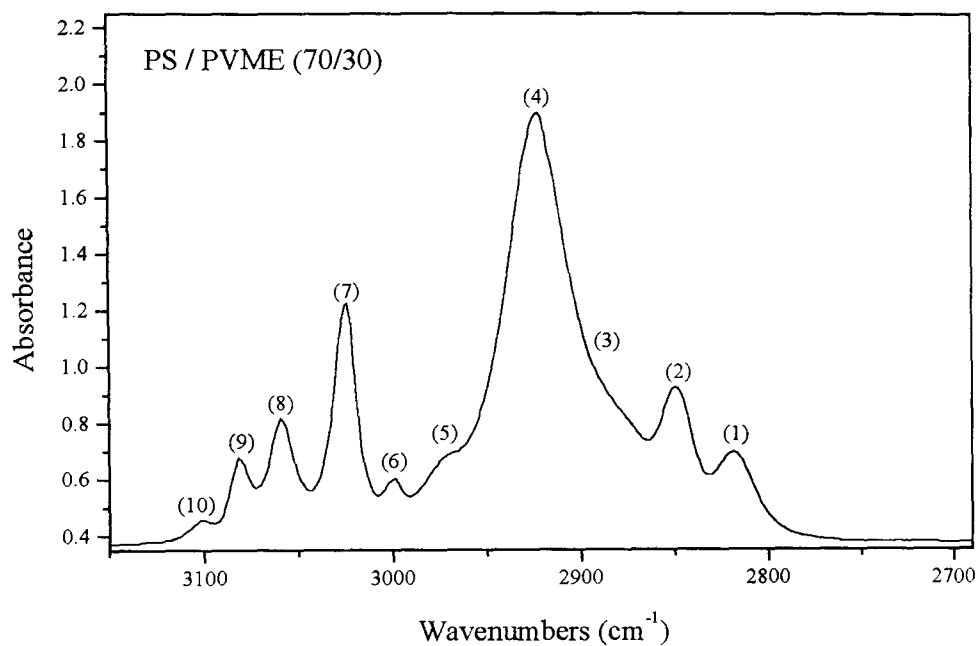
Figure 4.20   Infrared spectrum of 70:30 (w/w) PS/PVME blends in high frequency regions.
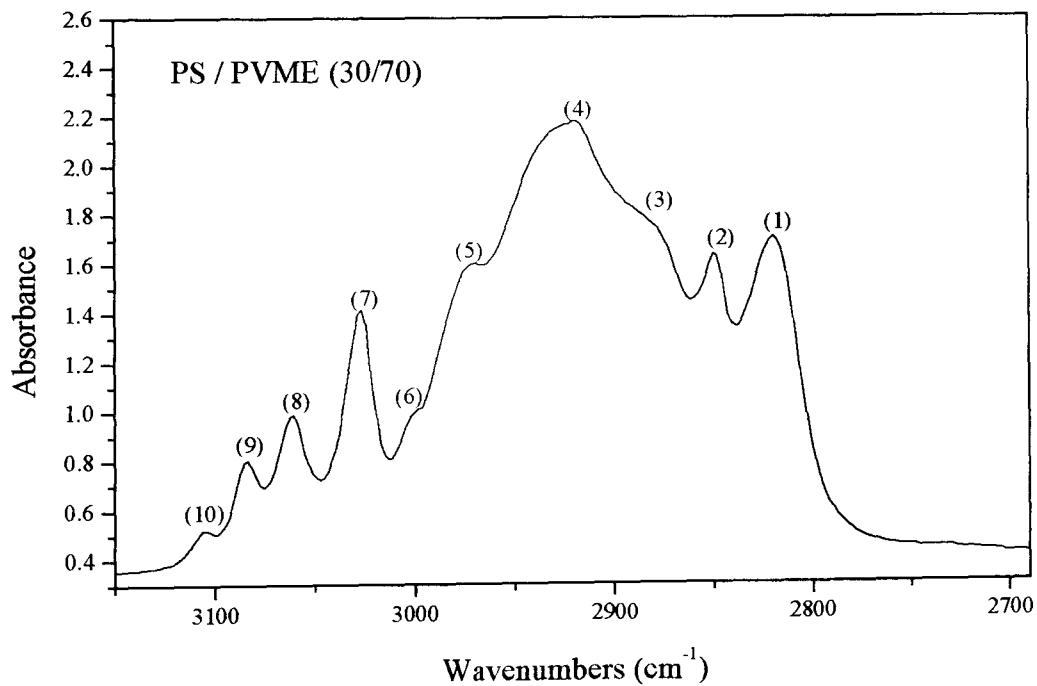
Figure 4.21   Infrared spectrum of 30:70 (w/w) PS/PVME blends in high frequency regions.
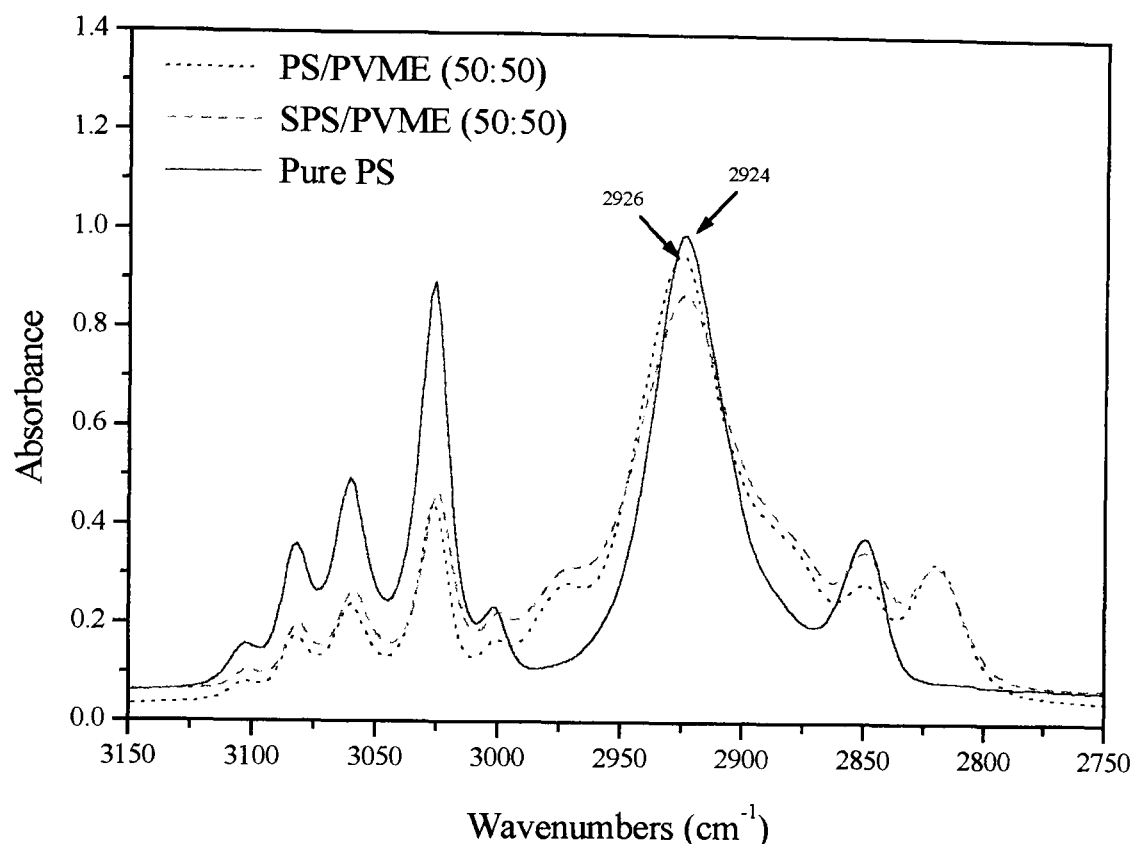
Figure 4.22 Infrared spectrum (2750 - 3150 cm^{-1}) of PS and 50/50 PS/PVME, SPS/PVME blends at room temperature.

Figure 4.23 shows the 1350 to 1650 cm^{-1} spectral range for PS, PVME and 50/50 PS/PVME blends. In this spectral range two bands assigned to the bending of CH_2 in the chain and to the bending of CH_2 unit are observed at almost constant wavenumbers of 1452 and 1493 cm^{-1} respectively [47,48] and the intensity of these absorption bands is almost the same. The antisymmetrical band of CH_3 group is also expected around 1455 to 1465 cm^{-1} and in fact a band near this frequency is observed in the spectrum of PVME. The proximity of CH_3 band (1462 cm^{-1}) to the one ascribed to CH_3 bending is probably the reason why it cannot be identified in all the spectra. For instance the bands at 1462 and 1452 cm^{-1} merge into one band and this band remains in all spectra of PS/PVME

blends. The fact that the band ratio 1452/1493 cm^{-1} is enhanced in the blend confirms its dependence on the number of CH_2 units. The presence of the shoulder at 1462 cm^{-1} clearly indicates that this is the case.

Figure 4.23 Infrared spectrum (1350 - 1650 cm^{-1}) of PS, PVME and 50/50 PS/PVME blends measured at room temperature. Absorption bands: 1, 1493 cm^{-1}, absorbance 0.907; 2, 1452 cm^{-1}, absorbance 0.92; 3, 1493 cm^{-1}, absorbance 0.476; 4, 1452 cm^{-1}, absorbance 0.593. 1-2 (0.013), 3-4 (0.117).

The spectra in the 1000 to 1250 cm^{-1} regions are interesting not only because of the presence of CH_3 rocking and C - O stretching mode, but also due to the presence of symmetric and asymmetric vibration of sulfonation groups[49,50]. The sulfonic anions have two active stretching vibrations: (1) a symmetric stretching

vibration at 1043 cm⁻¹ and (2) an antisymmetric stretching vibration at about 1200 cm⁻¹.

Figure 4.24 shows the spectrum of PVME: a strong doublet at 1085 and 1107 cm⁻¹ with a shoulder at 1132 cm⁻¹. The bands at 1100 cm⁻¹ have been usually assigned to the C - O stretching mode, but could also contain contributions from CH₃ rocking and C- C stretching modes [49]. It is seen that the intensity of the 1085 cm⁻¹ band is greater than that of the 1107 cm⁻¹ components in all the blends due to the contribution of 1069 cm⁻¹ of C-H in-plane bending vibration of PS ring. As the PVME content in the blend increases, the 1107 cm⁻¹ band becomes more prominent in comparison to the 1085 cm⁻¹ band. The SPS/PVME blend also shows similar changes to that of the PS/PVME blends except the appearance of sulfonation peaks at 1229, 1043, and 1011 cm⁻¹, as shown in figure 4.25.

Lu et al[14] reported that PVME has a strong doublet at 1085 and 1107 cm⁻¹ with a shoulder at 1132 cm⁻¹, and the relative intensity of this doublet varies considerably when the PVME sample is cooled or heated. Thus, they concluded that the relative intensity of this doublet was sensitive to the miscibility of the PS/PVME blends, and that the intensity of this 1085 cm⁻¹ peak was greater than that of the 1107 cm⁻¹ peak for the miscible blend.

According to these studies, the absorption band at high wavenumber (1107 cm⁻¹) in PVME increases with the inhomogeneity in the blends induced by heating. Since the relative intensity of the particular band at high wavenumber reflects the population of the rotation isomers of the ether group, the absorption spectra imply that the rotation of the ether groups of PVME chains in the PS/PVME blend is restricted by stronger attraction between the oxygen atoms of the ether unit of PVME chains and the phenyl rings of PS chains [14]. This conclusion contradicts our interpretation of IR spectra obtained by a more accurate data

analysis (as discussed below) and also the results obtained by quasielastic neutron scattering [16]. It can be seen from Figure 4.24; that the contribution from PS peak is small. In addition, the absorbance (peak height) is critically dependent on sample geometry, spectrometer throughput and temperature. Accurate subtraction can only be done if the baseline, specimen thickness and peak broadening are known. None of this procedure has been reported by Lu et al [14]. These authors also do not explain how molecular interaction will affect peak height. After a careful study of the behaviour of these peaks and subtraction of PVME and PS peaks, the conclusion was, that this evidence[14] for molecular interaction is unreliable
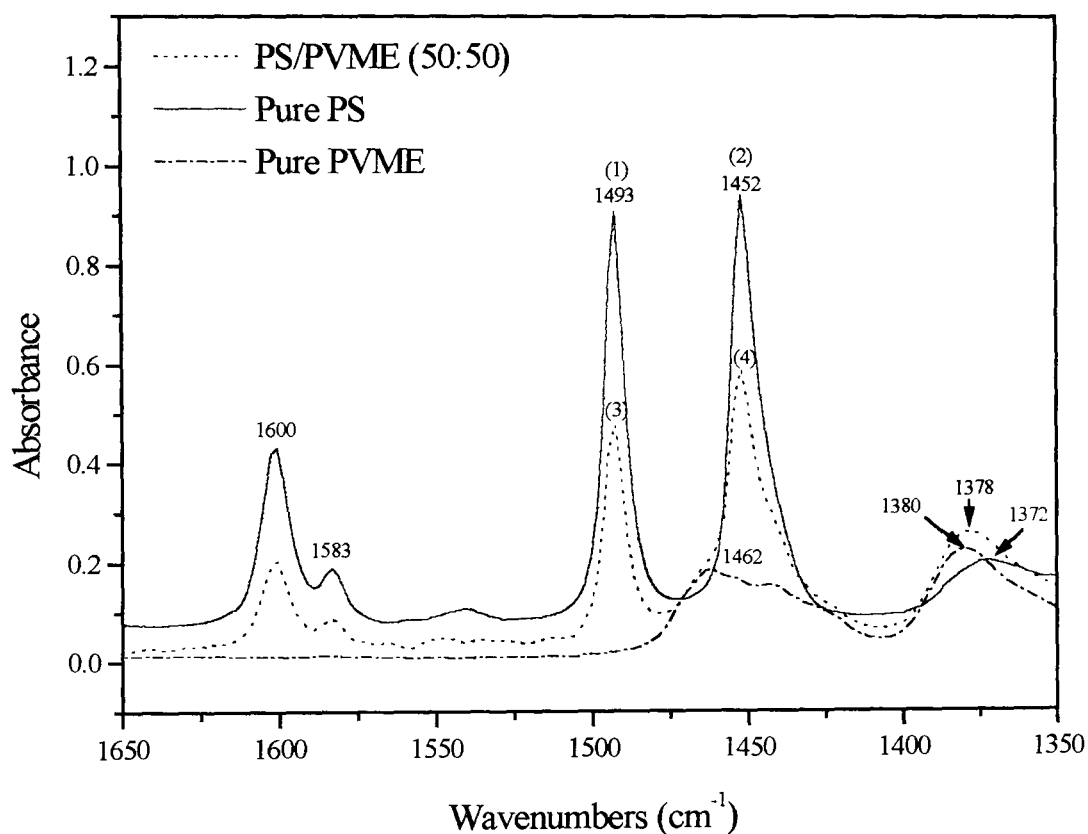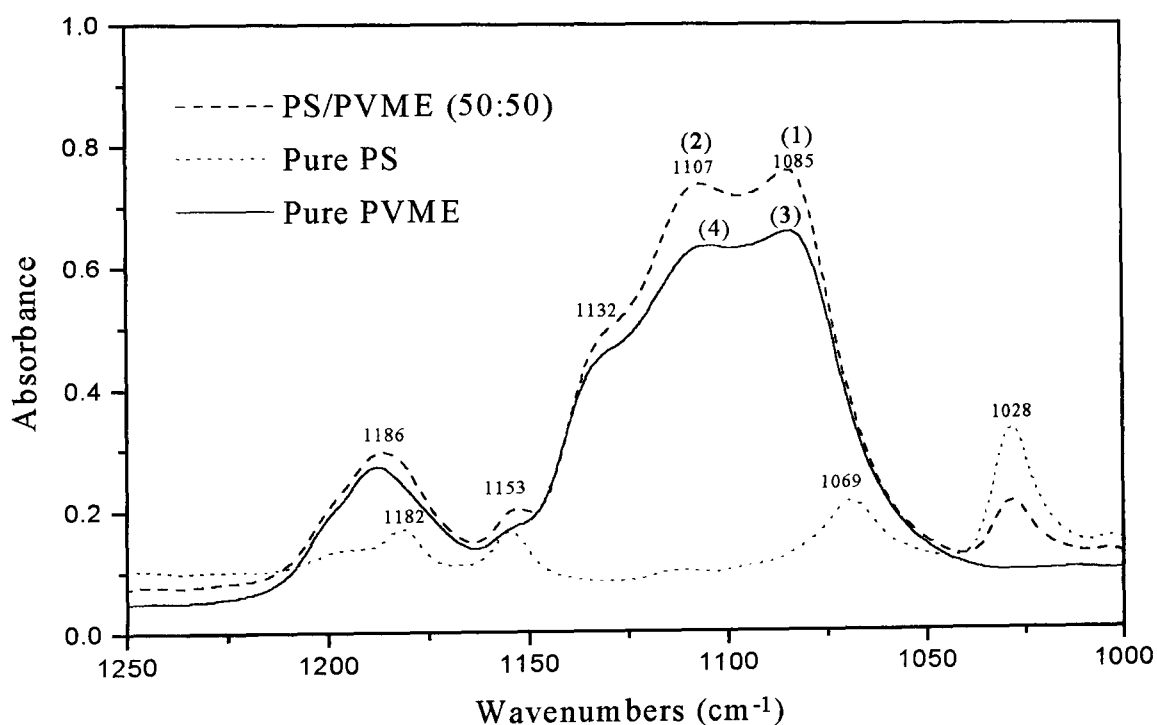

Figure4.24   Infrared spectrum (1000 - 1250 cm⁻¹) of PS, PVME and 50/50 PS/PVME blends measured at room temperature. Absorption band: 1, 1085 cm⁻¹, absorbance 0.760; 2, 1107 cm⁻¹, absorbance 0.728; 3, 1085 cm⁻¹, absorbance 0.655; 4, 1107 cm⁻¹, absorbance 0.635.
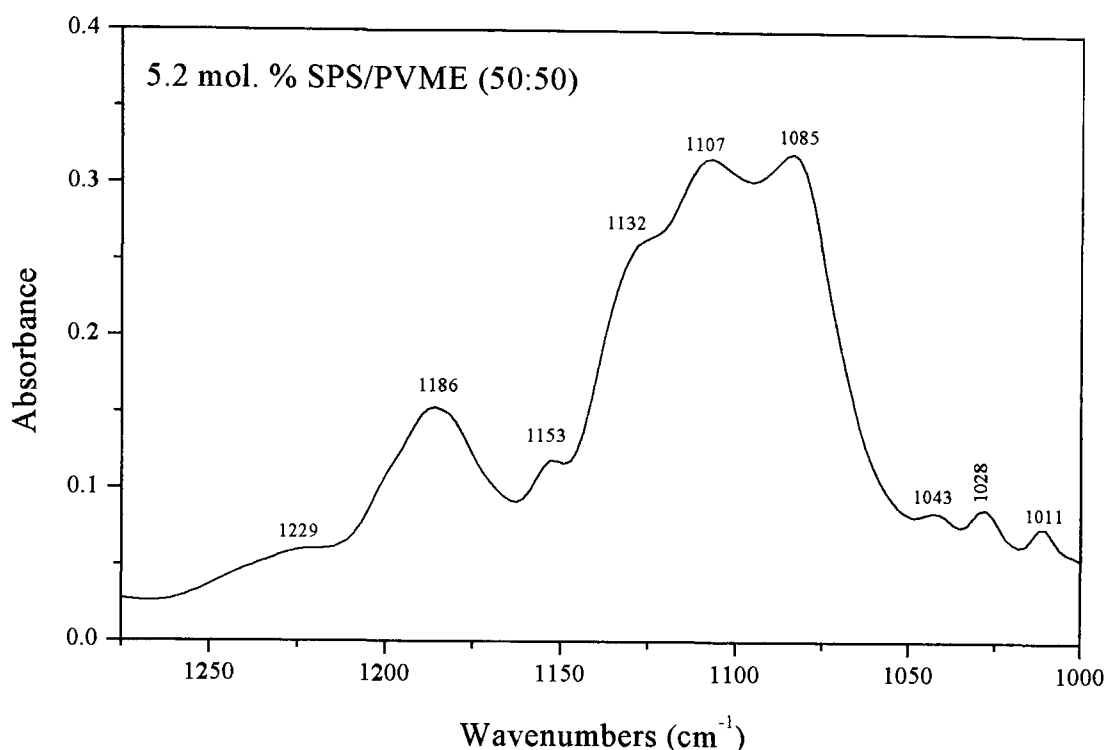
Figure 4.25 Infrared spectrum (1000 – 1275 cm^{-1}) of SPS/PVME (50:50) blends measured at room temperature.

In the 670 to 830 cm^{-1} region, there are two benzene ring vibrations which involve out-of-plane ring bending by quadrants as shown in figure 4.26. The absorption bands at 756 cm^{-1} in pure PS and 788 cm^{-1} of PVME, when combined show one intermediate absorption peak between these two, appearing at 758 cm^{-1} in the blends. The intensity of this band is higher than both absorption bands. On the other hand, as shown in figure 4.26, the C-H out-of-plane bending vibration of the phenyl rings on PS were also shifted with the concentration of PVME. This band is found at 700 cm^{-1} in (50:50) PS/PVME blend, but in pure PS it is located at 699 cm^{-1}. Lu et al[14] reported that this C-H out-of-plane bending vibration is most sensitive to phase compatibility. For incompatible blends of PS/PVME such as the film cast from trichloroethylene or chloroform solution,

the peak maximum is usually found at an intermediate position between the two

extremes.
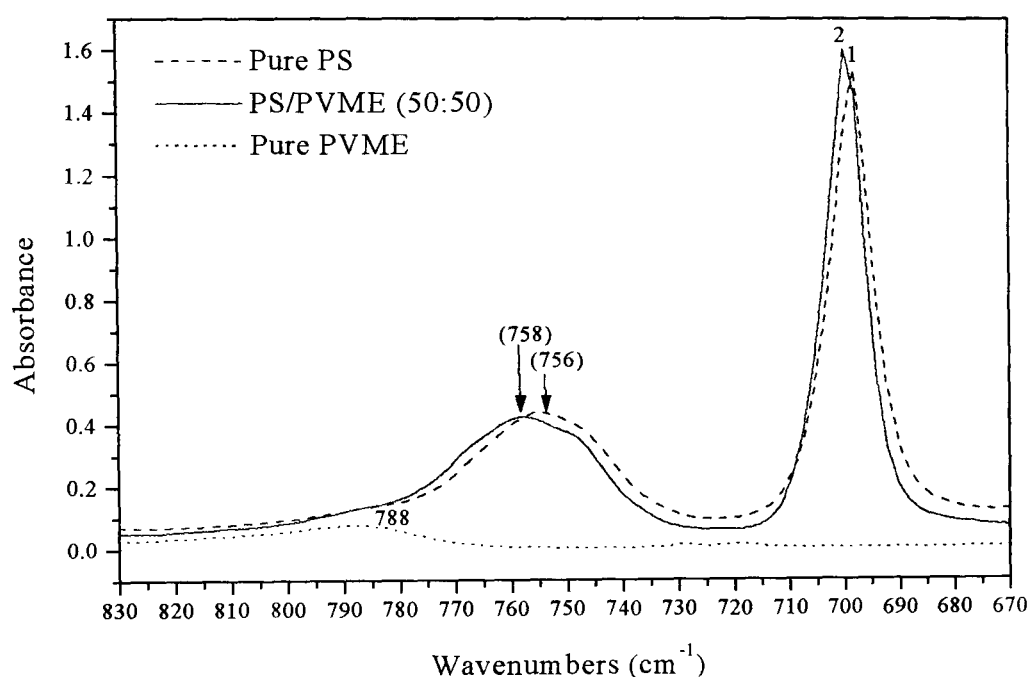
Figure 4.26   Infrared spectrum (670 - 830 cm^{-1}) of PS, PVME and 50/50 PS/PVME blends at
room temperature. C − H out-of-plane bending vibration of PS in bulk and
PS/PVME (50:50). 1, 699 cm^{-1}; 2, 700 cm^{-1}.

Therefore the vibrational frequencies of C − H bond on phenyl ring in PS at

different compositions of PS/PVME blends are plotted against the weight

fraction of PVME (figure 4.27). Careful examination of figure 4.27 shows that

the peak position moves to higher frequencies with increasing concentration of

PVME in the blends. The interpretation of these results [14] was that a certain

molecular interaction exists between the phenyl ring of PS and COCH$_3$ of

PVME. Hence this interaction is deemed to be an important factor which governs

the miscibility of the blend of PS/PVME.
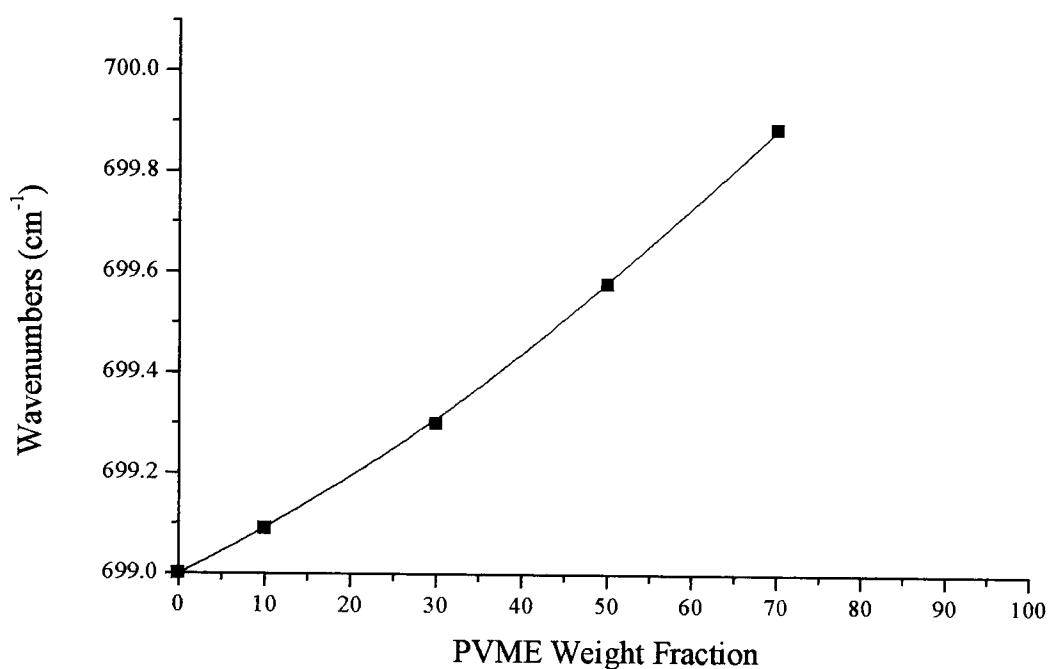
Figure 4.27. The frequency of the C – H out-of-plane phenyl ring of PS in blends with PVME, verses weight fraction of PVME, at room temperature.

To understand the role played by intermolecular interactions in the miscibility and phase behaviour of PS/PVME blends, it is crucial to examine the nature of interaction of homopolymers and blends at different temperatures. We were also particularly interested in whether such measurements can be used to distinguish between thermal behaviour of spectral changes observed on homopolymers and miscibility effects of PS/PVME blends. The changes in spectra of pure PS, PVME and 50:50 blend are shown in Figure 4.28 to 4.30 respectively. Spectra for different temperatures are plotted together, to show the spectral shift and peak broadening. Some peaks show no shift or broadening, others shift and broaden simultaneously. Only the peak at 758 cm^{-1} (Figure 4.30c) shows pure shift to lower wave numbers. The peak at 699 cm^{-1} is very intene and can be measured accurately for very thin samples only, but the shift is clearly visible. The peak height is also temperature dependent and some peaks increase with temperature, other decrease. This is most clearly observed for peaks at 1107 and 1085 cm^{-1}.
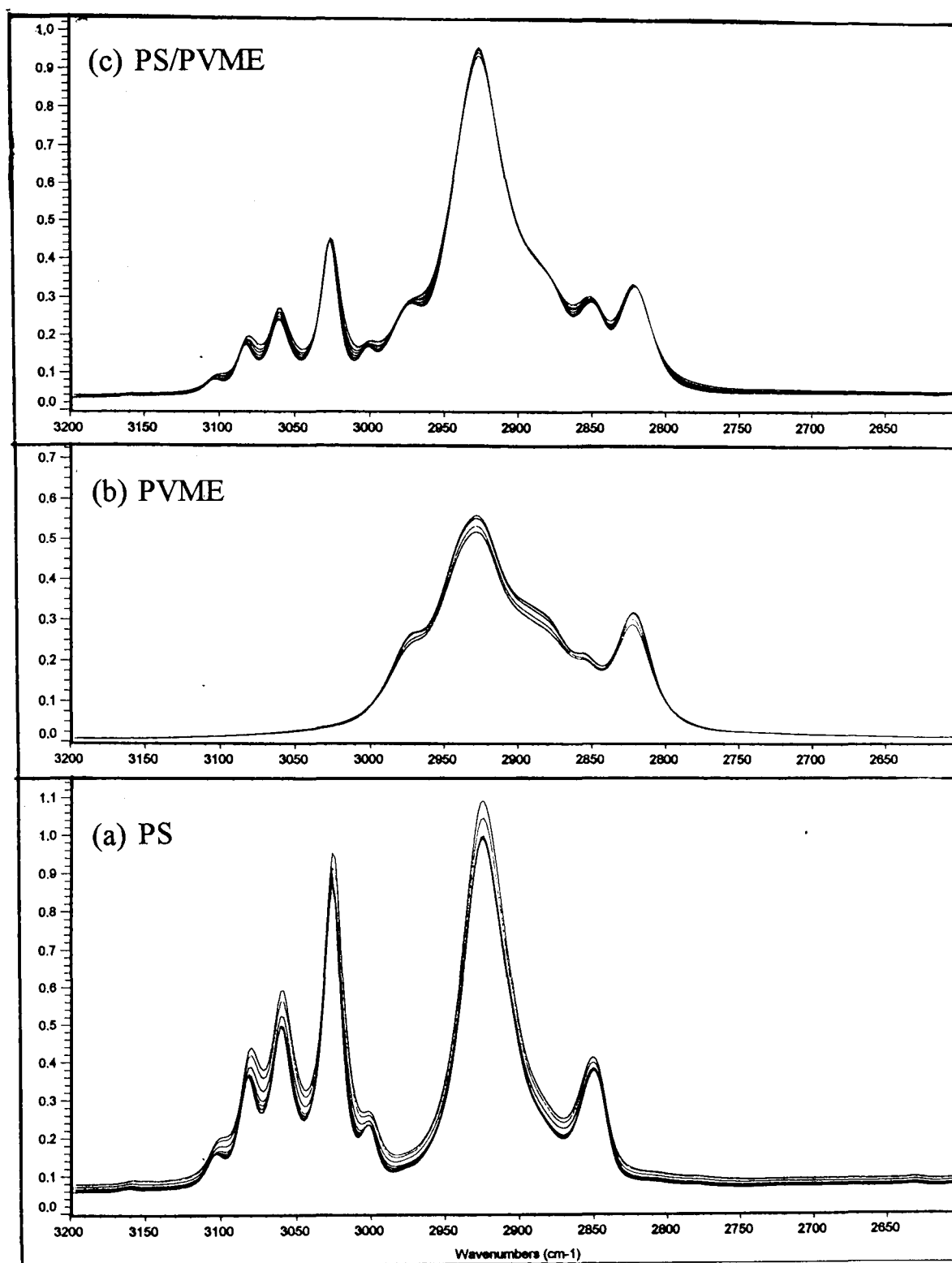
Figure 4.28   Infrared spectrum (3200 – 2500 cm^{-1}) of PS, PVME and 50:50 PS/PVME blends measured from room temperature up to 160°C in seven steps (25,50,75,100,125,150,160°C).
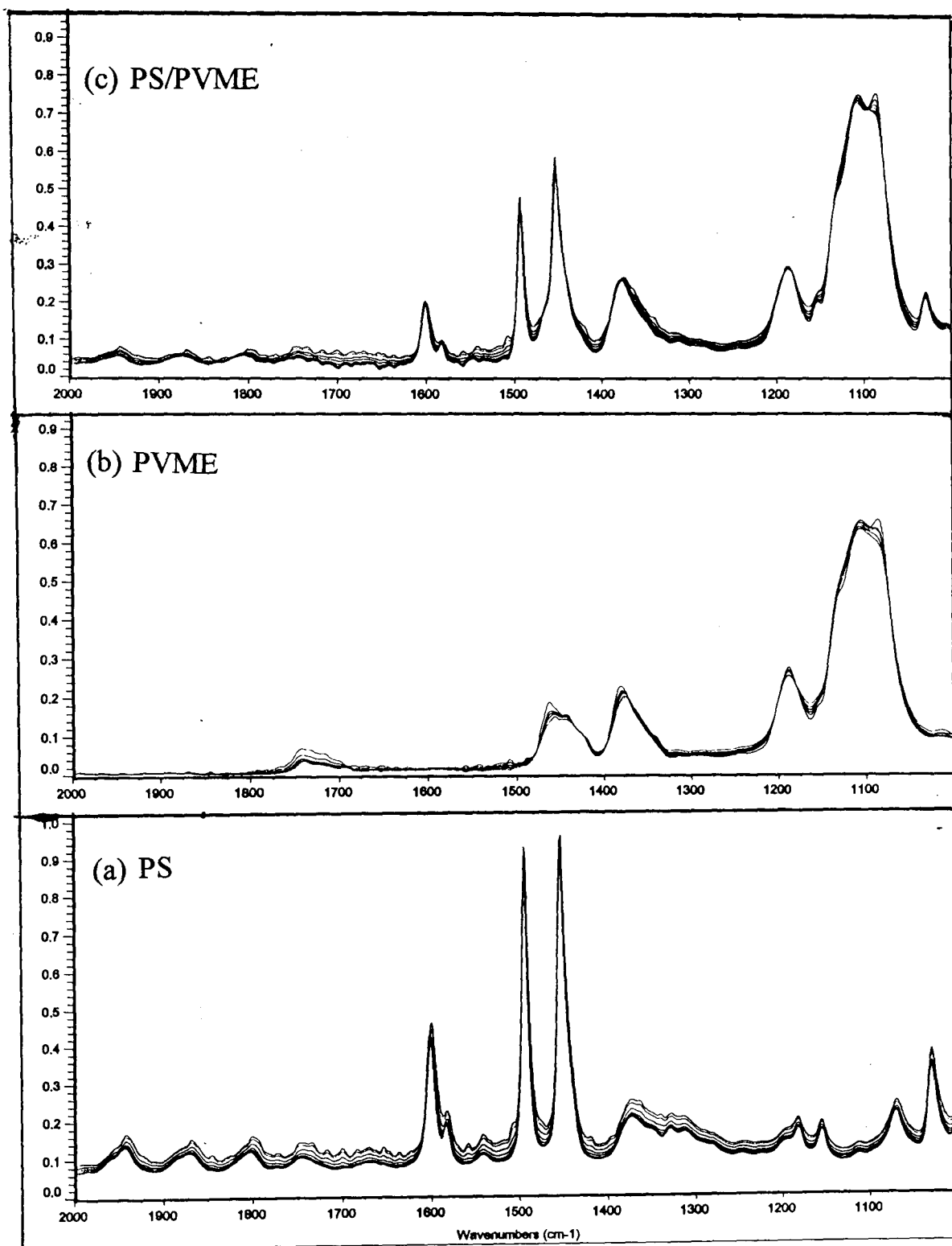
Figure 4.29 Infrared spectrum (2000 – 1000 cm⁻¹) of PS, PVME and 50:50 PS/PVME blends measured from room temperature up to 160°C in seven steps (25,50,75,100,125,150,160°C).
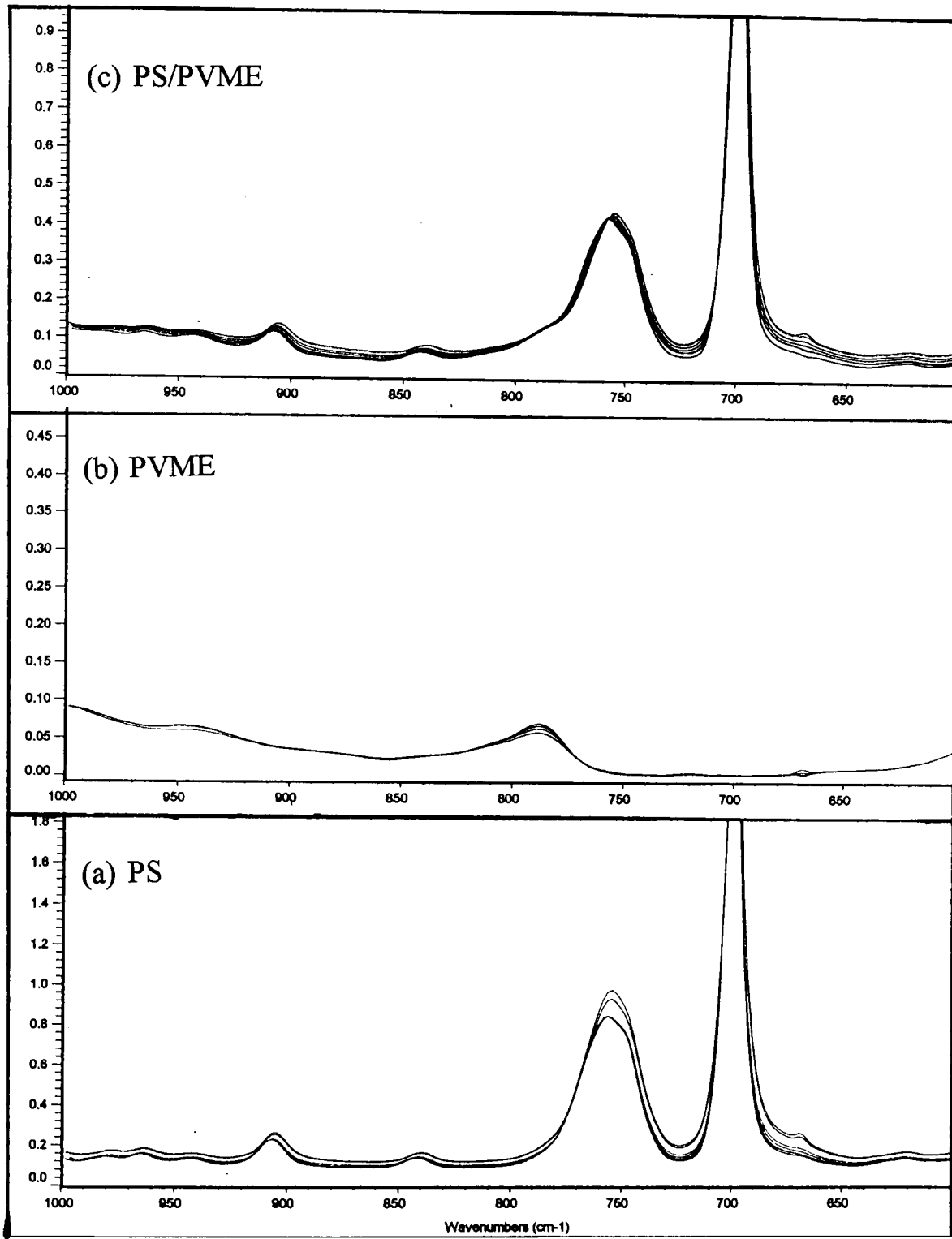
Figure 4.30 Infrared spectrum (1000 – 600 cm^{-1}) of PS, PVME and 50:50 PS/PVME blends measured from room temperature up to 160°C in seven steps (25,50,75,100,125,150,160°C).
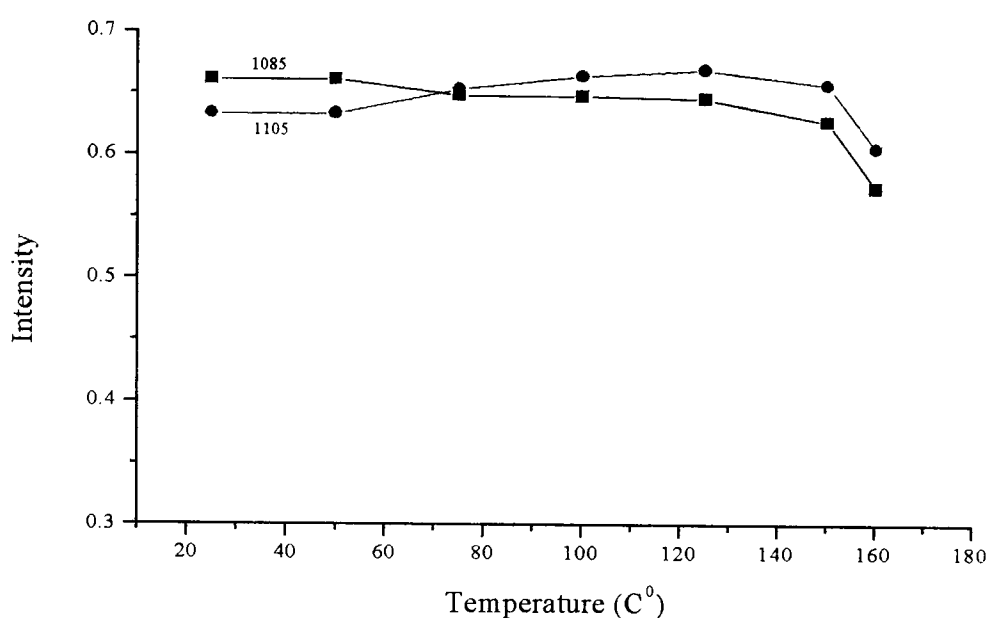
Figure 4.31 Relative intensity of doublet of 1100 cm^{-1} regions in pure PVME recorded from room temperature to 160°C.

Figure 4.29(b) and (c) show the FTIR spectra in the C − O stretching vibration of COCH$_3$ group in pure PVME and (50/50) PS/PVME blend, respectively. The relative intensity of the doublet at 1107 and 1085 cm^{-1} of PVME shows changes with temperature, but this change is similar to that observed in pure PVME as well as in blends. Their relative intensities changed substantially with temperature, but the position of these two bands did not change in pure PVME and also when blended with PS. The 1107 cm^{-1} component dominates at high temperatures, whereas the 1085 cm^{-1} component dominates at low temperatures, as reported previously [13,14,52]. The changes in peak height for this doublet are shown in Figure 4.31 for PVME and in Figure 4.32 for the blend. The reduction of peak height at 160°C for the PVME is most likely the result of spectrometer instability. The spectral shift can also be plotted and shows similar behaviour for both pure PVME and the blend. The only shift observed for all temperature is the 758 cm^{-1} peak, which is about 1.5 cm^{-1} higher for the blend than for PS for all

temperatures (see Figure 4.33). This is the only positive reliable result which indicates molecular interaction.
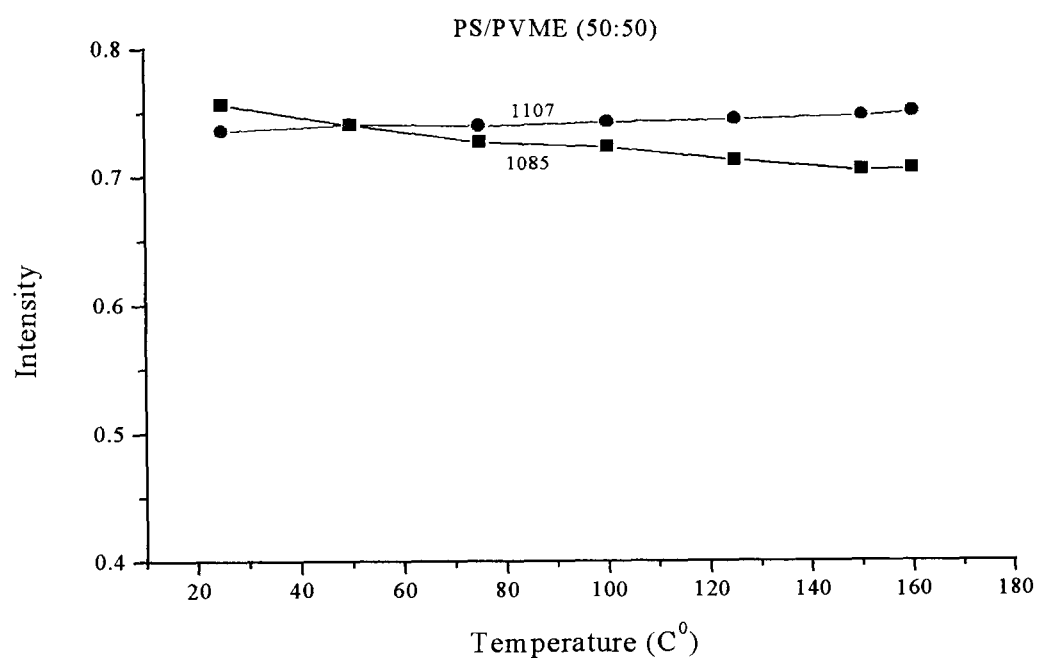
Figure 4.32   Relative intensity of doublet of 1100 cm^{-1} regions in PS/PVME (50:50) blends recorded from room temperature to 160°C.
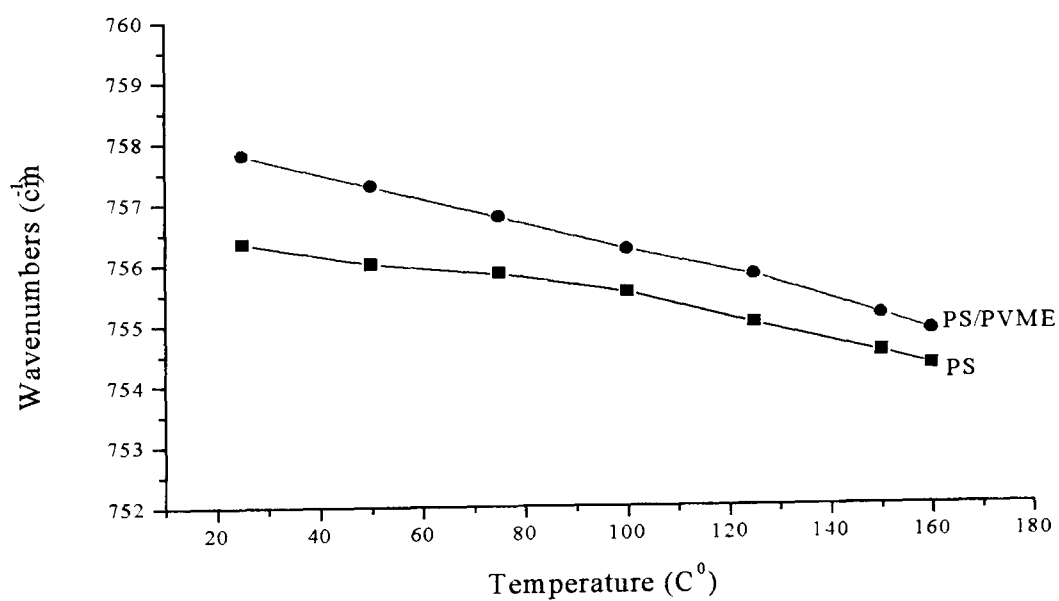
Figure 4.33   The frequency of the C – H out-of-plane phenyl ring of PS in blend with PVME at different temperature.

Our results are in good agreement with a quantitative analysis of local dynamic effects of the ether CH_3 group in PVME and the ester methyl group in PMMA, investigated as a function of temperature and blend composition using quasielastic neutron scattering by Arrighi et al [16]. They observed that the local dynamic of the ether CH_3 group of PVME in blends with PS is very similar to the pure polymer, whereas a strong influence due to blending was detected in the SCPE/PMMA blend. They concluded that the absence of any dynamic effect on methyl group rotation in the PS/PVME blend is considered to be a consequence of the dynamics of the PS units compared to that of SCPE in the SCPE/PMMA blend. They added that the weaker interaction between PS and PVME might be responsible for the differences observed in the two blends.

These results indicate that the miscibility observed in DSC experiments could be due to an interaction involving the ether lone-pair electrons of PVME and the phenyl ring of PS. If any specific interactions involving the C – O group are present, at best, they will be extremely weak. However, spectroscopic perturbations arising from interchain forces are simply too small to be observed with a high degree of confidence. Sulfonation of PS clearly shows changes in the FTIR spectra which means that FTIR spectroscopy is very sensitive to small chemical changes in the molecular structure. On the other hand the blends of SPS and PS with PVME show no clear differences in FTIR spectra. All the spectral changes reported in the literature could be related to the temperature dependence of spectra of homopolymers as shown in this work. This means that molecular dynamics rather than atomic vibration is affected by blending. In other words the molecular interactions responsible for changes in T_g are occurring on a molecular rather than atomic scale.

The shift in 758 cm^{-1} peak (or possibly the 699 cm^{-1} peak) is probably related to the changes in configuration of the benzene rings, which can be affected by the PVME environment. It can be concluded, that the IR spectroscopy is not a suitable technique for detection of molecular interactions, unless these are of chemical nature, as for example hydrogen bonds. Weak and unspecified molecular interactions cannot be detected and it is likely that these are primarily responsible for the miscibility of polymers.

4.4.3 Light Microscopy Results

The resolution of a light microscope is high enough to resolve objects less than a micron in size. This technique cannot resolve small phases in miscible blends, which are of the order of 100 – 200 nm, but is useful for study of larger phases obtained by mechanical blending and for study of diffusion layers.

Samples for transmission light microscopy must be of even thickness and thinner than the required resolution. Samples were prepared in this work by pressing the polymer between a glass slide and a cover slip at elevated temperature, to reduce the viscosity. Some samples were prepared by cutting, using a microtome with a glass knife. A Leitz Laborlux microscope has been used, equipped with polarized light, phase contrast, differential interference contrast and fluorescence. The magnification on a micrograph has been established by using a stage micrometer (calibrated scale).

Light microscopy of a mechanically blended PS/PVME (50:50) sample at 180°C shows phases of PS dispersed in PVME (Figure 4.34). It has been expected that on annealing at 110°C the PS phase will dissolve in PVME. Instead the PS phase conglomerated into larger, spherical particles (Figure 4.35). This shows that there

is a high surface tension between both phases and that the diffusion is not symmetrical, i.e. PS is swelling with PVME, but not dissolving in it. The phase diagram for mechanical blending and diffusion is therefore different than the phase diagram measured using solvents, which produces a homogenous mixture at the room temperature (Figure 4.36), after short annealing at 150°C the phase separation is however occurring as expected. The phases are large and growing with annealing time (see Figure 4.37).

25 μ m

Figure 4.34 Light micrograph (X 500) for PS/PVME 50:50 composition of mechanically blended sample at 180 °C.
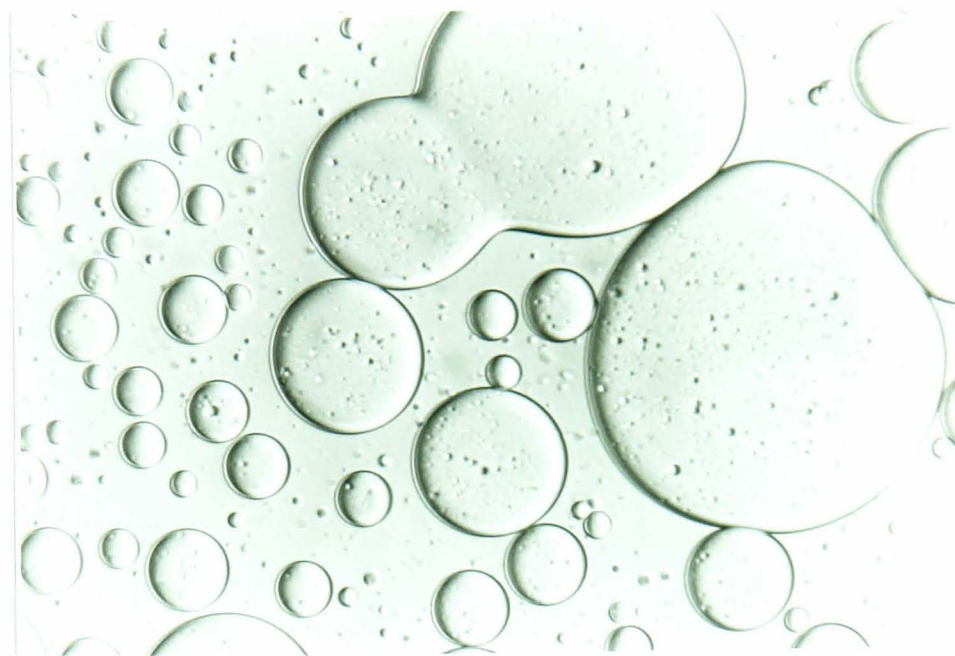
25 μ m

Figure 4.35   Light micrograph (X 500) for **PS/PVME** 50:50 composition of mechanically blended sample annealed at 110°C for 1 hour.
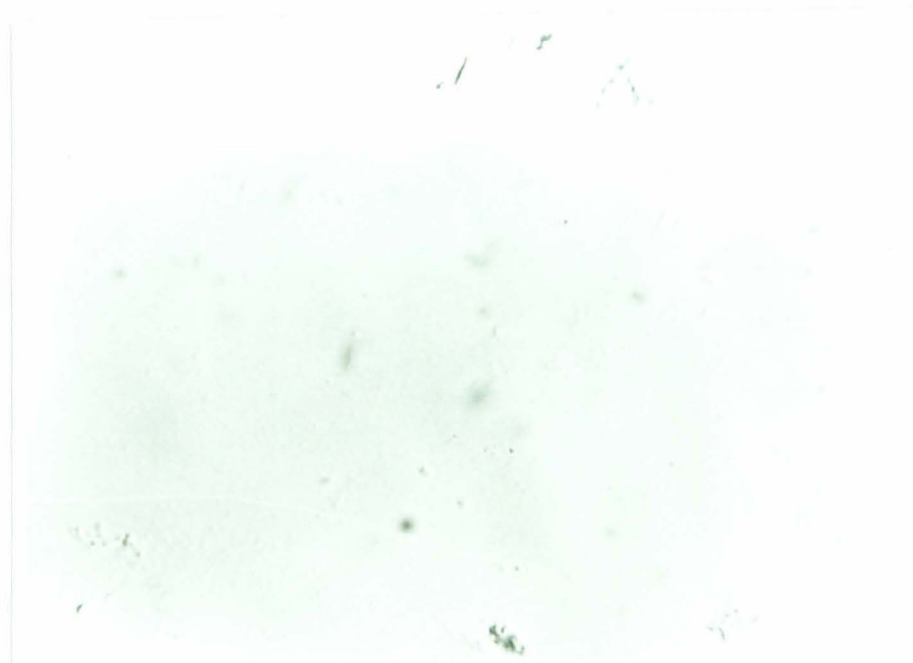
25 μ m

Figure 4.36   Light micrograph (X 500) for PS/PVME 50:50 composition of solvent cast samples.
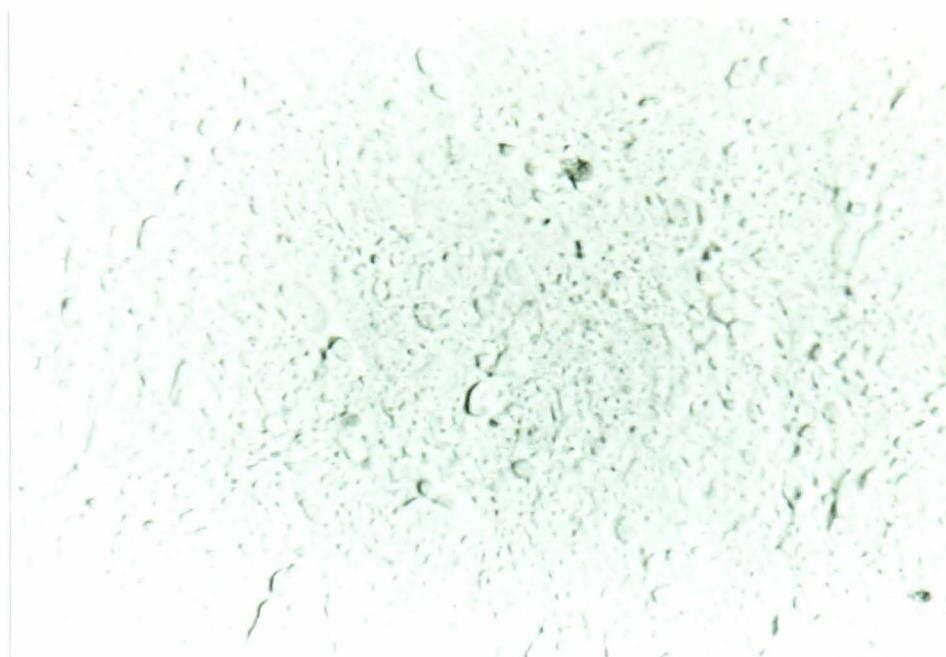
25 μ m

Figure 4.37 Light micrograph (X 500) for PS/PVME 50:50 composition of solvent cast samples annealed at 150°C for 15 min.

4.5   CONCLUSIONS

Miscibility and phase behaviour in blends of PS and SPS with PVME have been investigated by differential scanning calorimetry, optical microscopy and Fourier transform infrared spectroscopy. The blends prepared in this work are miscible in the amorphous state over all the composition range at low temperature as judged from the transparency of blend films and glass transition behaviour. The blends exhibit a single, composition – dependent glass transition temperature, which obeys the Gordon-Taylor equation, suggesting that the interaction between PS and PVME is fairly weak as previously reported by Bank et al [9].

Above 150°C, the PS/PVME blends underwent phase separation, which indicates the existence of a lower critical solution temperature (LCST). These blends are also believed to be phase-separated mainly by spinodal decomposition since phase separation was carried out above the cloud points (critical temperature) which are usually thought to be above the spinodal decomposition temperature. Based on the DSC studies, the phase separation process was investigated. The temperature range in which the phase separation occurred was determined by means of DSC. The blends displayed two glass transition temperatures when quenched in liquid nitrogen from temperatures above 150°C. It is observed that the rate of separation is very fast and the phases can only be preserved using the fastest possible cooling rate. The phase diagram of this blend system has the LCST at critical composition of between 20 and 30 wt % PS content. This is consistent with the tact that the molecular weight of PS is larger than PVME. The LCST is therefore located at the PVME – rich composition. As reported previously LCST depends on the molecular weight of each component in the blend [37].

The sulfonation of PS shows changes in the FTIR spectra, which means that FTIR spectroscopy is very sensitive to small chemical changes in the molecular structure. On the other hand the blends of SPS and PS with PVME show no differences in FTIR spectra. All the spectral changes reported in the literature have been shown in this work to be related to temperature dependence of spectra of homopolymers with the exception of 758 cm^{-1} peak. Furthermore, FTIR studies revealed that there is no chemical interaction such as hydrogen-bonding type interaction between PS and PVME present. It was suggested[14] that the ether lone-pair electrons of PVME and the benzene ring of PS might be involved. This has not been confirmed in this work. Our FTIR results correlate with a recently reported quantitative analysis of local dynamic effect of the ether CH_3 group in PVME and PS/PVME blends as a function of temperature using quasielastic neutron scattering by Arrighi et al [16]. They also observed that the local dynamic of the ether CH_3 group of PVME in blends with PS is very similar to the pure homopolymers. Therefore the miscibility observed by DSC does not support an interaction involving the ether lone-pair electrons of PVME and phenyl ring of PS. The miscibility of this system can therefore be considered to stem from the existence of intermolecular interactions between the components, which cannot be identified by FTIR spectroscopy.

Blends prepared by mechanical mixing have different behaviour. After mixing, two phases are observed by light microscopy and also two T_gs corresponding to pure homopolymers are measured by DSC. Only after long annealing at 110°C for 24 hours, a T_g at 67°C, corresponding to a 70/30 PS/PVME blend is observed. This shows that the diffusion of PVME in PS is very slow and that the phase diagram for blends obtained by the diffusion process is shifted to lower temperature or compositions.

References

1. Paul, D. R.; and Newman, S., Eds. *Polymer Blends;* Academic Press: New York, **1978**; Vols. I and II.

2. Olabisi, O.; Robeson, L. M.; Shaw, M. T. *Polymer-Polymer Miscibility*, Academic Press: New York, **1979**.

3. Utracki, L. A. *Polymer Alloys and Blends*, Oxford University Press: New York, **1989**.

4. Coleman, M. M.; and Moskala, E. J. *Polymer* **1983**, 24, 251.

5. Moskala, E. J.; Howe, S. E.; Painter, P. C.; and Coleman, M .M. *Macromolecules* **1984**, 17, 1671.

6. Ting, S. P.; Pearce, E. M.; and Kwei, T. K. *J. Polymer Sci., Polym. Lett. Ed.* **1984**, 18, 201.

7. He, M.; Lui, Y.; Feng, Y.; Jiang, M.; and Han, C. C. *Macromolecules* **1991**, 24, 464.

8. Percec, V.; Schild, H. G.; Rodriguez-Parada, J. M.; and Pugh, C., *J. Polym. Sci, Polym. Chem. Ed.* **1988**, 26, 935,

9. Bank, M.; Leffingwell, J.; and Thies, C. *Macromolecules* **1971**, 4, 43.

10. Nishi, T.; Wang, T. T.; and Kwei, T. K. *Macromolecules* **1975**, 8, 227.

11. Snyder, H. L., Meakin, P.; and Kwei, T. K. *Macromolecules* **1983**, 16, 227.

12. Tsujita, Y.; Kates, M.; Kinoshita, T.; and Takizawe, A. *Polymer* **1992**, 33, 773.

13. Garcia, D., *J. Polym. Sci., Polym. Phys. Ed.* **1984**, 22, 107, and 22, 1773.

14. Lu, F. J.; Benedetti, E.; and Hsu, S. L. *Macromolecules* **1983**, 16, 1525.

15. Larbi, B. C. F.; Leloup, S.; Halary, J. L.; Monnerie, L. *Polym. Commun.* **1986**, 27, 23.

16. Arrighi, V.; Higgins, J. S. *Macromolecules* **1995**, 28, 4622.

17. Mokdad, A.; Dubault, A.; and Monnerie, L., *J. Polym. Sci., Part B: Polym. Phys.* **1996**, 34, 2723.

18. Weiss, R. A.; and Lu, X. *Polymer* **1994**, 35, 09.

19. Zheng, S.; Huang, J.; and Yang, X. *European Polymer Journal* **1996**, 32, 06.

20. Zheng, S.; Huang, J.; and Guo, Q., *J. Polym. Sci., Part B: Polym. Phys. Ed.* **1997**, 35, 09.

21. Tsujita, Y.; Kato, M.; Kinoshita, T. *Polymer* **1992**, 32, 4, 773.

22. Wunderlich, B. in *Thermal Analysis in Polymer Characterisation*, (TuriE, ed.), 2, Heyden and Philadelphia, **1981**.

23. Parmer, J. F.; Dickinsion, L. C.; Chien, J. C. W.; and Porter, R. S. *Macromolecules* **1989**, 22, 1078.

24. Bank, M.; Leffingwell, J.; and Thies, C., *J. Polym. Sci., A-2* **1972**, 10, 1097.

25. Eisenberg, A. *Macromolecules* **1970**, 3, 147; Hird, R. B.; and Moore, R. B. *Macromolecules* **1990**, 23, 4098.

26. Gordon, M.; and Taylor, J. S., *J. Appl. Chem.* **1952**, 2, 493.

27. Fox, T. G. Bull. *Amm. Phys. Sco.* **1956**, 2, 123.

28. Pennachia, J. R.; Pearce, E. M.; Kwei, T. K.; Pulken, B. J.; and Chen, J. P. *Macromolecules* **1986**, 09, 973.

29. Tsujita, Y.; Kato, M.; Kinoshita, T.; and Takizawa, A. *Polymer* **1992**, 33, 04.

30. Schneider and Brekner., *J. Appl. Polym. Sci.* **1973**, 17,3175.

31. Belorgey, G.; and Prud'houmme, R. E. *J. Polym. Sci., Part B: Polym. Phys. Ed.* **1982**, 20,191.

32. Belorgey, G.; Prual' houmme, R. E.; and Aubin, M. _Polymer_ **1982**, 23, 1051.

33. Gunton, J. D.; Miguel, M. San.; and Sahni, P. S., in _Phase Transitions and Critical Phenomena, vol. 8_, Domb.C and Lebowitz . J. L., Eds.; Academic Press: London, **1983**.

34. Cahn, J. W. _J. Chem. Phys._ **1965**, 42, 93.

35. Fried, J. R.; MacKnight, W. J.; and Karasz, F. E. _J. Appl. Phys._ **1979**, 50, 6052 .

36. McMaster, L. P. _Macromolecules_ **1973**, 06, 760.

37. Nishi, T.; and Kwei, T. K. _Polymer_ **1975**, 16, 285.

38. Walsh, D. J.; and Dee, G. T. _Macromolecules_ **1989**, 22, 3395.

39. Kwei, T. K; Nishi, T.; and Roberts, R. G. _Macromolecules_ **1974**, 7, 667.

40. Casal, H. L.; Cameron, D. G.; and Mantsch, H. H., _J. Phys. Chem._ **1985**, 89, 5557.

41. Zerbi, G., _Advances in Infrared and Raman spectroscopy_, R. J. H. Clark and R.E . Hester, Eds.; Heyden, London, **1984**; Vol. 11, P- 301.

42. Snyder, R. G.; Hsu, S. L.; and Krim, _Spectrochim. Acta_ **1978**, 34A, 395.

43. Abbate, S.; Zerbi, G.; and Wunder, S. L., _J. Phys. Chem._ **1982**, 86, 3140.

44. Schlotter, N. E.; Porter, M. D.; Bright, T. B.; and Allara, D. _J. Chem. Phys. Lett._ **1986**, 132, 93.

45. Walczak, M. M.; Ch. Chung; Stole, S. M.; Widrig, C.; and Porter, M. D., _J. Am. Chem. Soc._ **1991**, 113, 2370.

46. Jabbari , E.; and Peppas, N. A. _Macromolecules_ **1993**, 26, 09.

47. Liang, C. Y.; and Krimm, Infrared spectra of high polymers. VI. Polystyrene, _J. Polym. Sci._ **1958**, 27, 241-54.

48. Randy, W.; and Painter, P. C. _Polymer_ **1981**, 22, 1633.

49. Snyder, R. G.; and Zerbi, G., _Spectrochim. Acta_ **1967**, 23A, 391.

50.   Colthup, N. B., Wiberly, S. E, *Introduction to infrared and raman spectroscopy*, Academic Press: New York, **1990**.

51.   Chang-Sik Ha and Won-Jei Cho, *Polymer* **1993**, *34,3*.

52.   Dong-Pil Kang, Chang. S. H and Won-J. C., *J. Polym. Sci., Polym. Chem.* **1989**, 27,1401.

CHAPTER FIVE

FTIR STUDY OF SULFONATED POLYSTYRENE

5.1   INTRODUCTION

The introduction of ionic groups into polymers results in a modification of their molecular structure and physical properties [1-7] such as chemical resistance, dimensional stability and mechanical strength. Recently several reviews appeared describing the properties of ionomers in both the solid state and solution [8-11] such as glass transition temperature (T_g), shear modulus of rubbery state (above the glass transition), dynamic mechanical behaviour, dielectric properties, and solution behaviour.

Ionomers are a class of ion-containing polymers, which have ions in concentration up to 10-15-mol % distributed on non-ionic backbone chains. The percentage of ionic groups (usually quoted as mole %) is calculated from the number of backbone atoms or repeat units to which ionic groups are attached [3]. It is believed that interactions between the ionic groups lead to two different types of ionic aggregates, namely *multiplets* and *ionic clusters*. According to a widely used model of ionomer microstructure, multiplets are small ionic aggregates consisting of a small number (eight or less) of interacting ion pairs, which act rather like physical crosslinks, and clusters are larger aggregates of phase-separated ion-rich regions that also contain segments of hydrocarbon chains [1,2,7,11]. However, the exact structures of the multiplets and clusters have not yet been fully elucidated.

Since the development of ionomers by DuPont in 1966[12], ionomers have been extensively studied in both industry and academia. Polystyrene-based ionomers in which the ionic groups are associated with the benzene rings belong to an important class of ionomers, the _random_ ionomers. In this regard, sulfonated polystyrene ionomers (SPS) are model polymers to gain a fundamental understanding of the properties of ionomers as well as the behaviour of associating polymers in general. This understanding is aided by a large number of studies already carried out on polystyrene and its availability in both deuterated and monodisperse form spanning a wide range of molecular weights.

As discussed in chapter three, infrared (IR) spectroscopy is a frequently used as an analytical tool in the study of polymers. The qualitative and quantitative information it generates can be related either to macroscopic properties or to molecular interactions[13]. IR spectroscopy has been used to investigate different types of ionomers from their pre-ionic form to their final ionomeric state under demanding operating conditions[11].

The aim of the present study is to investigate changes that occur upon sulfonation in the vibrational spectra of polystyrene and its ionomers and to relate these changes to the dynamical spectrum measured by inelastic neutron scattering (INS)[14]. Therefore we have studied the vibrational spectrum of hydrogenous atactic polystyrene with different selectively deuterated variants and a corresponding series of atactic sodium sulfonated polystyrene. This analysis will enable us to assign the peaks in order to identify where the sulfonation sites are. This information is vital for employing FTIR for the study of the chain conformation (e.g. clusters). It was hoped, moreover, to gain some insight into the changes occurring in the structure upon deuteration. This type of information

could help with understanding of process occurring in polymer blends: some ionomer blends are studied in the next chapter.

5.2   EXPERIMENTAL

5.2.1   Sample Preparation.

The sulfonated polystyrene sample was prepared at Exxon Research and Engineering Co. by Dr D G Peiffer, and the procedures are described below. The chemical structure of sulfonated polystyrene is shown in Table 5.1[14].

All the deuterated polystyrene samples used in this study were obtained through emulsion polymerization of the deuterated styrene monomer using potassium persulfate as initiator and sodium lauryl sulfate as the surfactant. The whole polymerization process was conducted under a argon atmosphere and is known to produce an atactic polymer. For example, a mixture of 90.0 ml of distilled water, 10.0 g of styrene -α,α,β-d$_3$, 1.0 g of sodium lauryl sulfate, and 0.1 g of potassium persulfate were stored into a 500 ml four-neck flask, vigorously agitated, degassed with argon gas and heated to 50°C for 24 h. Appropriate care was taken to eliminate any minor amount of residue surfactant. Subsequently the polymer was isolated from the emulsion by a large excess of acetone and dried in a vacuum oven at 65°C for 48 hours.
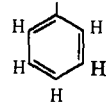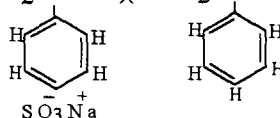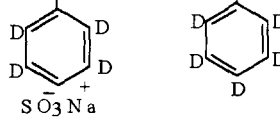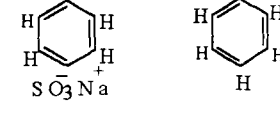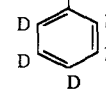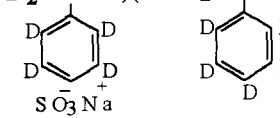
Sulfonation Procedure: These deuterated materials were then sulfonated by dissolving 2.7 g of poly (styrene-α,α,β-d$_8$) DH in 50.0 ml of 1,2-dichloroethane (1,2-DCE) at 25°C, 0.3 ml of acetic anhydride and 0.17 ml of concentrated

sulfuric acid were added. The solution was continuously stirred for 1 h at 50°C. The reaction was terminated by adding 0.45 g of sodium acetate dissolved in a mixture of 4.5 ml of methanol and 0.3 ml of water, which also neutralized all free acids. The filtered and neutralized ionomer was dried in a vacuum oven at 100°C for 48 h. Sulphur analysis showed negligible surfactant concentration. To calculate the sulfonation level, Dietert sulphur analysis was used. For this polymer, the sulfonate content was 7.4% (2.06 wt. % sulfur). All materials were characterised with gel permeation chromatography. Their corresponding weight-average molecular weight M_w and polydispersity ratio M_w /M_n are listed in table 5.1.

5.2.2   FTIR Measurement

Infrared spectra of these specimens were recorded by Dr. D. Vesely on a FTIR spectrometer _Nicolet 60 SXB_ used previously for the PS/PVME system (chapter four) at Material Engineering Department. The spectra were taken with resolution 2 cm^{-1} and were the average of 100 scans, within the wavelength range 400 – 4000 cm^{-1}. All infrared spectra were obtained at room temperature. The measurement was carried out either on thin pressed films at 160°C or by solid thin solvent-cast films in toluene. Thin films of polystyrene without sulfonation were pressed on a hot-stage at 160°C and sulfonated samples were obtained by casting at room temperature.

Table 5.1   List of the samples used in this study of atactic polystyrene with different selectively deuterated variants and different degrees of sulfonation.

sample	mol. wt (M_w/M_n)	av.mol. wt per monomer	structure of monomer
Neutral PS (C_8H_8), fully hydrogenous	600 000 (1.06)	104	
3.9 mol % sulfonated, fully hydrogenous	600 000 (1.06)	107.98	
6.3 mol % sulfonated, ring deuterated	1.171×10^6 (6.6)	110.68	
7.4 mol % sulfonated, chain deuterated $(-\alpha, \alpha, \beta\text{-}d_3)$	2.107×10^6 (2.4)	117.77	
perdeutero PS (fully deuterated)	1.39×10^6 (4.6)	-	
4.1 mol % sulfonated, fully deuterated	-	-	

5.3   RESULTS AND DISCUSSION

The measured infrared spectra of polystyrene in fully hydrogenous form and in their chain, ring and also fully - deuterated forms with different levels of sulfonation were analysed. The spectra obtained from fully hydrogenated PS are shown in figure 5.1. The spectra of chain deuterated, ring deuterated and fully deuterated forms are shown in figures 5.2 to 5.4, respectively. Upon careful inspection of these figures, it is apparent that important changes in the recorded spectra are observed, as discussed below.
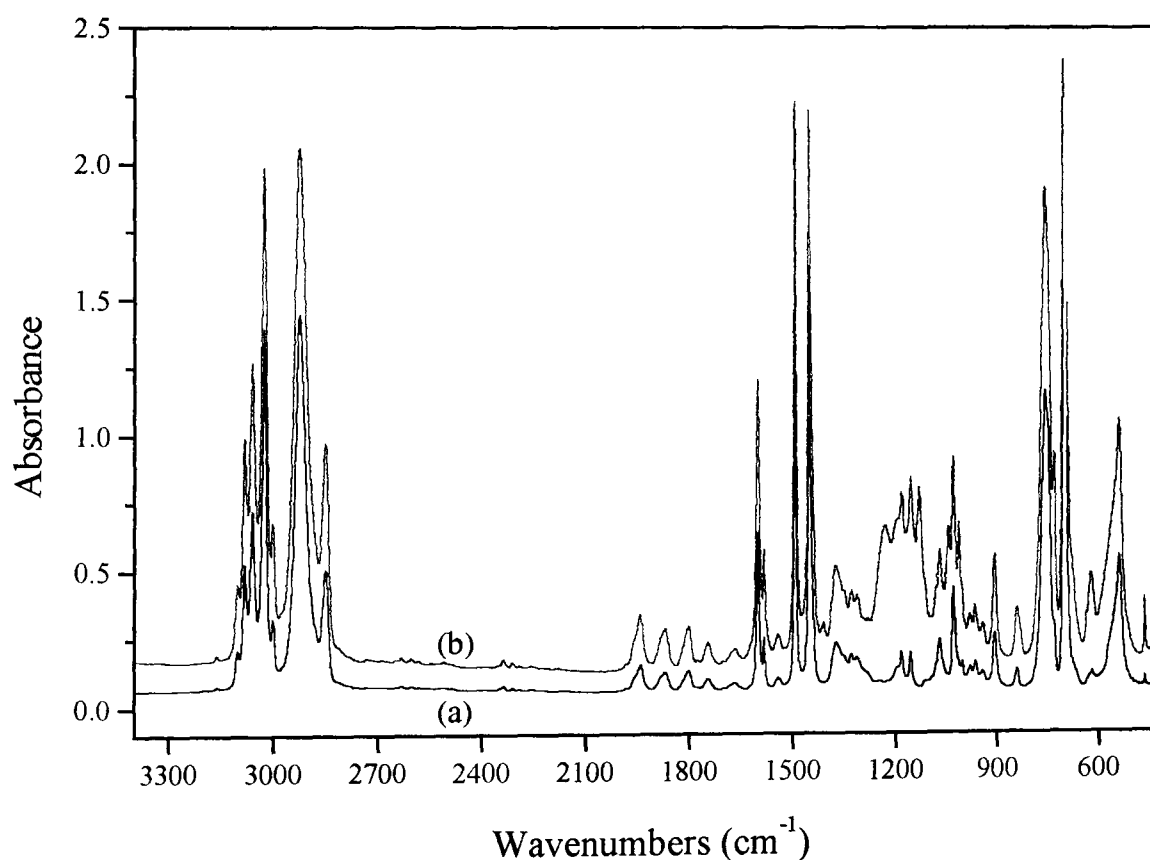
Figure 5.1   Infrared spectra of hydrogenous polystyrene, (a) pure polystyrene (b) 3.9 mol. % sulfonation polystyrene.

In Table 5.2, the observed vibrational frequencies and their assignments for fully hydrogenous polystyrene are listed. The characteristic bands of selectively deuterated samples are tabulated in Table 5.3. The comparison of all the spectra gives an indication where the substitution takes place. The position of the sulfonate group on the benzene ring of the styrene unit is also of interest, since it will have a profound impact on the local structure of a copolymer (PS – sulfonated PS).

Table 5.2 IR absorption assignment for fully hydrogenous polystyrene.

Assignment	Wavenumbers (cm^{-1})
C - H aromatic stretching vibration **(H-ring)**	3001 - 3103
C - H asymmetrical stretching vibration of CH_2 **(H-chain)**	2925
C - H symmetrical stretching vibration of CH_2 **(H-chain)**	2850
C - C stretching vibration of ring in plane	1601
C - C stretching vibration of ring in plane	1583
C - H stretching vibration of ring in plane **(H-chain)**	1493
C - C stretching vibration of ring in plane.	1452
S - O asymmetric stretching vibration of $-SO_3^-$ groups	1229
C – H bending vibration of ring in plane	1069
S - O symmetric stretching vibration of $-SO_3^-$ groups	1043
C – H bending frequency ring in plane	1029
C - H out-of-plane bending vibration	840
C - H out-of-plane bending vibration	757
C – H out-of-plane bending vibration **(H-ring)**	699
S – O asymmetrical bending vibration of $-SO_3^-$ groups	667
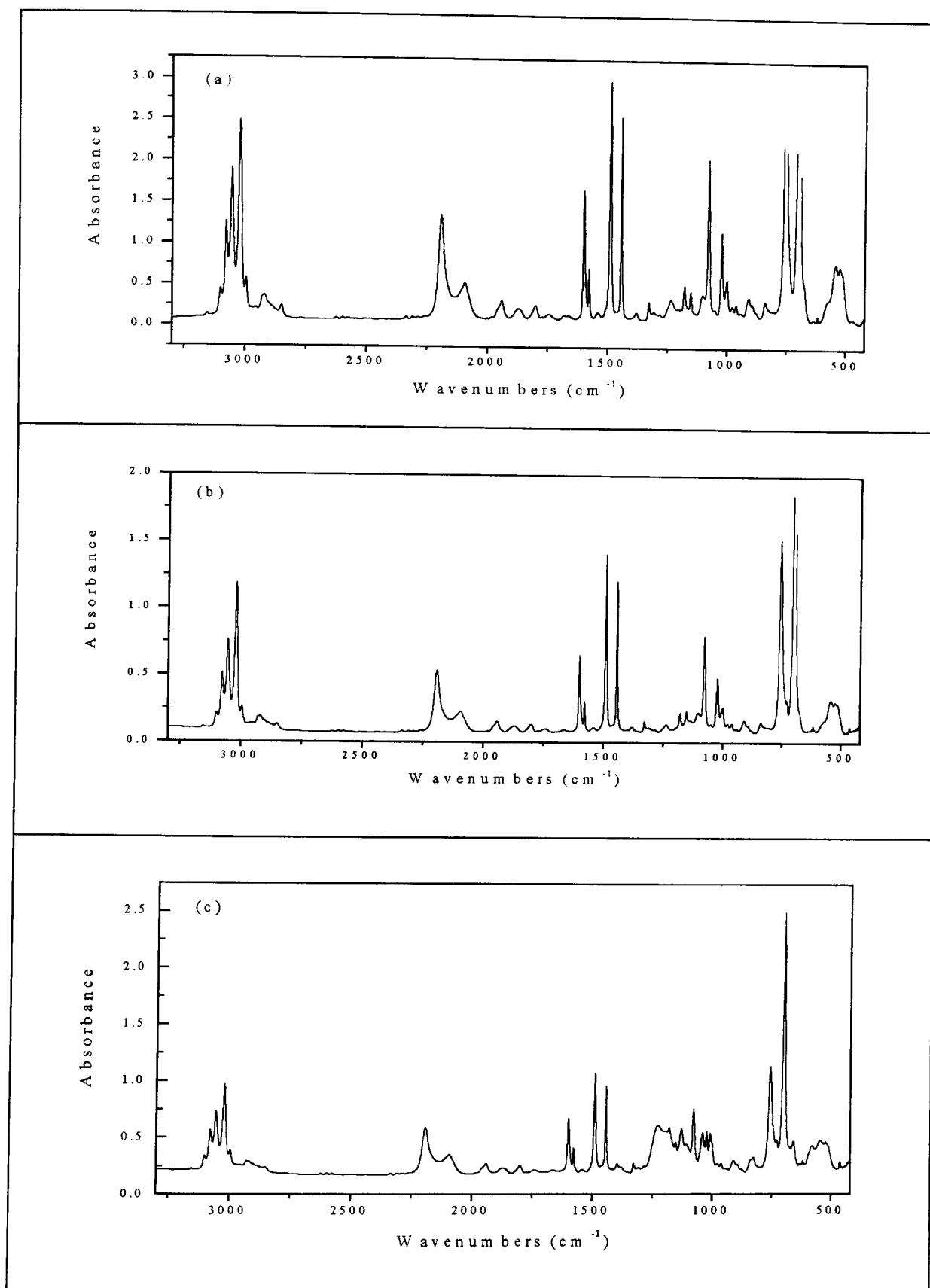
Figure 5.2   Infrared spectra of chain deuterated polystyrene, (a) 0.0 mol. % (b) 0.6 mol. % (c) 7.4 mol. % sulfonation.
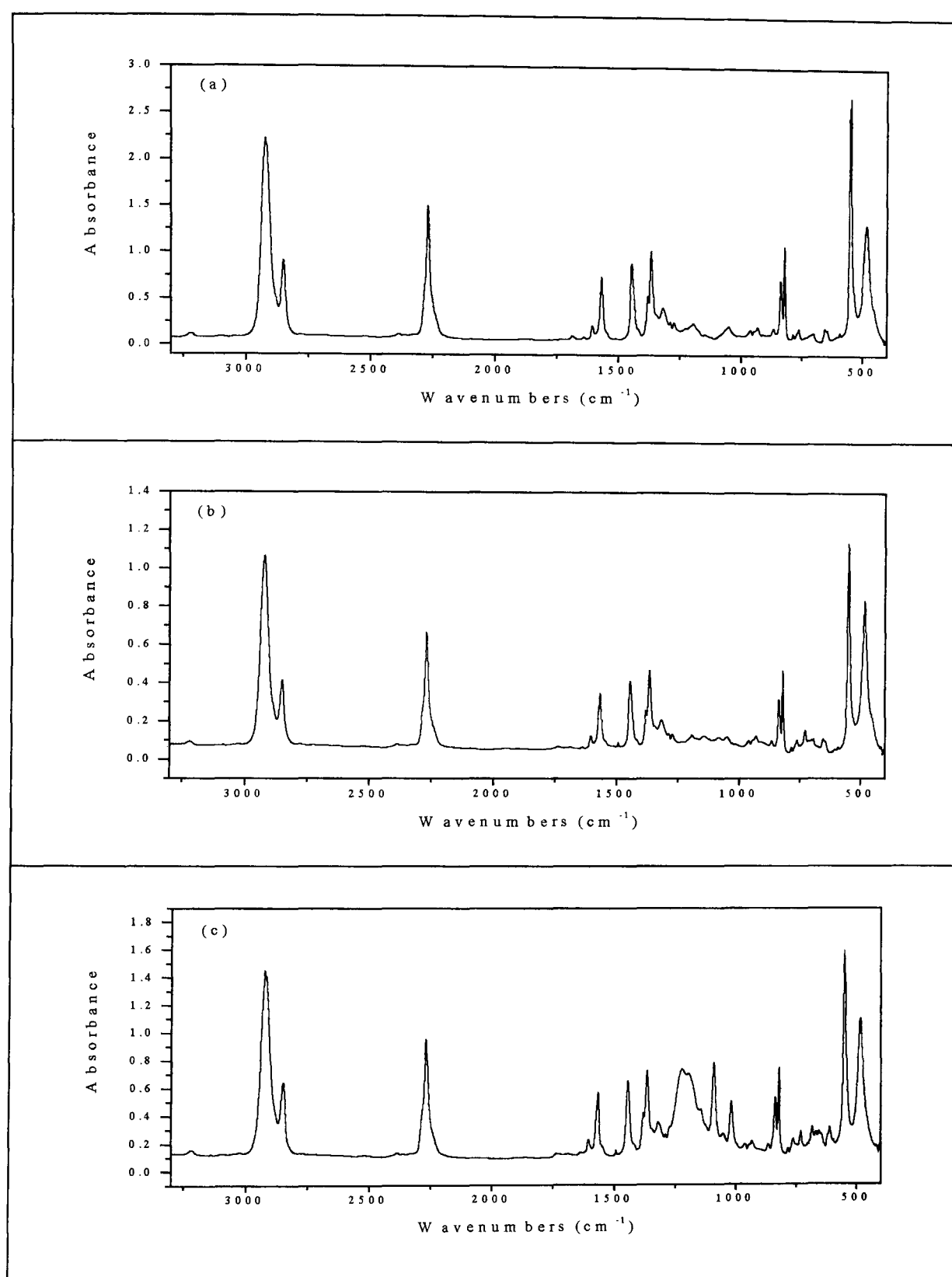
Figure 5.3   Infrared spectra of ring deuterated polystyrene, (a) 0.0 mol. %, (b) 0.8 mol. % (c) 6.3 mol. % sulfonation.
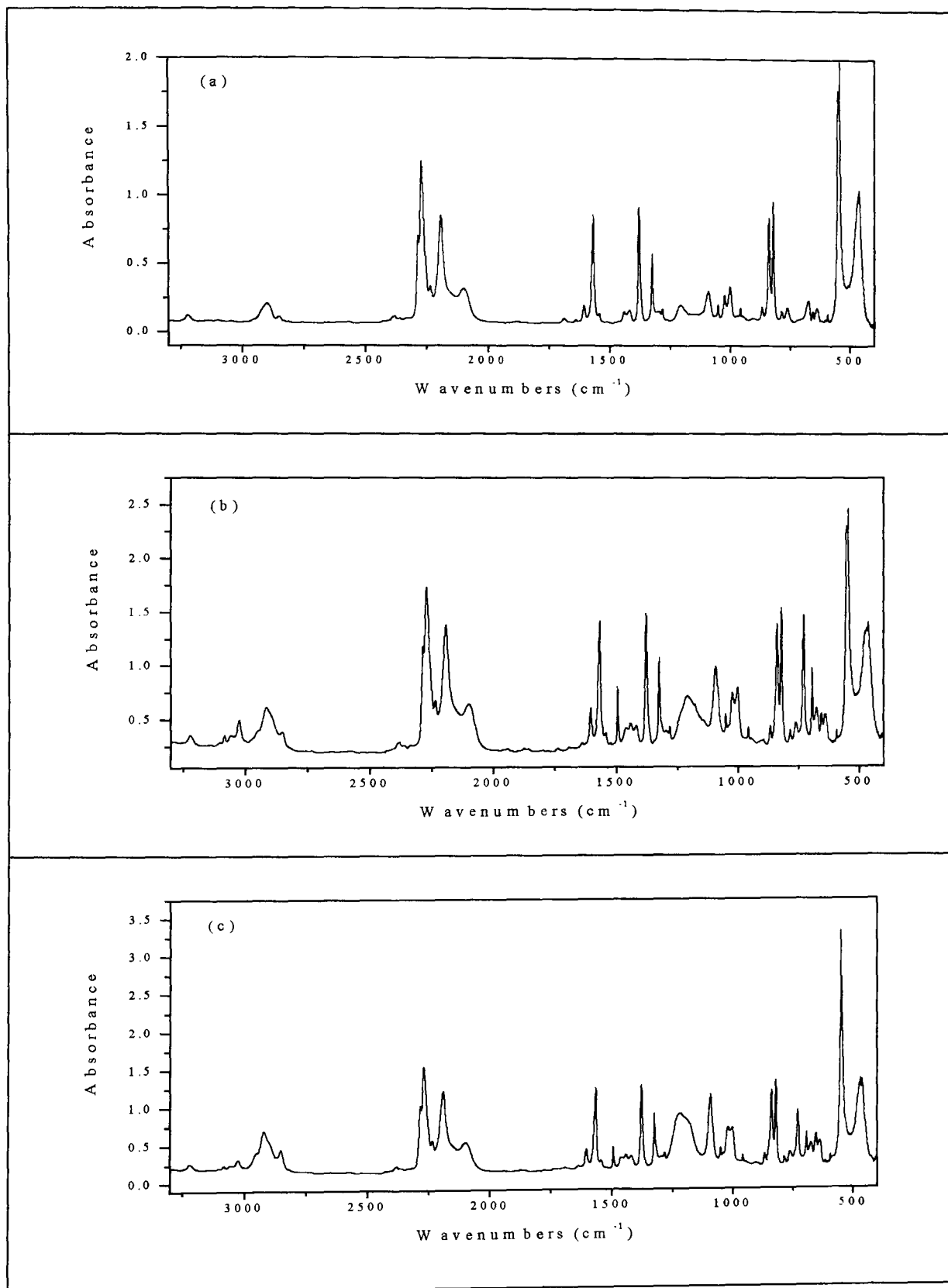
Figure 5.4   Infrared spectra of fully deuterated polystyrene, (a) 0.0 mol. % (b) 3.5 mol. %, (c) 4.1 mol. % sulfonation.

Table 5.3   IR absorption assignment for deuterated polystyrene.

Assignment	Wavenumbers (cm^{-1})		
	Chain Deuterated	Ring Deuterated	Fully Deuterated
C – H aromatic stretching vibration (H-ring)	3001 - 3103	-	-
C – H asymmetrical stretching vibration (H – chain)	-	2924	-
C – H symmetrical stretching vibration (H – chain)	-	2851	-
C – D asymmetrical stretching vibration (D – chain)	2194	-	2194
C – D symmetrical stretching vibration (D – chain)	2096	-	2100
C – D stretching ring vibration (D- ring)	-	2272	2272
C – C stretching vibration of ring in plane	1602	1607	1607
C – C stretching vibration of ring in plane	1580	1569	1569
C – H stretching vibration of ring in plane (H-ring)	1492	-	-
C – C stretching vibration of ring in plane	1446	1447	1441
S – O asymmetric stretching Vibration of -SO$_3^-$	1228	1226	1221
C – H bending vibration of ring in plane	1080	-	-
S – O symmetric stretching Vibration of -SO$_3^-$	1043	1053	1052
C – H bending frequency ring in plane	1025	-	-
C – D out-of-plane bending vibration (D- ring)	-	838	841
C – D out-of-plane bending vibration (D- ring)	-	823	822
C – H out-of-plane bending vibration (H- ring)	759	-	-
C – H out-of-plane bending vibration (H- ring)	699	-	-
S – O symmetric stretching Vibration of -SO$_3^-$	660	669	695
C – D out-of-plane bending vibration (D- ring)	-	551	548
C – D out-of-plane bending vibration (D- ring)	-	487	465
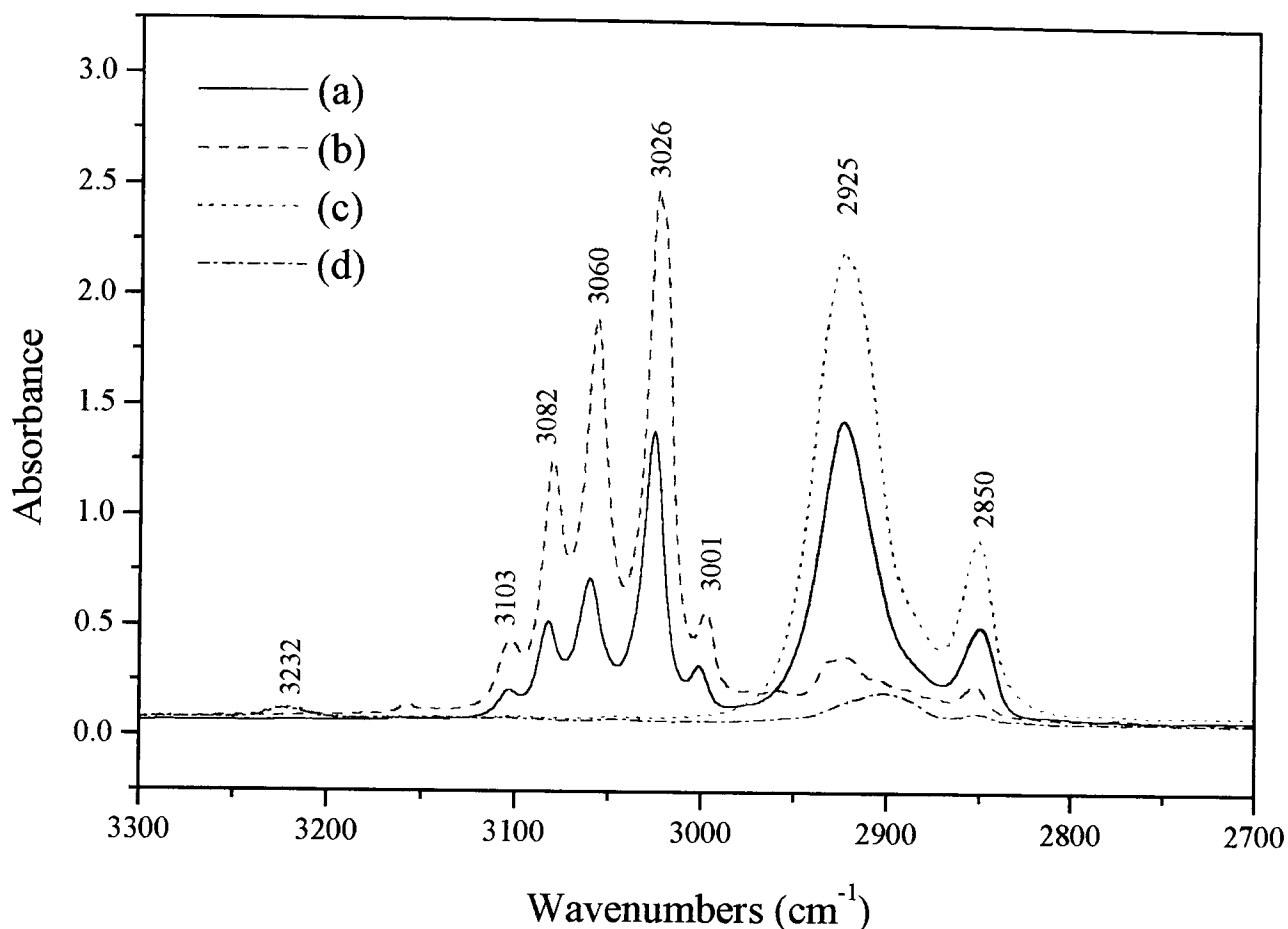
Figure 5.5   Infrared spectra of polystyrene in the high frequency in the 3300 to 2700 cm^{-1} region. (a). Fully hydrogenous (b). Chain deuterated (c). Ring deuterated (d). Fully deuterated polystyrene.

Figure 5.5 shows the infrared spectra of hydrogenous, chain deuterated, ring deuterated and fully deuterated polystyrene in the high frequency region from 2700 to 3300 cm^{-1}. The high frequency spectrum of fully hydrogenous polystyrene consists of two bands at 2850 and 2925 cm^{-1} of CH$_2$ symmetrical and asymmetrical stretching vibrations near the calculated [15] values of 2926 and 2853 cm^{-1}, with a series of C-H aromatic stretching bands around 3000 cm^{-1} (i.e. 3001, 3026, 3060, 3082 and 3103 cm^{-1}). The high frequency spectrum denoted

"b" in figure 5.5, of chain deuterated polystyrene exhibits the same bands as those appearing in the spectrum of hydrogenous PS around 3000 cm^{-1}. However, the two sharp peaks at 2850 cm^{-1} and 2925 cm^{-1} of C-H stretching vibration of CH$_2$ and CH groups nearly disappeared, yet still small shoulders are present in the chain deuterated and fully deuterated spectra ("d" in figure 5.5). The appearance of these shoulders implies that chain and "fully deuterated" samples are not fully chain deuterated. However in the ring deuterated spectrum ("c" in figure 5.5) only two bands of symmetrical and asymmetrical stretching modes of CH$_2$ groups are present at 2924 and 2851cm^{-1}, but the series of C-H aromatic stretching bands around 3000 cm^{-1} and a sharp peak of benzene ring vibration at 403 cm^{-1} have completely disappeared [14]. Also several other peaks disappear upon deuteration of benzene ring, as demonstrated later in this section. The assignment of the vibrational modes appearing in the fully hydrogenous spectrum ("a" in figure 5.5) is facilitated by comparing with the INS spectrum, since the deuterated moieties have an incoherent cross-section that is small compared to that of hydrogen (2 and 80 barns [1 barn=10^{-24}cm^2], respectively [14]).

Another interesting feature is the appearance of the band at 3232 cm^{-1} in the spectra of fully deuterated and ring deuterated polystyrene in figure 5.5. An absorption in this region is usually due to hydrogen – bonded O – H. But unfortunately this peak is found in both sulfonated and unsulfonated samples, and it is present only in the ring-deuterated and fully deuterated samples. However, no such absorption at this position was found in either the chain-deuterated and fully hydrogenous polystyrene with or without sulfonation. Therefore on this basis we cannot definitely assign this peak to a hydrogen bonded O – H group.

The spectra of 2350 to 1650 cm^{-1} regions are shown in figure 5.6. Traces A & B of figure 5.6 illustrate the spectra of ring deuterated and fully deuterated, and traces C & D represent chain deuterated and fully hydrogenous polystyrene spectra, respectively. It can be seen that upon deuteration of the benzene ring a sharp peak appears in the ring deuterated and fully deuterated spectra due to stretching vibration of the C – D group of the benzene ring. The chain deuterated and fully deuterated spectra exhibit two absorption features at 2100 and 2194 cm^{-1} which correspond to symmetrical and asymmetrical stretching vibration of the C – D modes for the deuterated analogues on the polystyrene chain. But in chain deuterated polystyrene the 2100 cm^{-1} peak shifts by four wavenumbers to lower frequencies at 2096 cm^{-1}. This indicates that deuterated analogues in chain deuterated PS affect the hydrogenous vibration of the ring. The above observation correlates with the double mass of D atom compared to that of H atom, as expected. The frequency position of the maximum absorbance of an IR band depends on the strength of the bonds and the masses of the atoms involved in the particular vibrational mode [15]. Thus these frequencies shift due to the mass variation (i.e. the substitution of deuterium atom for hydrogen). On the other hand the electron diffraction measurements of C$_2$H$_6$ and C$_2$D$_6$ showed a C – H bond distance of 1.1122 ± 0.0012 Å and C – D distance of 1.1071 ± 0.0012 Å[16] respectively, which shows that the interatomic bond is shorter for C – D bond.

In the range of 2000 – 1650 cm^{-1}, see figure 5.6, weak bands or combination bands are present in all fully hydrogenous and chain deuterated spectra. The pattern of these weak bands is characteristic of the substitution pattern of the ring. Because they are weak, these bands are most readily observed in spectra obtained from thick samples. The position of substitution on benzene rings can often be determined by the number of bands [15]. This procedure is limited by the

weak absorption of such overtone (or combination) bands. If there is a strong absorption in that region (such as a carbonyl stretch) the weak overtone bands are obliterated. These bands map out the vibrations of the ring pattern, which completely disappear in polystyrene spectra with deuterated ring and in the spectra of fully deuterated polystyrene. The ring-deuterated spectrum shows one band at 2272 cm^{-1} corresponding to C – D stretching mode of a deuterated ring. The same band is detectable in fully deuterated spectra with two additional small shoulders at 2286 and 2236 cm^{-1}. These bands are difficult to assign without unjustified speculation.
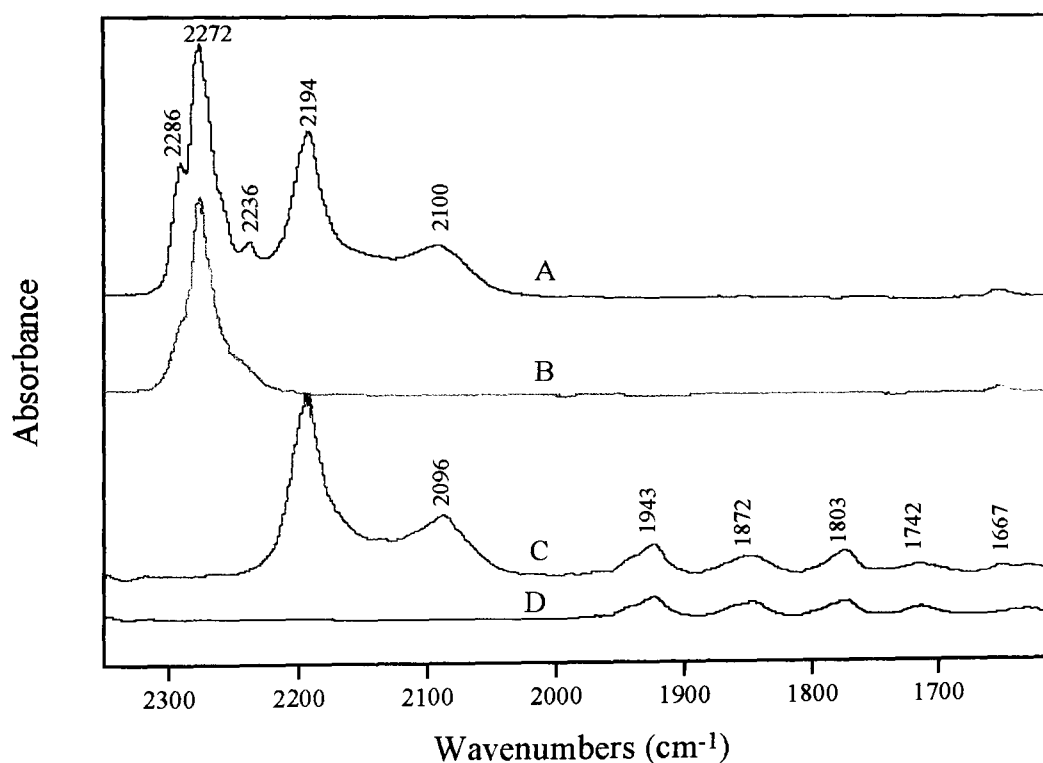
Figure 5.6   Infrared spectra of C - D stretching region. Trace (A) ring deuterated, (B) fully deuterated, (C) chain deuterated and (D) fully hydrogenous polystyrene.

Figure 5.7 (a) Infrared spectra of fully hydrogenous and chain deuterated polystyrene in the 1650 to 1400 cm^{-1} region: (———) fully hydrogenous; (------) chain deuterated.

Figure 5.7 (a) and (b) shows the 1400 cm^{-1} to 1650 cm^{-1} region of all samples of polystyrene spectra. In this spectral range the four bands can be assigned to the benzene ring vibrations. These vibrations mainly involve C = C stretching of ring bonds but there is little interaction with CH in plane bending vibration. The two bands are observed at almost constant wavenumbers of 1493 and 1452 cm^{-1} respectively [17,18], and the intensity of these absorption bands is almost the same in fully hydrogenous and chain deuterated polystyrene. But in chain deuterated

polystyrene the 1452 cm^{-1} peak shifts down by six wavenumbers to a lower frequency of 1446 cm^{-1}. However the vibration at 1492 cm^{-1} remains the same as in the fully hydrogenous polystyrene spectrum. These results suggest that in deuterated analogues of polystyrene (either ring – deuterated or chain – deuterated) the C = C vibration of the benzene ring is affected. Furthermore, two bands appearing in fully hydrogenous and chain deuterated polystyrene spectra (at 1583 and 1601 cm^{-1}) are also assigned to the benzene ring C = C stretching vibration. The position and intensity of these vibrations are also different for hydrogenous and deuterated samples.
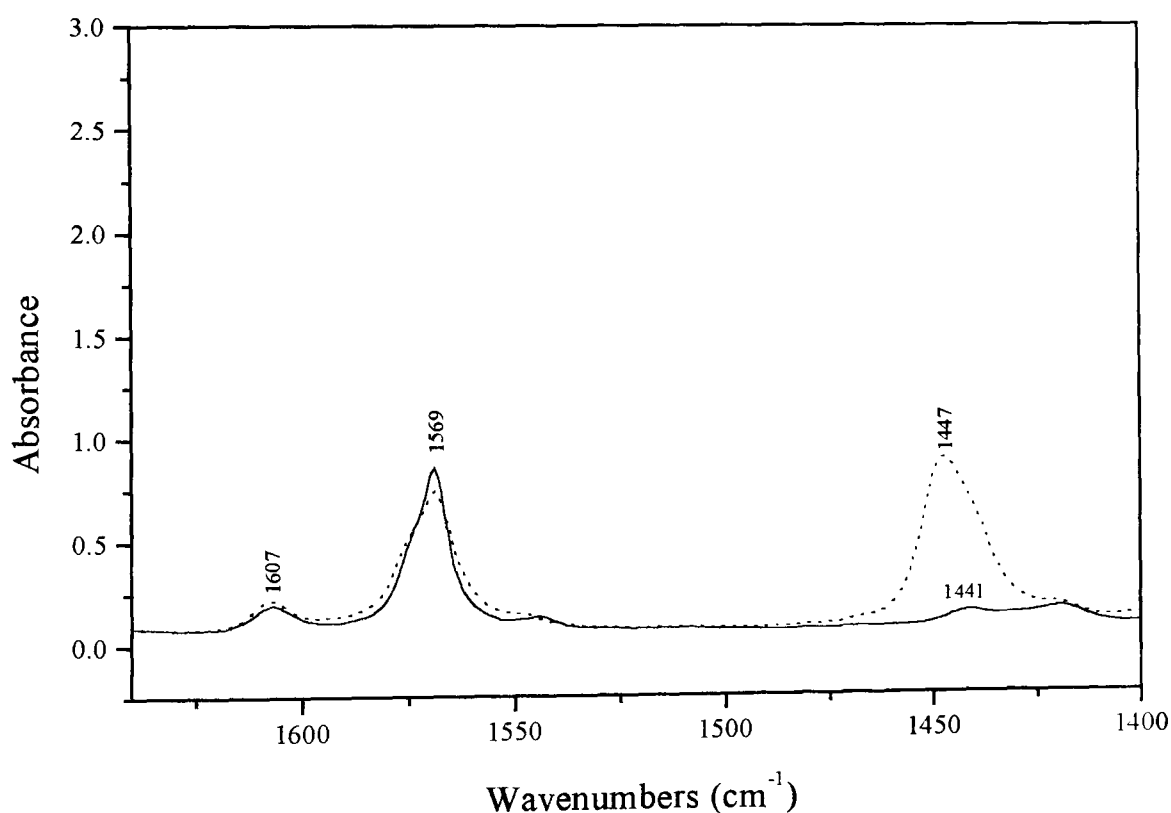
Figure 5.7 (b). Infrared spectra of fully deuterated and ring deuterated polystyrene in the 1680 to 1400 cm^{-1} region: (———) fully deuterated; (------) ring deuterated.

The spectrum of ring deuterated polystyrene shows a small peak at 1607 cm^{-1} with two extra peaks showing at 1569 and 1447 cm^{-1}, respectively. But the C – C bending vibration at 1493 cm^{-1} has completely disappeared in both fully deuterated and deuterated ring polystyrene spectra. Fully deuterated polystyrene spectrum exhibits only two peaks at 1607 and 1569 cm^{-1} with a very small peak at 1441 cm^{-1}, as shown in figure 5.7(b). This is difficult to explain without independent structural information, but it clearly shows the strong influence the deuteration has on the benzene ring vibration.

The spectra in the 1000 to 1400 cm^{-1} region are interesting not only because of the presence of symmetric and asymmetric stretching vibrations of the sulfonate anion, but also because the skeletal vibrations of the aromatic ring appear at 1029 cm^{-1} [19,20]. In this spectral range significant changes were observed in hydrogenous and deuterated samples with the increase of the sulfonation levels. The changes in this region are shown in figures 5.8 and 5.9, respectively. The fully hydrogenous and chain deuterated polystyrene are shown in figure 5.8 (a) and (b). Figure 5.9 (a) and (b) displays the ring deuterated and fully deuterated polystyrene respectively, with the different degree of sulfonation. There is no shift in the peak position and shape for aromatic ring vibration at 1029 cm^{-1} when spectra of sulfonated and pure polystyrene are compared.
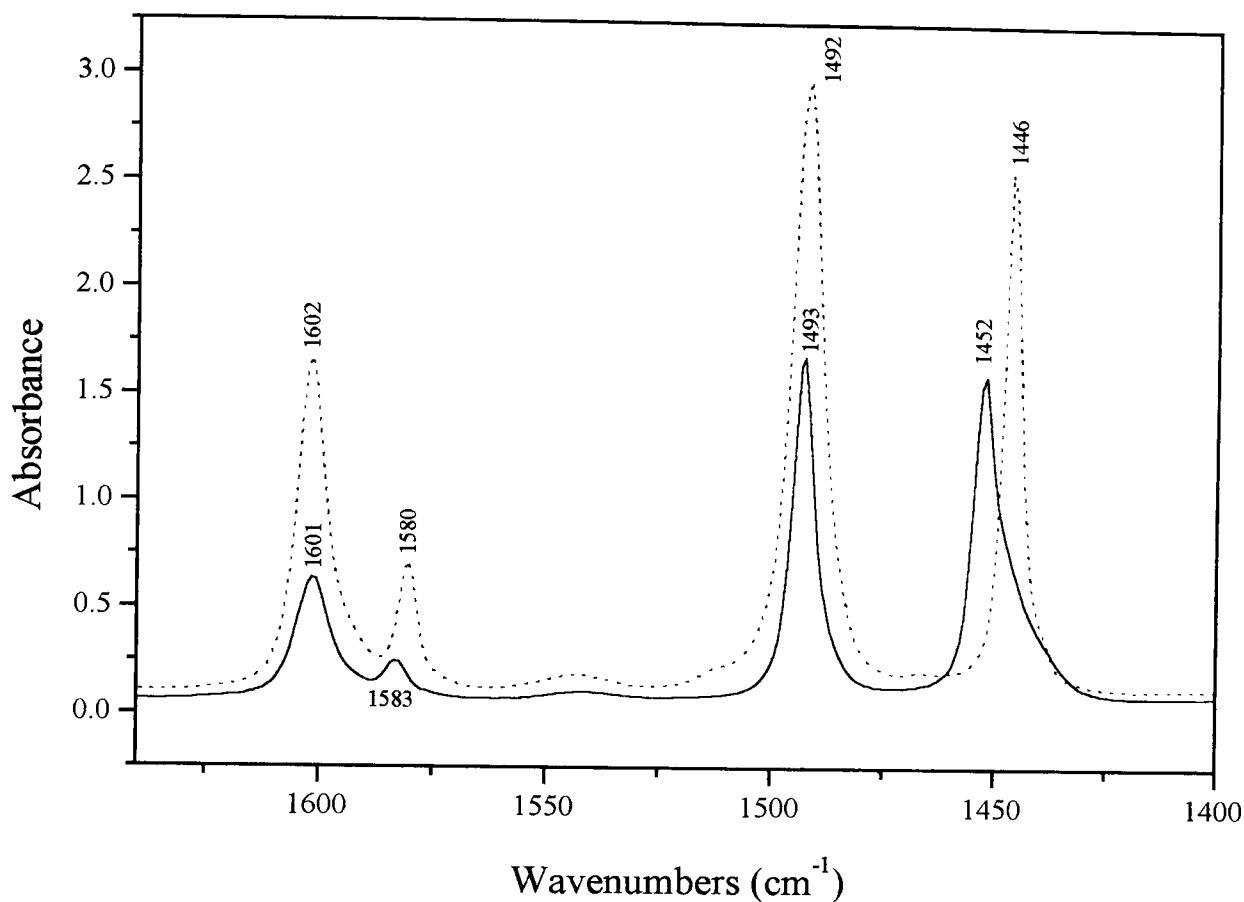
In the hydrogenous sulfonated polystyrene (SPS) spectrum, the bands at 1043, 1129 and 1229 cm^{-1} are associated with the sulfonate anion, -SO$_3^-$, and are sensitive to interactions of sulfonate group with its environment [20-23]. The band at 1229 cm^{-1} is assigned to the asymmetric vibration of the -SO$_3^-$ ion, in fully hydrogenous SPS (at 1228 cm^{-1} in chain deuterated SPS). In ring deuterated and fully deuterated SPS this peak is at 1226 and 1221 cm^{-1}, and shifts by 3 and

8 cm^{-1} compared to fully hydrogenous sulfonated samples, respectively. The shift of the asymmetric S – O stretching vibration is observed to move to lower wavenumbers as the deuterium concentration increases. However this band is shifted to higher wavenumbers with the increasing level of sulfonation in both deuterated ring polystyrene and fully deuterated polystyrene, as demonstrated in figure 5.8 and 5.9, respectively.
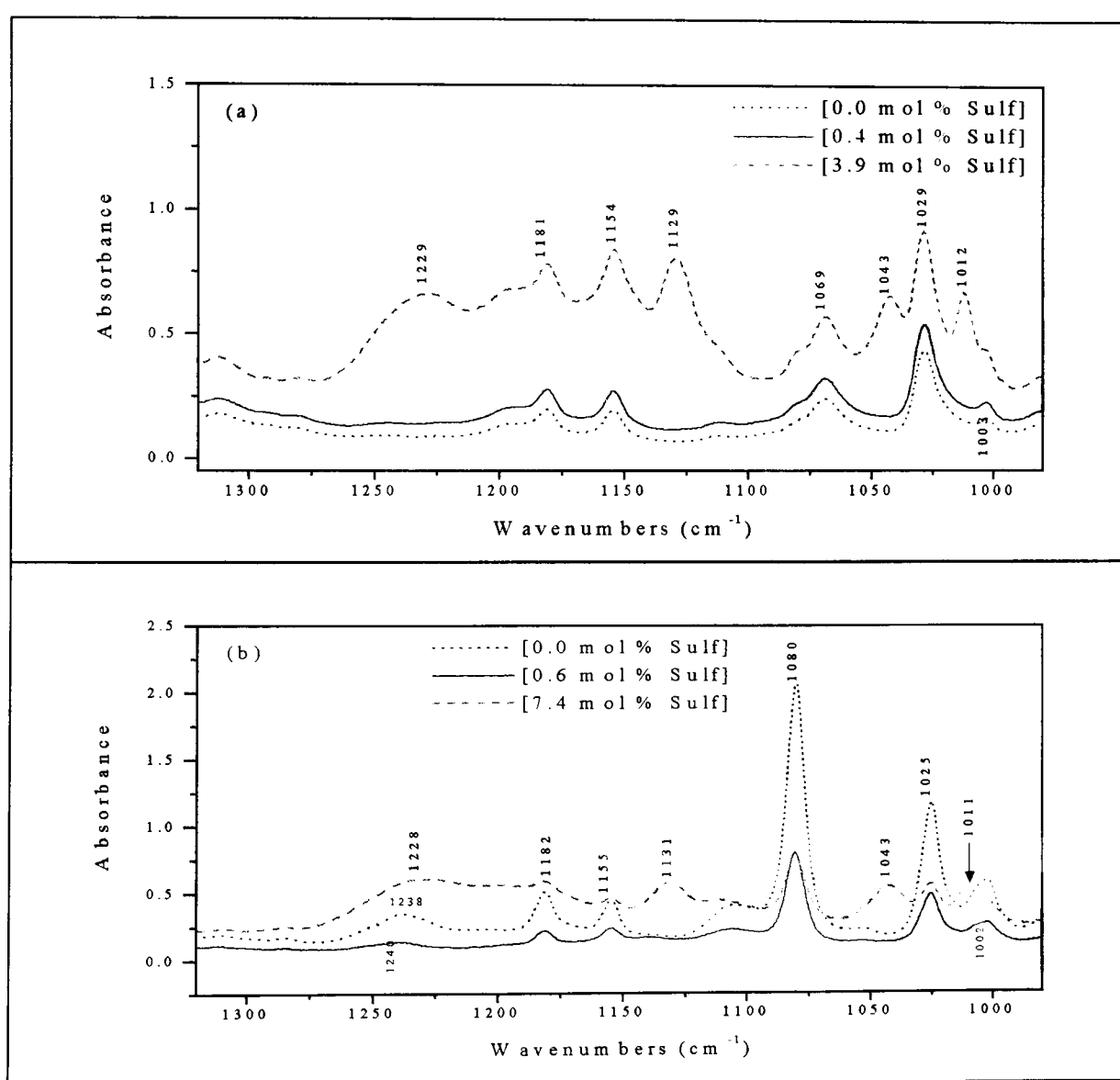
Figure 5.8   Infrared spectra of the S – O stretching region for (a) fully hydrogenous, (b) chain deuterated sulfonated polystyrene.
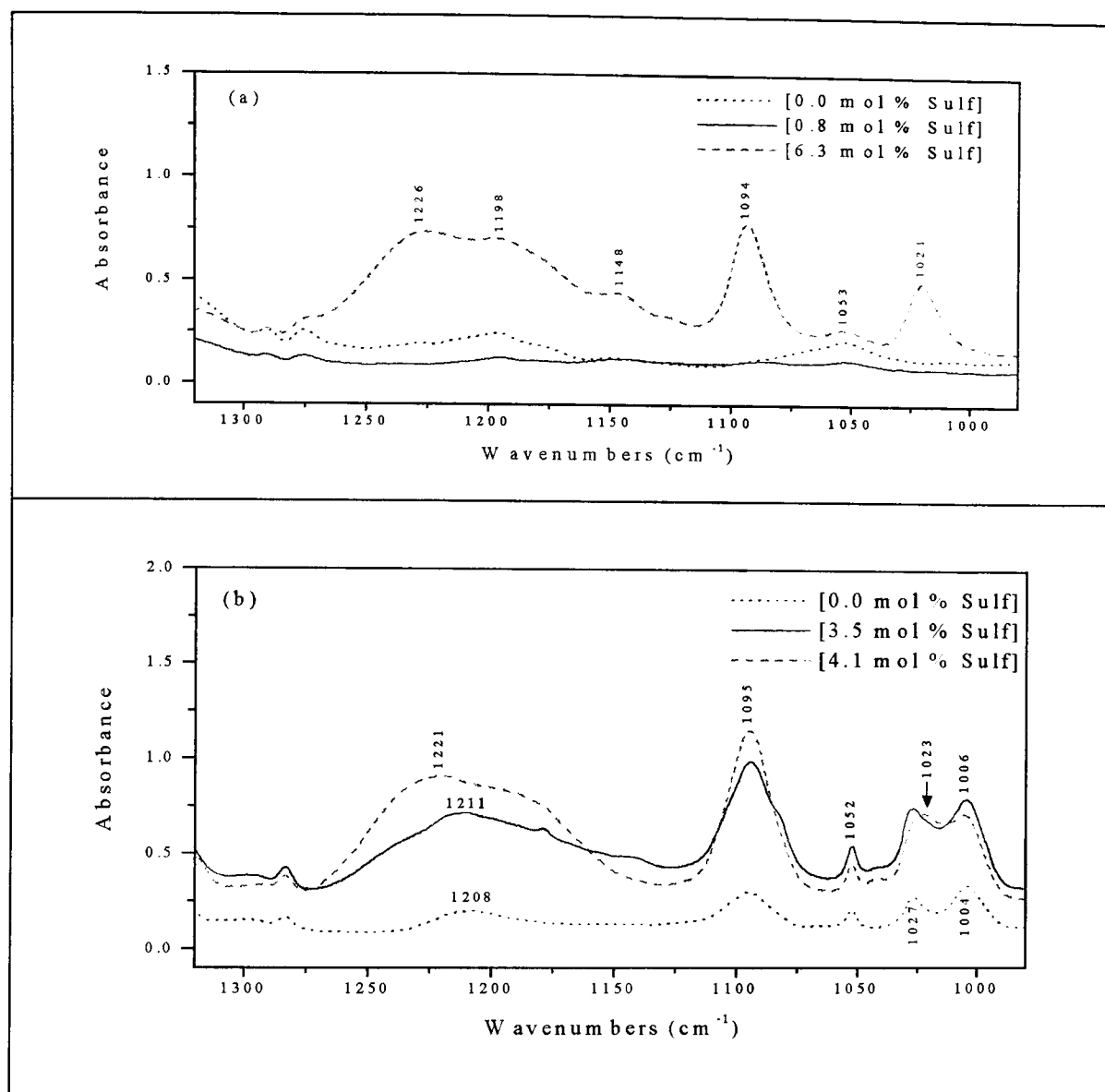
Figure 5.9   Infrared spectra of the S – O stretching region of (a) ring deuterated (b), fully deuterated sulfonated polystyrene.

Similar shifts were observed in the lower frequency range for the hydrogenous and deuterated SPS samples. The peak assigned to asymmetrical bending vibration of $-SO_3^-$ groups were observed to shift to higher frequency with sulfonation. Bands are observed at 667 cm^{-1} with developing peak at 731 cm^{-1} (which increases with the increasing degree of sulfonation) in the hydrogenous

and chain deuterated SPS. These bands were shifted upwards to 695 cm^{-1}, and an additional strong peak appeared at 731 cm^{-1} in fully deuterated SPS as shown in figure 5.10. The two C - H out-of -plane bending vibration present in fully hydrogenous and chain deuterated polystyrene at 699 and 757 cm^{-1} correspond to peaks for monosubstituted ring vibration [24]. But for ring deuterated PS these peaks are also shifted to 551 and to 465 cm^{-1} for both the ring deuterated and the fully deuterated polystyrene.
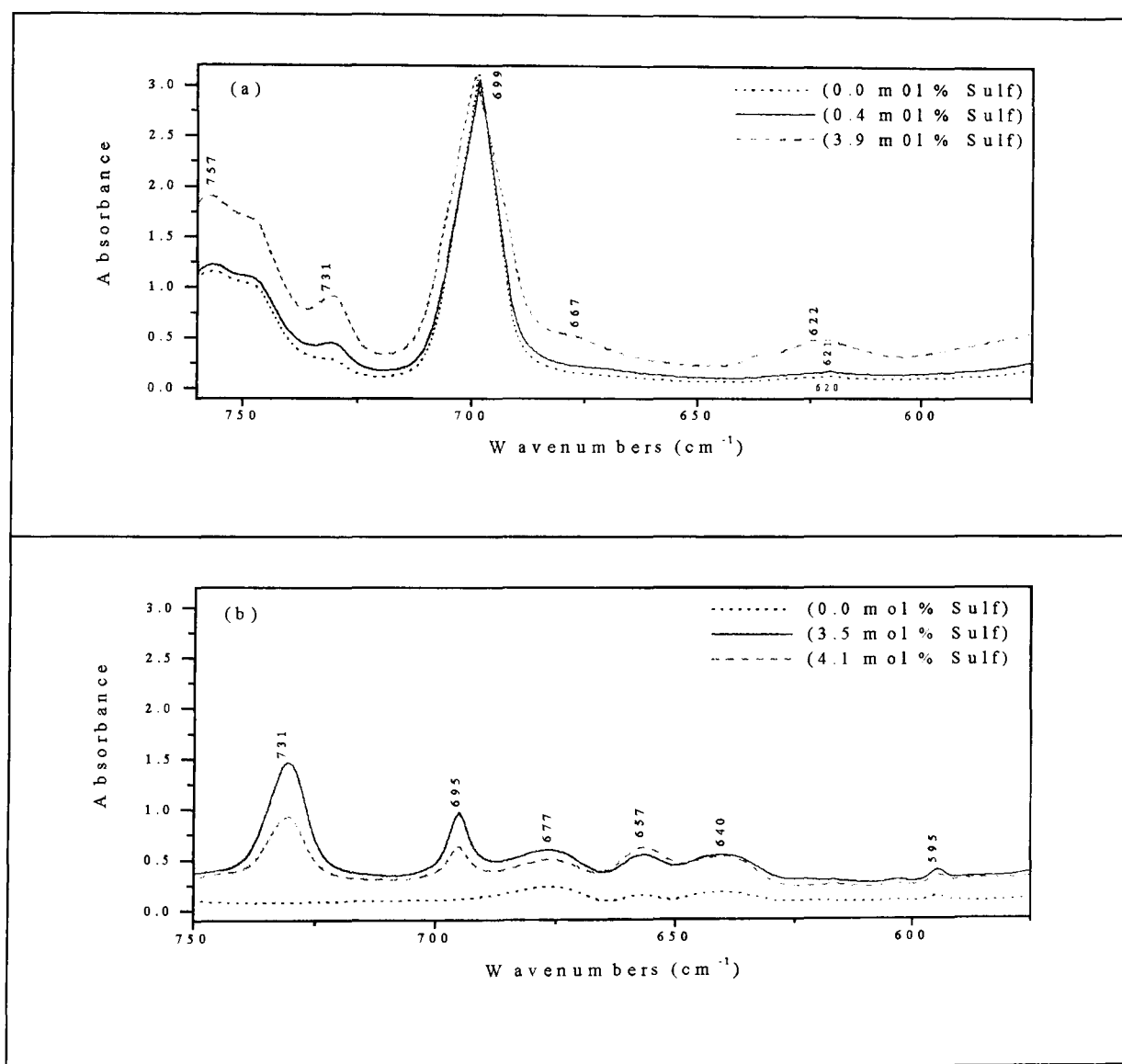
Figure 5.10 Infrared spectra of the S - O stretching region of (a) fully hydrogenous (b), fully deuterated polystyrene.

On the other hand, the $S = O$ symmetric stretching vibration band which appears at 1043 cm^{-1} in fully hydrogenous and chain deuterated SPS, shows the shift to higher wavenumbers at 1053 cm^{-1} with resence of an extra peak at 1021 and 1094 cm^{-1} in ring deuterated and fully deuterated SPS, respectively. Its trend is in the same direction as the latter, but a larger shift was observed. The large band width and the appearance of a new peak suggests that the $S = O$ absorption frequency threshold has been shifted to the higher frequency region, thus indicating the possibility of a formation of a stronger ionic field with the increasing deuterium concentration. The whole change in the spectral feature is believed to be due to the effect of increasing deuterium concentration; deuterium participates in cluster formation together with the sulfonate ions or local environment of $-SO_3^-$ group.

The additional evidence which supports the above conclusion is as follows: The asymmetric $-SO_3^-$ stretching vibration for fully hydrogenous SPS ionomers appears in the 1181 to 1250 cm^{-1} region. For fully deuterated SPS it appears as a very broad feature from 1150 to 1260 cm^{-1}, comprising two bands which become more distinct with increasing deuterium concentration, and its asymmetric stretching vibration is doubly degenerated. The splitting of this band and the positions of the peaks are sensitive to the effect of the increasing deuteration. The broad background in deuterated samples could possibly be due to the strong composite absorption of the $S = O$ and $D - O$ systems. Another visible change occurs around the 1200 cm^{-1} region in all sulfonated polystyrenes, where the spectra of vibrations fill the gap between 1150 – 1250 cm^{-1} with a broad band appearing on sulfonation. Therefore this result supports the outcome of a previous study [14] that sulfonation may destroy the short-range order within the sample and enhance the local chain mobility. The DSC measurement on PS samples show the disappearance of endothermic fusion peaks and the appearance

of a significant shift of T_g position towards higher temperature upon increasing level of sulfonation[25]. It is evident that upon increase in the level of sulfonation a change in the state of material has been produced [26]. This increase is attributed to ionic interactions occurring in the ionic domains, which increase the mobility of the ionomer backbone. The sulfonated spectra also display a peak around 1398 – 1461 cm^{-1}. This peak can be assigned to – SO_2 – group [27], indicating a presence of a small amount of non-ionic groups. The position of this peak is slightly changing, depending on the level of sulfonation and deuteration.

These observations are in agreement with those obtained by other workers on ionomer membranes. Kujawski et al [28] have recently reported work on Nafion, PESS and Raipore membranes. They conclude that the position of the symmetrical and asymmetrical stretching vibration of the sulfonic group differs for each membrane, and this difference may reflect the ionic strength of the sulfonic group in the membrane due to the chemical environment, and it also depends on the type of the sulfonic cation .The same behaviour was observed by Zundel[20] for cross-linked polystyrene sulfonate (PSS) ionomers, who also put forward that the strength of the electrostatic field around a cation depends on its ionic radius and is a controlling factor in determining how it will interact with the sulfonate group. The cation will alter the polarisation of the S – O bond, leading to a frequency shift and /or change in absorptivity.

The strong interaction with the cation produces a shift in frequency of symmetrical and asymmetrical stretching vibrations of the sulfonate group. The increase in field strength as the ionic radius of the cation decreases moves the symmetrical band to higher frequencies. The frequencies of the symmetric stretch

of the sulfonate group measured for sulfonate ionomers in their alkali metal cation forms are collected in Table 5.4.

Table 5.4   Values of ionic radius and electrostatic field with various cationic forms for sulfonate ion symmetric stretch band position of different ionomers.

Ionomer	IR band positions (cm^{-1})			
PSS[a]	1030	1042	1037	1031
PESS[b]	1046	1040	1036	1034
PFS[c]	1073	1064	1059	1055
FEP/PSS[d]	1055	1050	1045	1045
Cation	Li^+	Na^+	K^+	Cs^+
Radius (Å)	0.68	0.97	1.33	1.67
Electrostatic Field (esu.cm^{-1}x10^{-6})	3.18	2.08	1.36	0.98

a   See Zundel.[20]   b   See Kujawski et al.[28]

c   See Lowry and Mauritz.[29]   d   See Levy et al.[30]

Moreover, fully deuterated SPS spectrum contains a strong new peak, at 1495 cm^{-1} (not in unsulfonated spectrum), but ring deuterated SPS exhibits a very weak peak at the same wavenumber. However, fully hydrogenous and chain deuterated SPS did not show any change in this region which contains two bending vibration of C – H group at wavenumbers 1493 and 1452 cm^{-1} respectively, as demonstrated in figure 5.11. These results indicate that sulfonation will alter the distribution of deuterium in the sample and some

deuterium is replaced with hydrogen on the ring only. This is confirmed by the presence of C – H stretching vibration of hydrogenous moieties at around 3000 cm^{-1} as shown in figure 5.4 (b) and (c).
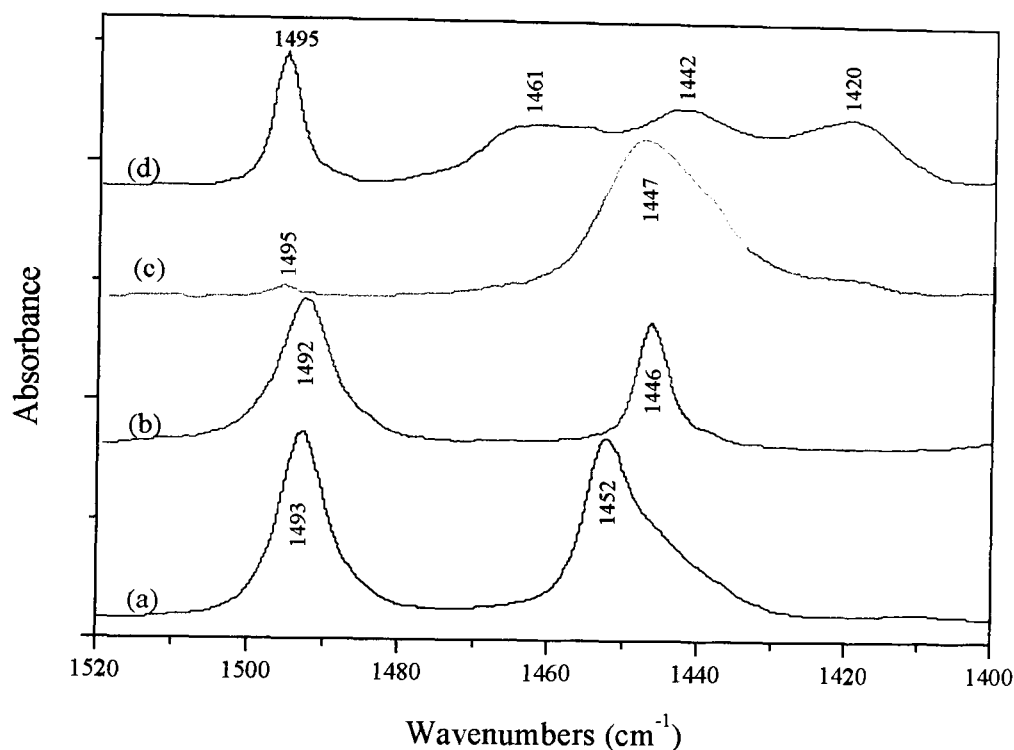
Figure 5.11 Infrared spectra (1400 – 1520 cm^{-1}) of sulfonated polystyrene. (a) Fully hydrogenous, (b) chain deuterated, (c) ring deuterated and (d) fully deuterated SPS.

The benzene ring vibration at 840 cm^{-1}, corresponding to C – H out – of – plane bending vibration [24] is very sensitive to the degree of sulfonation [20,23,27]. For para substituted hydrogen (the term *para* is the isomer of a disubstituted benzene ring in which the two groups are opposite each other in 1, 4 position, *ortho* 2, 6 and *meta* 3, 5 position of the benzene ring), this peak moves to about 820 cm^{-1}, it moves to 750 for ortho, and for metha substitution a double peak appears at 690

and 780 cm^{-1}, respectively [27,31]. This band has been found to change significantly in position and intensity with the sulfonation of fully hydrogenous and chain deuterated polystyrene as shown in figure 5.12 (a) and (b) respectively.
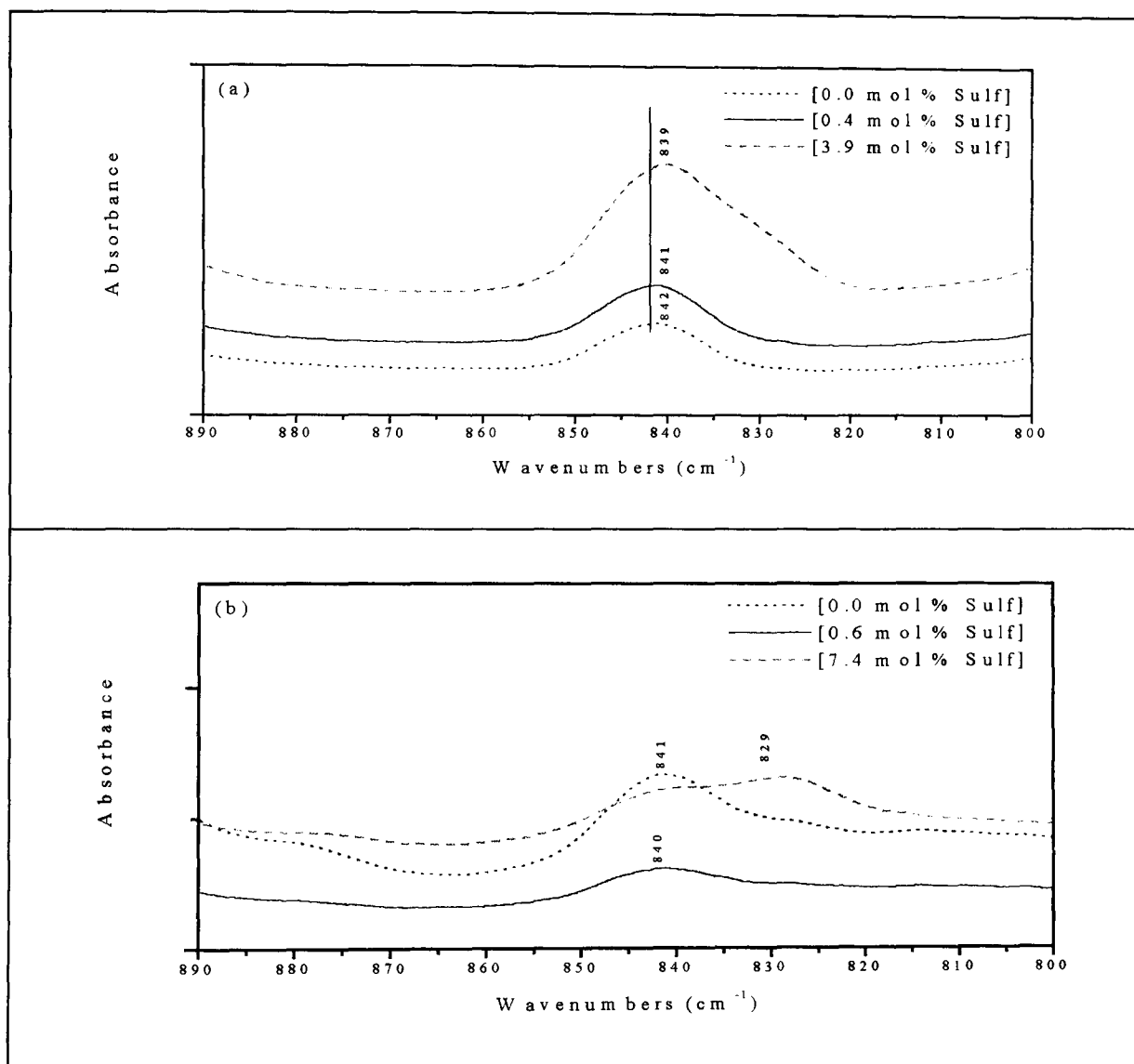
Figure 5.12 Infrared spectra of the C – H out – of – plane bending vibration, (a) fully hydrogenous and (b) chain deuterated sulfonated polystyrene.

Its intensity increases with increasing degree of sulfonation and is shifted down in frequency with increasing degree of sulfonation. It has been shown [32] that with addition of functional groups to the benzene ring, the 840 cm^{-1} band is shifted to

lower frequencies of about 820 cm^{-1}. In the case of PS ionomers investigated here, this peak appears at 829 cm^{-1} for 7.4 mol % sulfonation. This indicates that not all benzene rings are sulfonated, and a simple calculation of molecular weight (as given below) shows that for 7.4 mol %, only about one half of the rings are sulfonated. This corresponds well to the observed shift halfway towards the 820 cm^{-1} position.

-(- CH$_2$ - CH -)-

H $\bigcirc$ H $=$ 8C + 1S +3O +1Na +7H
H   H   8x12.01+1x32+ 3x16+1x22.99+7x1.008
SO$_3^-$Na$^+$ 96.08+32.06+48.00+22.99+7.056

Total Mw = 206.186

$$\frac{32.06}{206.186} = 0.15563 = 15\%$$

(Full sulfonation : every ring would be occupied)
Therefore
7.4 mol % x 2 = 14.8 ~15 %
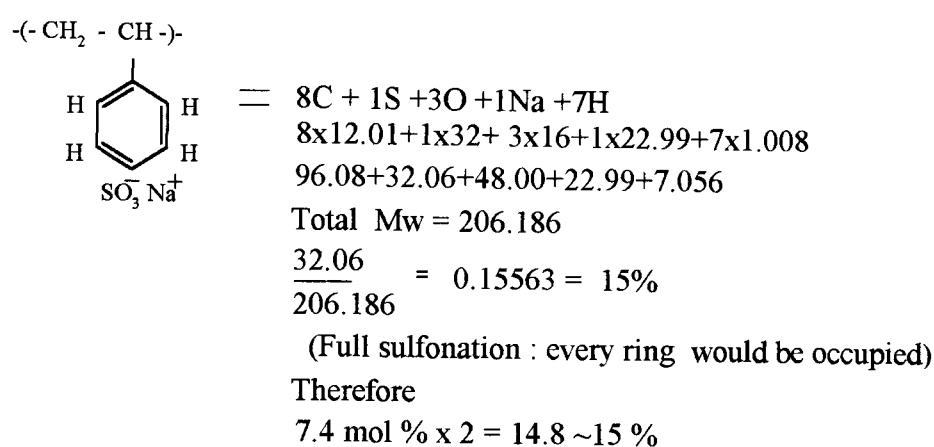
Unfortunately, this peak was not observed for polystyrene with ring-deuterated and fully-deuterated polystyrene due to a peak overlap: PS with deuterated rings shows two peaks (838 and 823 cm^{-1}) in this region [32] as shown figure 5.13 (a) and (b). The other band at 1003 cm^{-1} is assigned to the in – plane bending vibration of para – substituted benzene rings [33], which also increases with the sulfonate group being the substitute group. This peak has been found to change in position and intensity with the increasing level of sulfonation in both hydrogenous and deuterated sulfonated polystyrene as demonstrated in figure 5.8 and 5.9, respectively. The above observations of the para – substitute vibration suggest that the sulfonation group must be predominant at the para-position of the benzene ring.
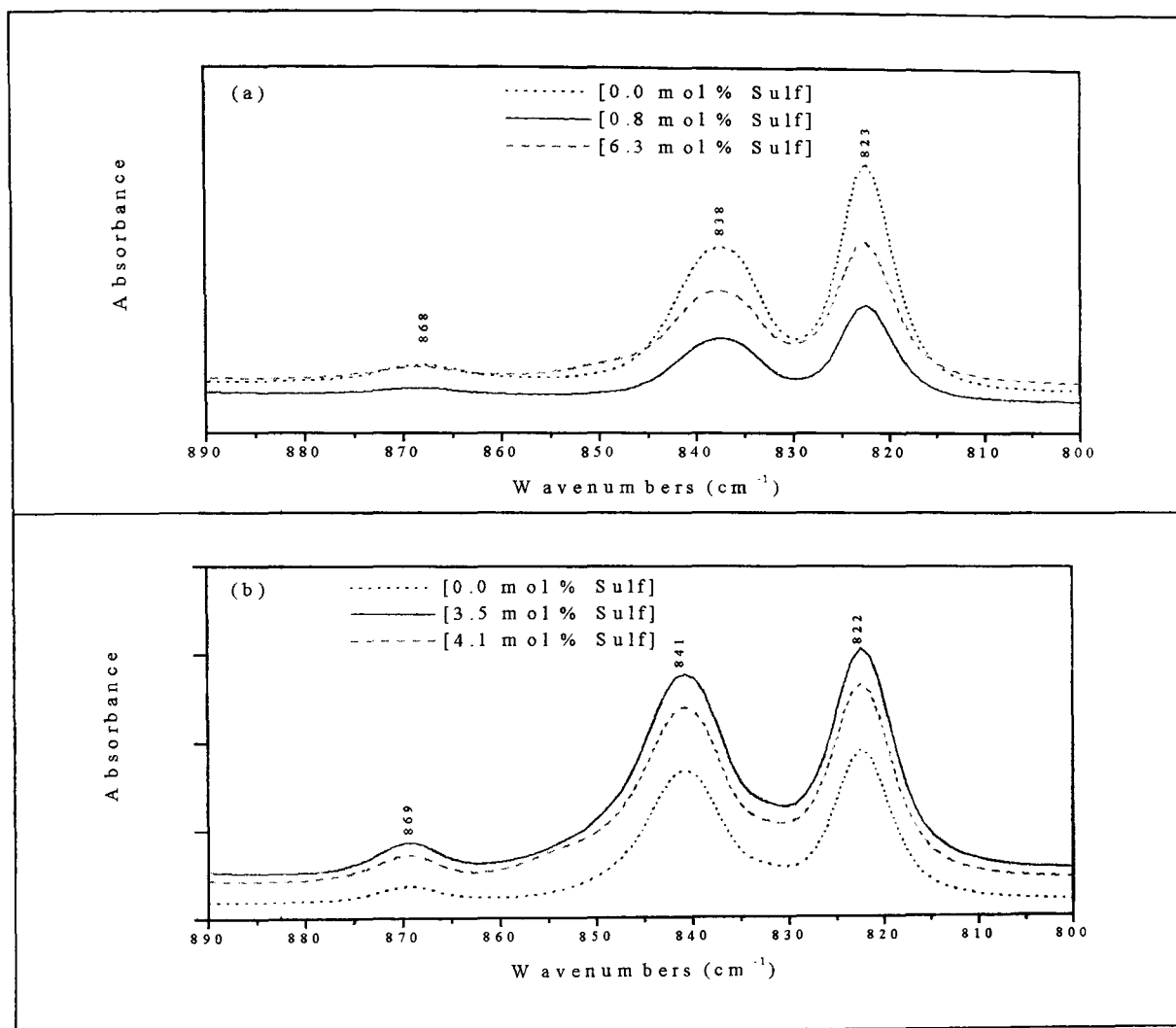
Figure 5.13 Infrared spectra of the deuterated ring vibration (a) ring deuterated and (b) fully deuterated sulfonated polystyrene.

This analysis has shown that the level of sulfonation and its location on the benzene ring can be clearly identified in IR measurements. It also shows the effect the deuteration has on the vibrational spectrum of the benzene rings (the peak shift of C – H vibration to C – D vibration and the C = C stretching vibration intensity and position are also different for hydrogenous and deuterated polymers). The presence of a small amount of – SO_2 – group has also been detected (1398 – 1461 cm^{-1} peak). It is however not possible without further

analysis and more accurate peak assignment to reveal the possible effects of clustering on the structure of the samples investigated.

5.4   CONCLUSIONS

In this study, we have confirmed the para - position of the sulfonate group on the benzene ring of the styrene unit. It is also expected from the consideration of chemical probabilities that such a substitution takes place exclusively at the para position. Moreover we have found that the spectrum of the chain deuterated and fully deuterated polystyrene revealed the presence of residual hydrogen on the chain. In this study, we have also demonstrated the changes occurring in the FTIR spectrum due to the process of sulfonation. These results clearly show that the vibrational bands depend on the strength of the bonds and the masses of the atoms involved in the particular vibration mode, as well as charge of the cation.

These results are also indicating the possibility of a formation of a stronger ionic field with the increasing deuterium concentration which participates in cluster formation together with the sulfonate ions. Moreover, FTIR measurements supports the outcome of previous study obtained by Gabrys et al [26] and Nickolson et al [25] that the process of sulfonation destroys the short-range order within the sample and enhance the local chain mobility.

Finally, the present studies of selectively deuterated functional groups allowed us to uniquely assign peaks which were not assigned previously to chain or ring vibration, namely 2194 cm^{-1} and 2272 cm^{-1}. It is also shown that the spectra are sensitive to a modification by deuteration or by sulfonation of adjacent functional groups (e.g. C – H vibrations of the chain)

References

1. Eisenberg, A.; King, M., *Ion containing Polymers, Physical Properties and Structure*, Academic press: New York, **1977**.

2. Utracki, L. A.; Weiss, R. A., Eds., *Multiphase Polymers: Blend and Ionomers*, ACS Symposium Series No.395. Am. Chem. Soc., Washington, DC, **1989**.

3. Macknight, W. J.; Earnest, T. R. *Macromol. Rev.* **1981**,16, 41.

4. Tant, M. R.; Mauritz, K. A.; and Wilkes, G. L, *in Ionomers, synthesis, structure, properties and applications*, Blacki Academic and Professional, London, **1997**.

5. Tant, M. R.; and Wilkes, G. L., *J. M. S.- Rev. Macromol. Chem. Phys.* **1988**, C28 (1), 1.

6. Fitzgerald, J. J.; and Weiss, R. A., *J. M. S.- Rev. Macromol. Chem. Phys.* **1998**, C28 (1), 99.

7. Eisenberg, A. *Macromolecules* **1970**, 3, 147; Hird, R. B.; and Moore, R. B. *Macromolecules* **1990**, 23, 4098.

8. Register, R. A.; X-hai, Yu.; and Cooper, S. L. *Polym. Bull.* **1989**, 22, 565.

9. X-hai, Yu.; Grady, B. P.; Reiner, R. S.; and Cooper, S. L., *J. Appl. Polym. Sci.* **1993**, 47, 1673.

10. Wilson, A. D.; Prosser, H. J.; Eds., *Development in ionic Polymers*, Applied Science, New York, **1983**. (b). Lundberg, R. D., *Encyclopedia of Chemical Technology*, 3rd ed., Supplement Volume, **1984**, 546.

11. Schlick, S, Ed., *Ionomers, Characterization, Theory and Applications*, CRC press: London, **1996**.

12. Rees, R. W. U. S. Patent 3264272, assigned to *E. I. Du Pont de Nemours & co.*, **1966**.

13. Seisler, H. W.; Holland-Moritz, k., *Infrared and Raman Spectroscopy of Polymers*, Marcel Dekker, New York, **1980**

14. Gabrys, B. J.; Huang, D.; Nardi, F.; Peiffer, D. G.; and Tomkinson, J. *Macromolecules* **1993**, 26, 8, 2007.

15. Englewood Cliffs, Prentice-Hall, N. J.; Inc., *Applications of Absorption Spectroscopy of Organic Compounds*, **1965**.

16. Bartell, H. B., *J. Chem. Phys.* **1965**, 42,851.

17. Liang, C. Y.; and Krimm, Infrared Spectra of High polymers. VI. Polystyrene, *J. Polym. Sci.* **1958**, 27, 241.

18. Randy, W.; and Painter, P. C. *Polymer* **1981**, 22, 1633.

19. Weiss, R. A.; and Padmavathy Rajagopalan, *J. Polym. Sci.: Polym. Phys. Ed.* **1995**, 33, 495.

20. Zundel, G., *in Hydration and intermolecular Interaction*, Academic Press: New York, **1969**; chap. 4.

21. Vasilis, G. Gregoriou, *Applied Spectroscopy* **1997**, Vol. 51, 4.

22. Lu, X.; Weiss, R. A. *Macromolecules* **1996**, 29, 1216.

23. Fan, D. X.; and Bazuin, C. G. *Macromolecules* **1995**, 28, 8209.

24. Varsanyi, G., *Vibrational spectra of Benzene Derivatives-* Academic Press: New York and London, **1969**.

25. Nickolson, L. K; Mahmood, K.; Gabrys, B, J; Vesely, D; and Peiffer, D. G., submitted to "Polymer".

26. Schärpf, O.; Gabrys, B. J.; and Peiffer, D. G., *ILL report 90 SC 26T, Part A, Part B*, Institute Laue - Langevin, Grenoble, France, **1990**.

27. Donald, L. P.; and Gary, M. L., *Introduction to Spectroscopy*, 2nd Edition, Saundero Golden Sunburst Series, **1996**.

28. Kujawski, W.; Nguyen, T. Q.; Neel, *J. Appl. Polym. Sci.* **1992**, 44, 951.

29. Lowry, S. R.; Mauritz, K. A., *J. Am. Chem. Soc.* **1980**, 102, 4665.

30. Levy, L. Y.; Jenard, A.; Hurwitz, H. D., _J. Chem. Soc. Faraday Trans._ **1980**, 76, 2558.

31. Norman, B. C.; Lawrence, H. D.; and Stephen, E. W., _Introduction to infrared and Raman Spectroscopy_, 3rd Edition, Academic Press: Inc., **1990**.

32. Charles, J. P., _The Aldrich Library of FTIR Spectra_, Edition one, Vol:2, Aldric chemical company. Inc., **1985**.

33. Painter, P. C., _J. Polym. Sci., Part B: Polym. Phys._ **1977**, 15, 1885.

CHAPTER SIX

NEUTRON REFLECTIVITY OF IONOMER BLENDS

This chapter contains a report on an investigation by neutron reflectivity of two ion – containing polymer blends. The work on lithium and zinc-salt of deuterated sulfonated polystyrene (d-SPS) with Polycarbonate (PC) blends is a joint project with Dr. R. A. Weiss, University of Connecticut, USA.

6.1   INTRODUCTION

The concentration profile at polymer-polymer interfaces characterises the interfacial structure. It not only is an important parameter for understanding the chemical and physical interactions at the interface, but also governs the interfacial adhesion, which ultimately controls the physical and mechanical properties of the blend [1].

The concentration profile at the interface is a result of the interfacial mixing of components across the polymer-polymer interface. Therefore, morphology, adhesion and final properties of the material hinge on the control of interfacial mixing. Moreover, observation of the degree of interfacial mixing at a certain temperature as a function of time provides information about the interdiffusion coefficient of the system.

Interfacial mixing takes place when two polymer surfaces are brought into contact and diffuse into each other [2], as a result of the interaction between the

two polymers[3]. The general theories regarding polymer interdiffusion and techniques used to study polymer-polymer interfacial mixing are described in two excellent reviews [4-6]. In this study, we focus our attention on polymer – polymer interdiffusion as the result of the interfacial mixing of a partially miscible system polycarbonate and a lightly sulfonated polystyrene ionomer pair. The interfacial development was investigated as a function of annealing time at 200 and 220°C. The interfacial width obtained after annealing the sample for time t_0 at 200°C and 220°C can be correlated with different times and temperatures at one temperature by using the WLF (Williams-Landel-Ferry) empirical equation as given below

$$\log \frac{t}{t_0} = \frac{c_1(T-200)}{c_2+(T-200)}$$

6.1

The constants c_1 and c_2 depend on the temperature range and can be found in the literature [7].

In a small molecular system, the diffusion is usually described by a Fickian equation with a constant diffusion coefficient [8]. In a polymer melt or a polymer solution when both components are mobile, a number of studies have shown that a concentration dependent diffusion coefficient is required, but Fickian theory is still applicable. As a result, theories predict that the movement of the interface is linear with the square root of the interdiffusion time toward the faster-moving species. This prediction has been experimentally verified [9-12].

In the case of a glassy polymer in small molecular solvents, however, transport phenomena in general cannot be explained by Fickian diffusion theory [13]. The diffusion process is "anomalous", since interdiffusion is influenced by the stress

relaxation of the glassy polymer as it is swollen by the penetrating solvent. In the limiting case, when the transport rate is entirely controlled by polymer relaxation processes, "Case II" diffusion is applied [14]. A characteristic of "Case II" diffusion is that as the mobile species penetrates into the glassy polymer, a sharp advancing boundary separates the inner glassy core from the outer swollen, rubbery shell, and this boundary advances at a constant velocity towards the glassy polymer. Most diffusion problems of practical interest in polymers cannot be explained by Case II and numerous [15-17] new mechanisms [18-20] have been proposed. In this work the diffusion rates, as predicted by different proposed models are correlated with new experimental data.

It is known that polystyrene is immiscible with bisphenol-A polycarbonate, whereas blends of sulfonated polystyrene with polycarbonate are miscible at all concentrations in the range of 8.7 – 13.7 mol. % sulfonation [21-23]. In previous studies Weiss et al [21-23] reported that blends of lightly sulfonated polystyrene ionomer (SPS) and bisphenol-A polycarbonate (PC) were partially miscible for a narrow range of the sulfonation of the ionomer. Both lithium and zinc-SPS/PC systems exhibit upper critical solution temperature (UCST) phase behaviour and a miscibility gap with respect to the sulfonate concentration. Fourier transform infrared spectroscopy revealed that no specific interactions involving either the carbonate carbonyl group or the metal sulfonate group occurred in these blends [22]. The miscibility was attributed to intramolecular repulsive interaction within the ionomer, the so-called copolymer effect.

A high resolution technique is required to probe the interface between the polystyrene ionomers and the polycarbonate. Therefore we have used neutron reflectivity to investigate the polymer-polymer interfaces since it provides

subnanometer resolution and high contrast when one of the two polymer components is selectively deuterium-labelled [24-26].

In this chapter we report some preliminary results from the application of the specular reflection of neutrons to the study of the nature of the interface between the two different cation lithium and zinc deuterated polystyrene with polycarbonate (PC), subjected to annealing treatment.

6.2   EXPERIMENTAL

6.2.1   Materials

The polymers used in this work were polycarbonate and deuterated sulfonated polystyrene with different metal cations (i.e. Lithium and Zinc). The structures of these polymers are shown below (page 169).

Polycarbonate (PC) was obtained from Aldrich Chemical Co., Inc. and had number average and weight average molecular weights of 12,100 and 22,600 g/mole, respectively.

Deuterated polystyrene (d-PS), with a number average molecular weight of 18,620 g/mole and polydispersity 1.03, was synthesized by Dr. Robson Storey at the University of Southern Mississippi, USA. The samples of d-LiSPS and d-ZnSPS were prepared by Yacob Ghebremeskel, using the method described below. Sulfonation level was determined to be 11.2 mol % for both samples.

The starting deuterated polystyrene was obtained through anionic polymerization. The sulfonation reaction of the deuterated polystyrene was carried out in dichloroethane at 60°C using acetyl sulfate to produce a polymer randomly substituted with sulfonate groups at the para position of the phenyl ring[27]. The reaction was terminated by adding a small amount of isopropyl alcohol. The resultant sulfonic acid derivative (d-HSPS) was recovered by steam stripping and dried under vacuum. d-HSPS was neutralized with an excess of lithium acetate in 90/10 toluene/methanol to produce the lithium salt of the ionomer (d-LiSPS), which was again recovered by steam stripping and dried

under vacuum. Sulfonation levels were determined by elemental sulphur analysis at Galbraith Laboratories, Inc. USA.

The characteristics of these samples are shown in Table 6.1. The molecular weight characteristics of the polymers were determined through GPC analysis, whereas the T_g temperatures were determined through DSC [21-23]. The neutron scattering length densities (Nb) were calculated from the respective elemental composition and mass density.

-(CH - CH₂)(CH - CH₂)-

SO₃⁻M⁺
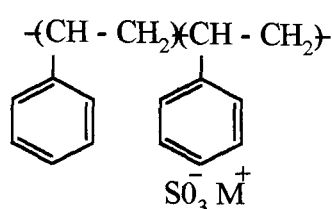
Sulfonated Polystyrene (SPS)
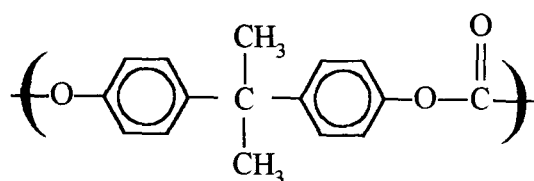
Polycarbonate (PC)

Table 6.1   Characteristics of samples used in neutron reflectivity experiments.

Polymer	M_n g/mol	M_w g/mol	T_g °C	Density g/cm³	Nb x 10⁻⁶ Å⁻²
PC	12,100	22,600	155	1.20	2.03
d-ZnSPS	18,620	18,750	120	1.17	5.7
d-LiSPS	18,620	18,750	120	1.17	5.97

6.2.2 Sample Preparation

The samples prepared for the neutron reflection experiment consisted of a bilayer film of d-ZnSPS and d-LiSPS on top of a thick layer of PC (both layers cast on a silicon wafer). Samples were prepared by Dr. Weiss's group at the University of Connecticut, USA. The sulfonation level of these dSPS was 11.2 mol %. Prior to spin – coating, the silicon disks were cleaned in a 70/30 sulphuric acid / hydrogen peroxide solution for 45 min. They were then rinsed thoroughly in deionized water and blown dry. The bottom layer was prepared by spin – coating (at 1350 rpm) from a 1% (weight) solution in a methylene chloride solvent directly on to a polished silicon wafer, with the aim of achieving a layer thickness of ~100 nm. After spin – coating, the thin PC film was first air – dried and then dried in a vacuum oven for 45 min. at room temperature. Half of these wafers were then coated with d-LiSPS, and the other half were coated with d-ZnSPS. A 1- % solution of d-LiSPS or d-ZnSPS in solvent mixture 90/10 toluene/methanol, was then spun cast onto the PC layer at 1750 rpm, leaving a coat of approximately 40 nm. Samples were stored in a dessicator until the time of the experiment to protect the samples from moisture.

Interfacial mixing was measured by placing the bilayer samples at the annealing temperatures of 200 and 220°C in a vacuum oven for different periods of time. Two samples were not annealed (as made) to compare with the annealed samples. A list of the annealing times is given in Table 6.2. The annealing times analysed were the same for both Zn-and Li-salts. After prescribed annealing period, the specimens were quenched by natural cooling to the room temperature for the neutron reflectivity measurements.

Table 6.2   Annealing times for the bilayer d-ZnSPS/PC and d-LiSPS/PC.

Annealing Code	Cumulative annealing time @ 200°C (hrs)
As made	0
B	1
C	3
D	5
E	7
F	14
G	60

The annealing temperature was chosen so that it was above the glass transition temperatures of both polymers where the polymer chains were mobile, in order to allow interfacial mixing to occur.

6.2.3   Neutron Reflectivity Measurements

The neutron reflectivity measurements were carried out at the ISIS pulsed neutron source, Rutherford Appleton Laboratory, on the CRISP reflectrometer[28]. Data were collected at three different incident angles, 0.25, 0.6 and 1.5°, and were then merged to form a single reflectivity curve. The reflection from the film was measured at the specular angle by a single well-collimated detector. The wavelength dependence of the reflected neutron intensity is obtained by a time – of – flight analysis.

The reflected intensity is converted to reflectivity by removal of the incident spectral shape (using an incident beam monitor), corrected for the detector efficiency and normalised to unity at total reflection. The procedure for modelling and fitting the reflectivity spectrum is documented elsewhere [29]. The calculation of the specular reflectivity profiles can be performed exactly for any model profile using the optical matrix method [30]. In this study least-square fitting method was used. However, before we proceed into the detail description of the experimental results it is in order to explain briefly the way that data were analysed.

6.2.4 Data Analysis

The NR data analysis was carried out using a combination of model-fitting techniques. Model-fitting is the standard approach towards NR data analysis. It works relatively well when there is enough prior knowledge of the system but it gives model-dependent results for the interfacial profile.

The procedure for the data analysis is as follow. The "Mulf" program was used throughout in combination with standard analysis programs to get accurate fitting. First a program called SLAB_FIT was initially utilised which provided model suggestions for the specific data set as the regularising parameter. The only input parameters of the program are the total sample thickness and the scattering length density (Nb) of the substrate. Therefore prior knowledge of the total sample thickness, for example through simulation in "Mulf", is crucial in obtaining physically meaningful solutions. The program then tries to produce the best fit for 1 layer, then 2 layers, and so on to a maximum of 20 layers. The program can be run interactively or non-interactively. After running this program the proposed models are checked for physical meaning, and there are two

possibilities: a) the program did propose a physically meaningful model or b) none of the suggested models is physically correct.

When a meaningful model is found the SLAB_REFINE program is utilised. This parameter-refinement model uses as input the parameter set obtained from SLAB_FIT and refines it using standard model fitting. The program compares the calculated profile from the suggested model with the experimental data and when the profiles are the same this model and parameter set are taken as the final result. This way a model-independent procedure is followed while at the same time physically meaningless solutions are rejected.

Before proceeding to the Results section (6.3) it is very important to make a distinction between what is considered as the interfacial width for the symmetric and asymmetric interfacial profile. From the data analysis the neutron scattering length density (Nb) of the system is obtained as a function of distance z perpendicular to the interface. If the interface has a Gaussian profile the interfacial width w is defined as

$$w = \sigma\sqrt{2\pi}$$

where σ is the Gaussian width or interfacial roughness. In cases of asymmetric interfaces that are not described simply as a single Gaussian (or tanh) profile then the width w is defined in a different way. It is defined as the distance covered by 82% of the total change in volume fraction between the two media as can be seen in figure 6.1.
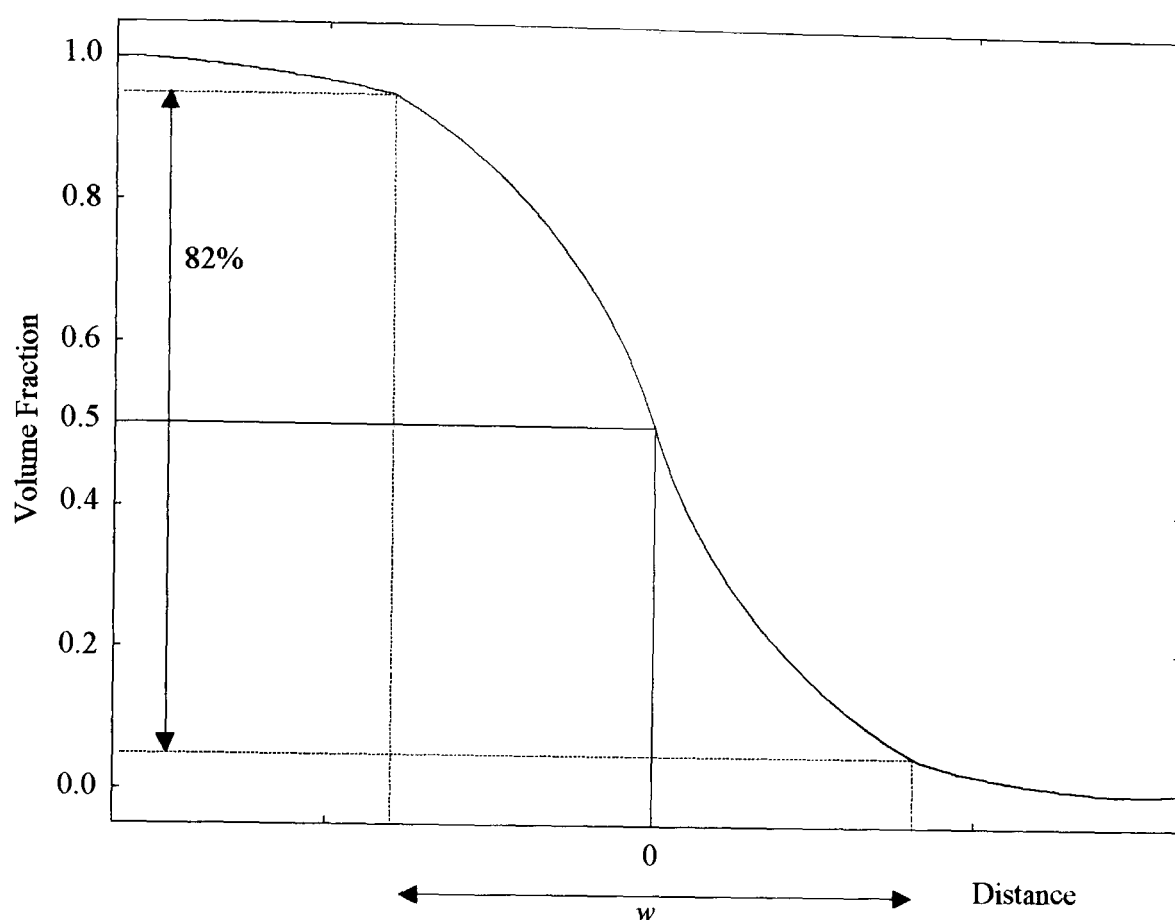
Figure 6.1   Definition of interfacial width w in the case of an asymmetric interfacial profile that cannot be described as a single Gaussian profile.

6.3   RESULTS AND DISCUSSION

Theory predicts that when two polymers, which are thermodynamically partially miscible are brought together and allowed to diffuse the initially sharp interface between them broadens due to the mutual diffusion of the two types of polymer chains. Intermixing across the interface will continue until an equilibrium width is reached. It is important to note that in this case the kinetics of formation of interfaces between chemically different polymers is controlled by thermodynamic as well as kinetic factors. NR experiments were carried out on the two different partially miscible systems d-ZnSPS/PC and d-LiSPS/PC.

6.3.1   d-ZnSPS/PC System

As stated in chapter three, the aim of a neutron reflection experiment is to measure the neutron specular reflectivity as a function of the wave vector transfer (or incident neutron wavelength since both quantities are simply related) perpendicular to the reflectivity surface.

A typical example of such a profile is given in figure 6.2, which corresponds to the reflectivity curves for an "as made" bilayer sample of d-ZnSPS/PC on a silicon substrate. The error bars represent the experimental data and the solid line is the calculated reflectivity profile for which the parameters in Table 6.3 have been used. The solid line in figure 6.2 represents the optimal reflectivity calculated using a symmetric Gaussian function model [24,29] for the scattering length density profile at the interface. In this model, the first derivative of the scattering length density with respect to the depth Z is Gaussian function shown below:

$$G(Z) = \frac{Nb}{(2\pi)^{1/2} < Z_\sigma >} e^{-\frac{z^2}{2<Z_\sigma^2>}}$$

Here, Nb is the scattering length density difference of the two bulk phases that form the interface, and $< Z_\sigma >$ is the standard deviation of the Gaussian function that characterises the interfacial width. The scattering length density, Nb, for d-ZnSPS, d-LiSPS and PC was calculated using the elemental composition of the polymers, tabulated values of the scattering length of each element and the mass density of the polymers, see Table 6.1. This left only three adjustable parameters: the film thickness, d, and the air-surface roughness or the ionomer/polymer

interfacial width, $<Z_\sigma^2>^{1/2}$ for fitting the interface model to the experimental data. The best scattering length density profile fit for the "as made" sample (see figure 6.3) gave an interfacial width "w" of 12 Å. This interfacial width corresponds to a relatively sharp initial interface for a partially miscible blend. The top layer of d-ZnSPS is 409 Å thick whereas the bottom PC layer is 1300 Å thick.
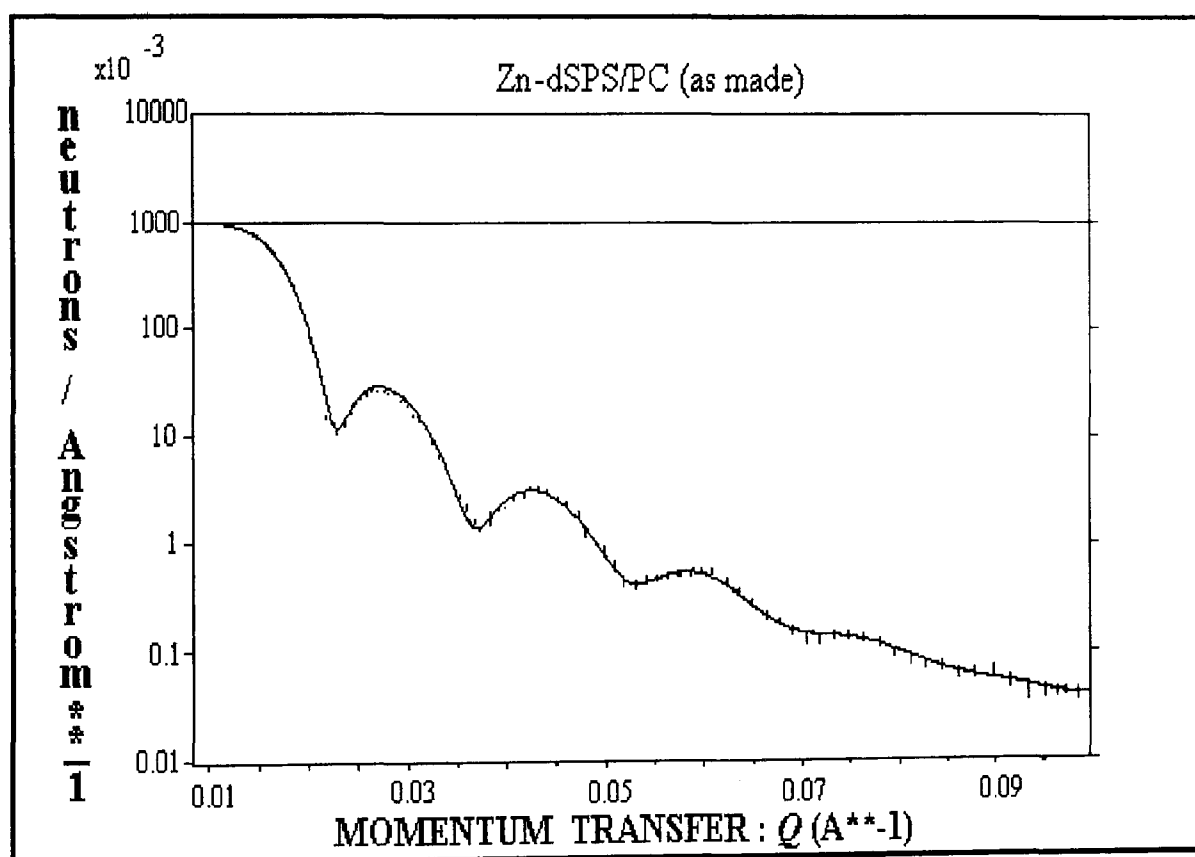
Figure 6.2   Neutron reflectivity profile of a d-ZnSPS/PC bilayer "as made" on a silicon wafer. The error bars represent the experimental points and the solid line curve is the best fit by using a symmetric interfacial model shown in the next figure.
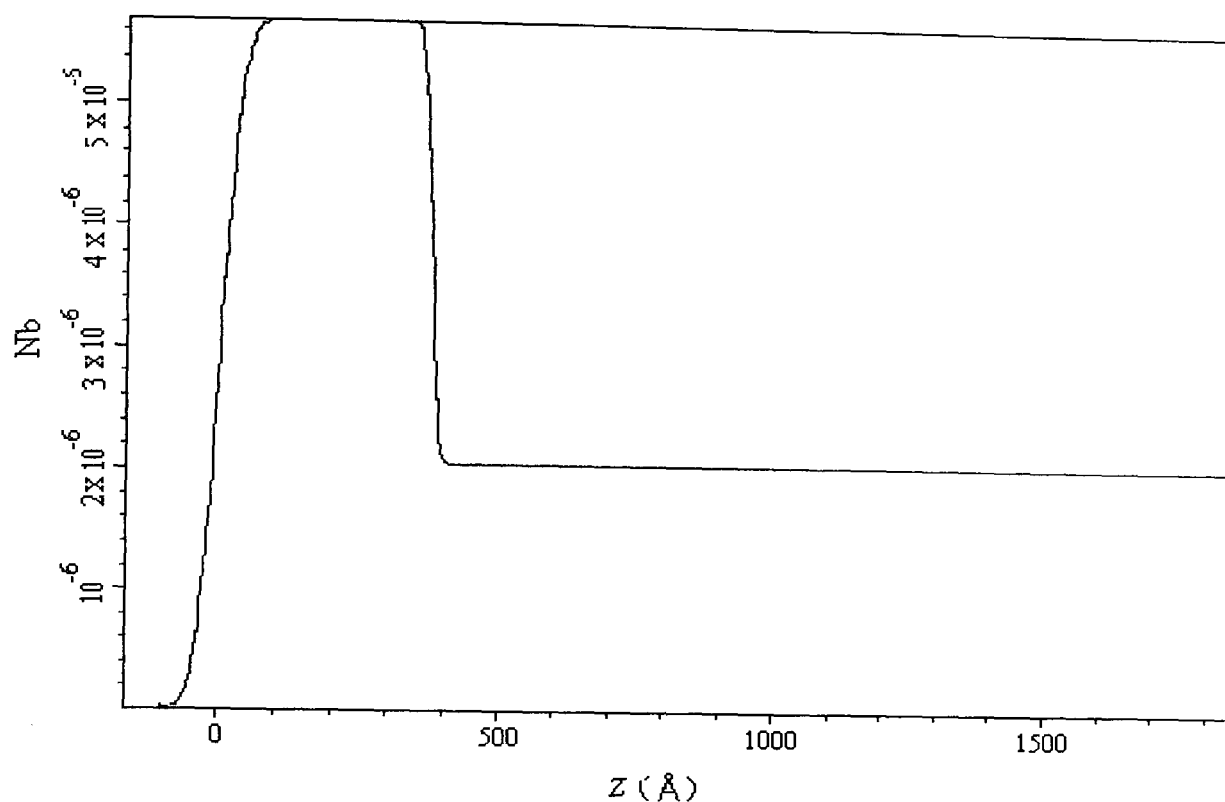
Figure 6.3   The profile of scattering length density as the function of the layer depth (*Z*) for a d-ZnSPS/PC bilayer on a silicon wafer, as made. The profile indicates d-ZnSPS layer thickness of 409 Å and an air/ionomer interfacial roughness of 23 Å, and were used to generate the solid line curve in the previous figure.

Figure 6.4 and 6.5 shows the reflectivity profiles and their best model fits for the d-ZnSPS/PC bilayer following the annealing sequences in Table 6.2. Experiments were carried out for the "as made" sample and after annealing at 200°C for several time periods. There was no measurable change in the profile following the initial annealing "A" therefore the relative profile has not been included in figure 6.4. The reflectivity data in these figures have been scaled for clarity. The

interference patterns arise from waves reflected at each interface. The dominant lower frequency fringes arise from the thinner top layer d-ZnSPS, whereas the superimposed high frequency fringes arise from the bottom thick PC layer. The rate at which these fringes damp depends on the interfacial width and nature of the polymer-polymer interface. It should be pointed out that the fits are very sensitive to the parameters describing the top d-ZnSPS layer and the interface but they are not sensitive to the parameters describing the bottom PC layer and the density of the substrate, since the scattering length density of d-ZnSPS is much larger than that of PC.
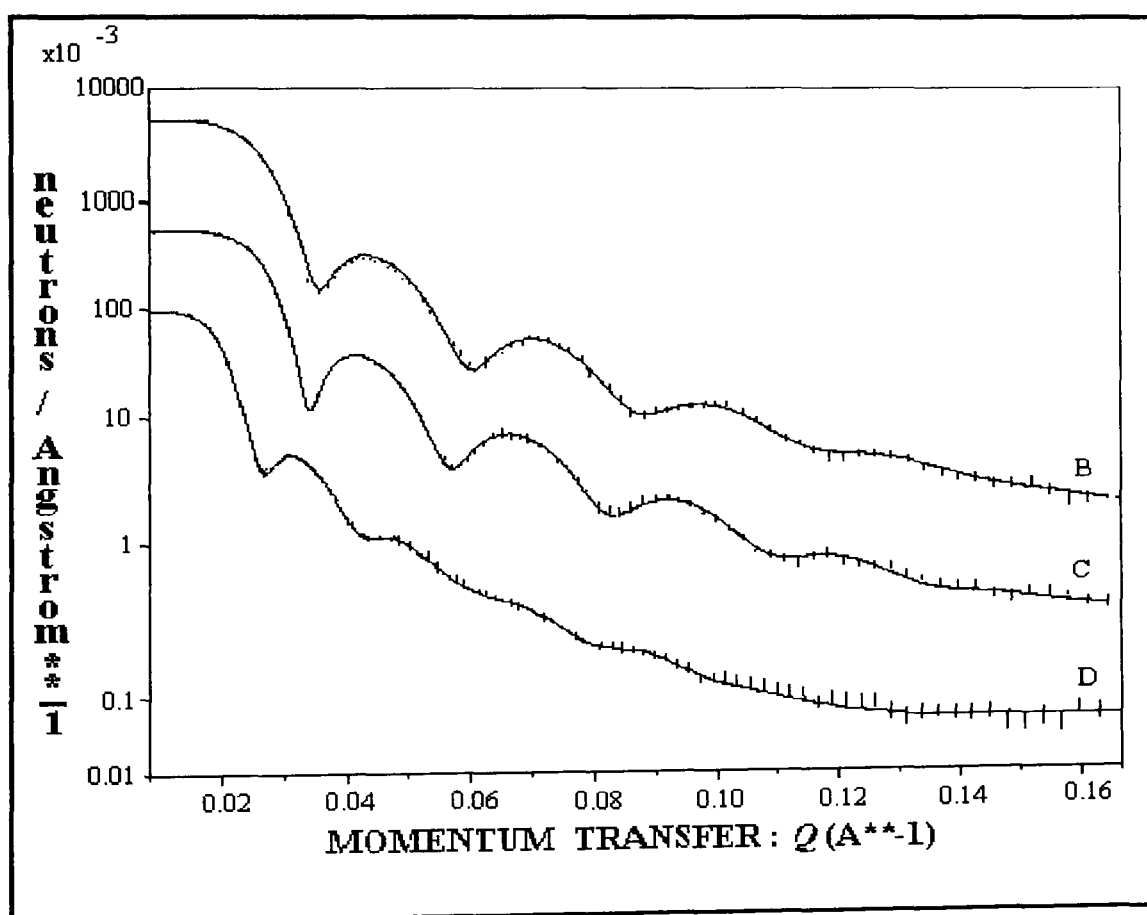
Figure 6.4   Neutron reflectivity profile with best fits of a d-ZnSPS/PC, annealed at 200°C for different periods of time. Curve (B) 1 hrs, (C) 3 hrs, and (D) 5 hrs.
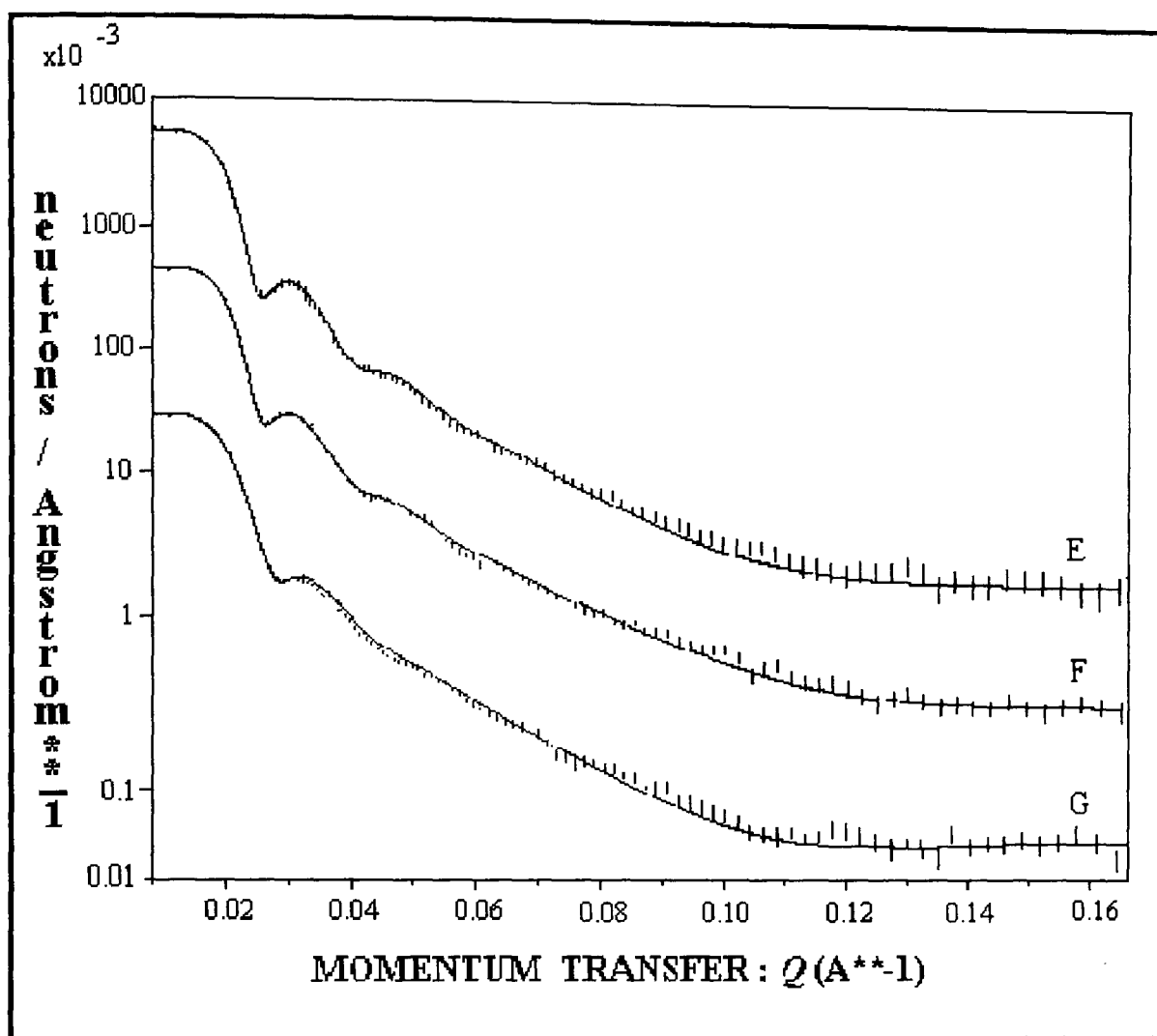
Figure 6.5   Neutron reflectivity profile with best fits of a d-ZnSPS/PC, annealed
            at 200°C for 7 hrs (Curve E), for 14 hrs (Curve F) and after
            annealing for 60 hrs (Curve G).

In order to obtain an initial quantitative assessment of the annealing process and
to indicate clearly the major processes in operation, the model fitting has been
made using a single bilayer with a diffuse Gaussian interface at the d-ZnSPS/PC
interfaces. In view of the lack of sensitivity of the main features of the reflectivity
profile to the thickness and density of the lower PC layer and the density of the
substrate these parameters have been held constant in the refinement procedure.

The fitted parameters (thickness and density) of the d-ZnSPS/PC layer, and the width of the interface are summarised in Table 6.3 respectively.

Table 6.3   Parameters used in the two-layer fits of the reflectivity profiles, where Nb and d are the scattering length density and thickness of the d-ZnSPS, $\sigma 1$ and $\sigma 2$ are the air – top layer and top layer – bottom layer root mean square roughnesses respectively. All the profiles have been fitted with the following constant parameters: Nb (PC) = 2.05 × 10^{-6} $Å^{-2}$, d (PC) = 1300 Å and Nb (silicon) = 2.07 × 10^{-6} $Å^{-2}$.

Annealing code	d (Å) d-ZnSPS	Nb× 10^{-6} $Å^{-2}$ d-ZnSPS	$\sigma 1$ (Å)	$\sigma 2$ (Å)
As made	409	5.45	23	12
B	398	5.70	20	12
C	388	5.73	19	32
D	389	5.68	20	40
E	384	5.61	19	50
F	380	5.78	16	56
G	340	5.76	20	63

Figure 6.6 gives the neutron scattering density profile of "as made" and of samples which followed the annealing sequences in Table 6.2. These scattering density profiles were actually used to generate the best reflectivity fits in figures 6.4 and 6.5, respectively. Figure 6.6 shows that as the polymer/polymer interfacial width increases as the layer of d-ZnSPS becomes thinner as a result of its dissolution into the interface. The "as made" sample is characterised by a more diffuse interface, which is 12 Å compared to the one for the d-LiSPS which is

4 Å (see section 6.3.2 Table 6.4). The "as made" interface can be simulated by a Gaussian interface towards the PC side. The top d-ZnSPS layer is 409 Å thick whereas the bottom PC layer is 1300 Å, after 1 hour annealing time the shape of the interface and the interfacial width remains the same. As the more mobile d-ZnSPS swells the less mobile PC, the interface shifts towards the d-ZnSPS without an apparent increase in the interfacial width. After 3 hrs annealing time the shape of the interface remains approximately the same, but the interfacial width has increased to 32 Å. After 5 hrs annealing time the interface changes shape as well as the interfacial width which reached 40 Å. After 7hrs annealing time the interfacial width reached 50 Å and after 14 hrs annealing time it increased slowly to 56 Å while the interface is characterised by a Gaussian interface towards the PC layer. The top d-ZnSPS layer gets slightly thinner as the d-SPS, which is a more mobile polymer, starts swelling the less mobile PC. After annealing at even longer times (60 hrs) the interfacial width reached 63 Å and the top layer reached to 340 Å. Given the uncertainty in deriving the interfacial width this value implies that the sample has reached the constant interfacial width of the system under these annealing conditions.

The question: how much of d-ZnSPS enters the PC rich layer and how thick is the PC rich layer, cannot be answered by modelling, as they are beyond the resolution of the neutron reflectivity technique. However, based on the mass preservation and the assumption of a total volume preservation, which requires the total film thickness and the total amount of d-ZnSPS remaining constant, the thickness of the PC rich layer and the concentration of d-ZnSPS in that layer can be calculated. Nevertheless, this calculation can determine whether d-ZnSPS is distributed homogeneously inside the PC layer or if it has a concentration profile from the d-ZnSPS/PC interface to the d-ZnSPS/air interface.
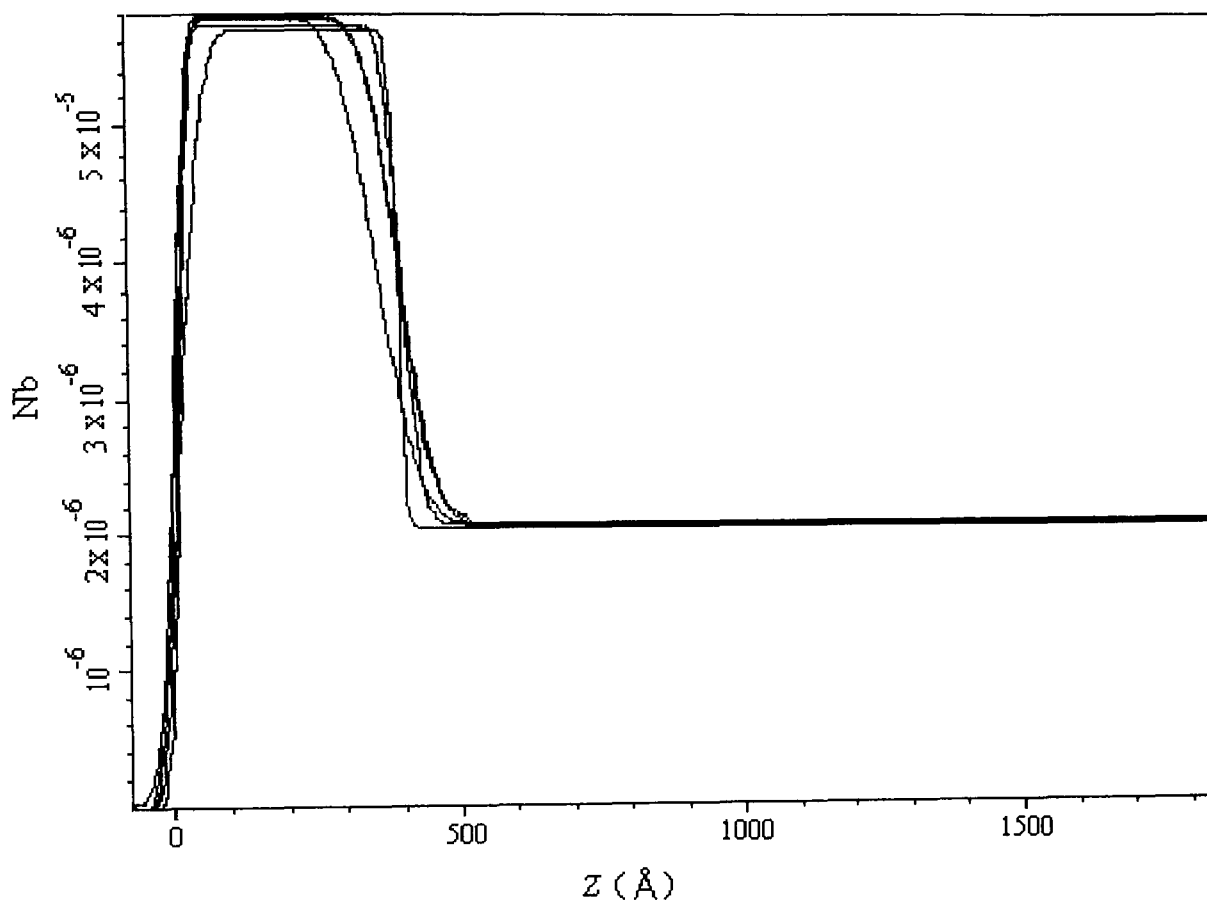
Figure 6.6   Evolution of the neutron scattering density profile at 200°C for the d-ZnSPS/PC bilayer. Thickness of d-ZnSPS layer and the interfacial profile are results of the fits. The thickness of PC rich layer and the scattering density value of PC rich layer are calculated based on the mass conservation of d-ZnSPS.

6.3.2   d-LiSPS/PC System

Figure 6.7 shows the reflectivity data (error bars) and the best fitting (solid line) obtained for the "as made" sample from d-LiSPS/PC bilayer. The interface can be described by a perfect Gaussian function whose interfacial width is 4 Å and surface roughness is 30 Å (see figure 6.8). The top d-LiSPS layer is 427 Å thick and the bottom PC layer is approximately 1300 Å. This indicates that the surface of the "as made" sample is not smooth.
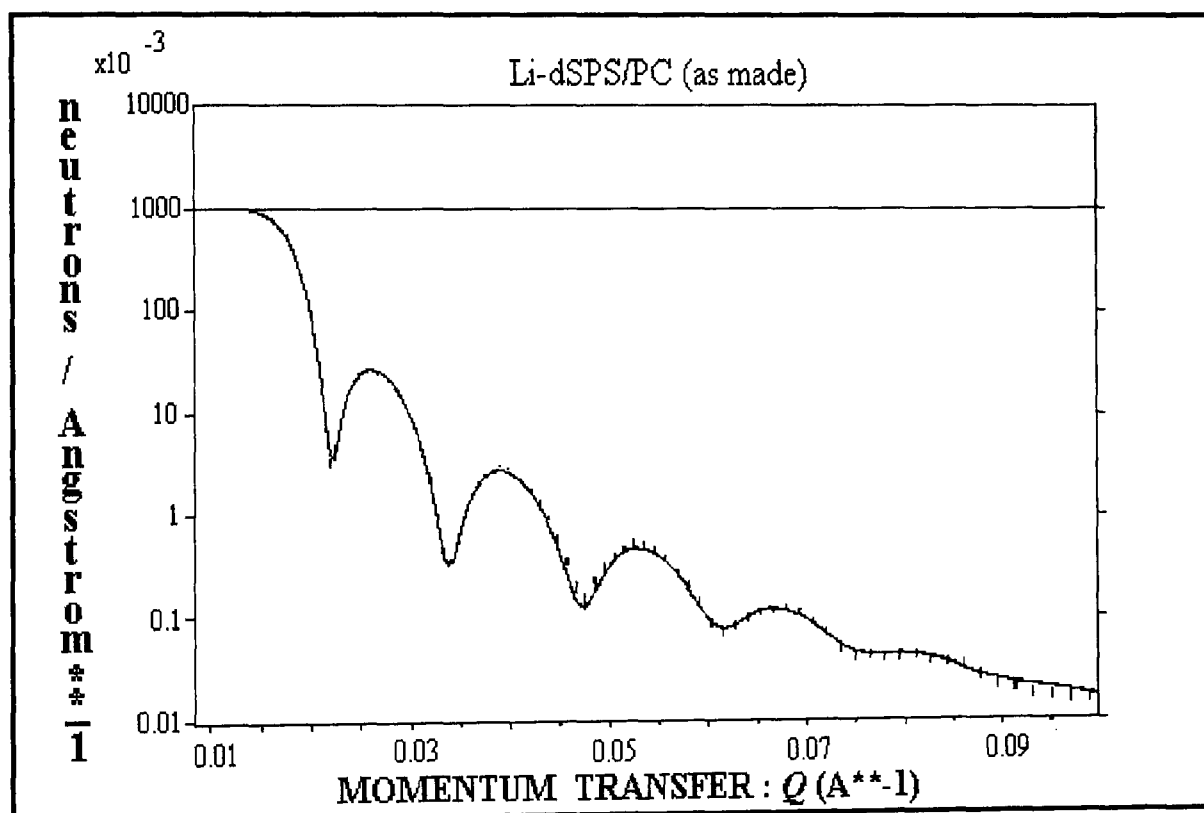
Figure 6.7   Neutron reflectivity profile of a d-LiSPS/PC bilayer "as made" on a silicon wafer. The error bars represent the experimental points and the solid line curve is the best fit by using a symmetric interfacial model shown in the next figure.
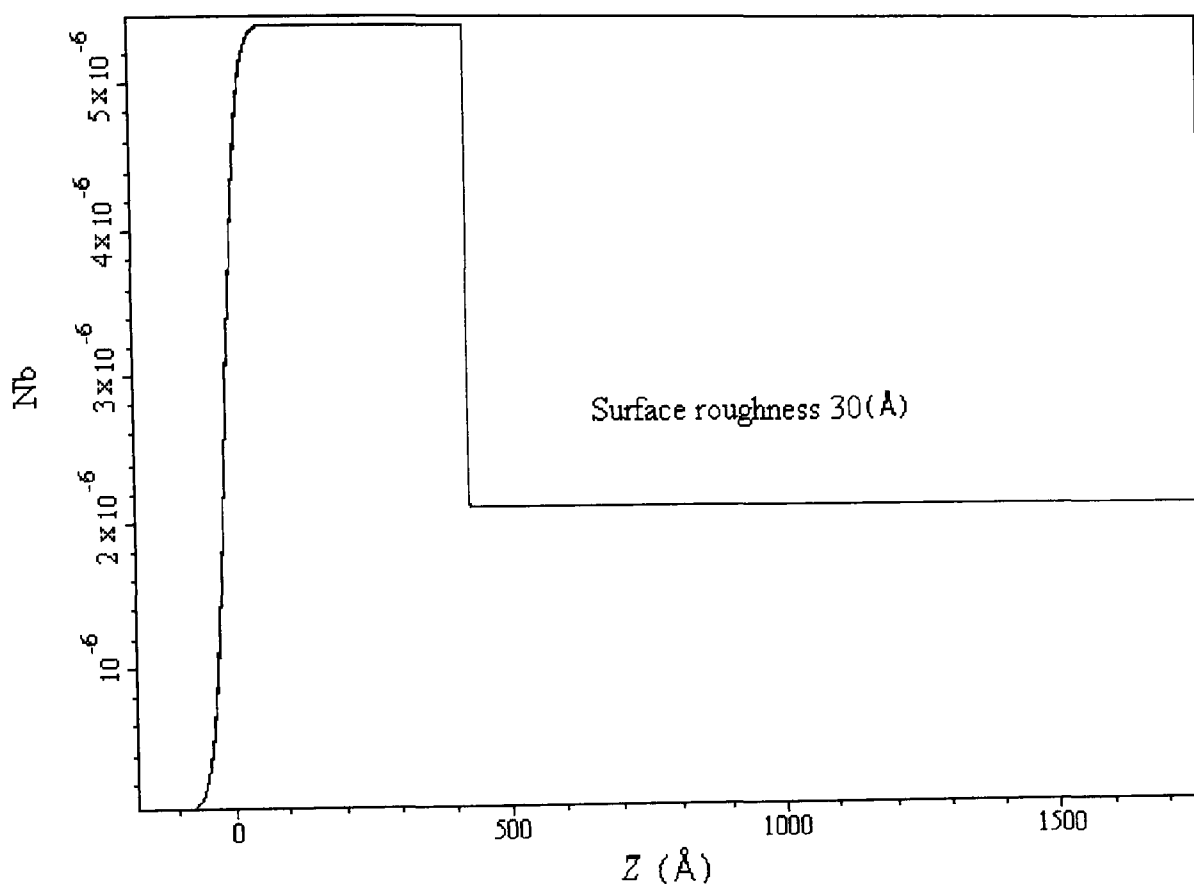
Figure 6.8   The profile of scattering length density as the function of the layer depth (Z)
for a d-LiSPS/PC bilayer on a silicon wafer, as made. The profile indicates
d-LiSPS layer thickness of 427 Å and an air/ionomer interfacial roughness
of 30 Å, and were used to calculate the solid line curve in the previous
figure (6.7).

Figure 6.9 and 6.10 shows the reflectivity profiles and their best model fits for the
d-LiSPS/PC bilayer following the same annealing sequences as with the
d-ZnSPS/PC system (see Table 6.2). The reflectivity data in these figures have
been scaled for clarity. The interference patterns arise from waves reflected at
each interface. The qualitative results obtained for the system with d-ZnSPS
apply here as well. A decrease in amplitude of the fringes with annealing time
indicates the presence of an interface. The period of the higher frequency fringes

increases as a result of thinning of the d-LiSPS layer. The entire model fitting has been made using a single bilayer with a diffuse Gaussian interface at the d-LiSPS/PC interfaces. As mentioned earlier, the reflectivity profiles are not sensitive to the parameters of the bottom PC layer and the density of the substrate, thus these parameters have been held constant in the refinement procedure. The fitted parameters (thickness and density) of the d-LiSPS layer, and the width of the interface are summarised in Table 6.4.

The effect of annealing on the reflectivity data can be seen directly in figure 6.9 and figure 6.10. The amplitude of the fringes decreases, which indicates the presence of an interface that increases in size with annealing time. Moreover, the period of the low frequency fringes increases indicating a thinning of the top d-LiSPS layer. The top film gets thinner with annealing while initially its scattering length density increases and eventually reaches a constant value. However from the fitting parameters (see Table 6.4) one can extract the following information about the system:

During the annealing B, C and D the thickness of the top layer increases. After annealing B the scattering length density of the d-LiSPS increases and then remains approximately constant during all the annealing steps. This suggests that during the first three annealing processes the d-LiSPS layer is stabilizing and that the chains are allowed to move and arrange themselves until they reach equilibrium.
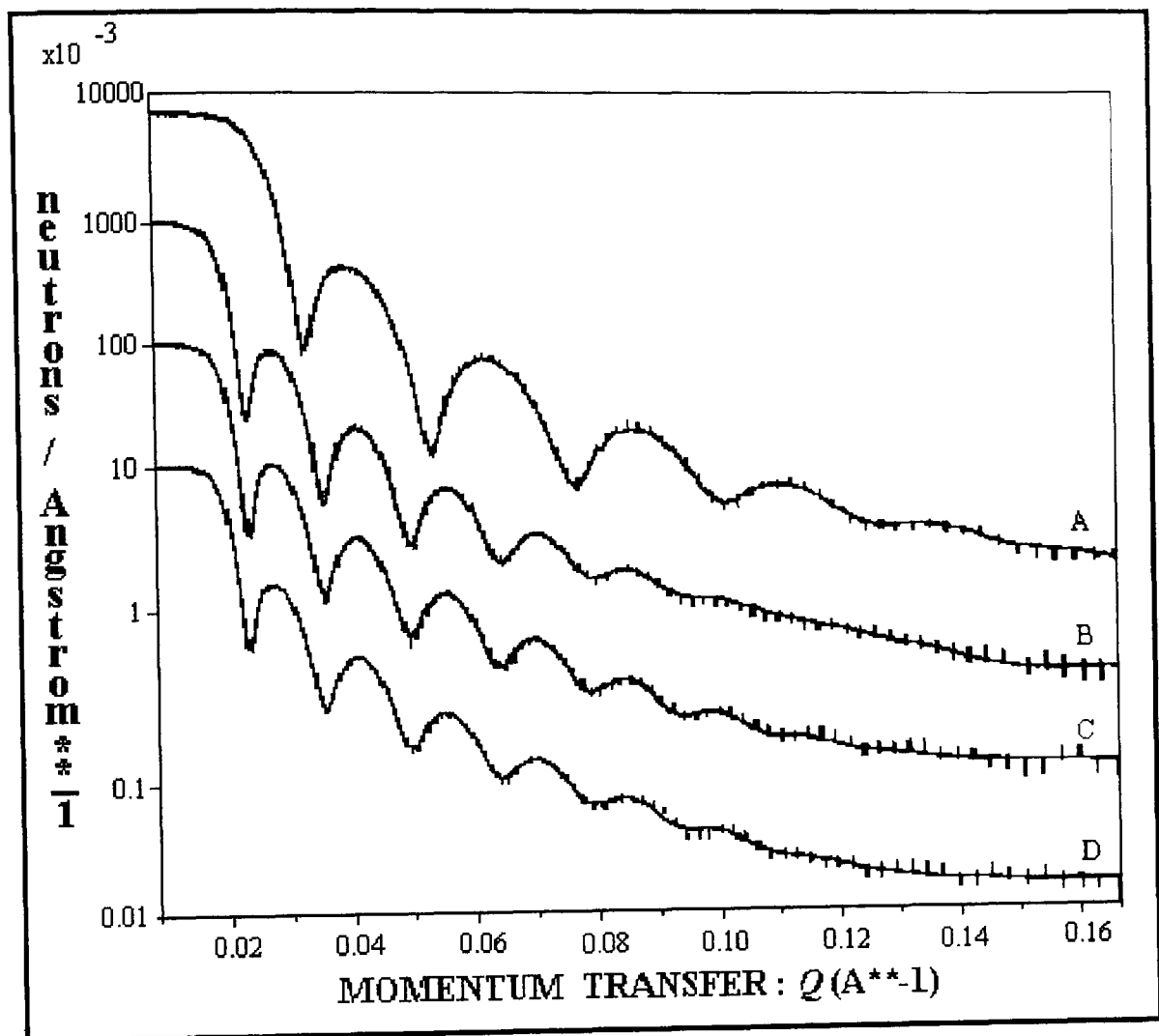
Figure 6.9   Neutron reflectivity profiles with best fits of a d-LiSPS/PC, annealed at 200°C for different periods of time. Curve (A) as made, (B) 1 hrs, (C) 3 hrs, (D) 5 hrs.

After annealing E, F and G the thickness of the top layer decreases and its scattering length density mostly remains constant. The width of the interface increases continuously and the air-ionomer roughness remains approximately constant. Several conclusions can be drawn from the results obtained before and after annealing the samples.

$x10^{-3}$

MOMENTUM TRANSFER : Q (A**-1)
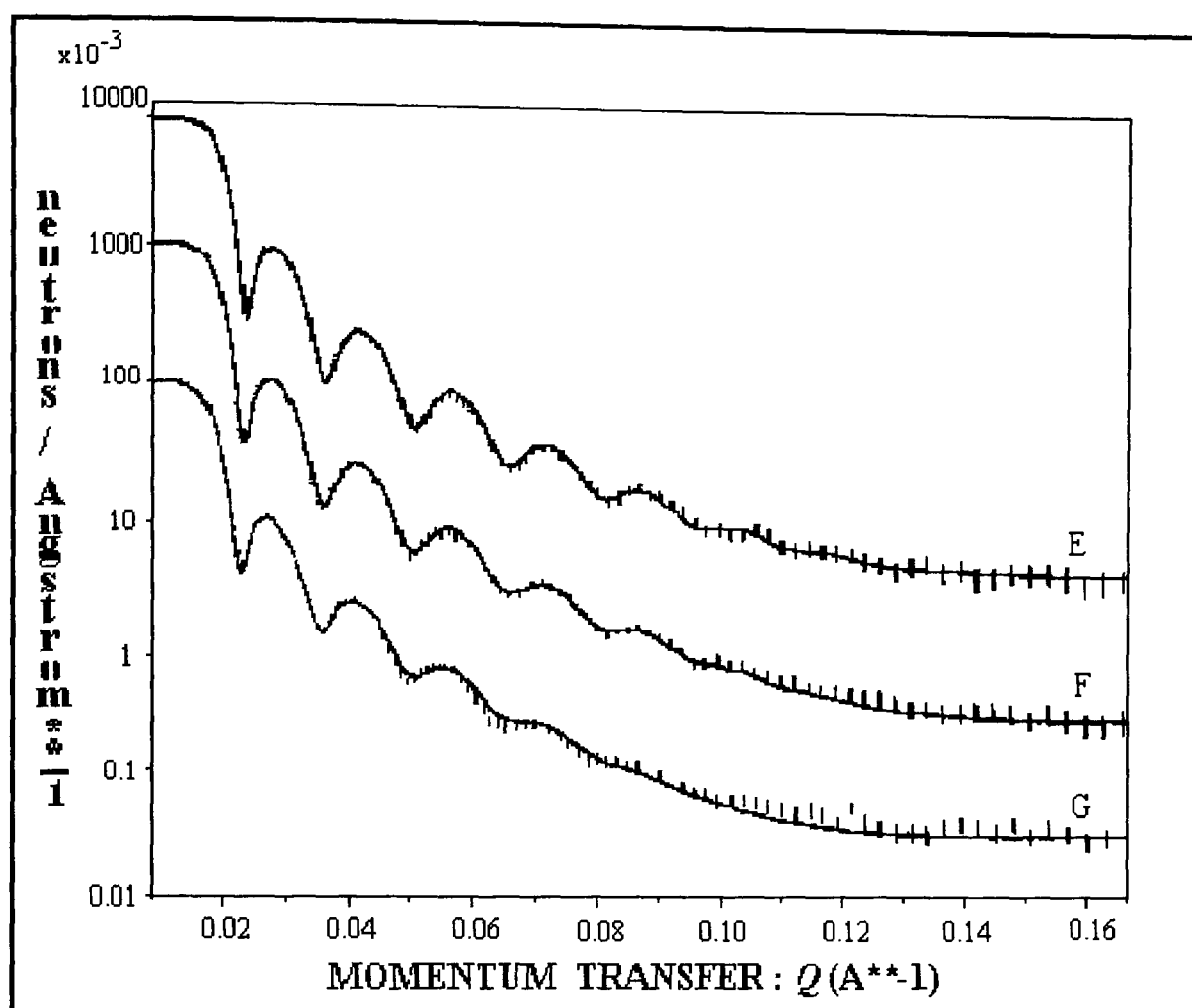
Figure 6.10 Reflectivity data and their best fits. Top curve (E): after annealing at 200C

for 7 hrs, middle curve (F): after annealing for 14 hrs and bottom curve (G):

after annealing for 60 hrs.

The top d-LiSPS layer gets thinner with annealing while its scattering length

density increases slightly and then remains constant. The surface undulations are

larger at the initial stages of annealing and the quality of the sample improves

gradually. The d-LiSPS chains are allowed to move and arrange and the root-

mean-square roughness d-LiSPS/PC therefore changes gradually. The surface of

the top layer becomes again more wavy with annealing and as d-LiSPS diffuses

into the bottom layer. The shape of the interface remains the same but the

position of the interface moves towards the d-LiSPS layer. These effects are clear from the change in the period of the fringes with annealing.

We should also point out why the interface appears large, then decreases and subsequently increases again. Because the top layer was prepared by spin coating directly onto the layer already on the substrate it is quite likely that the solvent has swollen the interface so that in the first couple of hours of annealing the system is simply changing to a new equilibrium state.

Table 6.4   Parameters used in the two-layer fits of the reflectivity profiles, where Nb and d are the scattering length density and thickness of the d-LiSPS, $\sigma 1$ and $\sigma 2$ are the air – top layer and top layer – bottom layer root mean square roughnesses respectively. All the profiles have been fitted with the following constant parameters: Nb (PC) = 2.05 $\times$ 10^{-6} Å^{-2}, d (PC) = 1300 Å and Nb (silicon) = 2.07 $\times$ 10^{-6} Å^{-2}.

Annealing code	d (Å) d-LiSPS	Nb$\times$ 10^{-6} Å^{-2} d-LiSPS	$\sigma 1$ (Å)	$\sigma 2$ (Å)
As made	427	5.38	30	4.1
B	412	5.50	22	5.2
C	416	5.64	11	21.0
D	416	5.75	11	22.4
E	402	5.78	11	23.1
F	402	5.75	13	26.8
G	402	5.75	15	34.0

The d-LiSPS/PC interface has been modelled as a symmetrical Gaussian, therefore implying that there is some mixing on both sides of the interface. As shown by the fitting parameters (Table 6.4) the top d-LiSPS layer gets thinner as the d-LiSPS, which is the more mobile polymer, starts swelling the less mobile PC. The PC has a higher molecular weight than the d-LiSPS. The direction of the shift of the interface is therefore always towards the fastest moving components, clearly indicating the occurrence of a swelling mechanism.

In conclusion, the results obtained from this experimental series are qualitatively the same as the ones obtained for the d-ZnSPS/PC system. The only difference lies in the fact that interdiffusion occurs over a shorter time range than before. In order to investigate the equilibrium interfacial width for this system NR experiments at longer annealing times would be necessary.

Having discussed the interfacial structure, we now proceed to discuss the kinetics of the interfacial mixing. Figure 6.11 and 6.12 show plots of the interfacial shift (ΔZ_i) as a function of annealing time, t, at 200°C for the d-ZnSPS/PC and d-LiSPS/PC bilayer, respectively. The experimental data clearly do not follows either case – II (curve "a") or Fickian diffusion (curve "b") equation, which indicates that the overall mixing process cannot be described solely by a polymer relaxation or a simple molecular diffusion mechanism. These results show that a relatively small increase in the interfacial width is observed. The initial fast increase is followed by a slow increase until the final constant width is reached.

In a previous paper [31] Weiss and Feng used neutron reflectivity to study the kinetics of interfacial mixing between the Lithium-salt sulfonated polystyrene and polyamide (mPA). They interpreted their data with two suggested models of

diffusion controlled mechanisms of mixing kinetic for a different temperature range. Similar to the above we have used the same proposed models to fit our experimental data.

Figure 6.11   Displacement of the d-ZiSPS layer front at 200°C as a function of annealing time for a d-ZnSPS/PC bilayer. Lines are the best fittings by using different kinetic models: (a) $\Delta Z_i = Bt$; (b) $\Delta Z_i = Bkt^{1/2}$; (c) $\Delta Z_i = B[1 - \exp(-kt)]$; (d) $\Delta Z_i = B[1 - \exp(-kt^{1/2})]$. In these equation, t is the annealing time, ΔZ_i is the interface shift, k and B are the fitting parameters.
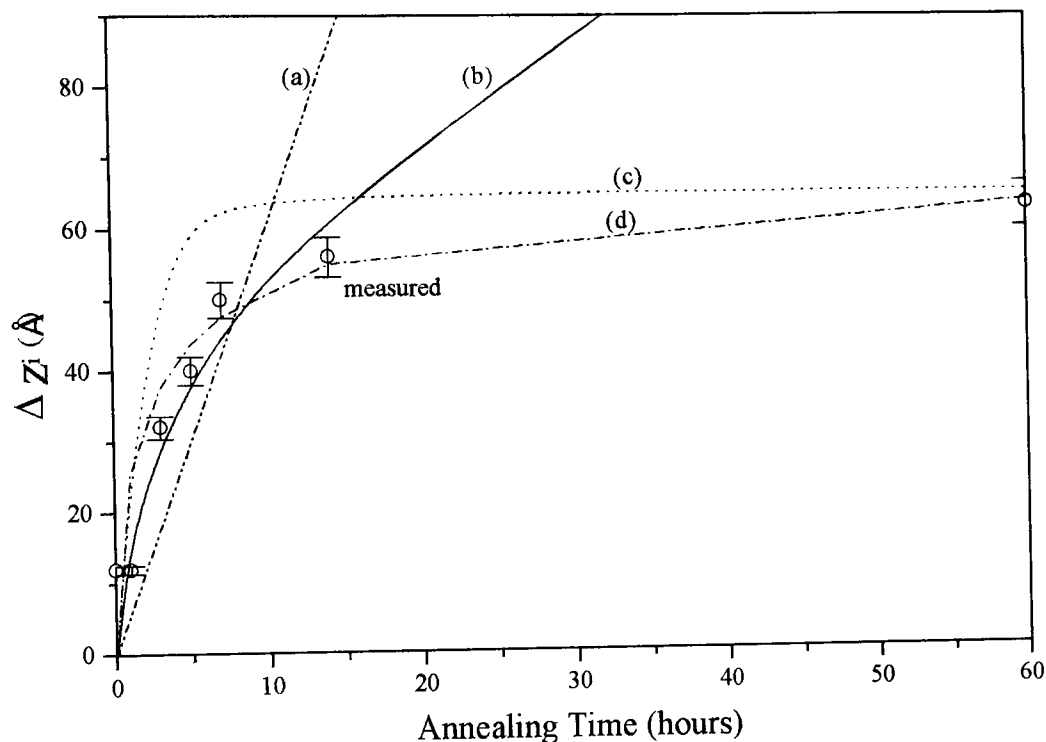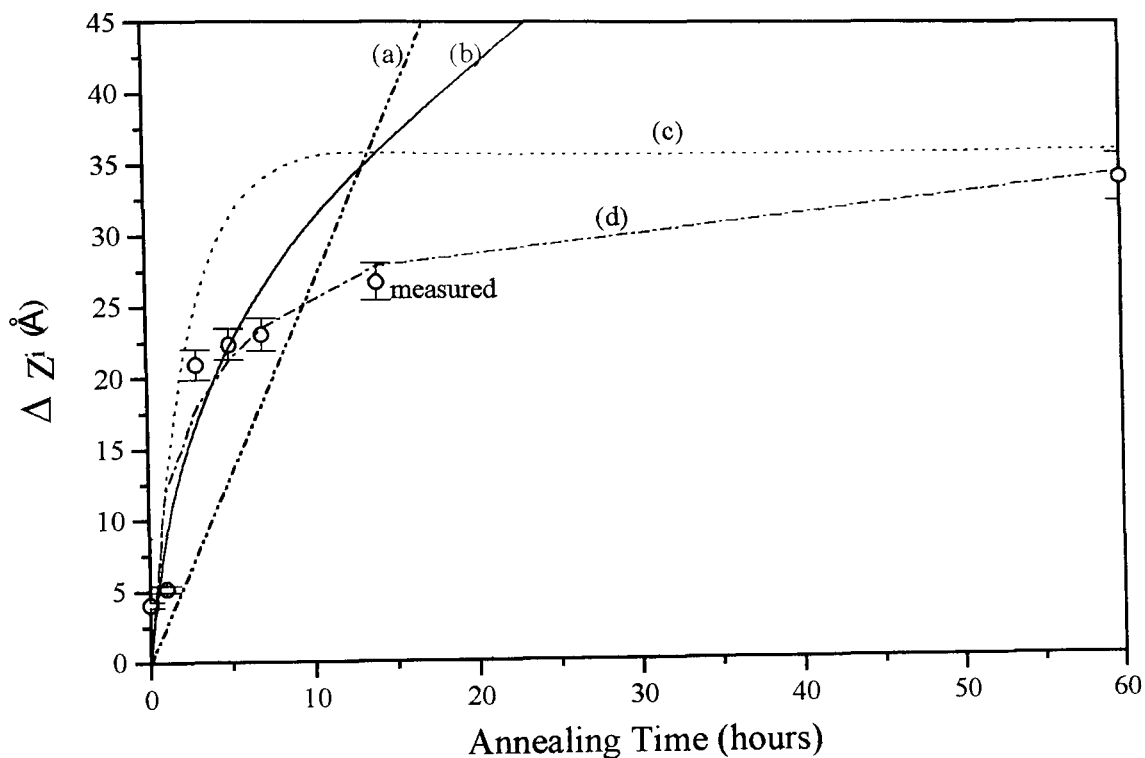
Figure 6.12   Displacement of the d-LiSPS layer front at 200°C as a function of annealing time for a d-LiSPS/PC bilayer. Lines are the best fittings by using different kinetic models: (a) $\Delta Z_i = Bt$;   (b) $\Delta Z_i = Bkt^{1/2}$;   (c)

$\Delta Z_i = B[1 - \exp(-kt)]$; (d) $\Delta Z_i = B[1 - \exp(-kt^{1/2})]$. In these equation, t is the annealing time, ΔZ_i is the interface shift, k and B are the fitting parameters.

In figure 6.11 and 6.12, line (b) and line (c) give the best fits to equations ($B[1 - \exp(-kt)]$) and ($B[1 - \exp(-kt^{1/2})]$) respectively. Within the experimental error, the equation ($B[1 - \exp(-kt)]$) does not fit the experimental data. On the other hand the equation ($B[1 - \exp(-kt^{1/2})]$) provided the best fit to the experimental data. The interpretation of this equation provided Weiss et al [31]

was that the diffusion is gradually and significantly slowed down by crosslinking mechanism. This is unlikely to be the case in this system of PS/PC, but it is obviously some form of chemical reaction or molecular rearrangement, which is responsible for the observed effects.

These results could be expected, as at 200°C the polymers are immiscible. It will be therefore useful to repeat the experiment with samples annealed in the miscible range. i.e. above the critical solution temperature (225°C)[23]. Another change that might have been beneficial would be to coat the deuterated layer underneath the PC instead of on top. This would provide greater contrast between the substrate and the lower layer while obviously maintaining the polymer/ionomer contrast. Unfortunately such samples and beam time have not been available for this work.

6.4   CONCLUSIONS

In this part of the study, we have demonstrated the effects of introducing intermolecular complexation on the interface of sulfonated polystyrene (SPS) and polycarbonate (PC) blends with different metal cations (i.e. lithium and zinc). Both systems are partially miscible and exhibit an upper critical solution temperature behaviour [22]. The diffusion in these systems with annealing at a temperature above the glass transition temperature of both polymers has been measured. The interfacial profiles obtained for these systems are described by symmetric Gaussian interfaces.

The results are qualitatively similar for both ionomers, but interdiffusion is slightly faster for d-ZnSPS/PC system. The diffusion process can be expected to

follow the function of square root time, until a thermodynamical equilibrium is reached. This will occur when a homogenous mixture is obtained. In the current observations the changes in the thickness layer are very slow and non-linearly dependent on the square roots time. This indicates, that the observed thickening of the interfacial layer is more affected by changes in planarity of the interface than by a true diffusion. In any case it can be concluded with certainty that the diffusion (if any) is extremely slow.

References

1. Paul, D. R.; Sperling, L. H., *Multicomponent Polymer Materials*, Advances in chemistry series 211; ACS, Washington, DC, **1986**.

2. Voyutskii, S. S., *J. Adhes*, **1971**, 3, 69.

3. de Gennes, P. G., *C. R. Acad. Sci.*, Paris, Seri. II, **1981**, 292, 1505.

4. Kausch, H. H.; Tirrell, M., *Annu. Rev. Mater. Sci.* **1989**, 19, 341.

5. Jabbari, E.; Peppas, N. A., *J. M. S., Rev. Macromol. Chem. Phys.* **1994**, C34(2), 205.

6. Higgins, J. S.; Bucknall, D. G., *Neutron Reflection Studies of Polymer-Polymer Interfaces*, Technical Report of Central Laboratory of the Research councils **1997**.

7. Ferry, J. D., *Viscoelastic Properties of Polymers*, 3rd Edn., J. Wiley and Sons, New York, **1980**.

8. Crank, J., *The Mathematics of Diffusion*, Claredon Press, Oxford, **1956**.

9. Brochard, B.; de Gennes, P. G., *Physico Chemical Hydrodynamics*, **1983**, 4, 313.

10. Brochard, B.; de Gennes, P. G., *Europhys. Lett.*, **1986**, 1(5), 211.

11. Kramer, E. J.; Green, P. F.; Palmstrom, C. J., *Polymer* **1984**, 25, 473.

12. Fernandez, M. L.; Higgins,J. S.; Penfold, J.; Shackleton, C., *J. Chem. Soc. Faraday Trans.*, **1991**, 87(13), 2055.

13. Hopfenberg, H. B.; Stannett, V. T., *The Physica of Glassy Polymers*, ch.9, Haward, R. N., Eds., Wiley, New York, **1973**.

14. Alfrey, T. Jr.; Gurnee, E. F.; Lloyd, W. G., *J. Polym. Sci.(C)*, **1966**, 12, 249.

15. Crank, J.; Park, G. S., *Diffusion in polymers*, Acad. Press, **1968**.

16. Frisch, H. L., *J. Phys. Chem.* **1958**, 62, 401.

17. Eyring, H., _J. Chem. Phys._ **1936**, 4, 283.

18. Crank, J. _J. Polym. Sci._ **1953**, 11, 151.

19. Frisch, H. L., _J. Chem. Phys._ **1964**, 41, 3679.

20. Douglas, J. F.; Johnson, H. E.; Granick, S., _Science_, **1993**, 262, 2010.

21. Lu, X.; Weiss, R. A., _Proc. Annu. Tech. Conf._, _Soc.Plast.Eng_ **1993**, 684-686.

22. Lu, X.; Weiss, R. A., _Macromolecules_ **1996**, 29, 1216.

23. Rui Xie; Weiss, R. A, _Polymer_ **1998**, 39, 2851.

24. Russell, T. P., _Mater. Sci. Rep._ **1990**, 5, 171.

25. Karim, A.; Mansour, A.; Felcher, G. P; Russell, T. P., _Phys. Rew. B._ **1990**, 42, 6846.

26. Fernandez, M. L.; Higgins, J. S.; Penfold, J.; Ward, R. C.; Shackleton, C.; Walsh, D. J., _Polymer_ **1990**, 31, 2174.

27. Makowski, H. S.; Lundberg, R. D.; Singhal, G. H., _US Patent_ **1975**, 3, 870, 841.

28. Penfold, J., _J. Phys. (Paris) C_ **1989**, 750.

29. Ankner, J. F., _In Surface X-Ray and Neutron Scattering_, Springer Proceedings in Physics **1992**, 61, 105.

30. Born, M.; Wolf, E., _Principles of Optics_, 6th _Edn._, Pergamon Press: Oxford, **1980**.

31. Feng, Y.; Weiss, R. A.; Han, C. C., _Macromolecules_ **1996**, 29, 3918.

CHAPTER SEVEN

CONCLUSIONS

7.1 CONCLUSIONS

The aim of this thesis was to investigate the miscibility of two different blends through a polymer – polymer diffusion. All the blends used in this work are partially miscible polymer blends. Although the PS/PVME blend shows LCST behaviour, the ionomer blends (d-LiSPS/PC and d-ZnSPS/PC) exhibit UCST behaviour. The standard characterisation of the model system PS/PVME blend was carried out using DSC, optical light microscopy and FTIR spectroscopy as a function of temperature and composition. It was determined, as briefly summarised below, that the given hypothesis about the miscibility of the PS/PVME blend being due to the specific interaction between the ether lone-pair electrons of PVME and the phenyl ring of PS has not been confirmed in this work by a more accurate IR data analysis and also the results obtained by quasielastic neutron scattering [1].

The DSC results show that the blends prepared in this work are miscible in the amorphous state over all the composition range at low temperature as judged from glass transition behaviour and the transparency of blend films. The blends exhibit a single, composition – dependent glass transition temperature that obeys the Gordon – Taylor equation. The predicted T_g's from the Gordon – Taylor equation for this blend fitted the experimental data quite well and yielded a K value of 0.25. This indicates that there is not any strong interaction like hydrogen

bonding type, if any specific interaction involving between PS and PVME are extremely weak. DSC results also show that the mechanical-blending samples have different behaviour to the samples prepared by solvent casting. The mechanical-blended system did not show a single T_g of the blend, unless annealed for one day at 110°C. The light microscopy experiments confirm to these results that the solvent cast samples and prepared by mechanical blended have different microstructures.

The DSC results also show that a phase diagram can be constructed by DSC techniques. The blends displayed two glass transition temperatures when quenched from temperature above 150°C, as shown by FTIR and light microscopy. In addition it is shown that the rate of phase separation is very fast and the phases can only be preserved using the fastest possible cooling rate (e.g. N_2). The phase diagram of this blend system has the LCST at critical composition between 20 and 30 wt % PS content, which correlates well with phase diagram already available in the literature [2-4].

FTIR spectroscopy failed to identify any perturbation of the ether lone – pair electron of PVME and the benzene ring vibration of PS as a result of blending the PS and PVME. It was found that the peak assigned to the C – O stretching mode of PVME at 1100 cm^{-1}, shows similar behaviour for both pure PVME and the blend. Moreover, i.r study as a function of temperature and blend composition show that the C – O stretching vibration of the $COCH_3$ group in pure PVME and (50/50) PS/PVME blends is very similar as recently reported, the same local dynamic effect of the ether CH_3 group in PVME and PS/PVME blend composition as a function of temperature using QENS [1]. Therefore the spectral changes in polymer blends as reported in the literature can be explained by

temperature changes in pure homopolymers with the exception of 758 and 699 cm^{-1} peaks. This indicates that molecular interactions, which are responsible for miscibility, are not detectable by infrared absorption and are therefore of unspecified strength and location. The FTIR spectra of SPS/PVME blends (Fig: 4.22 and 4.25) indicate that sulfonate groups on PS affect polymer miscibility through changes in configuration of molecules, rather than through direct interaction with the PVME, as suggested in the literature.

Parker and Vesely [5] have used polarised light microscopy and electron microscopy to measure and identify the interdiffusion layer in the blends poly(vinyl chloride)/poly ($\in$-caprolactone) (PVC/PCL). Similar analyses by optical light microscopy experiments have been tried on PS/PVME interdiffusion but have not been successful so far. A small amount of PVME was placed on the top of thin PS film produced by compression moulding. The light microscopy experiments were carried out after heating the samples above and below the glass transition temperature of PS. No interdiffusion layers were observed because of the low resolution and contrast, but also problems with sample preparation. However, it was observed that this experiment is very promising as a way of looking at the interdiffusion of two polymers with a very low degree of miscibility. Some changes must occur at the interface when the chains have reached the melt state and the two polymers are in contact.

The second system investigated was that of sulfonated polystyrene (PS)/polycarbonate (PC) blends with different cations, where the interfacial development for several annealing times at 200°C for the d-LiSPS/PC and d-ZnSPS/PC system was investigated. This was accomplished by carrying out neutron reflectivity (NR) experiments.

The diffusion in this system with annealing at a temperature above the glass transition temperature of both polymers has been measured. The interface can be simulated by a symmetric Gaussian interface. After a sufficiently long enough annealing time a constant interfacial width is observed in d-ZnSPS/PC system as is predicted for the case of partially miscible systems. Replacing d-ZnSPS with d-LiSPS gave similar qualitative results to the d-ZnSPS sample, but in this case the interfacial development occurred more rapidly than before. The time range investigated in this experimental set was not long enough to obtain the final equilibrium width. Further experimental investigation at longer annealing times is recommended at this stage in order to obtain the equilibrium interfacial width for d-LiSPS/PC system. Also the observed changes in the thickness layer are very slow and non-linearly dependent on the square roots time. This indicates, that the observed thickening of the interfacial layer is more affected by changes in planarity of the interface than by true diffusion. Therefore it can be concluded with certainty that diffusion (if any) is extremely slow.

To understand the changes occurring in the structure upon deuteration and sulfonation, a series of hydrogenous atactic polystyrene ionomers with different selectively deuterated variants was studied. It was observed that the formation of a strong ionic field with the increasing deuterium concentration which participates in cluster formation together with the sulfonate ions. It has also been found that the spectra are sensitive to a modification by deuteration or by sulfonation of adjacent functional groups (e.g. C – H vibration of the chain). These results also clearly show that the vibrational bands depend on the strength of the bonds and the masses of the atoms involved in the particular vibration mode as well as charge of the cation. Moreover, using the selectively deuterated functional groups

allowed to uniquely assign peaks, which were not assigned previously to chain or ring vibration.

7.2   RECOMMENDATIONS FOR FUTURE WORK

1). The major aim of this work, i.e. to correlate the diffusion rate, miscibility and phase diagrams has only partially been fulfilled. It will be necessary to study the diffusion rates for different temperatures using neutron reflectivity, and improve the techniques for light microscopy.

2). In order to establish fully phase diagrams, true solubilities have to be measured. This can be done with techniques currently not available to us, e.g. FTIR microscopy, X-ray microanalysis, fluorescence etc.

3). The role of molecular interactions is not easy to establish. This work has shown that the interactions are not specific, which makes the utilisation of vibrational techniques, like FTIR or NMR less useful. It will therefore be necessary to utilise some indirect methods, not yet fully developed, such as vapour pressure, contact angle, viscosity or enthalpy measurements.

4). The effect of changes in functional groups or ions has also not been clarified and it is essential to obtain data from a large range (wavenumbers) of compounds before some conclusions can be reached.

1. Arrighi, V.; Higgins, J. S. *Macromolecules* **1995**, 28, 4622.
2. Nishi, T.; Kwei, T. K. *Polymer* **1975**, 16, 285.
3. Walsh, D. J.; Dee, G. T. *Macromolecules* **1989**, 22, 3395.
4. Kwei, T. K.; Nishi, T.; Roberts, R. G. *Macromolecules* **1974**, 7, 667.
5. Parker, M. A.; Vesely, D. *J. Polym. Sci., Part B: Polym. Phys. Ed.* **1986**, 24, 1869.